University of Tennessee, Knoxville

TRACE: Tennessee Research and Creative Exchange

Doctoral Dissertations

Graduate School

5-2011

Development of a Rigid Body Forward Solution Physiological Model of the Lower Leg to Predict Non Implanted and Implanted Knee Kinematics and Kinetics

John Kyle Patrick Mueller
jmueller@cmb.utk.edu

Follow this and additional works at: https://trace.tennessee.edu/utk_graddiss

Part of the Biomechanical Engineering Commons

Recommended Citation

Mueller, John Kyle Patrick, "Development of a Rigid Body Forward Solution Physiological Model of the Lower Leg to Predict Non Implanted and Implanted Knee Kinematics and Kinetics. " PhD diss., University of Tennessee, 2011.
https://trace.tennessee.edu/utk_graddiss/1006

This Dissertation is brought to you for free and open access by the Graduate School at TRACE: Tennessee Research and Creative Exchange. It has been accepted for inclusion in Doctoral Dissertations by an authorized administrator of TRACE: Tennessee Research and Creative Exchange. For more information, please contact trace@utk.edu.

To the Graduate Council:

I am submitting herewith a dissertation written by John Kyle Patrick Mueller entitled "Development of a Rigid Body Forward Solution Physiological Model of the Lower Leg to Predict Non Implanted and Implanted Knee Kinematics and Kinetics." I have examined the final electronic copy of this dissertation for form and content and recommend that it be accepted in partial fulfillment of the requirements for the degree of Doctor of Philosophy, with a major in Biomedical Engineering.

Richard D. Komistek, Major Professor

We have read this dissertation and recommend its acceptance:

Mohammed R. Mahfouz, William H. Hamel, Aly Fathy

Accepted for the Council:

Carolyn R. Hodges

Vice Provost and Dean of the Graduate School

(Original signatures are on file with official student records.)

To the Graduate Council:

I am submitting herewith a dissertation written by John Kyle P. Mueller entitled "Development of a Rigid Body Forward Solution Physiological Model of the Lower Leg to Predict Non Implanted and Implanted Knee Kinematics and Kinetics." I have examined the final electronic copy of this dissertation for form and content and recommend that it be accepted in partial fulfillment of the requirements for the degree of Doctor of Philosophy, with a major in Biomedical Engineering.

Richard Komistek , Major Professor

We have read this dissertation
and recommend its acceptance:

William Hamel

Mohamed Mahfouz

Aly Fathy

Accepted for the Council:

Carolyn R. Hodges
Vice Provost and Dean of the Graduate School

(Original signatures are on file with official student records.)

Development of a Rigid Body Forward Solution Physiological Model of the Lower Leg to Predict Non Implanted and Implanted Knee Kinematics and Kinetics

A Dissertation
Presented for the
Doctor of Philosophy Degree
The University of Tennessee, Knoxville

John Kyle Patrick Mueller
May, 2011

To my grandparents,

Werner and Irene

Robert and Kathleen

Acknowledgements

I would like to acknowledge and thank, first and foremost, my major professor Dr. Richard Komistek. His support, insight, enthusiasm, vision, encouragement and belief in my abilities were the key elements in a support system that helped me finish this dissertation and complete my work at the Center for Musculoskeletal Research. He not only provided me the chance to work on this, but many other projects that included opportunities to work with industry, work with the best orthopaedic clinicians in the world, travel, speak, publish and learn many lessons I hope I will always remember. He is as inspiring in his personal life as he is in his professional, and I hope to live up to his expectations in both.

I would also like to acknowledge and thank my dissertation committee members Dr. Mohamed Mahfouz, Dr. William Hamel, and Dr. Aly Fathy not only for their support and helpful insight into my dissertation work but also for their overall support during my time at Tennessee. I would like to thank Dr. Thomas Kane for his time, knowledge of mechanics and musical interludes. Thank you to Dr. Doug Dennis for sharing his expertise in clinical orthopaedics and his support and patience. Also thank you to Drs. Brian Haas, Jan Victor, Shaw Akizuki, Hal Cates and all the surgeons and researchers I had the pleasure and opportunity to work with on various projects and publications.

To my fellow Center for Musculoskeletal Research lab mates, thank you for all your help and for your fellowship. I would like to especially thank Adrija Sharma, Sumesh Zingde, Filip Leszko and Matt Anderle for their generosity, ideas, discussions and overall help during my time at the lab.

I'd also like to thank Gary To, Diana Glaser and Mike Kuhn for their help over the years. Thank you to all of the undergraduates that worked on my projects and made me look good. Thank you to Rebecca Robertson. Mike Johnson, Chris Carr and Joe Mitchell thank you for the lunch breaks and thank you to everyone who has come through the lab and touched my life professionally and personally. CMR is a special place to be, take pride in all your work and keep the fridge clean!

I would like to thank my three brothers, my sisters, my nieces, my family and my friends and teammates for their support, encouragement and restful and laugh filled breaks from my work. Elizabeth Maurine, thank you.

Finally, I would like to thank my parents, Dale and Mary Ellen, for their countless sacrifices and limitless dedication to their family, inspiring me to work hard and challenge myself, their support in this and all my endeavors, and their love.

Abstract

This dissertation describes the development and results of a physiological rigid body forward solution mathematical model that can be used to predict normal knee and total knee arthroplasty (TKA) kinematics and kinetics. The simulated activities include active extension and weight-bearing deep knee bend. The model includes both the patellofemoral and tibiofemoral joints. Geometry of the normal or implanted knee is represented by multivariate polynomials and modeled by constraining the velocity of lateral and medial tibiofemoral and patellofemoral contact points in a direction normal to the geometry surface.

Center of mass, ligament and muscle attachment points and normal knee geometry were found using computer aided design (CAD) models built from computer tomography (CT) scans of a single subject. Quadriceps forces were the input for this model and were adjusted using a unique controller to control the rate of flexion, embedded with a controller which stabilizes the patellofemoral joint. The model was developed first using normal knee parameters. Once the normal knee model was validated, different total knee arthroplasty (TKA) designs were virtually implanted.

The model was validated using in vivo data obtained through fluoroscopic analysis. In vivo data of the extension and deep knee bend activities from five non-implanted knees were used to validate the normal model kinematics. In vivo kinematic and kinetic data from a telemetric TKA with a tibia component instrumented with strain gauges was used to validate the kinematic and

kinetic results of the model implanted with the TKA geometry. The tibiofemoral contact movement matched the trend seen in the in vivo data from the one patient available with this implant. The maximum axial tibiofemoral force calculated with the model was in 3.1% error with the maximum force seen in the in vivo data, and the trend of the contact forces matched well. Several other TKA designs were virtually implanted and analyzed to determine kinematics and bearing surface kinetics. The comparison between the model results and those previously assessed under in vivo conditions validates the effectiveness of the model and proves that it can be used to predict the in vivo kinematic and kinetic behavior of a TKA.

Table of Contents

List of Tables

Chapter 3: Materials and Methods

Appendix

List of Figures

Chapter 1: Background

Chapter 3: Materials and Methods

Bodies and Contact

Ligaments and Muscle Modeling

Initial Conditions, Parameters and Validation with Fluoroscopy

Broad Scope

Chapter 4: Validation

Normal Knee Extension

Normal Knee Deep Knee Bend

Teletibia TKA Deep Knee Bend

Chapter 5: Extension Model

Anterior/Posterior Tibiofemoral Positions

Quadriceps, Patella Ligament, Tibiofemoral and Patellofemoral Forces

Knee Ligament Forces

Chapter 6: Deep Knee Bend Model

Anterior/Posterior Tibiofemoral Positions

PID Controller

Quadriceps, Patella Ligament, Tibiofemoral and Patellofemoral Forces

Tibiofemoral Interaction Forces

Patellofemoral Kinematics

Patellofemoral Forces

Knee Ligament Forces

Ligament Slack Lengths

Chapter 7: Sensitivity Analyses

Appendix

Anatomical Definitions

Extension Model Progression

2D Patella Kinematics

Additional Deep Knee Bend Sensitivity Analyses

Nomenclature and Acronyms

BW = Body Weight
TKA = Total Knee Arthroplasty
UHMWPE = Ultra High Molecular Weight Polyethylene
NURBS = Non-uniform Rational B-splines
GUI = Graphical User Interface
PCR = Posterior Cruciate Retaining
CS = Cruciate Sacrificing
PS = Posterior Stabilizing
ACLR = Anterior Cruciate Ligament Retaining
AP = Anterior/Posterior
MIS = Minimally Invasive Surgery
GRF = Ground Reaction Force
EF = Elastic Foundation
RBSM = Rigid Body Spring Model
SES = Simple Elastic Solution
MH = Modified Hertzian
FEA = Finite Element Analysis
EMG = Electromyography
FE = Flexion/Extension
RP = Rotating Platform
PFJ = Patellofemoral Joint
TFJ = Tibiofemoral Joint
PFR = Posterior Femoral Rollback
PID = Proportional-Integral-Derivative
P = Proportional
DOF = Degree of Freedom
KKS = Kansas Knee Simulator
CT = Computed Tomography
IRB = Institutional Review Board
AR = Axial Rotation
MCL = Medial Collateral Ligament
ACL = Anterior Cruciate Ligament
PCL = Posterior Cruciate Ligament
LCL = Lateral Collateral Ligament
NKII = Natural Knee II
CPE = Congruent Polyethylene
UCPE = UltraCongruent Polyethylene
ML = Medial/Lateral
SI = Superior/Inferior
IE = Internal/External

> indicates vector
$\cdot$ dot product
$\dot{x}$ dot above indicates derivative of x with respect to time

Chapter 1: Background

The knee is a large diarthroidal or synovial joint serving as the attachment between two of the longest bones in the human body, the femur and the tibia. The joint is free to move, lubricated by synovial fluid, constrained by the joint geometry and soft tissue structures such as the meniscus and collateral and cruciate ligaments and contained in a joint capsule. The joint consists of three articulating surfaces. Between the tibia and femur, or the femorotibial joint, are articulating surfaces between the medial and lateral condyles. There is also a surface between the patella and femur called the patellofemoral joint.

The knee carries much of the load of the human body. During static standing, the two knees share the load from more than 80% of total body weight (BW). During daily activities like walking, running and playing sports the dynamic loads on the joints increase dramatically from the static loads experienced while standing. These increased loads can make the knee susceptible to osteoarthritis which breaks down the lubrication mechanism resulting in pain and stiffness at the knee joint. The breakdown of the cartilage between the femur and tibia and femur and patella can be extremely painful and debilitating resulting in the inability to perform daily tasks and loss of productivity. Osteoarthritis is ranked second only to heart disease as the leading cause of work disability.

Artificial joints are a last resort for the treatment of osteoarthritis. When the pain is too debilitating and all other treatments have been exhausted the articulating surfaces of the knee are replaced. The first artificial knee joints were designed 60 years ago. These were highly constrained hinge-like devices. Since then, increased knowledge of the mechanics of the knee has resulted in modern designs that allow for translational and rotational motion, intended to allow more natural movement.

In the modern knee replacement or total knee arthroplasty (TKA), the articulating surfaces of the knee are replaced by four components (Figure 1). A component manufactured with a biocompatible metal consisting of titanium or cobalt chromium alloy is used to resurface the distal end of the femur. The geometry of this component varies between manufacturer's designs and has evolved with increasing knowledge of the in vivo mechanics of TKA. Earlier components had a close to circular sagittal profile but lately the trend has been to more closely mimic the natural knee by reducing the radius of sagittal curvature of the articulating surface towards the posterior femur. Manufacturers also use different profiles for the medial and lateral condyles. All new designs have a rounded profile in the coronal plane on each condyle although the radius of curvature varies between designs.

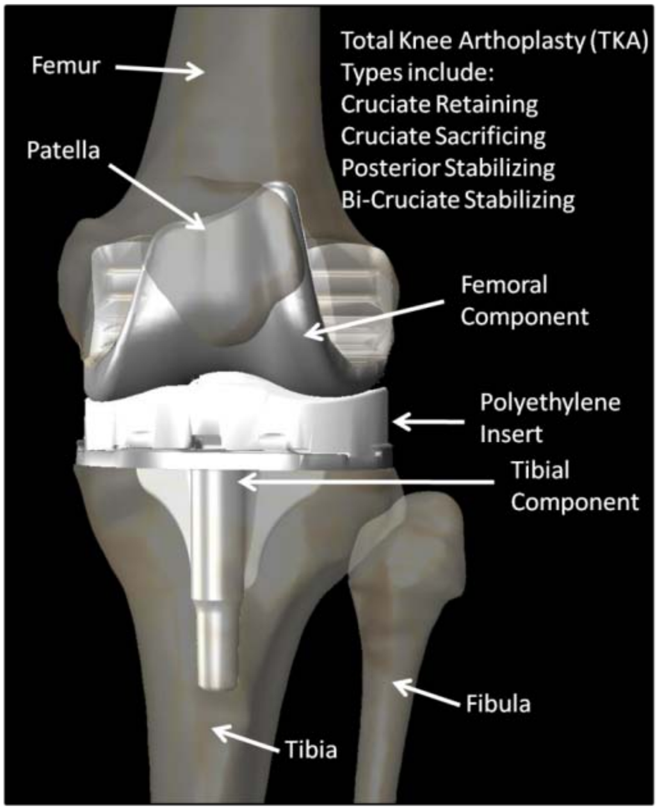

Figure 1: Diagram of a knee replacement or total knee arthroplasty (TKA).

The tibial component is typically a flat tray made of the same material as the femoral component and attaches to the boney architecture of the tibia in various ways depending on the manufacturer. This tray holds a piece of plastic, often referred to as a “tibial insert” or “polyethylene insert”, manufactured from wear resistant, cross-linked ultra-high molecular weight polyethylene (UHMWPE). The tibial insert acts as the bearing between the femur and tibia. The backside of the patella is resurfaced with a piece of plastic, sometimes referred to as a “patella button”. This button lies in a groove on the anterior surface of the femoral component and mimics the interaction between the normal patella and the trochlear groove on the non-implanted femur. This groove guides the motion of the patella which transfers force from the quadriceps to the tibia and acts as the extensor mechanism of the knee. The shape of the femur, the geometry of the insert and button, and the changes made to the soft tissue structures during the surgical procedure affect the mechanics (kinetics and kinematics) of the knee after replacement.

There exist several types of TKA devices and surgical procedures to implant them. Some implants use bone cement to secure the components to the naturally occurring boney architecture while others use a porous coating which is intended to promote bone growth into the component for fixation. Some use a hybrid approach which cements some components while, in the same knee, others are not cemented.

Different TKA also resect or retain the cruciate ligament structures. The cruciate ligaments, consisting of the anterior cruciate ligament (ACL) and the posterior cruciate ligament (PCL), provide stabilization to the knee. The ligaments have been extensively studied in vitro, but there are limitations to gathering in vivo data from the ligaments. Imaging studies have shown that the cruciate ligaments are taught and provide stabilization during certain stages of daily activity, but it is still unclear the extensive role each cruciate ligament plays and contributes to the overall motion patterns of the healthy knee. A question which still has not been answered definitively is, “How much does the geometry of the articulating surface and the soft tissue structures each affect knee motion?”

Goodfellow and O’Connor in their seminal 1978 article stated “The normal joint invites analogy with a well pitched tent which resists all forces tending to distort it by the development of tension in its guy ropes and compression in its pole." [Goodfellow and O'Connor, 1978] In 1978 it was unclear exactly what each soft tissue or bony structure contributed to the stability or motion of the knee and, although extensive in vitro and in vivo research has been performed in this area, it is still a question yet to be answered. The knee is such a complicated structure, and so unique from person to person, that all soft tissue and bony structures contribute to numerous aspects of behavior which is one of the reasons why the perfect solution to knee reconstruction has not been found.

Goodfellow and O'Connor also make the statement that "condylar replacement prosthesis may best confer stability upon the living joint if it is itself unstable." In this statement, it is assumed that they were referring to the bony and cartilage structures of the knees, which their sole job is to keep the bones apart, acting as the "tent pole", while soft tissue structures keep the bones together, acting as the "guy ropes". Based on this concept, Goodfellow and O'Connor stated that the replacement of the condyle should do nothing but resist movement of the femur into the tibia. This theory of design, plus attempting to solve problems such as wear and creep developed into the original Oxford Meniscal Unicondylar Knee [Goodfellow 1987], determined to be a successful design [Murray 1998]. This theory, however, assumes that all soft tissue is intact and works normally. Some patients receiving TKA do not have sound ligaments and the behavior of ligaments and muscles can change after the trauma they experience during a total knee replacement. Therefore, in the current marketplace there are several manufacturers of knee systems each with different products that function in different ways.

Most TKA are one of three types: (1) Posterior Cruciate Retaining (PCR) TKA, where the surgeon retains the PCL and resects the ACL, (2) Cruciate Sacrificing (CS) TKA, where the surgeon resects both cruciate ligaments, or (3) Posterior Stabilized (PS) TKA, where the surgeon resects both cruciate ligaments and the TKA design provides stabilization through mechanical constraints. PS TKA designs generally use a cam post system which has a post designed in the tibial insert that engages a cam on the posterior side of the femur, preventing the tibia from translating posteriorly (or femur translating anteriorly) with increasing knee flexion. Manufacturers also design implants with more conforming inserts which provide stabilization and more recently there is a bi-cruciate TKA, in which a dual cam system on the femur engages on both the posterior and anterior side of the post, guiding both anterior and posterior translation of the tibia. Although not used as frequently, ACL retaining (ACLR) TKA keep both cruciate ligaments, keeping many of the native soft tissue structures of the knee.

The attachment of the tibial insert to the tibial tray also has several variations. There are inserts which are locked or “fixed” to the tray and do not move. There are also rotating tibial inserts which rotate on the tibial tray and mobile bearing inserts which rotate and translate in the anterior/posterior (AP) direction similar to the “meniscal” design presented as the Oxford Knee.

Surgeons prefer different surgical approaches and techniques that offer advantages and disadvantages to both the surgeon and patient. Minimally Invasive Surgery (MIS) or a quadriceps sparing approach has become more popular in recent years and does not cut through the quadriceps, disrupts less soft tissue and leaves a much smaller scar allowing less blood loss and a quicker recovery for the patient. However, because the incision is much smaller than a traditional approach the surgeon cannot see as well and has less room to maneuver, increasing chances for error when implanting the devices. Different approaches alter the soft tissue structures in different ways.

Manufacturers design their TKA around the same basic principles, but execute these principles in their (slightly) unique way in order to develop a knee which out-performs competitor's TKA and to distinguish themselves in the medical device market. The question of which type of device (PCR, PCS, PS, ACLR, fixed bearing, mobile bearing, etc) and which procedure garners the best results continues to be a source of controversy in the arthroplasty field [Post 2009, Khanna 2009].

Chapter 2: Literature Review and Motivation

Arthroplasty is considered a useful and successful treatment for severe arthritis. However, failure due to polyethylene wear reduces the longevity of implants [Howling 2001, Currier 2005]. Efforts to improve the performance of polyethylene have, for the most part, been concentrated on the material properties and different manufacturing and packaging techniques. It has now been assumed that the wear, delamination and pitting of polyethylene has been reduced by developing highly cross-linked polyethylene and also using sterilization and packaging techniques which prevent oxidation of the material [Wroblewski 1999, Heimke 2002, Li 1994, Williams 1998]. Design also plays a role in lowering the stress and therefore wear in polyethylene. Goodfellow and O'Connor stated that high conformity leads to higher contact area and lower stress [Goodfellow 1978]. However, the more conformity the less the knee is allowed to move freely, and could lead to higher shear forces at the bone-component interface leading to loosening. Designers of TKA strive to find the optimal balance between conformity and simply providing the "tent pole" and keeping the bones apart, as discussed earlier.

Wear Studies

To date, wear studies are performed by analyzing retrieved inserts or using knee simulators. Analyzing insert retrievals is retrospective and can only provide data for implants that have been on the market for several years. Some researchers have been able to make conclusions relating patient activity and length of implantation to visible fatigue type wear [Rorhbach 2008, Lavernia 2001]. Other studies do not find data to support this relationship, but correlate types of wear present and the overall wear of the component [Crowninshield 2006]. Retrievals for the most part are either from revision surgeries or from autopsy retrievals. Samples from revision surgeries come from implants that have failed for any number of reasons. Typically nothing is known about the history of an implant retrieved during autopsy. The number of available retrievals is also limited and do not become available until years after the first of a newly designed device is implanted.

Wear simulators use standard force-motion profiles to test TKA designs in an in vitro environment over millions of cycles intended to simulate years of use [Walker 2000, DesJardins 2000]. Although essential in the testing of new TKA designs, studies of retrieved TKA bearings show more and different wear occurs in vivo than in vitro [Harman 2001]. Retrieval studies have shown that wear patterns are variable between patients and also TKA type and design [Wasielewski 1994, 1997, Currier 2005]. This variability is a function of different in vivo motion patterns between patients and between TKA which the in vitro testing standards do not reflect.

Cadaver Simulations

Cadaver simulators such as the Oxford Rig, the Purdue and Kansas knee simulators and others [Maletsky 2005, Kiguchi 1999, Patil 2005] attempt to recreate the in vivo kinematics and kinetics of the knee. However, concerns remain as to the effectiveness of using mechanical devices and cadaveric specimens to simulate in vivo conditions. A recent review comparing results from in vivo and in vitro studies concluded, although generally matching up well, the accuracy of knee kinematics after 30 degrees of knee flexion in cadaveric simulators may be questionable [Varadarajan 2009]. Although these simulators can provide accurate kinematics and retain the patellofemoral joint and other soft tissue structures, the rigs are not designed to repeat the millions of cycles required to simulate years of every day activity and can only test one implant at a time. Also, muscle forces are applied using non physiologic elements and are thus, input mechanically. Therefore, if the input to the simulator is incorrect and not simulating in vivo muscle conditions, the output could also be altered from truly in vivo mechanics. Even though most wear simulator designs can test several implants at once both options are expensive and time consuming.

Implant Design

When designing new TKA, a company generally uses an iterative process. A new idea or theory of design is implemented. An initial design and prototype is manufactured. Then engineers test the implant prototype in both cadaveric and wear simulators. After this first step the engineers and surgeons take what they learned from the original tests and adjust the design, coming to a second design iteration. The testing process is repeated and lessons learned applied to the next iteration…and so on. This is time consuming and expensive, taking months to complete the rigorous testing these companies require to ensure that the design they end with is a viable one worth the marketing, manufacturing and regulatory costs they incur to get the product on the market.

The expense and difficulties of using simulators and retrieval studies to evaluate design performance makes computational modeling of implant performance an attractive option, if the model is accurately evaluated using a viable error analysis. Modeling implant performance using a validated computer model is fast and it is cheap. Although wear is a complicated mechanism it is ideally a function of kinematics, contact kinetics and material properties. Previous inverse computational models have shown that the bearing forces increase in deeper weight bearing flexion [Komistek 2005, Sharma 2007]. As patients demand better performing TKA [Weiss 2002], and the marketplace becomes more competitive for implant companies, the need for computational tools that can investigate and predict the effects of design, patient parameters and surgical procedures on the kinematics and contact kinetics at the bearing surfaces becomes even greater.

Previous Models

There are an abundance of biomechanical mathematical models of the lower leg in the literature used in various fields. The sports medicine and physical therapy fields use models to investigate ligament reconstruction procedures and the rehabilitation exercises used to recover from injury. Investigators in the exercise science field study training activities to maximize effect and minimize risk of injury. Gait analysis is used in concert with mathematical models to study the surgical treatment of neurological disorders such as cerebral palsy and other gait and physiological abnormalities such as patella alta, varus or valgus deformities and conditions of the foot. Computational models are also used to estimate or predict mechanics after joint reconstruction to evaluate device design and surgical procedures.

These models can essentially be broken up into two main groups: inverse models and forward models. Inverse dynamic models use known motions as the input to the model to calculate force and moments acting across the joints. Forward models input forces into the model in order to predict the motions caused by said forces.

Inverse Knee Models and Contact Modeling

There are two ways to determine in vivo loads occurring at the bearing surface in joint replacements. The first is to determine the loads experimentally by instrumenting components with sensors and gathering the data through telemetry. This has been accomplished successfully in the hip [Lu 2001, Taylor 2001] and with varying success in the knee [D'Lima 2005, Heinlin 2009, D'Lima 2008, Burny 2000]. Before these implants, there was no way to determine loads occurring at joints in vivo, only cadaveric studies gave insight. The cost of designing, manufacturing and implementing these designs is high, and a limited number are implanted, always with the risk that the device will malfunction. However, the insight these devices have given into loads and moments occurring at artificial joints are extremely valuable to the validation of inverse dynamic models [Sharma 2007, Kim 2009].

Mathematical modeling is a much more accessible way to determine loads occurring in the human body. In a three dimensional model, each body, in this case a boney segment of the human body system, experiences a torque about each of the three axes and a force in each of the translational directions. Therefore, for each boney segment there are six independent, unknown forces and moments that can be derived. These forces and moments are the resultants of external forces, like gravity, ligament forces, muscle forces and interactive bearing surface forces. The human leg is a redundant system with the number of muscle forces being much greater than the number of equations of motion that can be derived for the human leg system.

To solve the redundant system of the leg, researchers have primarily taken two paths: optimization and reduction. Using optimization to solve for muscle forces in an inverse type solution has been in practice for nearly thirty years [Komistek 2005, Erdimer 2007]. Using ground reaction force data from a force plate and kinematic data from either video motion analysis or other means of data collection such as fluoroscopy, the resultant forces and torques about each joint can be determined using equations of motion. During static optimization the muscle forces are determined by minimizing an objective function (e.g. total muscle force or muscle force stresses) while satisfying constraints. The constraints make the muscle forces equal to the joint torques and also keep the muscle forces below a maximum allowable force for each muscle. Additional time/joint angle dependant constraints are also used to increase the accuracy of the results. Minimizing the total muscle force squared or muscle stress cubed are common examples of the objective function, however what to minimize, and also the involvement of co-contracting muscles are still sources of controversy and constitute some of the major assumptions in this type of modeling. Muscles obtained from the traditional algorithms tend to result in knee interaction forces that are higher than observed in vivo [Komistek 2005, Lin 2009]. Another disadvantage of finding the muscle forces using this approach is that the optimization scheme can be computationally expensive.

Recently, Lin et al. used a surrogate elastic foundation model in concert with an inverse model similar to that reported by Anderson and Pandy [Anderson 2001] and fluoroscopic data from a patient performing treadmill gait, motion analysis data and force plate ground reaction force (GRF) data from normal gait and in vivo force data from a telemetric TKA [Lin 2009]. Using CT scans of the femur and tibia/fibula from a patient similar in stature to that of the patient analyzed and a CAD model of TKA obtained from CT scans of the patient were virtually implanted in a similar surgical orientation as seen in the patient. This TKA/normal model combination was then fit to the center of rotation of the knee determined from fluoroscopy. Using an inverse total body model which represented the knee as a hinge, the investigators calculated the joint torques while the surrogate elastic foundation model, which is used to improve computational time over the traditional elastic foundation model, was also able to calculate interaction forces occurring in the telemetric TKA. Static optimization was then used to find the muscle forces at each time step. The objective function was to minimize the activation of each muscle while constrained by the joint torques from the inverse model and also the interaction forces at the knee determined by the instrumented TKA. Previous inverse models using optimization to determine muscle forces do not take into account the interaction forces. This model, by adding in vivo interaction forces to the objective function, narrowed the design space further constraining the possible results of the optimization, resulting, most likely in a solution closer to that which actually occurs in vivo [Lin 2009].

The second method of determining muscle forces in the leg during inverse dynamics simulations is the reduction technique which reduces the number of unknowns so that the system becomes determinant. Several models in the literature have used this method [Komistek 1998, 2005, Sharma 2007, 2008, Lu 1997, Morrison 1970]. Two common assumptions in the reduction technique are that certain muscles do not greatly influence the system and, therefore, are not included and certain muscles groups such as the quadriceps, which is a set of 4 muscles, are grouped and represented by one unknown force. The advantage of this technique for inverse solutions is it reduces unknown forces so that the mathematical model is a system of linear equations that can be solved quickly to find one solution.

To determine the tibiofemoral contact mechanics of a TKA using an inverse mathematical model, investigators have for the most part used two methods. The first method is to assume a rigid femur and a deformable tibial insert modeled using an elastic foundation (EF) [Blankevoort 1991, Li 1997, Pandy 1997, Nuno 2001]. This method is also referred to as a rigid-body-spring-model (RBSM). The EF is a bed of springs with properties intended to represent the material properties of UHMWPE. The contact pressure is determined by calculating the area of the springs which are deformed. A concern for this type of modeling is that these springs are one dimensional and the action of a particular spring in the model does not affect the neighboring springs. This does not reflect the true behavior of most materials, which when deformed in one direction also deform in the orthogonal directions, represented by Poisson's ratio. This can result in higher predictions of contact pressure as the calculation is essentially the interference between the femur and tibial insert [Sharma 2008].

The second method combines rigid body dynamics and then finite element analysis to determine contact stresses. Rigid body dynamics, the type of analysis used in Kane's dynamics, assumes a body does penetrate another body in contact. Therefore the contact between the femur and tibia or patella and femur is assumed to be point contact. In inverse dynamics, the position of the femur relative to the tibia, along with other inputs such as ground reaction force and ligament and muscle insertion, determine the muscle and ligament forces around the knee and, therefore, determine the interactive forces acting between the femur and tibia. These kinematics are obtained from some type of experimental or observational technique. The error of these systems is well above the amount of deformation which occurs in polyethylene during daily activity [Mahfouz 2003, Sharma 2008]. Therefore, the affect of not including the penetration of the femur into the insert on the lower extremity kinematics does not affect the overall accuracy of the dynamic model nearly as much as the inherent error in the experimental observation, which cannot be avoided. Assuming rigid contact, a model can determine the interaction forces occurring at the contact points. The position of the body and interactive forces occurring at the contact point can then be used as the input to a static finite element model, which calculates the stresses occurring at the tibial insert at specific increments from the simulation.

For years Finite Element Analysis (FEA) has been the gold standard for determining stresses at the tibiofemoral and patellofemoral interface [Andriacchi 1983, Lewis 1998]. The preprocessing time and subsequent CPU time required to carry out an FEA analysis is a limitation to this type of investigation despite the increase in accuracy over elastic foundation models.

Two other types of articulating modeling are simple-elastic-solution (SES) [Bartel 1985] and modified Hertzian (MH) theory used by Pandy et al. [Pandy 1998] and others [Eberhardt 1990]. Li et al. compared EF or RBSM, FEA, MH and SES and determined that for static deformation both FEA and EF methods better calculated stress-strain distributions and that the EF methods was the easiest to use, most computational efficient and determined contact pressures the best out of all of the methods [Li 1997]. In a more recent comparison of EF and FEA methods in a forward solution model of a force controlled wear simulator performing a gait cycle, Halloran et al. found that EF methods matched well with the FEA methods when measuring the stress/strain and contact pressures and the EF was 98% faster than the explicit FEA method used (6-7 hours vs. 10 minutes) [Halloran 2005]. Another paper compared MH, FEA, EF and modification to the EF technique meant to improve accuracy by only counting springs in the deformation area if they are deformed above a certain value, thus reducing the contact area. The authors tested the techniques on generic geometry meant to represent TKA and found that MH lacked accuracy, FEA was accurate but time consuming and that EF and the authors modified version of EF was much quicker and the authors modified technique was close to the accuracy of FEA in a fraction of the time [Perez-Gonzalez 2008].

Even more recently Lin et al. and others presented papers proposing and implementing the use of surrogate EF models to determine contact mechanics in diarthroidal joints. Surrogate models can be used to replace either FEA or EF models. They do not improve on the accuracy of these models but on the computational speed. Lin reported that this method decreases the calculation of contact pressures for an entire gait cycle from 10 minutes for an EF model to seconds for the elastic foundation, further decreasing the computational cost associated with this type of simulation without losing any significant amount of accuracy from traditional EF calculations [Lin 2009, Halloran 2009].

Sharma et al. developed a method which vastly decreases the computational time required for an FEA analysis while avoiding the inaccuracies associated with elastic foundations [Sharma 2009, Sharma 2008]. A validated rigid body model of a TKA, using in vivo kinematics obtained from fluoroscopy, ground reaction force-plate data and anthropometric inputs for segment inertial parameters and ligament and muscle attachments was used to determine tibiofemoral interaction forces of both the medial and lateral contact points. A spring network model was then developed which models the tibial insert geometry and material properties of UHMWPE. The tibial insert geometry was discretized into nodes. These nodes were interconnected by springs which simulate the material properties of polyethylene. Since the nodes were interconnected, the behavior of one node affected the neighboring node, representing Poisson's ratio. Tests of this method show that results comparable to FEA analysis can be obtained in seconds of CPU time as opposed to the hours required for FEA. The combination of the highly accurate in vivo kinematics from fluoroscopy, the results of a validated rigid body model and the technique of using a spring network to represent deformable contact on the tibial insert is a system which relatively quickly calculates accurate contact mechanics of an existing TKA.

Inverse knee models generally solve for the muscle and interaction forces using the three torques and three forces associated with each body of the model. Ligament forces are determined by defining position vectors within the system, which are known because the in vivo kinematics are known. Ligament forces, if included, are applied using linear or nonlinear spring models and are a function of the ligament element length or strain [Abdel-Rahman and Hefzy 1998, Blankevoort 1991, Crowninshield 1976, Shin 2007]. Anatomical studies have found that the major ligaments within the knee are made of bundles [Peterson 2006, Amis 2006, LePrade 2007] except for the LCL [Meister 2001]. This has been applied to the modeling of the knee, where each bundle is represented by one or more spring elements [Blankevoort 1991]. Mommersteeg found the optimal number of elements to represent each ligament is 4 to 7, with fewer than 4 being sensitive to insertion point measurement errors and more than 7 being redundant [Mommersteeg 1996].

Each of these bundles act differently throughout knee flexion, however, a consensus on exactly how each ligament bundle behaves has not been reached [Fuss 1989]. The lack of consensus on exactly when ligaments engage during flexion is probably due to two main factors:

1) Obtaining in vivo data on ligaments during dynamic maneuvers is difficult without invasive procedures

2) ligaments are patient specific in that the relaxed length, width, stiffness and attachment areas vary (although slightly) from subject to subject probably causing specific bundles to act slightly different from patient to patient.

There is a whole field of research focused on modeling ligaments using FEA. More recently they have been integrated into musculoskeletal models [Weiss 2001, Peña 2006, 2007]. Whether using one-dimensional spring models or the more complicated three-dimensional FEA models, the accuracy depends on what the investigator chooses as the relaxed length which dictates exactly when and how much force the ligament model applies to the system.

Predictive Forward Models

The previously mentioned inverse dynamics models are used as observational tools which can help determine the performance of devices which already exist and have been in use for years. Although any data regarding the in vivo behavior of these devices is useful, even the lessons learned are not validated until changes in a device are implemented and years later evaluated again. This probably accounts for some of the reason why most of the TKA in use today are a variation on one design and, although some advances have been made, the design of TKA really hasn't changed much in the past 20 years. Is this lack of development because the current designs are as good as they are going to get? Or because companies lack the tools to quickly and accurately predict the effects of a design change and therefore do not want to take on the risk of implementing a change and waiting years to determine the changes effect on performance?

Smith and Nephew, Inc. (Memphis, TN) claims their Journey® Bi-Cruciate TKA to be a leap forward in design, branching off from the traditional design based on the original Insall TKA. The company claims that the development of this TKA started from scratch and the majority of the design iterations were tested using a forward solution dynamic model developed by LifeMod/KneeSIM (Sacramento, CA). The use of a forward solution model can be powerful, in that it can predict the kinematics and kinetics of a newly designed device. Like all models, they should be evaluated using a rigorous error analysis, or the results could be attributed to GIGO (garbage in, garbage out).

All of the contact mechanic calculation methods previously discussed at length in the inverse model section, rigid body, EF, FEA, surrogate EF and FEA and spring networks can be applied in a predictive forward solution model.

The most common forward solution knee models presented in the literature are quasi-static with either rigid [Wismans 1980, Abdel-Rahman and Hefzy 1998, Dhaher and Kahn 2002] or deformable contact surfaces [Blankevoort 1991, Pandy 1997, 1998, Kwak 2000, Cohen 2001, 2003, Chao 2003, Elias 2004]. Quasi-static forward solution models with deformable contact are split into two main categories: FEA and EF. These models are placed in an initial orientation (e.g. 30 degrees of flexion) and the model is perturbed. Inertial properties and any viscoelastic characteristics of the soft tissue are not included in these models. Generally quasi-static forward solution models are used to investigate the laxity of a joint and/or the contribution of ligaments in constraining the knee during various tests. An example of a simulation performed with one of these models is of the AP drawer test doctors and trainers perform to test the laxity of the ACL [Bertozzi 2007, Pandy 1998] or to simulate passive flexion [Pandy 1997].

Another way these quasi-static models are used are as post-processing tools to inverse dynamics problems or gross body forward dynamic simulations which use idealized representations of the knee (hinge). The muscle forces for these simulations are generally found using optimization in concert with or validated by electromyography (EMG) data. Optimization schemes also try to minimize the difference between calculated and observed kinematics but generally minimize the activation or energy consumption of the muscles through use of a Hill Type muscle model [Shelbourne 2005, Anderson 2001]. The contact forces, muscle forces, joint torques and joint angle is then put into a joint specific model which includes ligaments and knee geometry and a static problem at specific instances of time throughout the simulation is solved determining the more specific tibiofemoral or patellofemoral orientations and forces or stresses [Fernandez 2008, Shelbourne 2005, Anderson 2001].

The details of quasi-static models in the literature vary with different amounts of physiological architecture, like ligaments and muscles, included. The initial conditions and the way in which investigators set these conditions in the models also vary along with the methods used to mathematically represent the articulating geometry. The articulating geometry have been represented in different ways including spheres and planes , representing the femur and tibia, respectively, polynomial surfaces, surface patches, non-uniform rational B-splines (NURBS) and basis functions.

In the introduction to a 2004 article, Curuntu and Hefzy summarized the current-state-of-the-art of dynamic knee models with the following statement: *"A single 3-D anatomical dynamic model that includes both tibio-femoral and patellofemoral joints does not yet exist''* [Curuntu and Hefzy 2004]. Bei and Fregley disagree and state that Piazza and Delp [Piazza and Delp 2001] have the only dynamic model [Bei and Fregley 2004]. A few models have been presented since this disagreement in 2004.

The early forward dynamic models were 2-D and used rigid contact and non-linear spring models to guide motion [Moeinzadeh 1983, Tumer 1993, Abdel-Rahman and Hefzy 1993]. In order to truly represent the complexities of the knee these models had to be expanded to three-dimensions [Curuntu and Hefzy 2004]. Most of these models use contact modeling as an integrated part of the overall musculoskeletal model. They are the means by which geometry is represented as a constraining force and contact pressures or stresses and therefore interaction forces between bodies are determined. Therefore the contact method will be discussed along with the multi-body simulations presented in the literature. Existing three-dimensional dynamic models geared toward the orthopedic industry and TKA lie within one of three scopes: 1) simulate a TKA in a wear simulator, 2) simulate a normal knee or TKA in cadaveric simulator or 3) the physiological implanted or non-implanted lower leg throughout an activity.

Wear Simulator Models

Simulations of TKA wear simulators started like most others, simply. Godest et al. modeled Stanmore knee simulator with motions and forces in the sagittal plane using the I-DEAS™

Package and MSC.ADAMS (MSC Software, Inc, Santa Ana, CA) integrated kinematic solver [Godest 2000]. The bodies were modeled in 3-D as rigid and the femur was placed in a fixed rotation with an applied axial load. An AP drawer test was then performed to determine the force needed to displace the tibia in the AP direction. These models of wear or testing apparatus have expanded from quasi-static 2-D models [Godest 2000, Sathasivam and Walker 1997] to quasi-static 3-D models [Rawlinson 2006, Godest 2002] and probabilistic [Laz 2006]. Quasi-static models take the input functions of the gait simulation used in these tests, which include flexion of the femur, AP translation of the femur, an axial force and the IE rotation of the tibia and discretized them at several instances in time. With the constraints in place that exist in the simulator, including springs in the AP direction off the tibial insert, these models apply input from the simulator into the system, allowing the other degrees of freedom to settle into equilibrium. Where the tibia and femur eventually rest in equilibrium determine what these models refer to as the resulting kinematics. These tests are repeated with the inputs from each discretized point of the investigators choosing. Validation of these systems consist of comparing the results at these discrete points to the corresponding points in time during a dynamic physical wear test in the machine with the same TKA design.

Recently models have begun to take into account the inertial properties of these systems and perform dynamic 3-D simulations [Fregly 2003, Halloran 2005, Moran 2008, Taylor 2003, Landon 2009, Giddings 2001, Lin 2009] which simulate a wear test continuously over time as opposed to discretely and quasi-statically at certain instances of time. The models are set up with the same constraints and degrees of freedom as the simulators and use the same time varying inputs as the simulators for the displacements and axial force. The method to calculate contact mechanics in the dynamic models vary from EF [Fregly 2003, Landon 2009] to modifications of the EF method [Lin 2009] and implicit [Giddings 2001] and explicit [Halloran 2005, Taylor 2003] FEA methods. The trend in dynamic modeling of the normal or implanted knee is to calculate the dynamics of the system and the pressure and stresses occurring at the contact interface concurrently. Note: depending on the frequency and speed of the simulation, and the extent to which viscoelastic properties play a part, some in the research field still consider simulations which are continuous and use continuous time-varying input functions quasi-static.

Wear simulators are the industry standard for testing the performance of a TKA. Computationally modeling these systems would prove beneficial to a company as opposed to manufacturing an implant prototype and taking up weeks of wear testing time and the associated costs. These models are also useful for "let's see what happens when…" tests because the inputs and boundary conditions for the tests can be changed however the investigator wants without the risk of damaging the machine or wasting time. For example, the alignment of the femoral component or the ML placement of the femoral component can be adjusted for investigation [Laz 2006, Taylor 2003]. These models could also be useful in helping determine new kinematic and force profile standards for wear testing. However, as mentioned before, the current standard kinematic and kinetic profiles used as the inputs to these tests are generic gait patterns and also ideal conditions [Walker 2000, DesJardins 2000] and results from wear testing do not necessarily match up with wear from implant retrievals [Wasielewski 1994, 1997, Currier 2005]. A computational model of a wear simulator, although valuable to industry, is simulating a test which does not necessarily provide an accurate prediction of an implant's performance in vivo.

Cadaveric Knee Simulator Models

Cadaveric knee simulators like the Purdue Knee Simulator, Kansas Knee Simulator (KKS) and the Oxford Knee Rig are used to investigate both the normal knee and the implanted knee [Maletsky 2005, Kiguchi 1999, Patil 2005]. Computational models were developed for these simulators initially to assist in their design and then also as a means of analytically performing the simulations. One of the advantages of modeling a cadaveric simulator is that the boundary conditions of the system are consistent between tests. The KKS has been computationally modeled in several studies [Guess 2005, Maletsky 2005, Baldwin 2009] as has the Oxford [Lanovaz and Ellis 2009, Elias 2004] and Purdue Simulators [Halloran 2005]. The KneeSIM™ software which is an industry standard in orthopaedics for computational simulations also replicates a knee simulator.

Guess and Maletsky used MSC.ADAMS to place a TKA in an already existing model of the KKS [Maletsky 2005] and represented the femoral and tibial articulations with ellipsoids, the patella as a partial sphere and the trochlear groove as toroids [Guess 2005]. Deformable contact was modeled with a RBSM type contact model. The contact forces were calculated from the integral of the spring forces over the contact area. The contact area was found using Hertzian contact theory using material properties and the articulating geometry. The TKA was a PS type TKA, however the cam and post mechanism were not included in this model. Ligaments were also excluded, however the simulator they were attempting to model did not have a cadaver lower leg only bars to hold the TKA in place and metal patella to transfer forces to across the knee. Torques in both the internal and external directions were applied to both the model and physical simulators. With an IE rotational test the simulation was in 104% error with the actual machine with a friction coefficient of 0.05. Raising this to 0.08 reduced the error to 54%. The goal of this model was to determine the forces needed to input to the physical simulator to achieve a desired flexion.

A more recent model of the KKS used Abaqus/Explicit™ (SIMULIA Inc., Providence, RI) to simulate a deep knee bend and investigate the patellofemoral kinematics. Two cadaver lower legs were put through a deep knee bend simulation in the KKS before implantation and then after implantation with a TKA and these cadavers were then input to the computational model. The tibiofemoral kinematics and quadriceps forces determined during the simulator tests were the inputs for this model. Model elements included the patella surface and trochlear surface interaction, the quadriceps tendon and patella ligament, and both the medial and lateral patellofemoral tendons. Simulations of the exercise took between 1.0 and 6.0 hours. Tibiofemoral kinematics from the KKS varied between specimens and also after the specimen was implanted with a TKA. As others have determined [Halloran 2005] the difference between the resulting kinematics when using RBSM and deformable contact was negligible and the speed of the RBSM contact simulations was two to four times faster than using deformable FEA contact. The forces or stresses at the patellofemoral contacts were not in the scope of this study, however, so no comparison was made regarding the forces. Ligament prestrains were manually adjusted to achieve the position of the patella before the simulation.

Haloran et al. presented a model of the tibiofemoral joint, modeled as if in a Stanmore wear simulator, similar to those describe above, and the patellofemoral joint was modeled as if in the Purdue cadaveric simulator [Haloran 2005]. The contact forces were determined as a function of the penetration distance of the master into the slave surface. The tibiofemoral analysis was modeled as a Stanmore wear simulator while the patellofemoral analysis was modeled as a Purdue knee simulator with tibiofemoral kinematics used as an input to the model. Using rigid body techniques with softened contact predicted nearly identical AP and IE kinematics as the fully deformable model. CPU time was far less in the rigid body model compared to the deformable body analysis going from several hours to several minutes. This study compared the pressure results from both the rigid and deformable contact analysis and determined that the difference between the two was worth the large decrease in computation time. The tibiofemoral joint and patellofemoral joint were analyzed during two separate simulations using unique boundary conditions for each. The patellofemoral joint and tibiofemoral joint act in concert. Ideally a dynamic model should include both.

A recent model of a TKA implanted cadaver in the Oxford Knee Simulator includes both the tibiofemoral joint and patellofemoral joint but also includes ligaments [Lanovaz 2009]. The goal of this study was to develop a dynamic model of the implanted knee which includes the patellofemoral and tibiofemoral joint, does not prescribe any kinematics and determines joint contact stresses. The simulation was that of an Oxford knee rig performing a closed-chain extension. The computer simulation was done in LS-DYNA (Livermore Software Technology Corp., Livermore, CA). Two separate cadaver lower legs were implanted with a CR TKA. The bone models were obtained with CT scans and TKA components were virtually implanted using their CAD models. Six ligament bundles, including the two for the PCL and the posteromedial capsule were included in the model. Parametric tests were also performed [Lanovaz 2009].

At the beginning of the simulation, the bodies were placed in their initial poses and the tension in the quadriceps actuator, the same force used in corresponding cadaver simulations, was applied [Lanovaz 2009]. The bodies were allowed to settle into equilibrium for a specific amount of time and then the simulation was run using the actuator forces from the cadaveric simulation. Although the position and force of the medial and lateral condyles were not reported separately for the tibiofemoral joint, both joint translations and rotations of the FEA simulation matched well with the kinematics from the in vitro tests. The forces and moments also matched well with the forces from the cadaver simulations.

The parametric tests, although performed with generic bony geometry, determined that the kinematics of the tibiofemoral joint was most affected by the MCL initial strain, tibial insertion of the patella ligament in the ML direction, femoral MCL insertion, patellar thickness and femoral PCL insertion. The initial strain of a ligament determines how tight it is during the activity. Ligament modeling will be discussed in detail later. The patellofemoral joint kinematics were most affected by the patellofemoral coefficient of friction, tibial patella ligament insertion, femoral MCL insertion, MCL initial strain and patellar thickness. The tibiofemoral forces on the medial and lateral side were most affected by the collateral ligament initial strains and insertion points and the tibial patella ligament insertion points [Lanovaz 2009].

Physiological Dynamic Models

The last group of dynamic models are those that attempt to model the physiological knee performing an activity. These models can range from single joint models which take all degrees of freedom to full body models which use optimization to determine the muscle forces but use idealized joints (like a hinge for the knee). Some models combine both elements.

Curuntu and Hefzy developed a model which simulated the knee extension exercise. Ligaments were represented as they typically are in the literature using a non-linear spring model which uses a relaxed length calculated from the length of the ligament in full extension [Abdel-Rahman and Hefzy 1998, Blankevoort 1991, Crowninshield 1976, Shin 2007]. If the strain of the ligament based on this relaxed length is below 0.0, no force is applied, if it is greater than 0.0 but under the linear strain threshold, the force is modeled with a quadratic function of the current length minus the relaxed length. Above the linear strain threshold the force function is linear with respect to the change in length. As mentioned above, one of the issues with these models is determining the relaxed length especially when models become patient specific [Curuntu and Hefzy 2004].

Two planes for both tibial condyles and the articulating geometry of the femur and patella expressed using Coons parametric bicubic surface patches were used to describe the geometry of the knee in Curuntu and Hefzy's model [Curuntu and Hefzy 2004]. A cadaver was discretized and the "corners" found on the cadaveric articulating surfaces were then connected by patches.

A local coordinate system for each surface allows any 3-D Cartesian position to be found on the surface using 2 coordinates from the local system. Using rules that do not allow penetration of one surface into another and also rules that ensure the normals occurring on the tibia and femur at both tibiofemoral interactions and again for two contact points at the patellofemoral joint are collinear, the rigid contact mechanics of the system are represented [Curuntu and Hefzy 2004, Hefzy and Yang 1993].

Piazza and Delp created a truly dynamic forward model of the reconstructed total knee using rigid body dynamics which simulated the step-up task in vivo [Piazza and Delp 2001]. The initial position and velocity were input to the model along with muscle activation from EMG and the rotations of the hip and ankle. Unlike other previously mentioned full body models [Fernandez 2008, Shelbourne 2005, Anderson 2001], the tibiofemoral and patellofemoral joints were both 6 degrees of freedom giving the model a total of 12 degrees of freedom and the geometry was described using three-dimensional polyhedral meshes. A collision detection algorithm was used to determine the number of contact points in the knee. Muscle inputs were derived from muscle activations from EMG which were input to a Hill-type muscle model along with passive and active force-length curves. The contact forces on the medial and lateral side were determined using an algorithm that allowed for separation of either condyle but did not allow for inter-body penetration. This allows for liftoff to occur, however as the author states, this method may also account for the inaccuracies in the contact force results as there are more than one solution for the interaction forces if there are several contact points. The flexion and internal rotation results were acceptable when compared to a TKA analyzed during a step-up activity using fluoroscopy, however the anterior/posterior translations were high for the simulation when compared to experimental results. The author contributes this to the possibility that the diminished axial compression force and the lack of friction force may limit the constraint of the model. Overall this is one of the only models that attempts a forward dynamic simulation and compares it to in vivo data from fluoroscopy. Collision detection and the method employed to derive contact forces has an advantage over some rigid body models in that different models do not need to be created for different contact conditions (model allows for condylar lift-off with one contact or normal articulation with two contacts). However, using meshes in general in forward solution modeling can lead to discontinuities which can affect the ability of the solver to continue [Piazza and Delp 2001].

Bei and Fregly introduced a system of representing geometry using trimmed NURBS. The contact pressures were calculated with RBSM. Since the algorithm is used in conjunction with multi-body dynamics software, the contact forces are needed so the pressure is multiplied by the area of the deformed springs. This article is geared towards describing the contact algorithm they used, however it is also cited as one of the few dynamic simulations in the literature [Bertozzi 2006]. This model is not purely forward, however, as the dynamic model of gait presented prescribes the flexion extension (FE) angle, internal-external (IE) rotation and AP translation of the femoral component obtained from fluoroscopic analysis while the medio-lateral (ML) and superior inferior (SI) translations and varus-valgus (VV) rotation were calculated with forward dynamics. An axial load was placed on the femoral component which was loaded off center 70% and 30%, medially and laterally, respectively [Bei and Fregley 2004].

No patellofemoral joint, ligaments or other soft tissue structures are included in the musculoskeletal model.

More recently explicit finite element models, like those mentioned above which model cadaveric simulators, have been used to determine kinematics while modeling the musculoskeletal, soft tissue and articulating geometry while also calculating the contact stresses [Barink 2005, 2008]. Barink et al. constructed a finite element simulation of a deep knee bend starting at 70 degrees of flexion comparing high flexion with standard PS Rotating Platform (RP) TKA (Sigma RP and Sigma RP-F) with the patellofemoral joint included [Barink 2008]. The femur was fixed and GRF applied to the tibia which is allowed to move in all 6 directions relative to the femur along with the patella relative to the femur. The tibia was constrained at the ankle with a torsional spring to simulate friction between the foot and the ground. Force was applied to the patella representing the quadriceps force by resisting movement using actuators. No ligaments besides the patellar ligament were included but damping was included in the model to prevent oscillation and numerical problems [Barink 2008]. An earlier model by this author [Barink 2005] took 24 hours to complete an extension maneuver. The publication of this latest model did not indicate the computational time.

Kessler et al presented a study in which a cadaveric and computational simulation of an open-kinetic-chain knee extension was performed. The computational model was developed using MSC.ADAMS and rigid body models. The bony ligament attachments from the cadaver were scaled to a medium sized male model and a Scorpio CR fixed bearing TKA and a Scorpio CR RP design were virtually implanted in the computational model. Quadriceps angle off of the patella was placed at 5.0 degrees valgus and contact was calculated between the femur and the tibia, the patella and the trochlear groove and the quadriceps tendon and the trochlear groove. Actuators attached to the proximal quadriceps tendon translated proximally along the femur creating a moment about the tibiofemoral joint. Kinematics of the tibiofemoral joint, patellofemoral joint and contact forces at each were calculated during the dynamic simulation. The simulation was validated using cadavers implanted with instrumented TKA. The kinematics and kinetic data from the simulation fell within the range of the cadaveric data and followed the trends well except for patellar lateral shift after 60 degrees. After validation determined that the model was getting satisfactory results, simulations were performed where the femoral component was malrotated +/- 3 degrees from the epicondylar axis for different simulation using a fixed bearing and rotating bearing TKA.

KneeSIM which uses MSC.ADAMS as its computational engine is the orthopaedic industry standard for dynamic forward simulation of TKA. Morra et al. have several publications which use this software to simulate activities [Morra 2008, Morra 2006] along with Innocenti et al. [Innocenti 2008]. The results these researchers achieve along with others that use ADAMS are validated with experimental data to varying degrees. Criticism of ADAMS however has been stated about the way the software calculates “rigid contact” [Sharf 2006]. Many of the models reviewed in this introduction use a bed of springs on a rigid body to determine the contact pressures. If the contact force is desired, it is determine from these pressures and the contact area. ADAMS uses a penalty method. The most rudimentary application of the penalty method uses a simple linear relationship

$$F = kx^n$$

where *F* is the force applied at the calculated contact point, usually the center of an ellipse determine using Hertzian contact theory, *x* is the penetration of the point into the other body and *k* and *n* are the stiffness coefficient and the power exponent, respectively [Sharf 2006]. This is called a compliant model, the larger the coefficient *k* and the power *n*, the more rigid the contact becomes. MSC.ADAMS uses a slightly more complicated formulation of the compliant contact model

$$F = kx^n + b(x)\dot{x}$$

where *b* is a cubic function of the penetration and acts as a damping factor [Sharf 2006]. This damping factor allows for energy dissipation during collision, which could be useful if modeling condylar lift-off. This software continues to evolve the way it deals with contact, however it still may be difficult to determine the values that should be used for the coefficients (*b* and k) and the exponent *n* [Sharf 2006], especially in a complicated contact scenario like that seen in the knee. The second is when normal non-colliding contact is the case, as it is for the majority of the time in the tibiofemoral joint and the patellofemoral joint during weight-bearing activities, there is a dissipation of energy, which does not hold true to the true nature of rigid body contact [Sharf 2006]. These concerns are fairly minor when you look at the power and functionality of the KneeSIM software, however it may indicate why contact forces are rarely reported in studies that use this model. The main issue to consider in the KneeSIM model is that it evaluates TKA in a model of a knee simulator. The model is not truly physiological with separate quadriceps muscles, hamstring muscles and a trunk which can rotate at the hip, changing the location of the trunk COM relative to the knee and foot and location of the ankle joint. The goal of the computational TKA analysis described in this dissertation is to determine the TKA performance in vivo.

When dealing with a simulation as complicated as the knee in three dimensions, all the elements going into the model need to be well understood and have some basis in the physical world. It can be hard to predict exactly what effect adding even something minor into the model will have. Just like Goodfellow and O'Connor's analogy of the knee as a tent, every element included in the model has a role in dictating the results it puts forth.

Chapter 3: Materials and Methods

The development of the forward solution computational model of the knee described in this dissertation report was a progression from an initial simplistic model representing a non-weight bearing exercise with idealized structures and joints to a more advanced model that was more complicated in nature, having a greater number of physiological parameters. A stepwise approach was utilized, allowing for verification of the model and assurance that each element of the model was implemented correctly. The end result of this research project was two very different models. The first is a rigid body model representing a non-weight bearing active leg extension and the second, a model of a weight bearing deep knee bend.

Both rigid body models were developed using AUTOLEV® (Online Dynamics, Inc., Palo Alto, CA, USA), a symbolic manipulator specifically designed to determine the equations of motion of multi-body systems using Kane's Dynamics (Kane, 1985). Kane's Dynamics is a vector based method. These vectors are expressed in coordinate systems or reference frames which are attached to bodies with mass and inertial properties or to massless frames. The position vectors, forces and constraints applied to the model are all based on vectors with a direction and magnitude expressed in these reference frames. The equations of motion and code to execute the simulation are output in C. This code can be modified to add any elements to the model which cannot be expressed within the AUTOLEV® software. Once an executable file is compiled, the parameters of the model can be changed without recompiling, allowing the user to change geometric constraints, subject's body mass, implant orientation, ligament stiffness and any number of other parameters. This approach is valuable for conducting a sensitivity analysis, verifying which parameters each model is sensitive to during each of the activities.

Bodies and Contact

Non-Weight Bearing Extension

The non-weight bearing model simulates an active extension exercise with the lower leg hanging at 90° and extending through activation of the quadriceps to full extension (0° or parallel to the ground). The model consists of 4 bodies with mass and inertial properties (Figure 2 and Table 1). Each of these bodies has a coordinate system comprised of orthogonal unit vectors. The 1> directional unit vector for each of the respective coordinate systems (for example FEMUR1>) points in the anterior direction, 2> points in the superior direction and 3> points in the lateral direction (Figure 1). The pelvis and femur are represented by respective bodies PELVIS and FEMUR, each fixed to the lab global coordinate system (N).

The patellofemoral joint (PFJ) is represented by the interaction at the patella interface represented by bodies PAT and FEMUR. The tibiofemoral joint (TFJ) is represented by the interaction between the tibia, represented by bodies TIBIA and FEMUR. TIBIA has 3 degrees of freedom constrained by the motion of two contact points which are kept from penetrating the femur using two auxiliary generalized speeds and an additional constraint in the mediolateral translation. PAT has three degrees of freedom constrained by the movement of two contact points and also a constraint which prescribes patella flexion as a function of knee flexion. The forces required to constrain the movement of the contact points represent the interaction forces for the medial and lateral condyles of the TFJ and for the two contact points representing the PFJ.

Physiological origins for the hamstrings and quadriceps muscles are used to apply a force to the model which drives the extension of the tibia. The quadriceps force vectors represent the physiological muscles which make up the quadriceps, the vastus medialus, vastus intermedius, vastus lateralus and rectus femoris. Each of these muscles is represented by four equally distributed force vectors which are modeled at the insertion and origin attachment sites. The hamstrings are also modeled according to their insertion site on the tibia and origin site on the femur with four force vectors representing each the medial (semimembranosus and semitendinosus) and lateral (biceps femoris) muscles of the hamstring. A modified proportional-integral-derivative (PID) controller was also developed to control the rate of flexion by adjusting the quadriceps force.

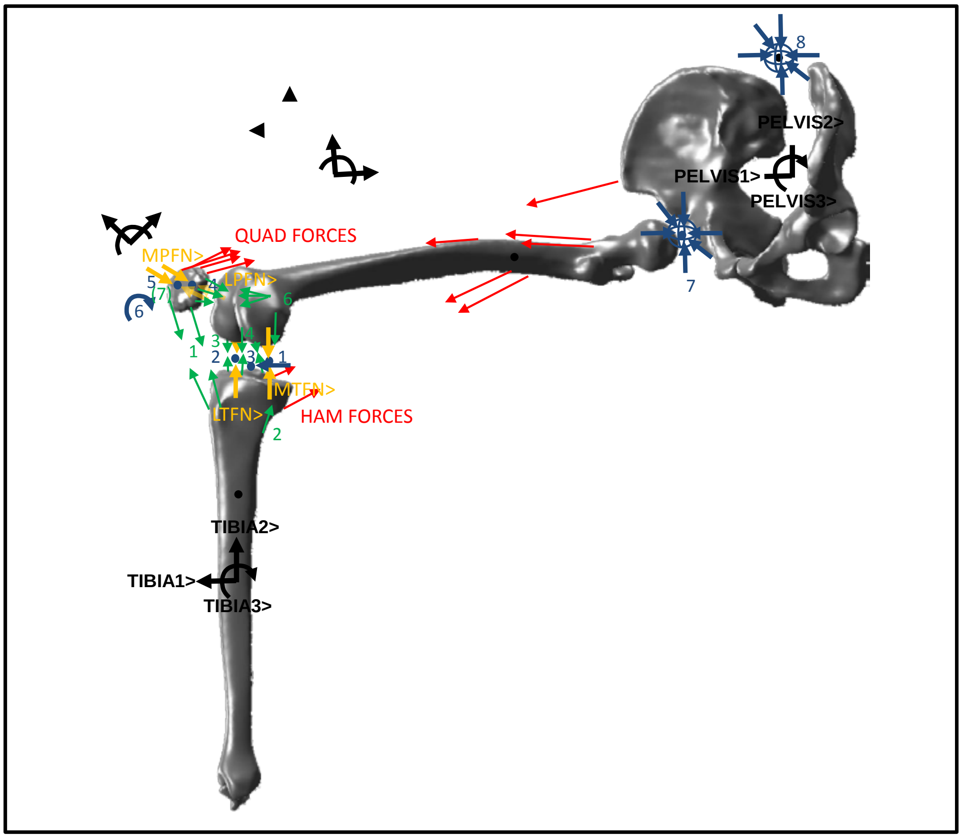

Figure 2: Free Body Diagram of active extension model of a right leg. The PELVIS is constrained to N (Lab) in all 6 DOF and the FEMUR is constrained to the PELVIS in all 6 DOF. The TIBIA and PAT bodies have three degrees of freedom each. A constraint at a point on the tibia near the joint center constrains M/L movement of the TIBIA in the FEMUR3> direction. Green numbers and arrows represent ligament forces modeled as non-linear springs. Blue numbers represent constraints. Yellow arrows represent geometric constraints and blue arrows represent constraints that are an assumption of the model. See Table 1 for more details.

Table 1: Description of Active Non-Weight Bearing Extension model. Refer to Figure 2.

SUMMARY OF ACTIVE NON-WEIGHT BEARING EXTENSION MODEL OF A RIGHT LEG	
GRAVITY	Gravity acts in the –1*N2> direction
BODIES	-PELVIS (fixed), FEMUR (fixed), PATELLA (3 DOF), TIBIA (3 DOF) -Mass and inertial properties calculated from literature -Orthogonal system of unit vectors established for each body 1> points anterior 2> points superior 3> points lateral
CONSTRAINT FORCES (BLUE NUMBERS AND BLUE AND YELLOW ARROWS ON Figure 2)	1. Medial TF Geometric Constraint force acting between FEMUR and TIBIA in the MTFN> direction 2. Lateral TF Geometric Constraint force acting between FEMUR and TIBIA in the LTFN> direction 3. Constrain M/L Movement of the TIBIA in FEMUR3> 4. Medial PF Geometric Constraint force acting between FEMUR and TIBIA in the MPFN> direction 5. Lateral PF Geometric Constraint force acting between FEMUR and TIBIA in the LPFN> direction 6. Constrain Rotation of PAT in PAT3> with Knee Flexion 7.FEMUR is constrained in 6 DOF to PELVIS 8. PELVIS is constrained in 6 DOF to N (Table)
LIGAMENT FORCES (GREEN NUMBERS AND ARROWS ON Figure 2)	1. Patella Ligament Medial and lateral, Two Bundles Each 2. Medial Collateral Ligament Three Bundles includes wrapping 3. Lateral Collateral Ligament One Bundle 4. Posterior Cruciate Ligament and Anterior Cruciate Ligament Two Bundles Each 5-6. Lateral and Medial Patellofemoral Ligaments Three Bundles for Each
ACTIVE MUSCLE FORCES (IN RED ON Figure 2)	-QUAD FORCES are applied to PAT at the insertion points and FEMUR at the muscle origin points. Controlled using a PID controller with an additional acceleration feed-back loop element and a proportional controller which stabilizes PAT tilt -HAM FORCES may be applied to the insertion point on the tibia and origin point on the femur and are a function of knee flexion
IMPORTANT ASSUMPTIONS	-Rigid body model does not allow for condylar lift-off. As long as the TF constraint forces (1,2 above) are in compression this is a reasonable assumption -PAT flexion is prescribed as a function of knee flexion -TIBIA translation in FEMUR3> is constrained -Contact point on FEMUR and on PAT are prescribed as a function of flexion -Geometry represented by constraining the velocity of contact points in the direction of the tibial or trochlear groove surface normals (LTFN>, MTFN>, LPFN>, MPFN>) to 0. -Ligaments are modeled as non-linear springs with damping

Articulating Geometry

An important assumption of the model is that the TFJ contact points on the femur are specified as the lowest point on the femur as a function of knee flexion. These contact points were found using a graphical user interface developed for this project in Matlab 7.8.0 R2009b (The MathWorks, Inc. Natick, MA, USA) (Figure 3). The PFJ contact points on the patella were also specified as a function of flexion. This assumption was verified with data collected for this investigation. If the location of the tibia was known, the position of the TFJ contact point could be found in the tibial reference frame. An assumption of the tibiofemoral contact point on the femur throughout the flexion cycle, allowed the geometry to be defined for both the femur and the tibia. The motion of the tibia on the femur was constrained to a specified geometry of the tibial articulating surface (Figure 4) or in the case of the patellofemoral joint, the trochlear groove (Figure 5).

The tibial or trochlear groove articulating geometries were defined by finding the two sequential angles necessary to "aim" a vector in space (Figure 6). These two angles were mapped in a specified reference frame on either a normal tibial CAD model obtained from a CT scan (Figure 7) or from the CAD model of a TKA polyethylene insert (Figure 8-Figure 9). A multivariate polynomial function was fit to the angular data over the tibial surface so that the orientation of the geometry normal direction was described over the articulating surface.

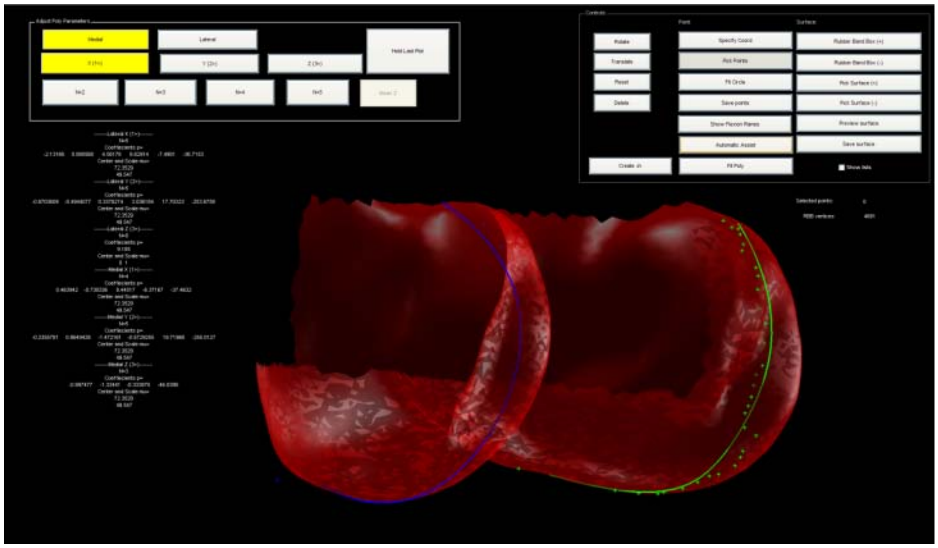

Figure 3: Screenshot of a graphical user interface (GUI) developed to determine the assumed contact points on the femur for this model. This is the posteromedial view of the normal knee femoral condyles with the path of the contact points found using the GUI.

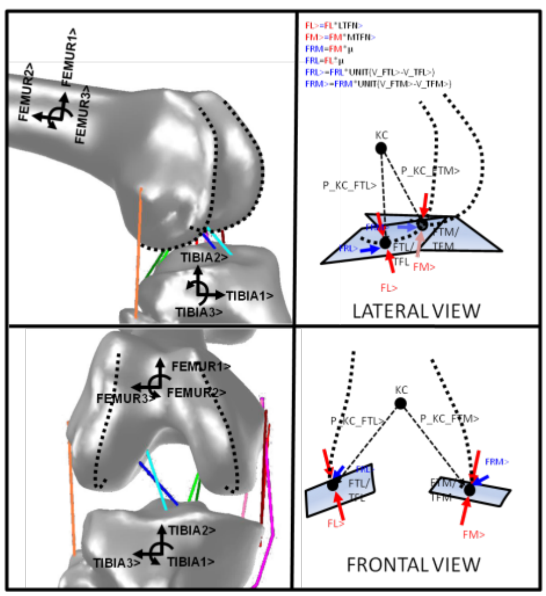

Figure 4: Diagram showing how tibiofemoral contact is modeled with tibial geometry. The geometry of the medial and lateral femur is expressed as a point on the medial (FTM) and lateral (FTL) condyle. FTM and FTL change position in the femoral reference frame as a function of flexion. TFL and TFM are the tibial contact points. The distance between TFL and FTL and TFM and FTM is set to 0>. TFL and TFM can translate along planes set parallel to the boney geometry of the tibia (velocity in normal LTFN> and MTFN> are constrained to 0) at the position of TFM and TFL in the tibial reference frame. Medial (FM>) and lateral (FL>) contact forces are in the LTFN> and MTFN> directions, respectively. FRL> and FRM> are friction forces.

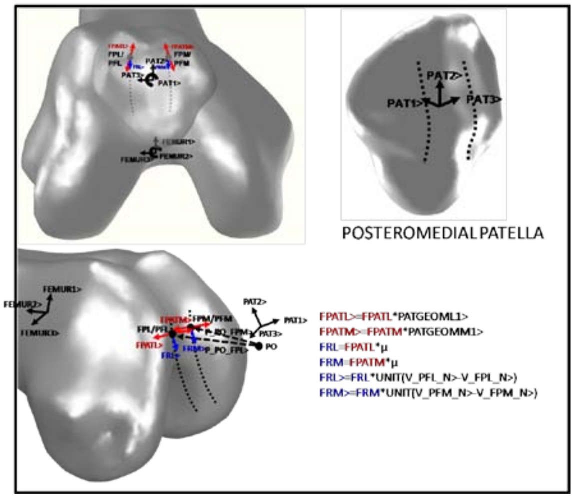

Figure 5: Diagram showing how patellofemoral contact is modeled with trochlear geometry. The geometry of the medial and lateral backside patella is expressed as a point on the medial (PFM) and lateral (PFL) surface. PFM and PFL change position in the patella reference frame as a function of flexion determine from flouroscopic analysis of the patellofemoral contact point. FPL and FPM are the femoral contact points. The distance between PFL and FPL and PFM and FPM is set to 0. FPL and FPM can translate along planes set parallel to the boney geometry of the trochlear groove (velocity of the contact points is 0 in the direction of thenormal MPFN> and LPFN>) at the position of FPM and FPL in the femoral reference frame. Medial (FPATM>) and lateral (FPATL>) contact forces are in the MPFN> and LPFN> directions, respectively. FRL> and FRM> are friction forces.

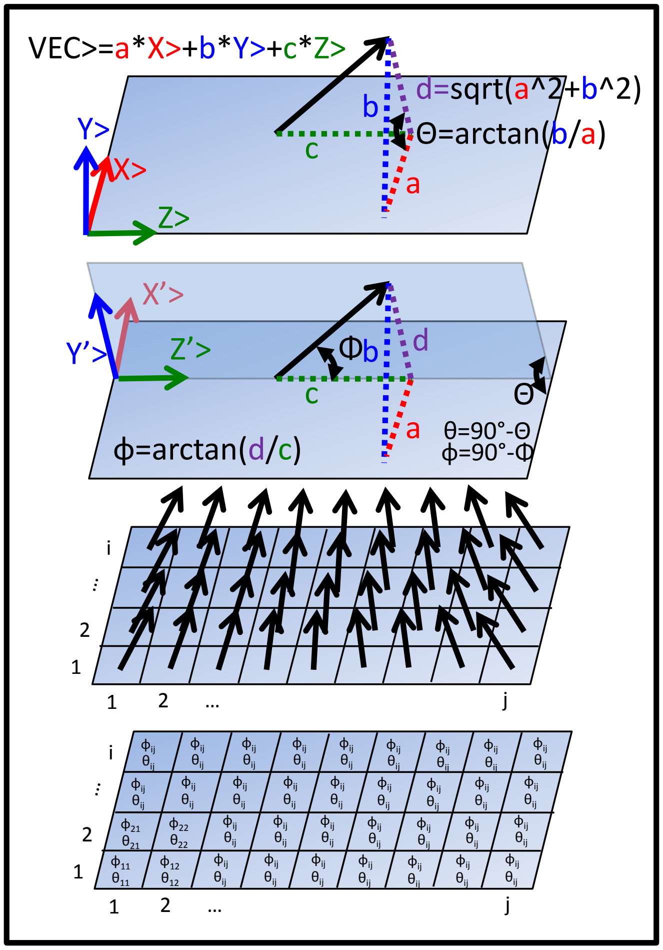

Figure 6: Demonstrating how a vector can be described using two sequential rotations, one about X> and one about Y'>. Multiple vectors can be expressed over a grid to represent the normal vectors from geometry. Rotations can be expressed as polynomials or spline functions.

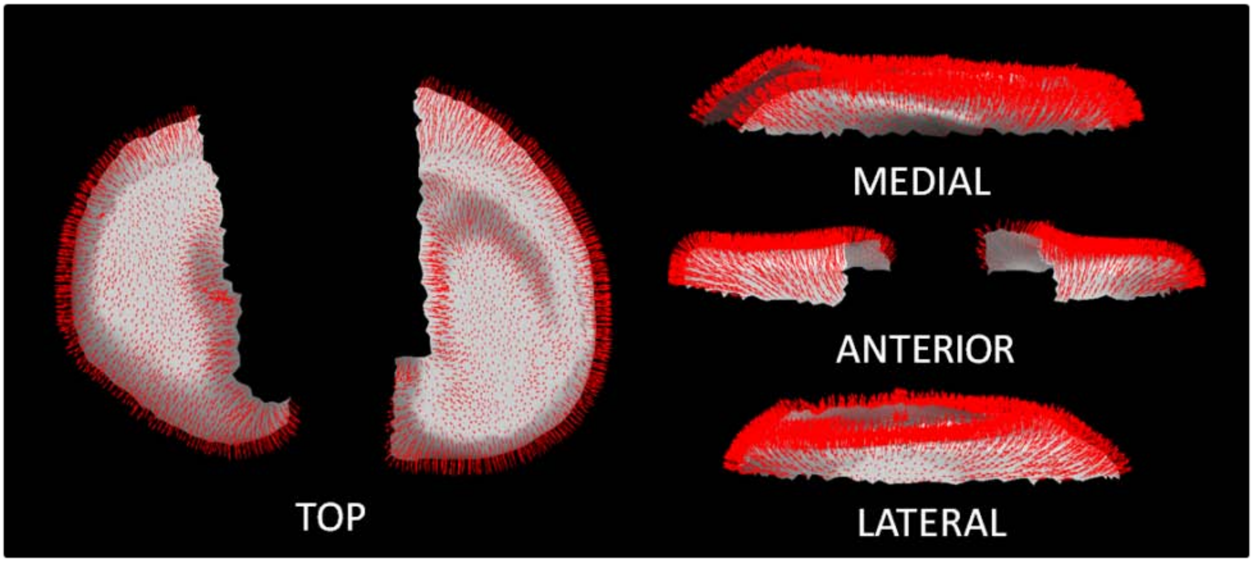

Figure 7: Proximal surface of a right normal tibia with the normals from each face of the CAD model displayed.

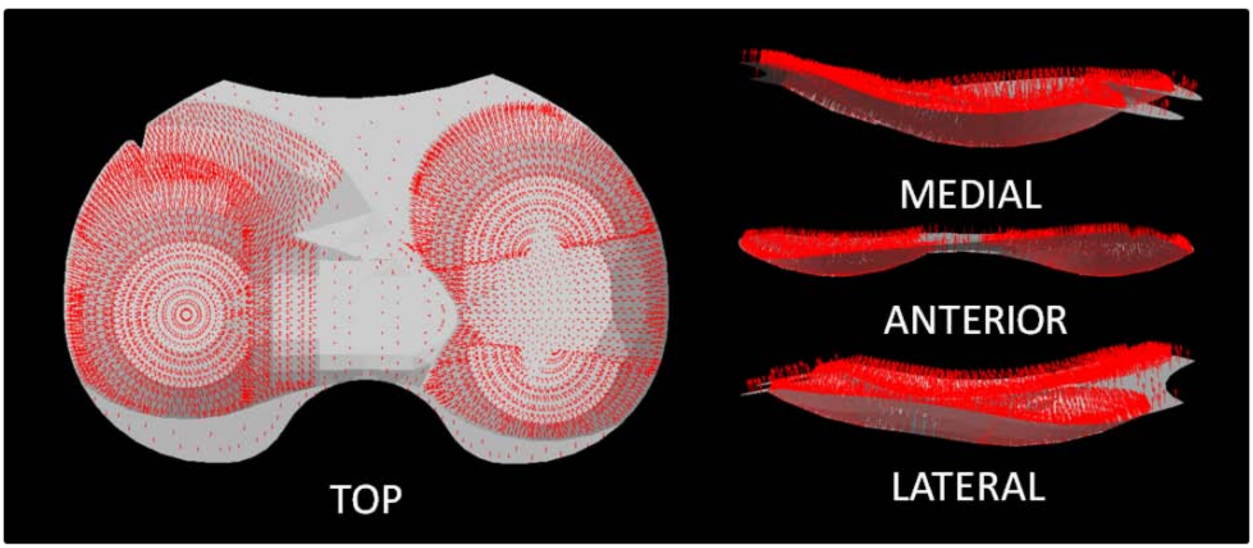

Figure 8: Articulating surface of the Medial Pivot® polyethylene insert by Wright Medical Technology, Inc. (Memphis, TN) with normals from each face of the CAD model displayed.

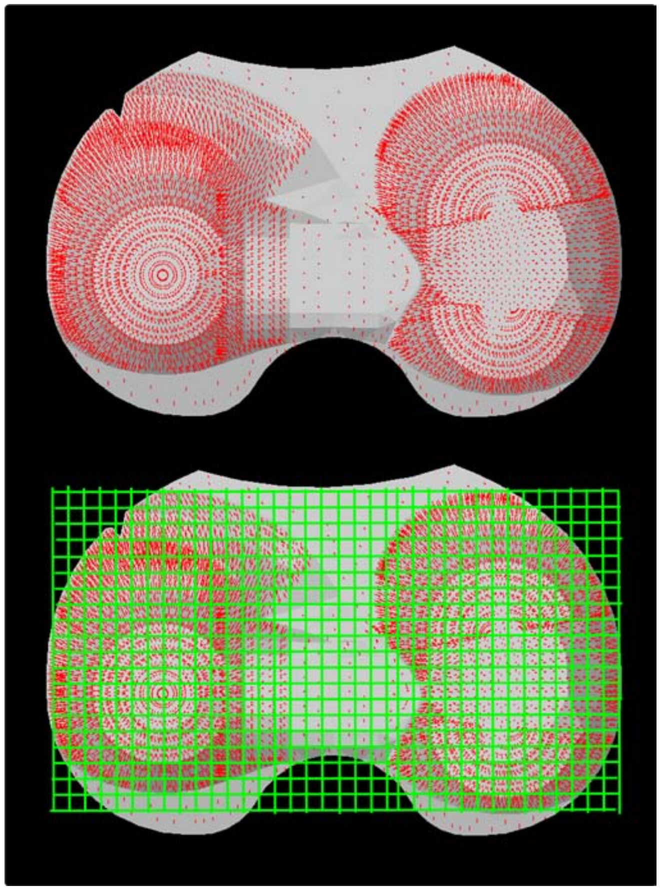

Figure 9: Normal vectors from the faces of a Medial Pivot® TKA polyethylene insert from Wright Medical Technology, Inc. These vectors can be mapped in the AP (up/down in this diagram) and ML (left/right) and a function can be fit to represent the two angles needed to find the orientation of the normal vectors.

This function could then be altered to change the articulating geometry while keeping all other parameters of the model similar in nature. Software was developed to calculate the multivariate polynomial and insert this geometry to the model (Figure 10). Multivariate polynomials from first to fifth degree were fit to the angular data and the polynomial that best represented the geometry and/or had the highest coefficient of determination (R^2) was used in the simulation. By discretely integrating the angular data over the geometric surfaces, an estimation of the geometry could be viewed and compared to the actual geometry (Figure 11).

The coefficients of the polynomial model could also be edited if needed. For the models included in this dissertation the mediolateral conformity (the second rotation angle about the 1> direction or in the coronal plane) was set to a constant value so that only the sagittal curvature was represented. This same process is also used to represent the trochlear groove contact geometry of the patellofemoral joint. However, as the knee goes farther past 90 degrees flexion, this representation becomes inaccurate and assumed orientation of the normal is used.

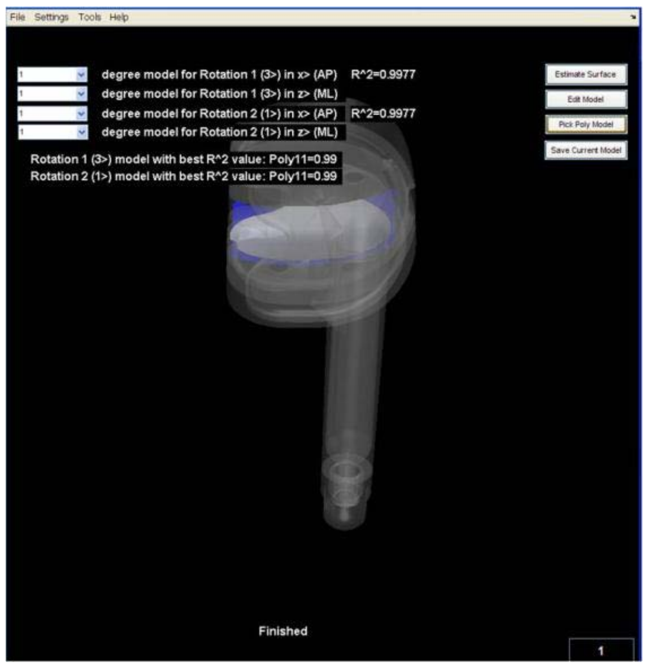

Figure 10: Software developed to calculate and choose the best polynomial representation of the angles representing the normal directions of the tibial or trochlear groove geometry. In the case of the Teletibia TKA lateral insert geometry, shown in this image, the polynomial which fit best was first degree with an R^2 value of 0.9977.

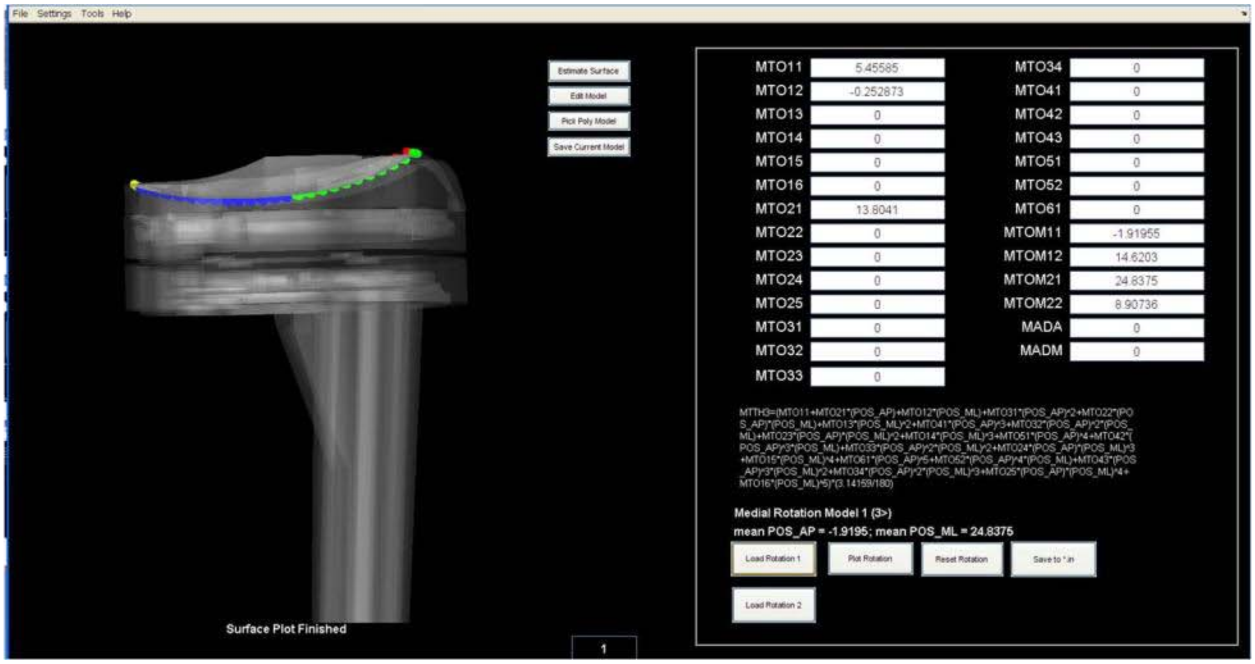

Figure 11: View of software developed to edit the multivariate polynomial and view the estimated geometry compared to actual geometry of the implant. The implant in this figure is the Teletibia TKA. The estimated geometry for the lateral insert is shown with the colored dots. Notice that the estimated sagittal curvature matches well with the actual curvature of the implant.

The position and orientation of the TIBIA reference frame relative to FEMUR was known. Therefore, the location of the medial and lateral contact points could be found in the TIBIA reference frame. The orientation angles were mapped on the tibia or polyethylene insert in the TIBIA1> and TIBIA3> directions relative to reference point TIBREF. Therefore, the orientation angle values, using the position vectors from TIBREF to the medial and lateral contact points, TFM and TFL, can be found. The components of these position vectors needed to find the orientation angles were found by taking the dot product of the position vector from TIBREF to TFM or TFL (TIBREFTFM> or TIBREFTFL>, respectively) with the TIBIA1> and TIBIA3> directional unit vectors.

$$\mathrm{TIBREFTFM1} = \mathrm{TIBREFTFM}{>} \cdot \mathrm{TIBIA1}{>} \tag{1.1}$$

$$\mathrm{TIBREFTFM2} = \mathrm{TIBREFTFM}{>} \cdot \mathrm{TIBIA2}{>} \tag{1.2}$$

$$\mathrm{TIBREFTFL1} = \mathrm{TIBREFTFL}{>} \cdot \mathrm{TIBIA1}{>} \tag{1.3}$$

$$\mathrm{TIBREFTFL2} = \mathrm{TIBREFTFL}{>} \cdot \mathrm{TIBIA2}{>} \tag{1.4}$$

Using the values from equations 1.1 to 1.4 the orientation of the medial and lateral normal vectors, LTFN> and MTFN>, were calculated.

$$Orientation\,of\ MTFN > = f(TIBREFTFM1, TIBREFTFM2) \tag{1.5}$$

$$Orientation\,of\ LTFN > = f(TIBREFTFL1, TIBREFTFL2) \tag{1.6}$$

The equation for the position of the contact points in each of these frames was then found.

$$POSTFM_{MTFN} = TIBREFTFM > \cdot\ MTFN > \tag{1.7}$$

$$POSTFL_{LTFN} = TIBREFTFL > \cdot\ LTFN > \tag{1.8}$$

The derivative of equations 1.7 and 1.8 over time is the velocity of the contact points in the direction of the normal vectors. This equation is a function of the six generalized speeds $(U1 - U6)$ governing the velocity of the tibia.

$$VELTFM_{MTFN} = \frac{dPOSTFM_{MTFN}}{dt} = f(U1, \dots, U6) \tag{1.9}$$

$$VELTFL_{LTFN} = \frac{dPOSTFM_{MTFN}}{dt} = f(U1, \dots, U6) \tag{1.10}$$

The results from equations 1.9 and 1.10 represent two simultaneous equations which were rearranged to solve for two of the generalized speeds in terms of the remaining four. An additional ML constraint was also placed on the tibia. In the case of the TFJ constraints, the translational generalized speeds in the TIBIA1>, TIBIA2> and TIBIA3> directions were constrained, leading to a tibial system with three degrees of freedom, but this system can rotate and translate in all six directions. The constraining forces at the medial and lateral contact points are applied in the LTFN>, MTFN> and FEMUR3> directions.

The articulating geometry of the PFJ is represented in a very similar manner as described previously for the TFJ. However, instead of defining the contact points defined on FEMUR in the TIBIA reference frame, the medial and lateral contact points defined on PAT, PFM and PFL, respectively, were found in the FEMUR reference frame. Assuming the orientation angles representing the normals in the medial and lateral trochlear groove, MPFN> and LPFN>, respectively, are mapped in the FEMUR2> and FEMUR3> directions from a reference point FEMREF the components of the position vectors from FEMREF to PFM and PFL in FEMUR2> and FEMUR3> were found and the remaining calculations are performed to find the two simultaneous equations.

$$\text{FEMREFPFM2} = \text{FEMREFPFM>} \cdot \text{FEMUR2>} \tag{1.11}$$

$$\text{FEMREFPFM3} = \text{FEMREFPFM>} \cdot \text{FEMUR3>} \tag{1.12}$$

$$\text{FEMREFPFL2} = \text{FEMREFPFL>} \cdot \text{FEMUR2>} \tag{1.13}$$

$$\text{FEMREFPFL3} = \text{FEMREFPFL>} \cdot \text{FEMUR3>} \tag{1.14}$$

$$Orientation\ of\ MPFN >= f(FEMREFPFM2, FEMREFPFM3) \tag{1.15}$$

$$Orientation\ of\ LPFN >= f(FEMREFPFL2, FEMREFPFL3) \tag{1.16}$$

$$POSPFM_{MPFN} = FEMREFPFM > \cdot\ MPFN > \tag{1.17}$$

$$POSPFL_{LPFN} = FEMREFPFL > \cdot\ LPFN > \tag{1.18}$$

$$VELPFM_{MPFN} = \frac{dPOSPFM_{MPFN}}{dt} = f(U7, \dots, U12) \tag{1.19}$$

$$VELPFL_{LPFN} = \frac{dPOSPFL_{LPFN}}{dt} = f(U7, \dots, U12) \tag{1.20}$$

In the case of the patella, the simultaneous equations 1.19 and 1.20 can be solved for the translational generalized speeds in PAT1> and PAT3> directions.

The geometry is defined and constrained through the velocities in the model, if the initial position is correct and the time step is small, the speed constraints should constrain the model to the spatial constraints. If the time step is too large and there is a large amount of movement between time steps, there is a risk of the contact point leaving the defined surface. Therefore, the time step for the model is kept small, around 0.0001 seconds.

Weight Bearing Deep Knee Bend

The DKB model consists of the same number of bodies as the extension model (Figure 13). However, TIBIA translation is constrained to the floor (N) at the ankle center and the rotation of TIBIA is prescribed as a function of knee flexion. PAT has the same 3 degrees of freedom (DOF) as described in the extension model, but now the FEMUR has 3 DOF, rather than the TIBIA. Like the TIBIA in the extension model, the FEMUR is constrained by the motion of the two contact points. An important change to the deep knee bend model is the constraining of the motion of the femoral head in the medial/lateral direction. This constraint acts as the stabilizing effect of the contralateral leg which prevents large M/L translation. With or without this stabilization, the model does run to completion (140 degrees flexion). However, with the constraint the position of the femoral head moved unrealistically far medially, especially in later flexion, resulting in unrealistic amounts of tibiofemoral axial rotation leading to unstable tibiofemoral kinematics, also affecting the PFJ kinematics. The 3 degrees of freedom are all rotational in nature, but the femur does have freedom to translate in all three directions. However these translations are dependent on the tibiofemoral geometry and the hip constraint applied at the femoral head. The TFJ contact positions on the femur are still found the same way as in the extension model using the GUI mentioned previously (Figure 12).

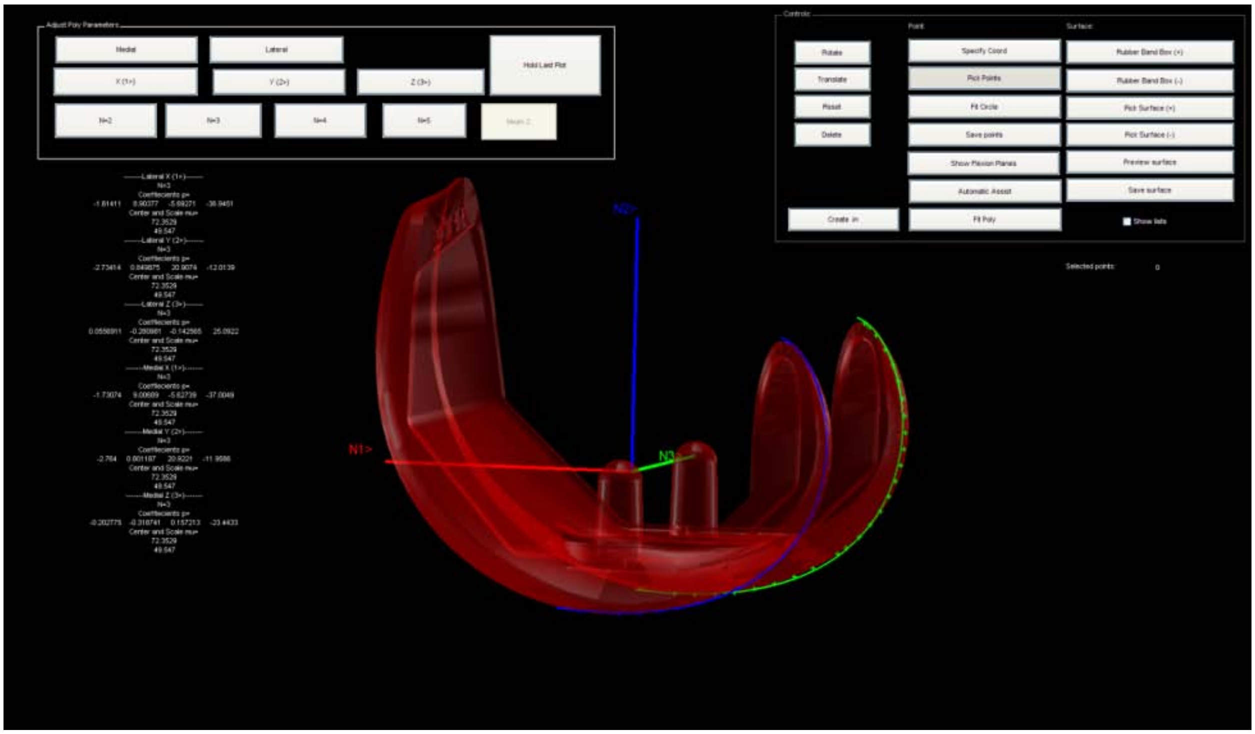

Figure 12: Screenshot of a graphical user interface developed to determine the assumed contact points on the femur for this model. This is for a TKA femoral component in this case for the Teletibia TKA used in one of the deep knee bend models.

The PELVIS represents the upper body or trunk of the subject. The mass center is placed at the center of mass of the trunk. The translation of PELVIS is constrained to the femoral head on FEMUR. The rotation of the trunk is prescribed as a function of knee flexion. Pelvic flexion is prescribed because a subject tends to lean forward while performing a deep knee bend.

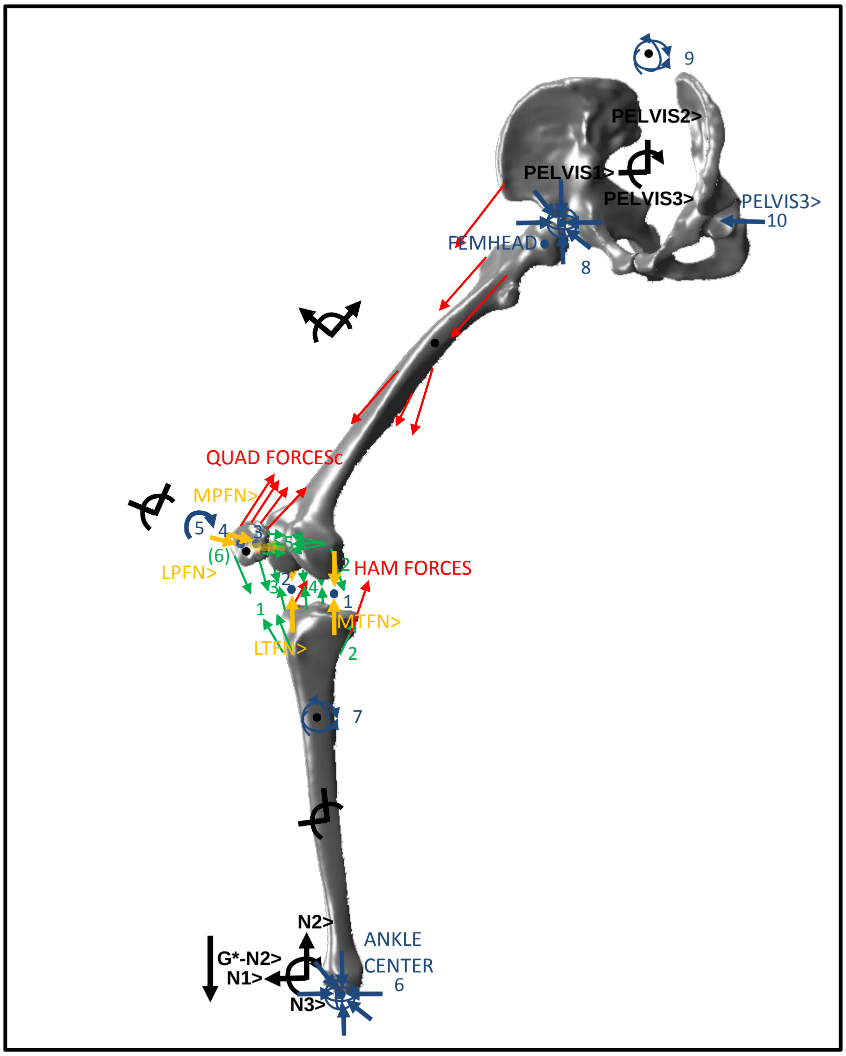

Figure 13: Free Body Diagram of the weight bearing deep knee bend model including joint constraining forces applied using geometry, ligament forces, active muscle forces, ground reaction forces, hip forces, opposite leg force in medial/lateral direction. This model includes four bodies, TIBIA, PAT, FEMUR and PELVIS (TRUNK). The TIBIA body is constrained in all three rotations and translations at the ANKLE CENTER in N. The FEMUR has three degrees of freedom although it can move in all 6 degrees of freedom. The translational speeds are constrained at the medial and lateral contact point and at the FEMORAL HEAD in the PELVIS3> direction. The PAT body representing the patella has two contact points with the FEMUR and three DOF. The ligaments forces are modeled as spring-damper systems with two spring elements per bundle. The QUAD and HAM forces are inputs to the model and are applied at attachement points on the patella and tibia, with origins on the FEMUR and PELVIS. Each force vector in this diagram represents four distributed force vectors applied to the respective bodies. The QUAD FORCES are controlled with a controller, which stabilizes the patella, embedded with a modified PID controller, which controls flexion, with an additional flexion acceleration feedback.

Table 2: Description of Weight Bearing Deep Knee Bend model. Refer to Figure 13 for picture.

SUMMARY OF WEIGHT BEARING DEEP KNEE BEND MODEL OF A RIGHT LEG	
GRAVITY	Gravity acts in the –1*N2> direction
BODIES	-PELVIS (3 rotations specified, fixed to femoral head), FEMUR (3 DOF), PATELLA (3 DOF), TIBIA (3 rotations specified, fixed to N (ground) at the ANKLE CENTER) -Mass and inertial properties calculated from literature -Orthogonal system of unit vectors established for each body 1> points anterior 2> points superior 3> points lateral
CONSTRAINT FORCES (BLUE NUMBERS AND BLUE AND YELLOW ARROWS ON Figure 2)	1. Medial TF Geometric Constraint force acting between FEMUR and TIBIA in the MTFN> direction 2. Lateral TF Geometric Constraint force acting between FEMUR and TIBIA in the LTFN> direction 3. Medial PF Geometric Constraint force acting between FEMUR and TIBIA in the MPFN> direction 4. Lateral PF Geometric Constraint force acting between FEMUR and TIBIA in the LPFN> direction 5. Constrain Rotation of PAT in PAT3> with Knee Flexion 6.TIBIA translation constrained to N (ground) at ANLE CENTER 7. 3 TIBIA rotations specified as function of knee flexion 8. PELVIS translation is constrained to the femoral head on FEMUR (FEMHEAD) 9. 3 PELVIS rotations in N are specified as a function of knee flexion 10. Mediolateral translation of the point on FEMUR, FEMHEAD, in the PELVIS3> direction is specified as a function of flexion
LIGAMENT FORCES (GREEN NUMBERS AND ARROWS ON Figure 2)	1. Patella Ligament Medial and lateral, Two Bundles Each 2. Medial Collateral Ligament Three Bundles includes wrapping 3. Lateral Collateral Ligament One Bundle 4. Posterior Cruciate Ligament and Anterior Cruciate Ligament Two Bundles Each 5-6. Lateral and Medial Patellofemoral Ligaments Three Bundles for Each
ACTIVE MUSCLE FORCES (IN RED ON Figure 2)	-QUAD FORCES are applied to PAT at the insertion points and FEMUR at the muscle origin points. Controlled using a PID controller with an additional flexion acceleration feedback element and a controller which stabilizes PAT tilt -HAM FORCES may be applied to the insertion point on the tibia and origin point on the femur and are a function of knee flexion
IMPORTANT ASSUMPTIONS	-Rigid body model does not allow for condylar lift-off. As long as the TF constraint forces (1,2 above) are in compression this is a reasonable assumption -PAT flexion is prescribed as a function of knee flexion -The mediolateral constraint at FEMHEAD acts as the stabilization provided by the contralateral leg -Contact point on FEMUR and on PAT are prescribed as a function of flexion -Geometry represented by constraining the velocity of contact points in the direction of the tibial or trochlear groove surface normals (LTFN>, MTFN>, LPFN>, MPFN>) to 0. -Ligaments are modeled as non-linear springs with damping

Ligaments and Muscle Modeling

Quadriceps and Hamstring Forces

The active muscle forces used as input to this model play an important role in determining the kinematics and kinetics occurring in this weight-bearing knee model. The location of the origin and insertion sites were determined using CAD models built from computed tomography (CT) scans of a subject with a normal knee (IRB# UT 7756B & Sterling 3088) (Figure 14).

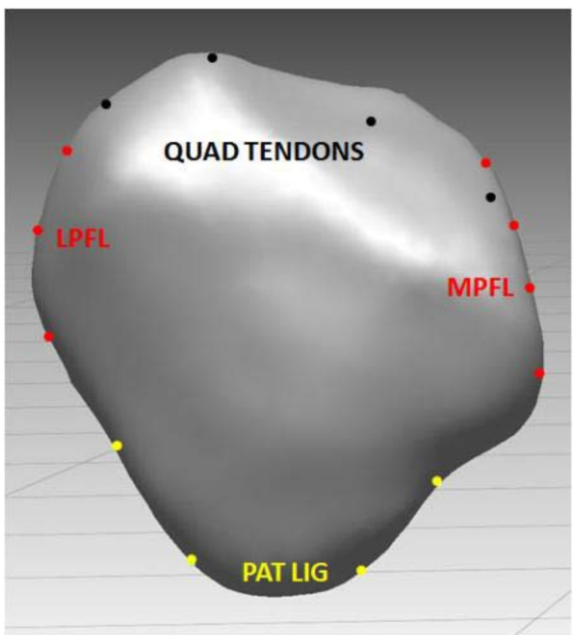

Figure 14: Anterior view of the patella with points for insertion of the patella ligament (PAT LIG), LPFL, MPFL and the quadriceps tendon.

The quadriceps force is applied to the femur, patella and through the extensor mechanism and the patella ligament, the tibia and controls the motion of the leg and contributes to the interaction forces at the TFJ and PFJ. From 0 to approximately 70-90 degrees knee flexion, the four quadriceps muscles are each modeled as equal and opposite forces acting on the femur and the patella. Quadriceps muscle wrapping on the femur is modeled in greater degrees of flexion as frictionless. The summation of the force vectors at the wrapping point are applied to the wrapping via points (Figure 15). There is one wrapping point for each quadriceps muscle element (four for each of the four quadriceps muscles). The hamstrings, modeled as four medial and four lateral elements on the tibia and the femur apply a small co-contraction force during both the extension and weight bearing flexion models.

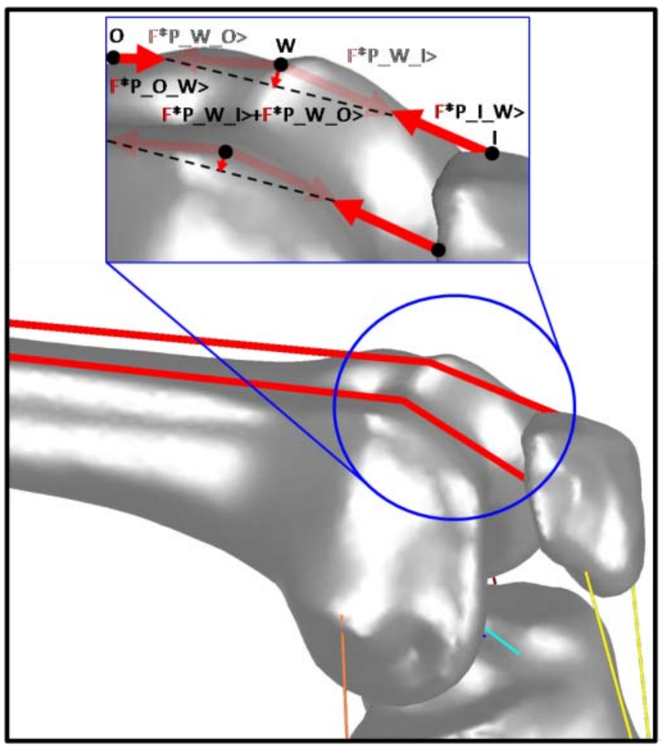

Figure 15: Close-up of the calculation of forces occurring at a wrapping point. Points O, W and I are the origin of the quad muscle, wrapping point and insertion, respectively. F is the quad muscle force and P_I_W> and other vectors are unit vectors pointing from the first point in the name to the second. This same concept is also applied to wrapping ligaments such as the MCL.

Quadriceps Force Controller

The force in each of the four muscles making up the quadriceps femoris is determined by a factor ranging between 0.1 and 6. An example of initial values for these factors for the vastus lateralis (Q_{VL}), vastus intermedius (Q_{VI}), rectus femoris (Q_{RF}) and vastus medialis (Q_{VM}) are 0.5, 4.0, 0.9 and 0.5 respectively. The magnitude of the force vectors representing each muscle is determined by multiplying this factor with a variable, Q_T, resulting in a total quadriceps force of Q_{TOT}.

$$Q_{TOT} = Q_T * (Q_{VL} + Q_{VI} + Q_{RF} + Q_{VM}) \tag{1.21}$$

Before the implementation of the controller, Q_T was a function which changed with knee flexion. This method worked well for the extension model because quadriceps forces from cadaver tests were used as an initial guess and simple adjustments to the function generally gave good and expected results. A function based on values from literature even worked well enough to test many of the early iterations of the DKB model. However, in order to truly represent a deep knee bend and get the knee model to flex at a desired rate, the value of Q_T needed to be adjusted using a technique, equation or process that was more sophisticated than simply a temporal function or function of flexion.

The controller used to adjust the quadriceps force went through several iterations. It was assumed that a PID controller would theoretically work well for an activity like a DKB because it is generally accepted that the quadriceps force increases as the knee goes into deeper flexion. Also, it is known that increasing quadriceps force results in an increased extension moment, which decreases the rate of flexion. One of several challenges in implementing a PID controller in a computational knee model which flexes to deep flexion, however, is tuning the controller. The conditions of the system change constantly as the knee goes into deeper flexion. Gains which work well from 0 to 45 degrees of flexion will not necessarily work well after 45 degrees of flexion. After quadriceps wrapping comes into effect the conditions of the system changed more than anticipated. Also, the goal is not only to reduce the error between the actual and desired flexion but also to get reasonable quadriceps force results. A set of gains may result in low error, but result in erratic jumps in the quadriceps force which are not realistic. If the gains are too low, the error may be too high or there may be oscillations in the results.

The resulting controller which worked best adjusted Q_T according to the error between desired knee flexion, $\theta_{FEM_{3des}}$ and actual knee flexion, θ_{FEM_3}. Two of the several other options explored used two process variables, either velocity or acceleration. Both of these methods performed reasonably well when purely looking at the error between desired and actual velocity or acceleration. However, the goal in this case was to complete the exercise simulation from full extension to maximum flexion in a certain amount of time, with constant flexion rate and acceleration. The overall time to complete the simulation using velocity or acceleration as the process variable was greater or less than the goal time by unacceptable margins. As would be expected smaller errors between desired and actual flexion velocity or acceleration result in larger errors in desired flexion.

Using only knee flexion as the process variable worked reasonable well. However, the performance was below expectations and unrealistic oscillations in the flexion rate were still present no matter how well the controller was tuned. The advantage of using a computer model is that the control scheme can be changed easily. Feedback loops can be added or removed with no cost in materials and little cost in time. An additional feedback loop using the error between the desired and actual flexion acceleration was added to the controller (Note: this is not the second derivative with respect to time of the flexion error, but the angular acceleration of the femur about TIBIA3>, which adds an additional process variable to the controller). Practically, using information about the angular acceleration of the femur allows the controller to proportionally adjust the quadriceps force according to what will happen, which should improve performance.

Theoretically it makes sense that adding an angular acceleration error loop would improve performance. The net torque of a body about an axis of rotation is governed by the equation, $\tau_{net} = I\alpha$. For all cases presented in this dissertation the desired angular acceleration, α, was $0.0°/s^2$. Therefore the desired net torque, τ_{net}, about the instantaneous axis of rotation (which lies somewhere between the femur and tibia within the knee joint) was 0.0 Nm. Once the femur reached the desired angular rate and acceleration, the controller adjusted the quadriceps force to counteract the external forces which apply a torque about the knee. Ideally, this adjustment in the quadriceps force should result in a net torque of 0.0 Nm. The PID controller was close to finding the ideal quadriceps force while not considering angular acceleration. However, by adding an adjustment proportional to angular acceleration error the quadriceps force could be "fine tuned" to more closely counteract the external torques, resulting in a net torque closer to 0.0 Nm. By themselves, the PID controller or the angular acceleration loop adjustment did not perform well. Combining them, however, raised performance and stability to a level which was acceptable for this system.

The controller was implemented around the differential equation solver (Figure 16). Before the solver ran and after the previous time step, which occured in this model every $intgstp$ seconds in model time (usually 10^{-4} seconds), the difference in the actual flexion and the desired flexion was determined,

$$e(t) = \theta_{FEM_3}(t - intgstp) - \theta_{FEM_{3des}}(t - intgstp) \tag{1.22}$$

the instantaneous derivative of this error $de(t)/dt$ and the integral of this error, $\int_0^t e(t)dt$ were also calculated. These values were multiplied by their respective PID gains (K_p, K_i, K_d, respectively). A flexion acceleration feedback element is also added to the controller. The flexion acceleration error is determined by subtracting the actual flexion acceleration from the desired flexion acceleration

$$ae(t) = \frac{d^2\theta_{FEM_3}(t - intgstp)}{dt^2} - \frac{d^2\theta_{FEM_{3des}}(t - intgstp)}{dt^2} \tag{1.23}$$

and a gain, K_{fa}, is multiplied to this error value. These values are added together.

$$Q_{Tadjust} = K_p * e(t) + K_i * \int_0^{t-intgstp} e(t)dt + K_d \frac{de(t)}{dt} + K_{fa} * ae(t) \tag{1.24}$$

This value is then added to the previous value of Q_T and the new value is input to the solver.

$$Q_T(t) = Q_T(t - intgstp) + Q_{Tadjust} \tag{1.25}$$

The gains are all positive values so that if the actual flexion is higher than the desired flexion (positive $e(t)$) or if the derivative of the error is positive or the integral is positive then these terms will all increase the overall quad force, Q_T and if they are negative, they will decrease Q_T.

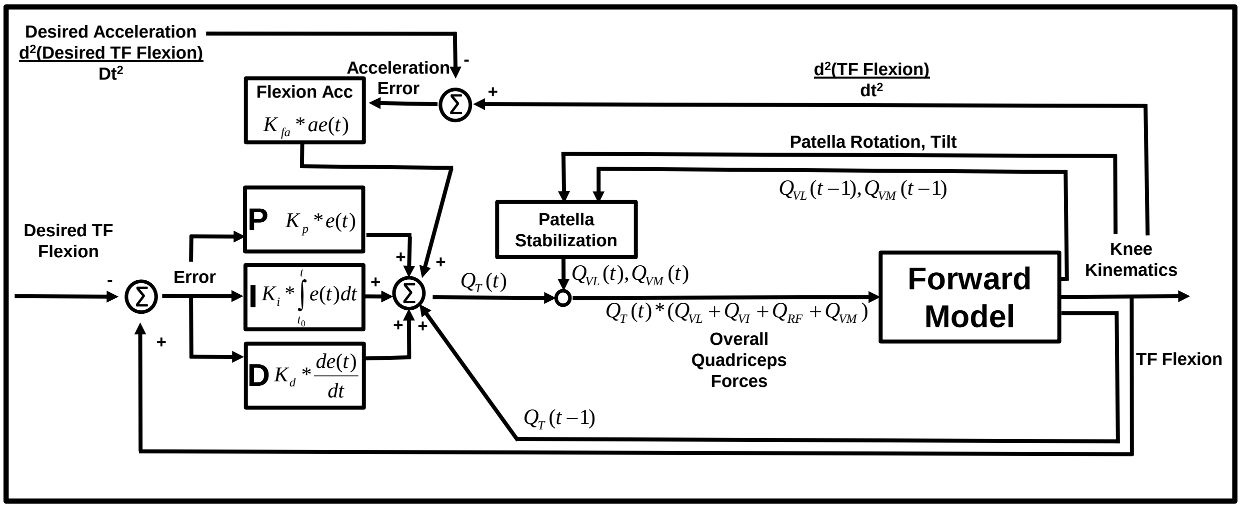

Figure 16: Diagram of position-integral-derivative (PID) controller with an additional flexion acceleration feedback loop used to adjust the quadriceps force to control flexion. The controller is implemented around the solver (box labeled Forward Model in this diagram) and adds or subtracts to the value of Q_T before every time step (time step is 1 for this diagram). Within this controller there is another controller which stabilizes the patella by adjusting Q_{VL} and Q_{VM}, the factors for the vastus medialis and vastus lateralis (details in Figure 17).

A recurring problem with the DKB simulations was instability of the patellofemoral joint, especially in patella tilt (rotation about PAT2> direction (Figure 13)), θ_{PAT_2}. In order to stabilize the patella, a controller which adjusts the factors for the vastus lateralis, Q_{VL} and the vastus medialis, Q_{VM}, was implemented (Figure 17). The patella stabilization controller always adds or subtracts a force to the appropriate muscle that is proportional to the amount of tilt that occurs from the previous time step to the current time step. There is also a constant force added or subtracted from the appropriate muscle if the amount of tilt occurring between time steps is increasing in the direction of tilt (see the upper most box in Figure 17). Unlike the flexion controller, instead of a desired tilt, the error, e_{PAT_2}, is determined by using the previous time step tilt angle as the desired tilt and therefore calculates e_{PAT_2} using equation 1.26.

$$e_{PAT_2}(t) = \theta_{PAT_2}(t - intgstp) - \theta_{PAT_2}(t - 2 * intgstp) \tag{1.26}$$

The difference in error, $de_{PAT_2}(t)$ is determined by subtracting $e_{PAT_2}(t - integstp)$ from $e_{PAT_2}(t)$.

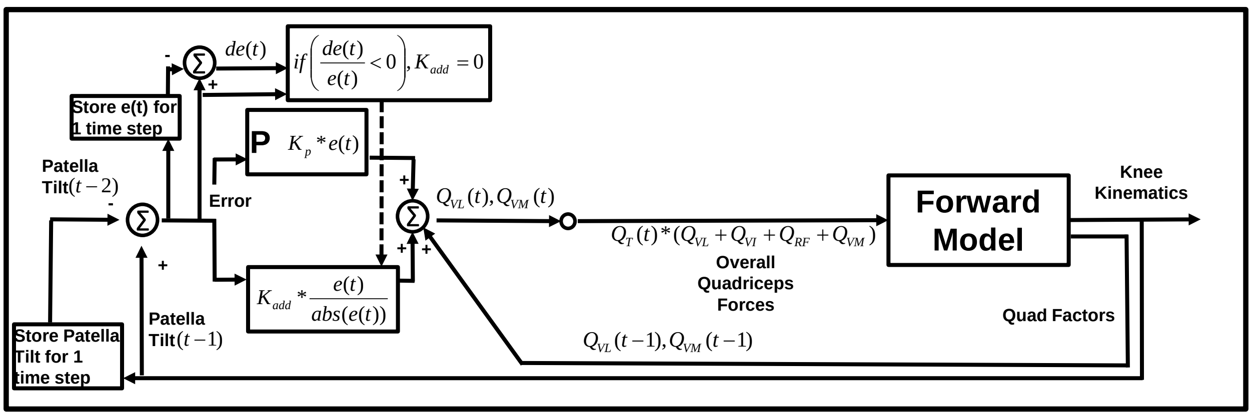

Figure 17: Diagram of the controller for patella stabilization. $e(t)$ in this diagram is $e_{PAT_2}(t)$ and Patella Tilt is θ_{PAT_2}, discussed in the text. This is implemented in line with the flexion controller (Figure 16).

Ligament Attachment

Like the quadriceps, the ligaments were represented by linear vectors in the model. Several bundles for each ligament are included in the model, represented by two spring-damper elements each. The attachment sites for all of the ligaments could be determined by examining the boney surface of the models obtained from CT scans and with assistance from the literature

(Figure 14, Figure 18 and Figure 19). Although error in this process is inevitable, using multiple spring elements for each bundle makes the model a more forgiving to these errors.

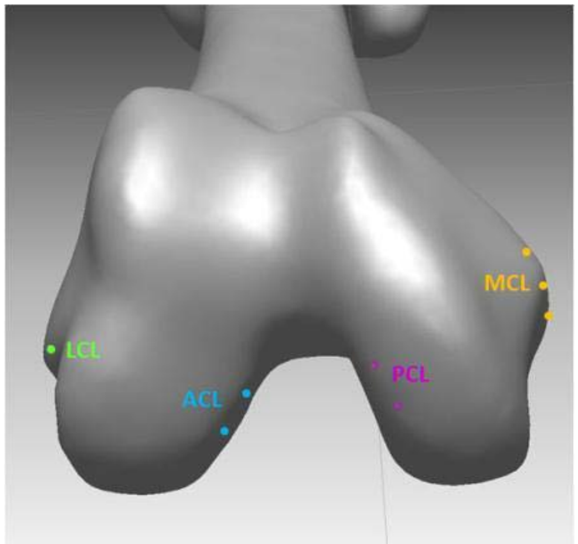

Figure 18: Distal view of a femur segmented from computed tomography scans with points chosen to determine the coordinates of the bony landmarks for the ACL, PCL, MCL and LCL.

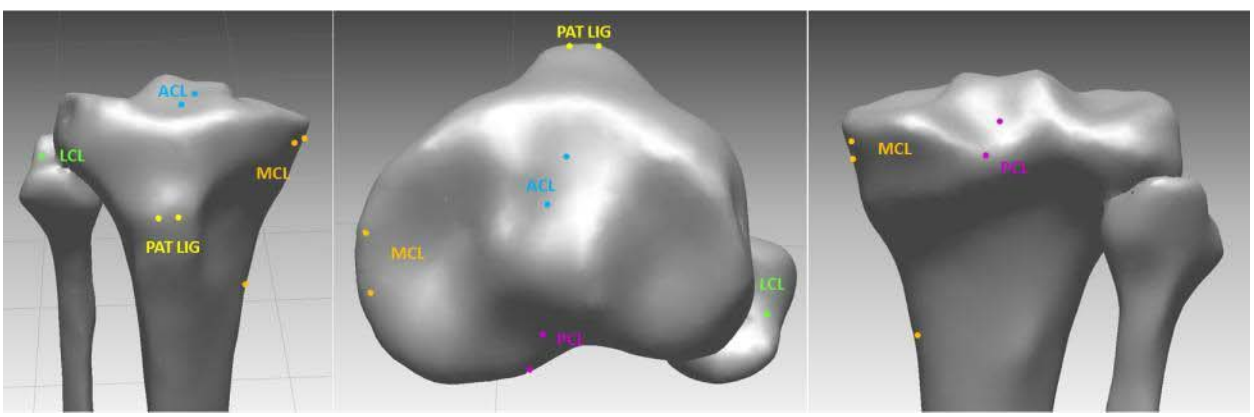

Figure 19: From left to right: Anterior, proximal and posterior view of the tibia showing with points for the ACL, PCL, MCL, LCL and patella ligament insertion points.

The medial collateral ligament (MCL) was modeled with the ligament directional force wrapping around the tibial bone. The forces at the wrapping point were determined using the same method as the quadriceps wrapping (Figure 15). The wrapping point affects the length of the ligament, which affects the force, and also the direction of the force applied.

Ligament Spring Model

Non-linear spring models previously published [Shin 2007] which use ligament strain are used to calculate a part of the ligament forces.

$$F_{Lig\ Spring} = \begin{cases} 0, & \varepsilon \leq 0 \\ k/2\,(L - L_0), & 0 \leq \varepsilon \leq 2\varepsilon_1 \\ k[(L - (1 + \varepsilon_1)L_0], & 2\varepsilon_1 \leq \varepsilon \end{cases} \tag{1.27}$$

$$\varepsilon = \frac{L - L_0}{L_0} \tag{1.28}$$

$$\varepsilon_1 = 0.03 \tag{1.29}$$

$$L = Ligament\ Length \tag{1.30}$$

$$L_0 = Ligament\ Slack\ Length \tag{1.31}$$

The slack length of the ligaments are not known and are considered patient specific. In most cases, these slack lengths were adjusted from values typically used in literature to get realistic results. Usually a slack length, determined using a reference strain, is calculated using the initial length of the ligament during a particular exercise.

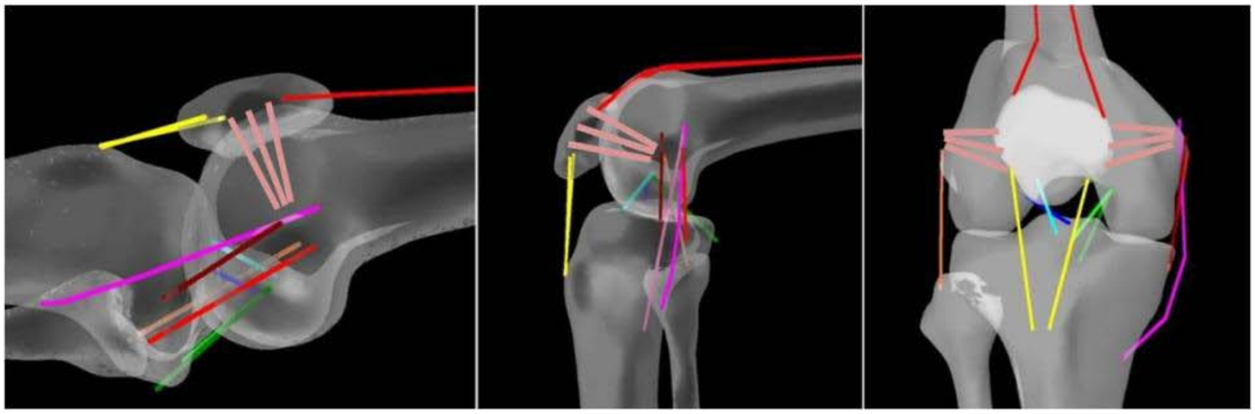

Figure 20: From Left to Right: Medial view of the knee in full extension, medial view of the knee model in flexion and anterior view of the knee model in flexion showing wrapping MCL bundle and wrapping quadriceps tendon over the femur.

Ligament Damping

A damping element is added to the ligament force calculation to reduce oscillations in the model. The damping coefficients, c, which reduced oscillation the best were chosen. The damping force is calculated using the following equations.

$$F_{Lig\ Damping} = \begin{cases} 0, & 0 \geq \varepsilon \\ c * dL/dt, & 0 < \varepsilon \end{cases} \quad (1.32)$$

Ligament Preloads

It is hypothesized that there is a preload which exist in each of the ligaments. These preloads are thought to be constant and separate from the spring forces calculated with the previous equations. With ligament preload added in, the total force in the ligament is represented with the following equation.

$$F_{Ligament} = F_{Ligament\ Preload} + F_{Lig\ Spring} + F_{Lig\ Damping} \quad (1.33)$$

To test the hypothesis that ligaments have preloads, a calculation of the preloads was performed which included the spring forces of the ligaments. To calculate the ligament preloads, the tibia is placed in an initial position and the force in addition to the ligament spring force required to keep the tibia from falling off the femur were calculated. This is a static problem with known gravitational forces acting on the tibia and foot. The goal is to solve for six unknown out of plane forces (posterior cruciate ligament (PCL), anterior cruciate ligament (ACL), MCL, lateral collateral ligament (LCL) and medial and lateral patella ligament forces) which make the three rotational and three translational speeds of the tibia equal to zero (Figure 21).

This is a static problem which could be solved by hand. However, the easiest way to do this is to convert the dynamic code created in AUTOLEV® to a static code, fixing the PATELLA body and setting all six generalized speeds for the TIBIA body to zero, adding the spring ligament forces and solving for the ligament preload forces. Therefore, anytime a new extension model is created, the static code can be run first and the preload values can be calculated. The ligament spring forces calculated at the initial position were applied to the model and then the preloads of the ligaments are calculated. If any preloads turn out to be negative (or in compression), then it was assumed that no preload exists for this ligament, the value is set to 0, just the spring force (if applicable) is applied to the model and the values for the remaining ligament preloads are recalculated until a solution with all positive numbers is reached.

There were options for how to calculate the preloads in each ligament. One option was to have a force in each ligament bundle. Depending on whether the patella ligament was included this results in 12 forces to be solved for using six equations motion. This is an underconstrained problem requiring the use of optimization which can be inefficient. Another option was to start with four forces for each of the knee ligaments and two for the patella ligament, making six simultaneous equations with six total forces and six equations. If one is removed because the spring force in the ligament and/or the calculated preload is in compression, then the system becomes overconstrained.

To solve an overconstrained system

$$Ax = b \tag{1.34}$$

where A and b are known and where the columns of A are longer than x, a least squares method was used which was efficient and gave a reasonable solution. The backslash command in Matlab® (The MathWorks Inc, Natick, MA, USA)

$$x = b \backslash A \tag{1.35}$$

finds a solution for x using QR factorization. This method requires that columns and rows of A be independent from each other, or that A be "full rank." The preloads were only found in the normal knee model and carried throughout the extension and weight-bearing deep knee models of the normal knee.

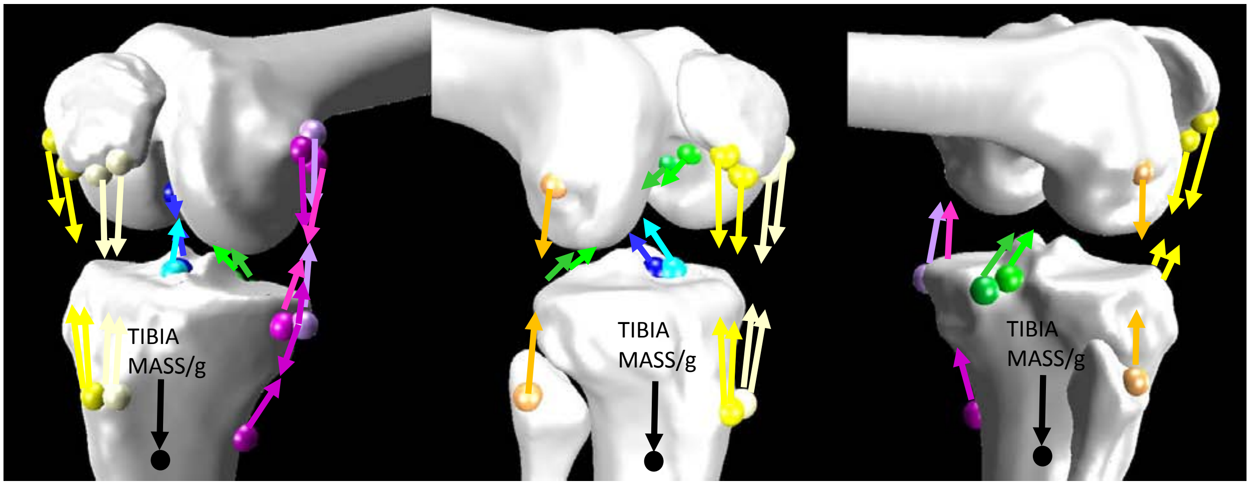

Figure 21: Close up view of the force vectors acting on the tibia from the various bundles of the ligaments of the knee and extensor mechanism. Each arrow represents two force vectors used in the calculation of ligament preloads. The goal is to find the force value for each ligament group which counter acts the mass of TIBIA and the FOOT (not shown). The spheres in this picture represent the actual attachment points used.

Initial Conditions, Parameters and Validation with Fluoroscopy

IRB approval (IRB# UT 7756B & Sterling 3088) was obtained to analyze five normal subjects and 20 implanted subjects for a study to compare normal knee kinematics to the ADVANCE® Medial-Pivot Knee (MP) (Wright Medical Technology, Inc, Memphis, TN). Five normal subjects underwent CT scans of the right leg. Three-dimensional CAD models were assembled from these CT scans (Figure 24). Patients implanted with the TKA and the five subjects with normal knees were asked to perform an active extension exercise (Figure 22). Starting with their knee hanging off a table at approximately 90° flexion the subjects were asked to extend their knee to full extension (0° flexion or parallel to the ground) . All subjects were also asked to perform a weight bearing deep knee bend (similar to going down to tie ones shoe) (Figure 23). Both of these exercises were performed under fluoroscopic surveillance.

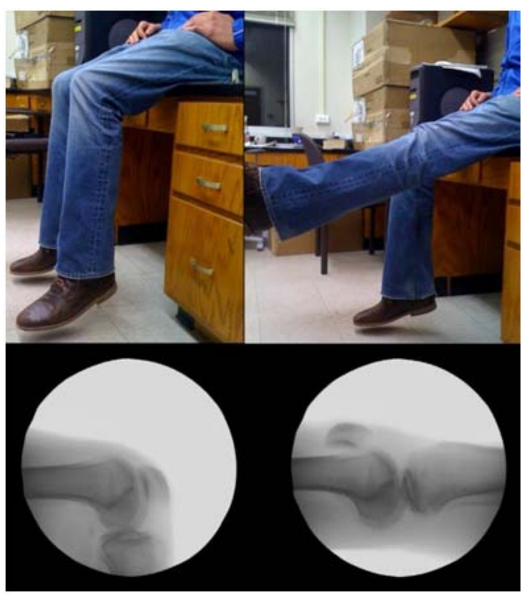

Figure 22: A subject not in this study demonstrating the non-weight bearing extension activity at initial extension and full extension (top, left to right) and sample fluoroscopy images of a normal knee from both increments (bottom, left to right).

Figure 23: Subject demonstrating a deep knee bend to maximum weight bearing flexion while under fluoroscopic surveillance.

Images were digitally captured from the fluoroscopic videos of both exercises every 20 degrees flexion and analyzed using a previously described method [Mahfouz et al. 2003] to extract 3-D tibiofemoral in-vivo kinematic data using the CAD models of either the TKA components or the normal knee CAD models (Figure 25-Figure 29). This kinematic data included medial and lateral tibiofemoral contact position and orientation angles of the femur relative to the tibia. Two-dimensional patella kinematics were also measured from the fluoroscopy images using software developed for this study to determine patella flexion angles over knee flexion and to estimate the patellofemoral contact points on the patella (Figure 30). The initial deep knee bend and extension forward simulations were meant to represent a normal knee. Once the model of the normal knee was giving reasonable results compared to the normal data collected from this study, TKA geometry was virtually implanted to this normal knee model. The results of the TKA simulation were then compared to the results of the in vivo kinematics collected using fluoroscopy from this study.

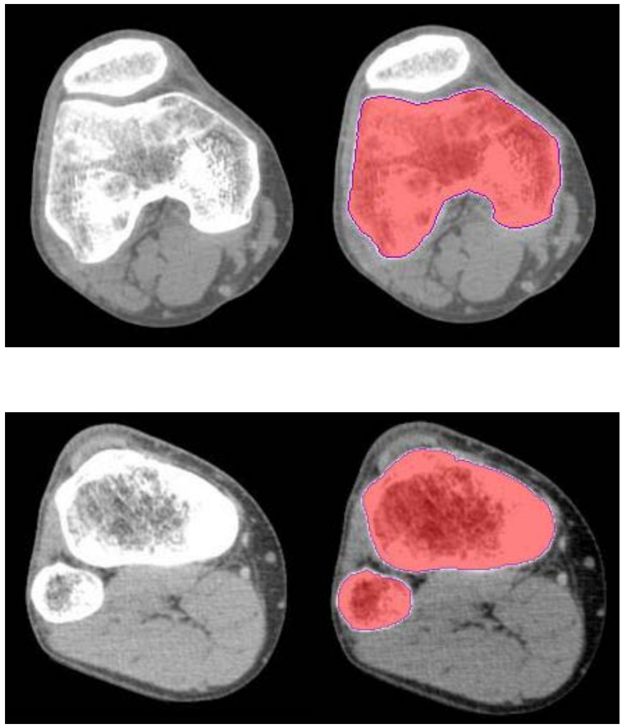

Figure 24: Sample CT image from the distal femur (top left) and proximal tibia and fibula (bottom left) and same images with the femur, tibia and fibula bones selected (right) used to create normal tibia models.

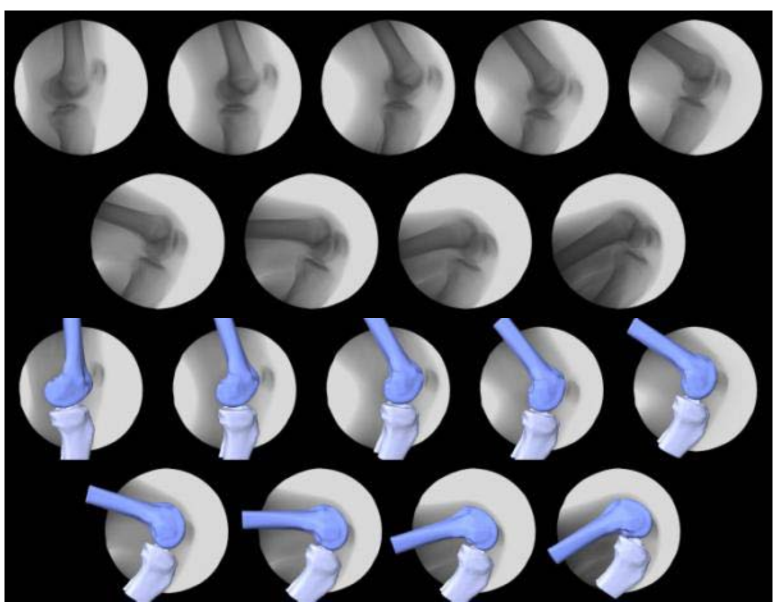

Figure 25: Fluoroscopy images from every 20 degrees of flexion during a weight bearing deep knee bend (top) and images with corresponding CAD models created from CT scans of the normal bone registered to the 2D image extracting 3D in vivo tibiofemoral kinematics (bottom).

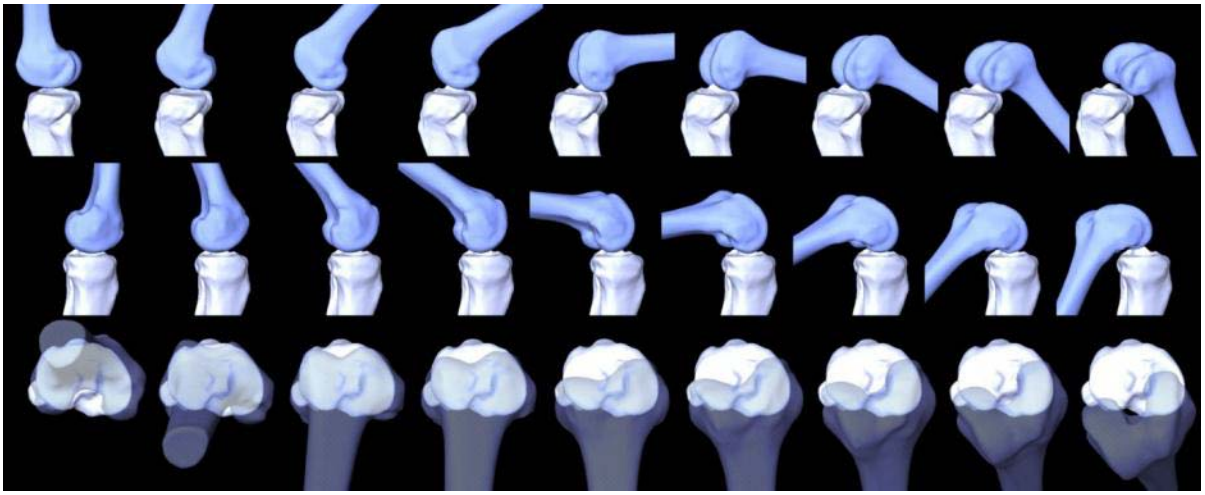

Figure 26: From top to bottom: Lateral, Medial and Top view of a sample normal knee subject performing DKB.

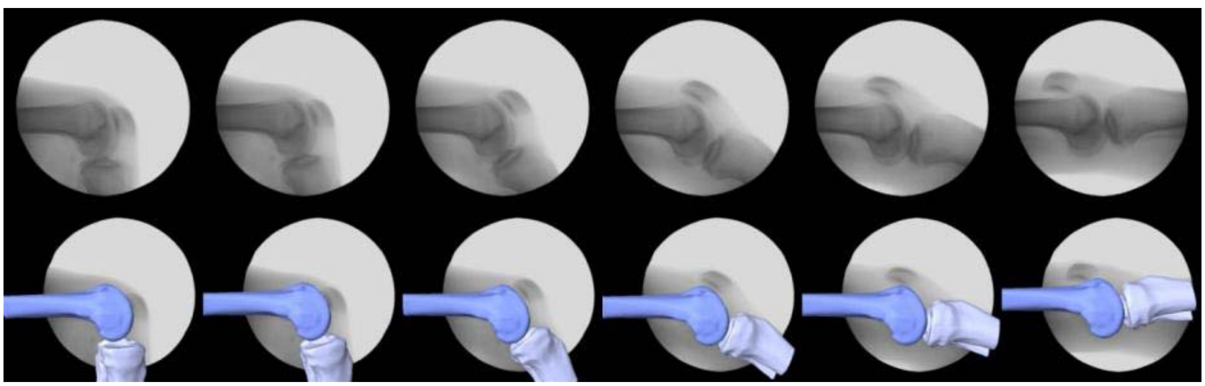

Figure 27: Fluoroscopy images from every 20 degrees of flexion during a non-weight bearing active extension activity (top) and images with corresponding CAD models created from CT scans of the normal bone registered to the 2D image extracting 3D in vivo tibiofemoral kinematics (bottom).

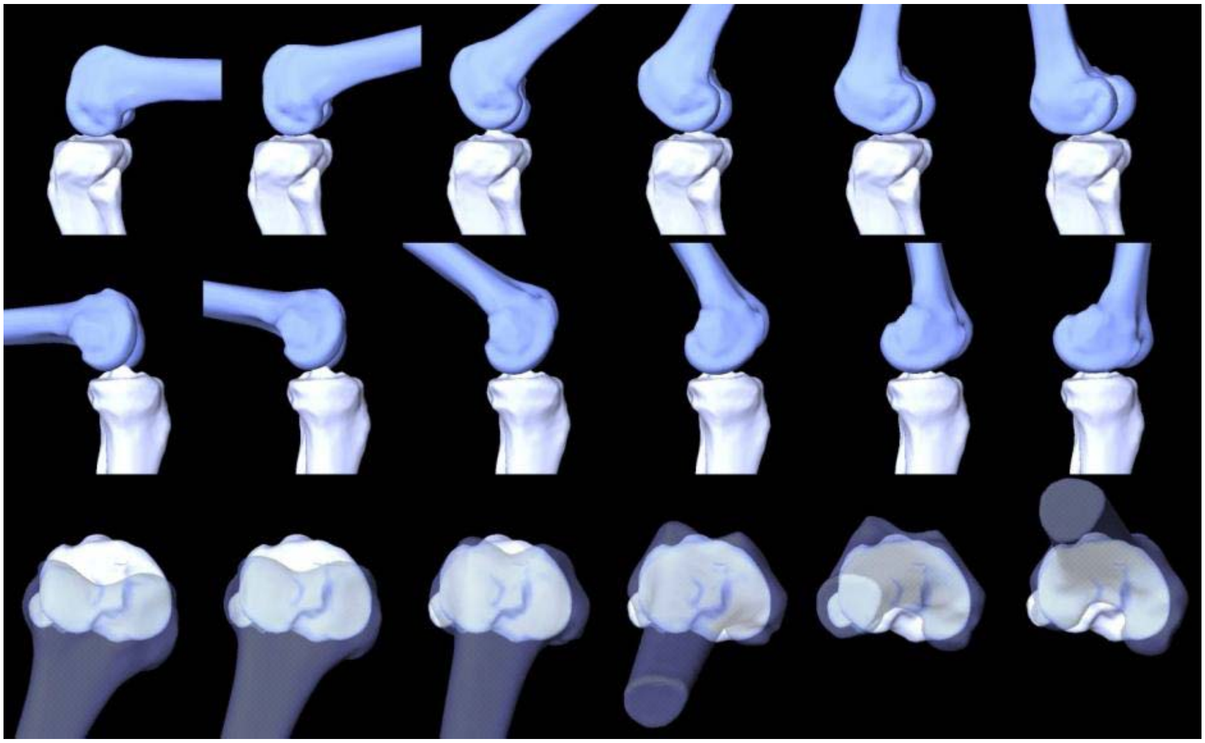

Figure 28: From top to bottom: Lateral, Medial and Top view of femoral kinematics relative to the tibia from a sample normal knee subject performing active non-weight bearing extension activity.

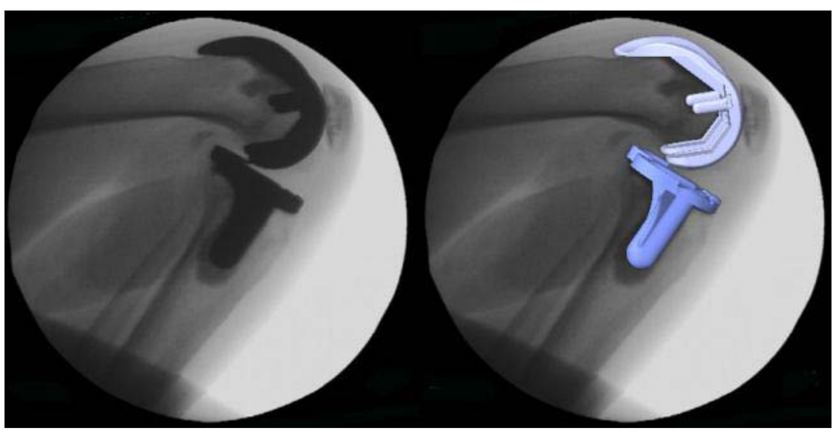

Figure 29: Digital fluoroscopic image of a Medial Pivot TKA at maximum flexion during a weight bearing deep knee bend activity and the corresponding image with a the metal component CAD models registered to the flurosocopic image extracting in vivo tibiofemoral contact kinematics.

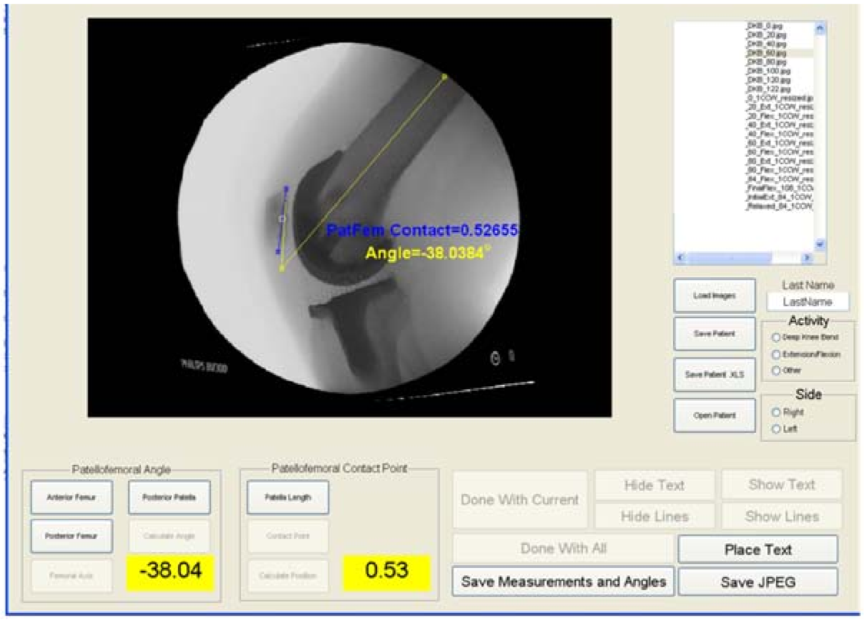

Figure 30: Screen capture of 2D patella kinematics software developed for this project. Sample image shows results from a subject implanted with a Medial Pivot TKA performing a deep knee bend at 40° flexion.

Previous IRB approved fluoroscopic TKA kinematic studies were also used to compare to simulation results of different TKA designs. Fluoroscopic kinematics and force data from a patient with a telemetric tibial component (Depuy, Inc., Warsaw, IN, USA) [D'Lima 2005, Sharma 2007] was used for comparison of tibiofemoral kinematics and tibiofemoral contact forces for the deep knee bend simulation.

A study which evaluated patients implanted with 40 Natural Knee II® (NKII) TKA with Congruent polyethylene (CPE) or Ultra-Congruent polyethylene (UCPE) inserts performing weight bearing deep knee bends (Zimmer Inc., Warsaw, IN, USA) [Mueller 2009] was also used (Figure 31). The purpose of this in vivo study was to compare tibiofemoral contact kinematics of the NKII cruciate retaining TKA with a CPE insert design to the kinematics of the patients implanted with the same femoral and tibial component design but with the UCPE insert (Figure 32). The UCPE is used when the patient's PCL is found to be weak or torn and is meant to stabilize femoral component kinematics in the anterior direction and act as a cruciate substituting TKA.

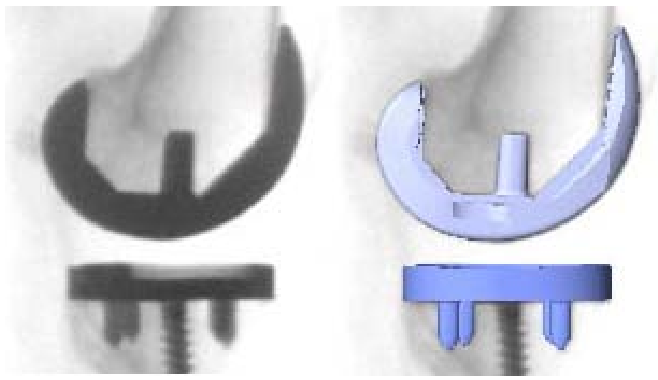

Figure 31: Close up fluoroscopy image of one of 20 knees implanted with a Natural Knee II TKA (left). Patient shown has an UltraCongruent polyethylene insert and the image was captured from fluoroscopic video at full extension during a deep knee bend. Image on the right includes the metal TKA components registered to the image on the left.

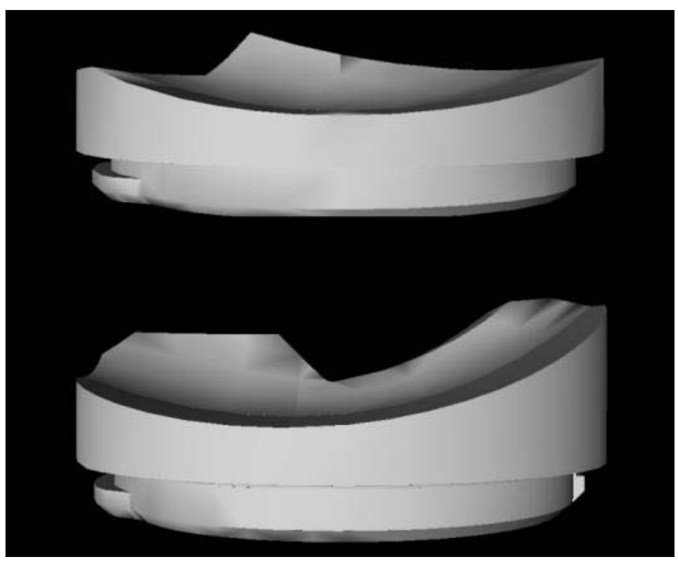

Figure 32: Congruent polyethylene (CPE) (top) and UltraCongruent polyethylene (UCPE) (bottom) inserts used in the Natural Knee II TKA designs. Notice the different sagittal curvatures, especially the slope of the anterior (right) surface and the more posterior "well point" position in the UCPE insert.

Another study used for comparison examined 22 Axiom® ACLR fixed bearing TKA (Wright Medical Inc, Memphis, TN, USA) [Mueller 2007] performing a weight bearing deep knee bend (Figure 33). One additional study used the kinematics from one Hermes® (Ceraver-Osteal Inc, France) ACLR fixed bearing TKA performing the same exercise (Figure 34). Deep knee bend kinematics and kinetics were also simulated using a preproduction ACL-R fixed bearing TKA (Figure 35). No in vivo kinematic data is available for this TKA.

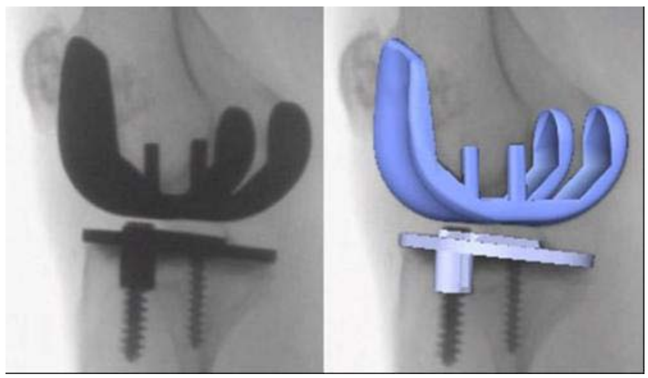

Figure 33: Close up fluoroscopy image of one of 22 knees implanted with an Axiom® ACL-Retaining Fixed Bearing TKA and analyzed using fluoroscopy at full extension during a deep knee bend.

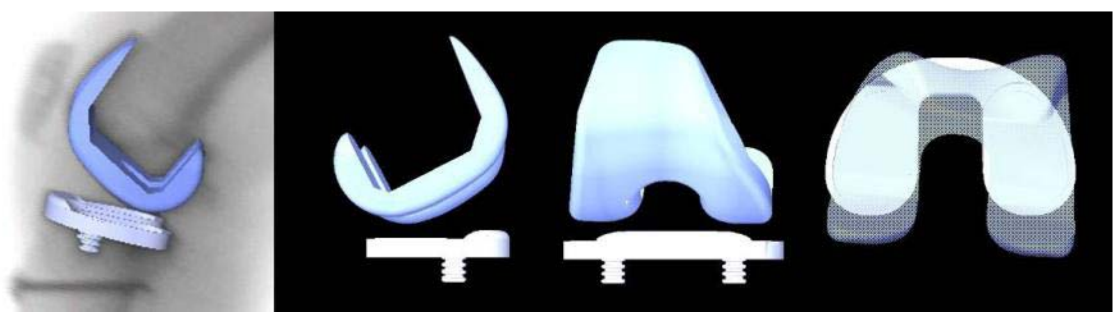

Figure 34: Close up fluoroscopy image of a knee implanted with a Hermes® ACL-R fixed bearing TKA during a weight bearing deep knee bend with registered metal TKA component CAD models (left) and lateral, frontal and proximal views (second from left to right) of the CAD models in the in vivo orientations.

Figure 35: Simulated position of the Preproduction ACL-R TKA during a deep knee bend. These orientations are not from fluoroscopy or from in vivo data as this implant has not yet been analyzed.

The data from these studies were used as validation or comparison and were also used to determine the initial conditions of the simulation. For the normal knee simulation, which used parameters obtained using CT models and data from one of the five normal subjects, the initial in vivo orientation of the femur relative to the tibia for that specific subject was used. The results of the simulation were then compared to the kinematic results of all of the subjects analyzed. Then the different TKA mentioned above were theoretically implanted using the normal subject's knee. Since patient specific data was not available for the TKA subjects analyzed in these studies, the average initial in vivo orientations of the femoral component relative to the tibia was used as a guide for starting the simulations. For the TKA, the simulation results were compared to all of the in vivo tibiofemoral kinematic data for the respective TKAs analyzed in this study, except for the preproduction TKA which has not been put on the market.

Broad Scope

The ultimate goal in producing this model was to integrate it with the contact model developed by Sharma in 2008 [Sharma 2008, 2009]. Sharma used a validated inverse model to determine contact forces using motions obtained from fluoroscopy. These motions and forces were then applied to a contact model which was able to determine contact pressure and stress with the accuracy of finite element in seconds instead of hours (Figure 36). This successfully validated forward dynamic model could replace the fluoroscopy and inverse model portions of this process (Figure 37) resulting in a virtual knee simulator that can accurately predict kinematics and contact stresses from an implant not yet manufactured or implanted.

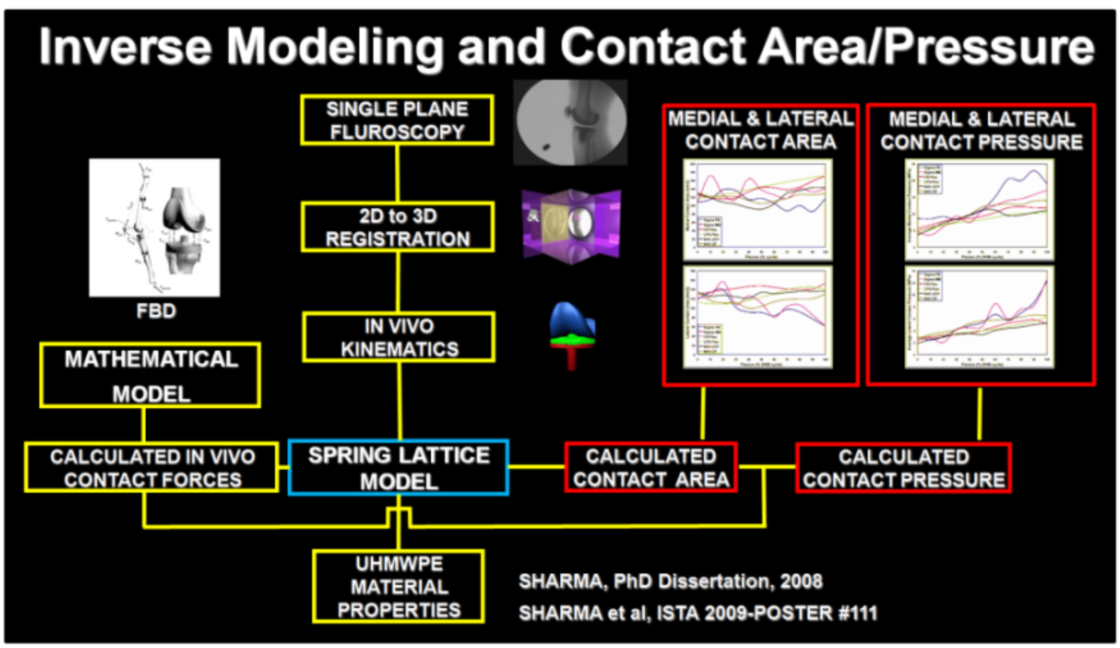

Figure 36: Diagram showing the process of modeling TF contact forces with a validated inverse dynamic model and using the results of that as input to a spring lattice contact model to quickly and accurately determine contact stress and pressures [Sharma 2008].

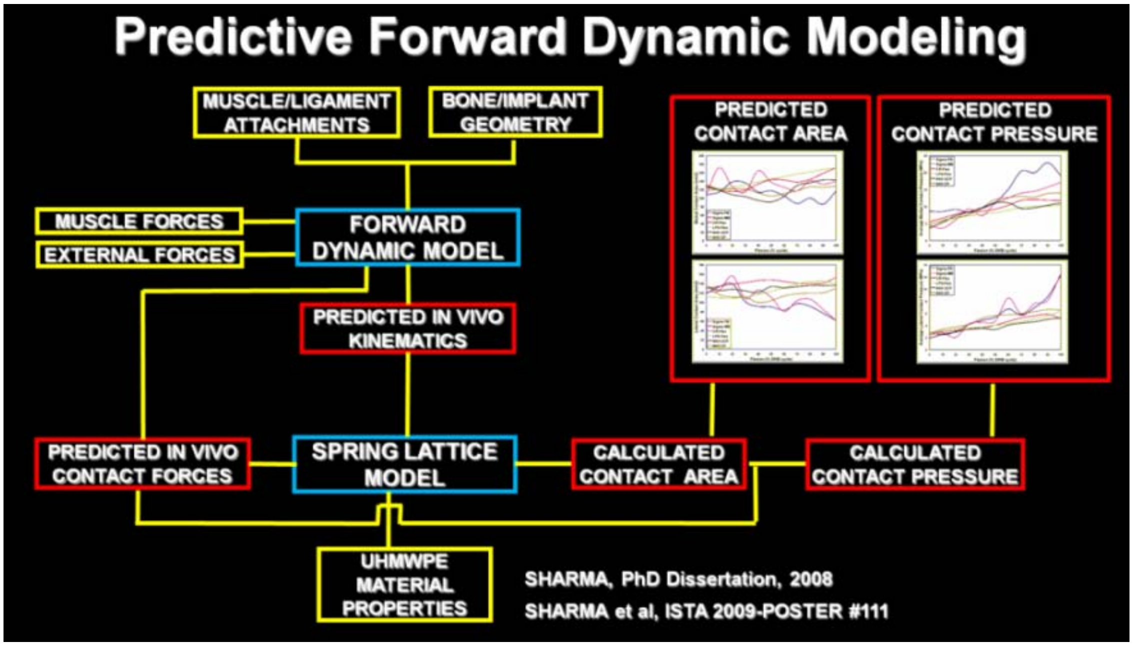

Figure 37: Diagram showing the potential for a virtual knee simulator by replacing the kinematics from fluoroscopy and forces from the inverse model using the predictive dynamic forward model.

Chapter 4: Validation

A comparative analysis was conducted, comparing the normal knee model that was derived for this dissertation to in vivo kinematics determined using fluoroscopy from five normal knees for both non-weight bearing and weight bearing activities. The deep knee bend model of the normal knee was then virtually implanted with the geometry of a telemetric TKA device that utilized strain gauges to measure force at the tibial base plate [D'Lima 2005]. The kinematic results of the model were compared to the fluoroscopic data from a patient that has been implanted with the telemetric device, while performing a deep knee bend [Sharma 2007]. The kinetic results from the forward model simulation were then compared with the telemetric force data collected and experimentally derived during the fluoroscopic trials. Included for comparison were the results, previously discussed from an inverse dynamics model which used the same kinematic data ([Sharma 2007]

Normal Knee Non-Weight Bearing Extension Model

The geometry, soft tissue attachment points, COM locations and segment masses were determined using CAD models built from CT scans of one of the subjects (Subject 3) (Figure 38-Figure 40 and the subject's mass. The CT scans only included the distal and proximal portions of the femur and tibia/fibula, leaving out a good portion of the shaft in these bones. The position of points needed in this portion of the CAD model were estimated. The initial position of the models for the simulation was determined using the in vivo position of Subject 3 determined from fluoroscopy (Figure 41) and the model was run from 90° flexion to full extension (0° flexion) (Figure 42).

Although this data is subject specific, the results of the normal model (Figure 42) are compared to all five subjects to determine whether the kinematic output from the model matches the trends documented using fluoroscopy (Figure 43 and Figure 44). Ligament spring values were taken from literature, however, the slack length of the ligaments were adjusted to get reasonable results from the model.

The greatest difference between the simulation and in vivo data for the lateral anterior/posterior contact position occurred at 60 degrees of knee flexion, where the simulation was 3.2 mm more posterior than the in vivo data (Figure 43). The movement matched well with the overall trend of all five normal knees which depicted, except for Subject 5, a general movement in the anterior direction as the knee extended. The lateral contact movement of the model was most similar to Subject 3 from which the majority of the parameters including ligament and muscle origin and insertion points, segment COM and femoral geometry used in this model were measured.

There was more anterior movement of the medial contact point through extension (Figure 44) than for the lateral condyle contact (Figure 43). This is consistent with the relationship between the medial and lateral condyle contact movement determined using the model. The medial condyle contact position in the model did not match as well with Subject 3 as on the lateral condyle contact. The greatest difference occurred at 20 degrees of knee flexion, where the simulation was 6.9 mm more anterior than the in vivo data.

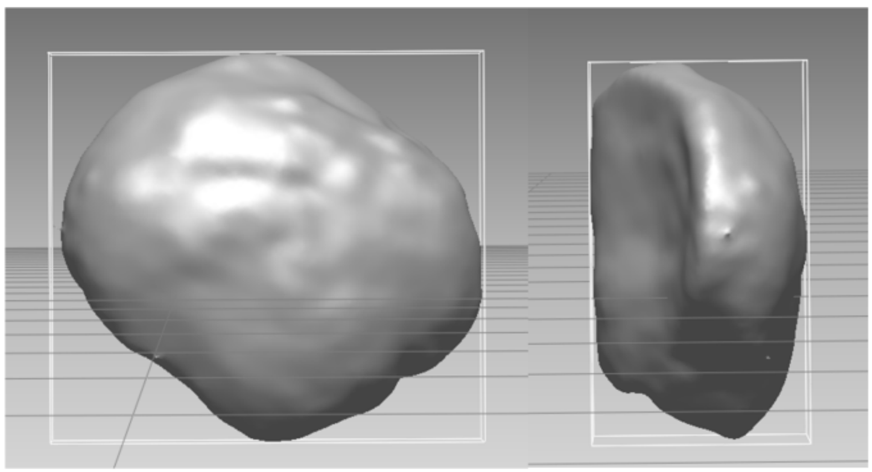

Figure 38: Frontal (left) and lateral (right) views of the CAD model of the patella developed from CT scans of a single subject (Subject 3) as viewed in RapidForm2006 (Inus Technologies, Inc., Seoul, Korea) with model bounding boxes. The position of points such as the patella ligament, quadriceps and medial and lateral patellofemoral ligaments attachments are found by using anatomical landmarks, if visible, or using guides from literature. The center of mass is also calculated using the size of the segment and formulas from literature.

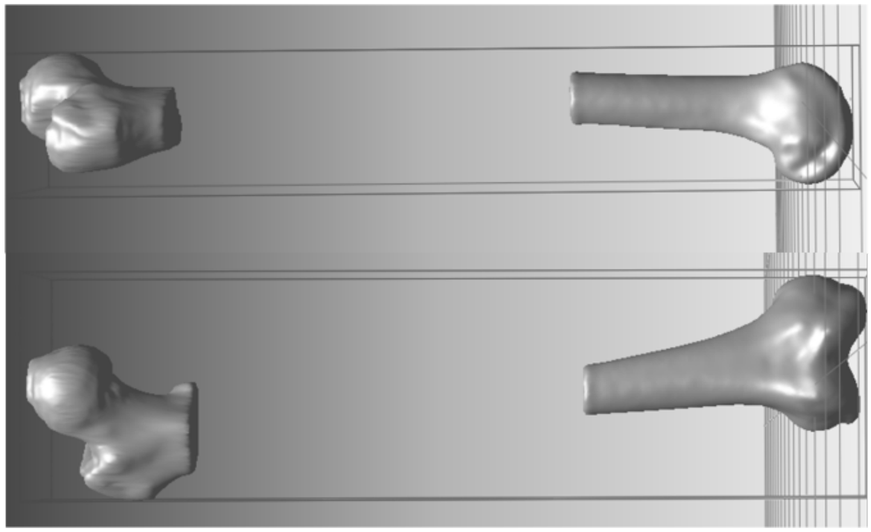

Figure 39: Lateral (top) and frontal (bottom) views of the CAD model of the femur developed from CT scans of a single subject (Subject 3) as viewed in RapidForm2006 (Inus Technologies, Inc., Seoul, Korea) with model bounding boxes. The position of points such as the knee ligament, quadriceps and hamstring and medial and lateral patellofemoral ligaments attachments and the center of the femoral head are found by using anatomical landmarks, if visible, or using guides from literature. The center of mass is also calculated using the size of the segment and formulas from literature. The shaft of the femur is not continuous as CT scans were only performed on the areas visible in the image. Any points needed in the area of the model which is not available are estimated.

Figure 40: Lateral (top) and frontal (bottom) views of the CAD model of the tibia/fibula developed from CT scans of a single subject (Subject 3) as viewed in RapidForm2006 (Inus Technologies, Inc., Seoul, Korea) with model bounding boxes. The position of points such as the knee ligament, hamstring were found by using anatomical landmarks, if visible, or using guides from literature. The center of mass is also calculated using the size of the segment and formulas from literature. The shaft of the tibia/fibula is not continuous as CT scans were only performed on the areas visible in the image. Any points needed in the area of the model which is not available are estimated.

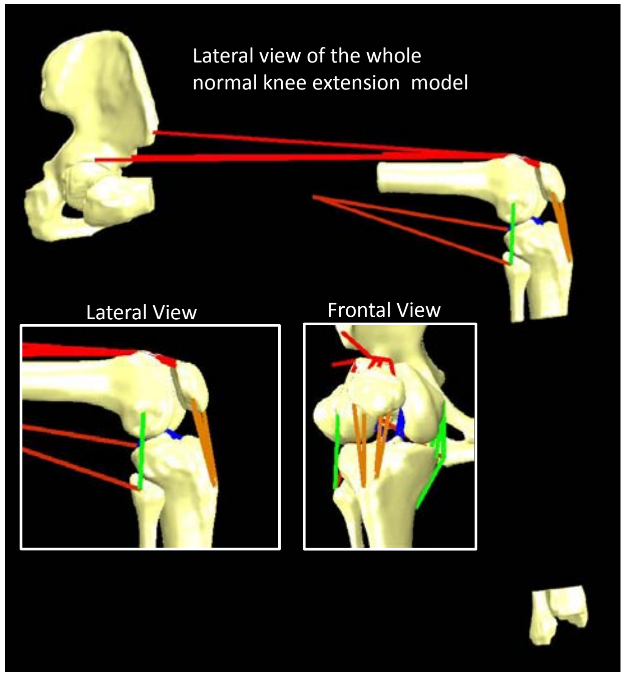

Figure 41: Lateral view of the whole extension model with closeup of the knee from the lateral and frontal view (inlays). There is a break in the femoral shaft and the tibia and fibula bones because CT scans were only taken of the parts visible to reduce radiation exposure to the subject as specified by this project's IRB. The pelvis is a sample pelvis taken from another patient.

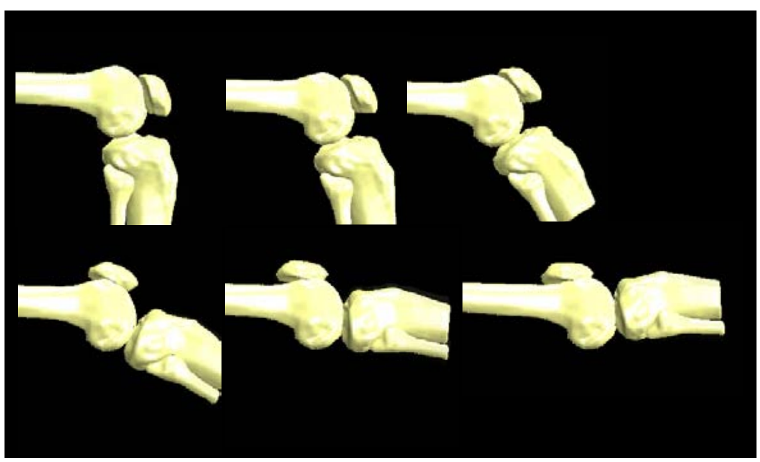

Figure 42: Lateral view of the progression of the normal knee through the non-weight bearing extension simulation. Muscles and ligaments athough they exist in the model are not shown.

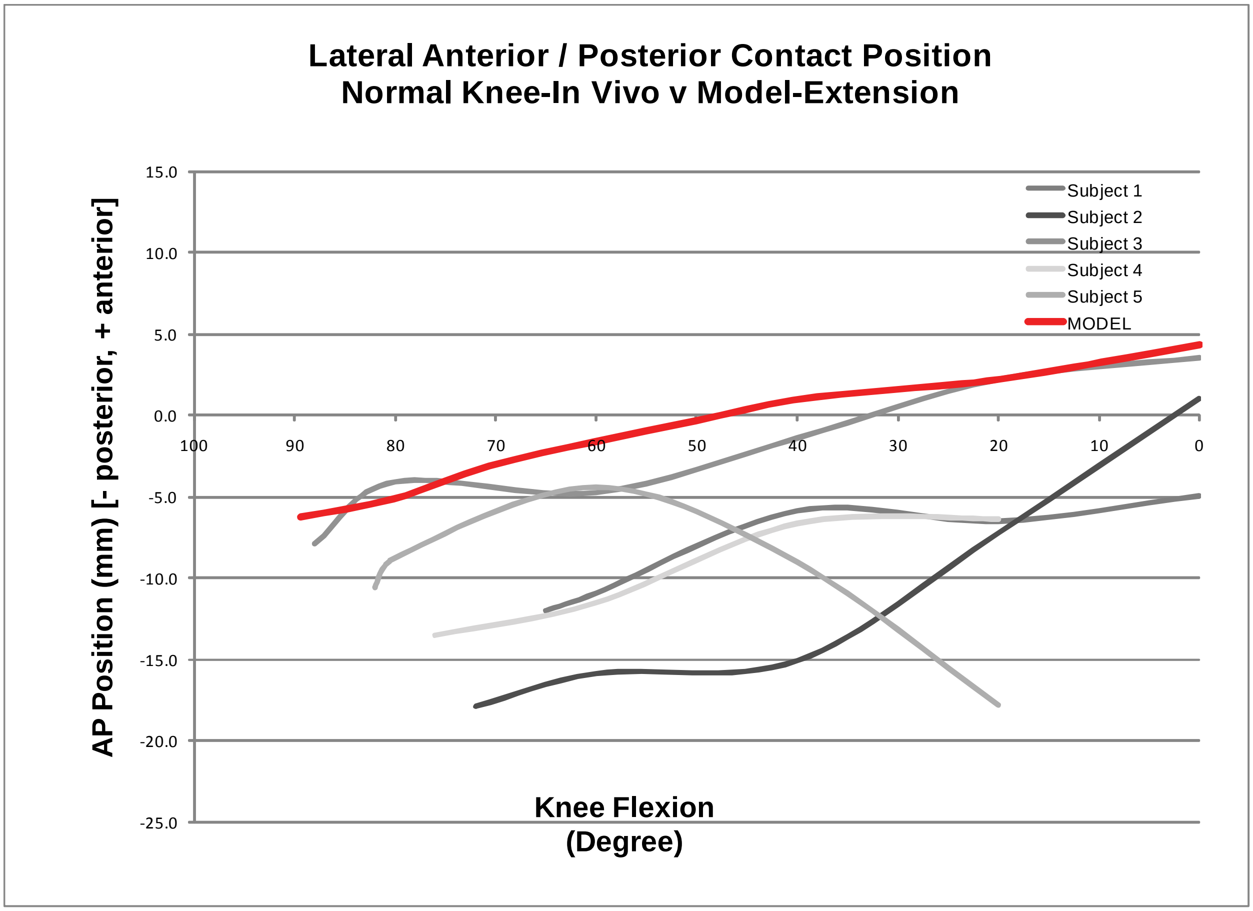

Figure 43: Lateral anterior/posterior femorotibial contact position data from fluoroscopy and forward model simulation for a non-weight bearing extension activity. Geometry and soft tissue attachments were determined using models constructed from CT scans of Subject 3.

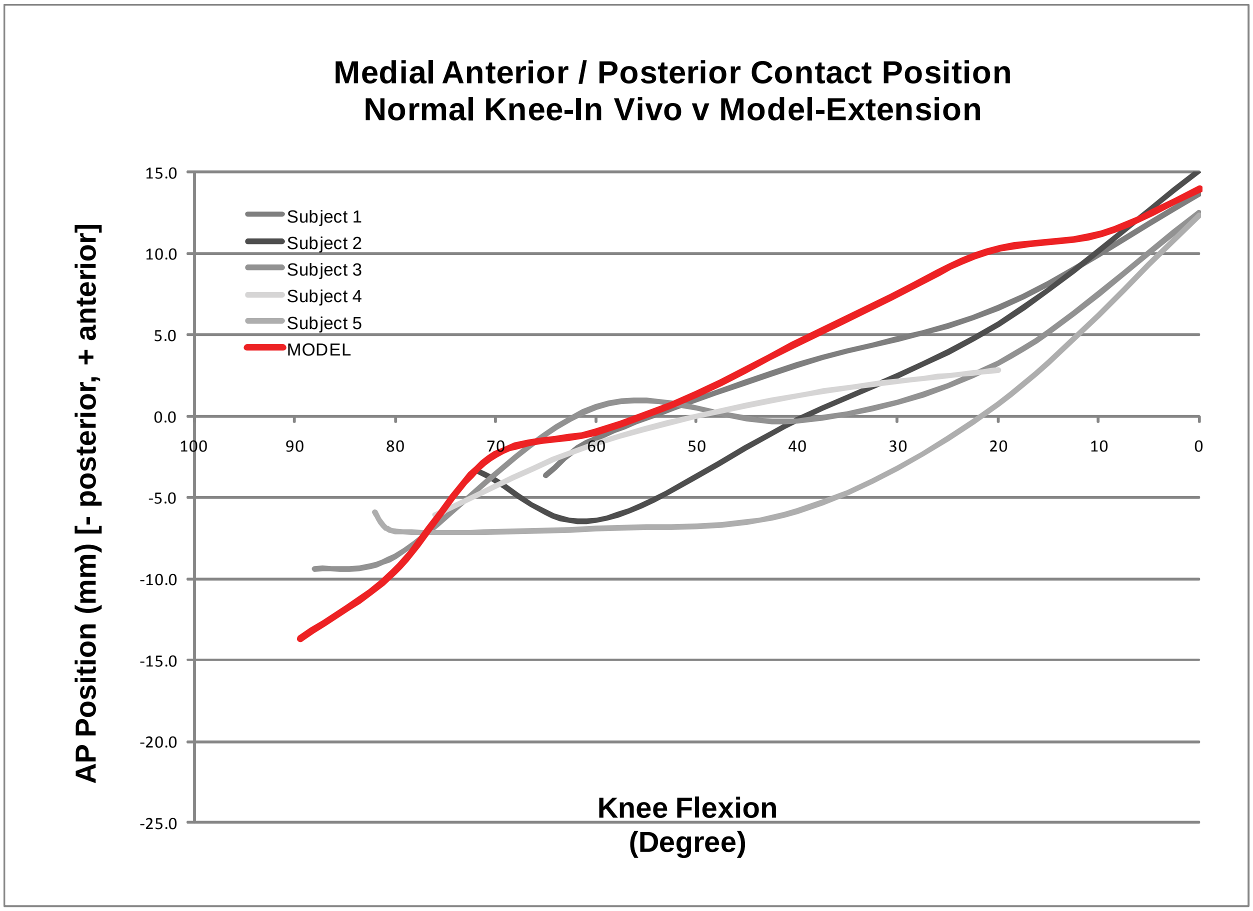

Figure 44: Medial anterior/posterior femorotibial contact position data from fluoroscopy and forward model simulation for a non-weight bearing extension activity. Geometry and soft tissue attachments were determined using models constructed from CT scans from Subject 3.

Normal Knee Weight Bearing Deep Knee Bend Model

The simulated lateral contact point movement matched up well with what was derived in the in vivo study (Figure 46). The trend in the in vivo data was to move in the posterior direction quickly from full extension (0 degrees) to 30 degrees of knee flexion and then to gradually move posteriorly throughout flexion. This trend was also determined to occur in the results derived using the model. Also, the results from the model were similar to Subject 3 with the greatest difference, besides the initial position, being 2.1 mm posterior, occurring at 140 degrees flexion.

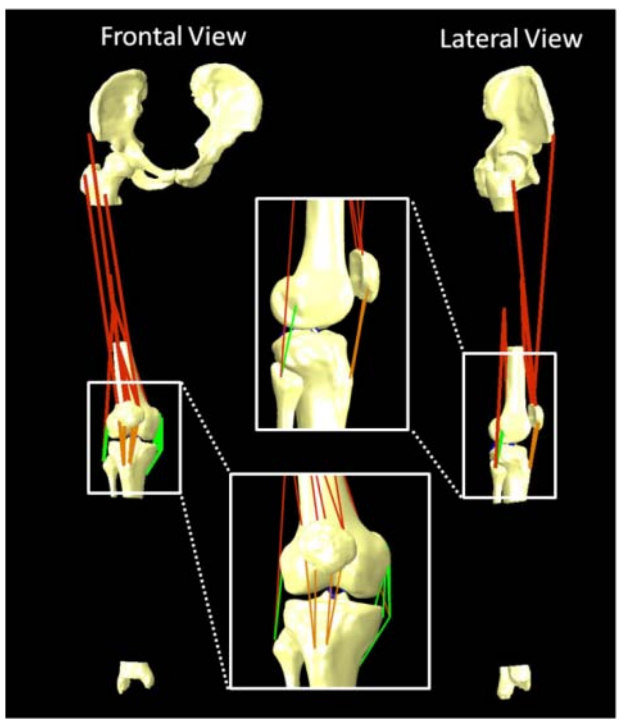

Figure 45: View of the normal deep knee bend simulation at full extension with close up of knee from the lateral and frontal views (inlays).

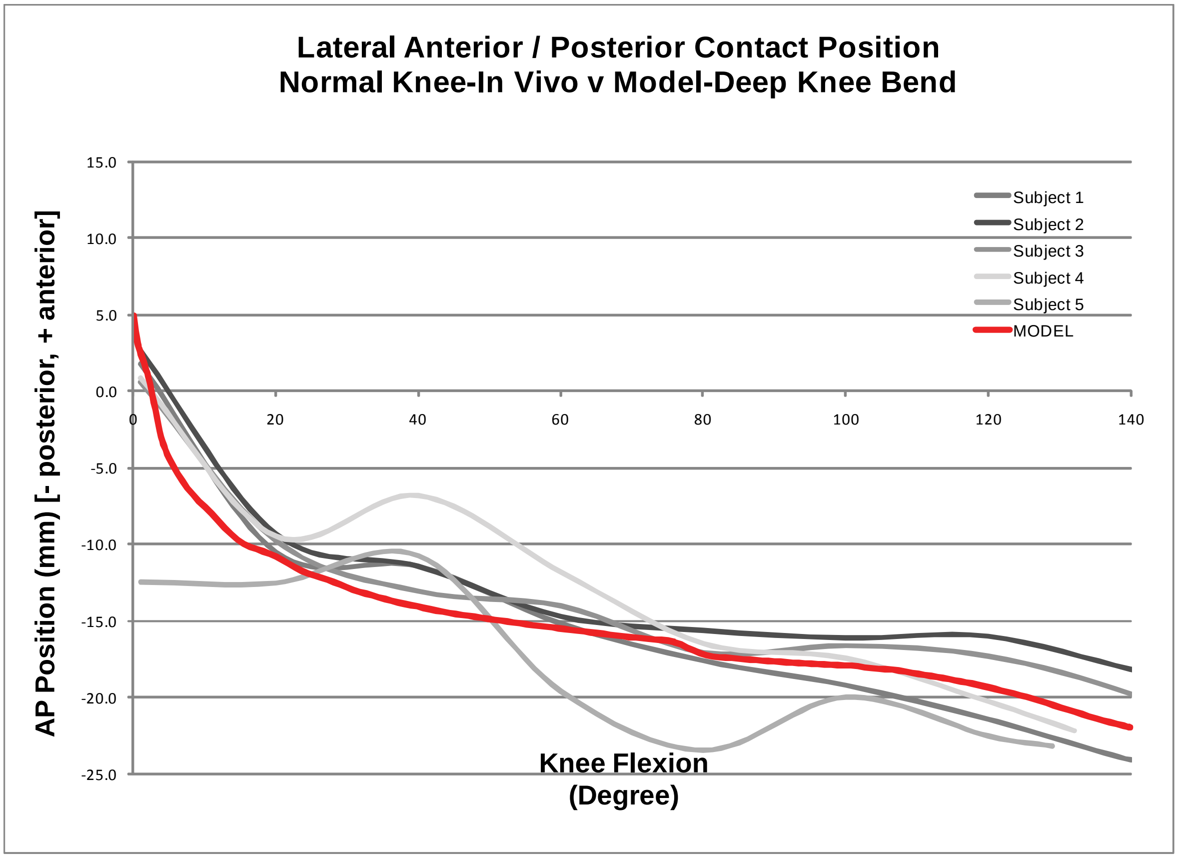

Figure 46: Lateral anterior/posterior femorotibial contact position data from fluoroscopy and forward model simulation for a weight bearing deep knee bend activity. Geometry and soft tissue attachments were determined using models constructed from CT scans of Subject 3.

Similar to the medial condyle in the non-weight bearing simulation, the medial condyle contact positions from the model did not match as well to the in vivo data as the lateral condyle contact positions (Figure 47). The contact point stayed more anterior on the tibia during the simulation. However, the overall movement is similar to the patterns depicted in vivo. The in vivo data was determined to move in the posterior direction during the first 30 degrees of flexion and then for the remainder of the activity, the movement is variable from subject to subject, usually with some anterior slide, unlike the lateral contact point which continues to move posterior. The simulation predicted similar relative movement of the contact point from

30 degrees to maximum flexion. However, from 0 degrees to 30 degrees, the movement was less in magnitude than the in vivo data results. The overall pattern of movement for the contact point was fairly similar to the in vivo data on the medial side.

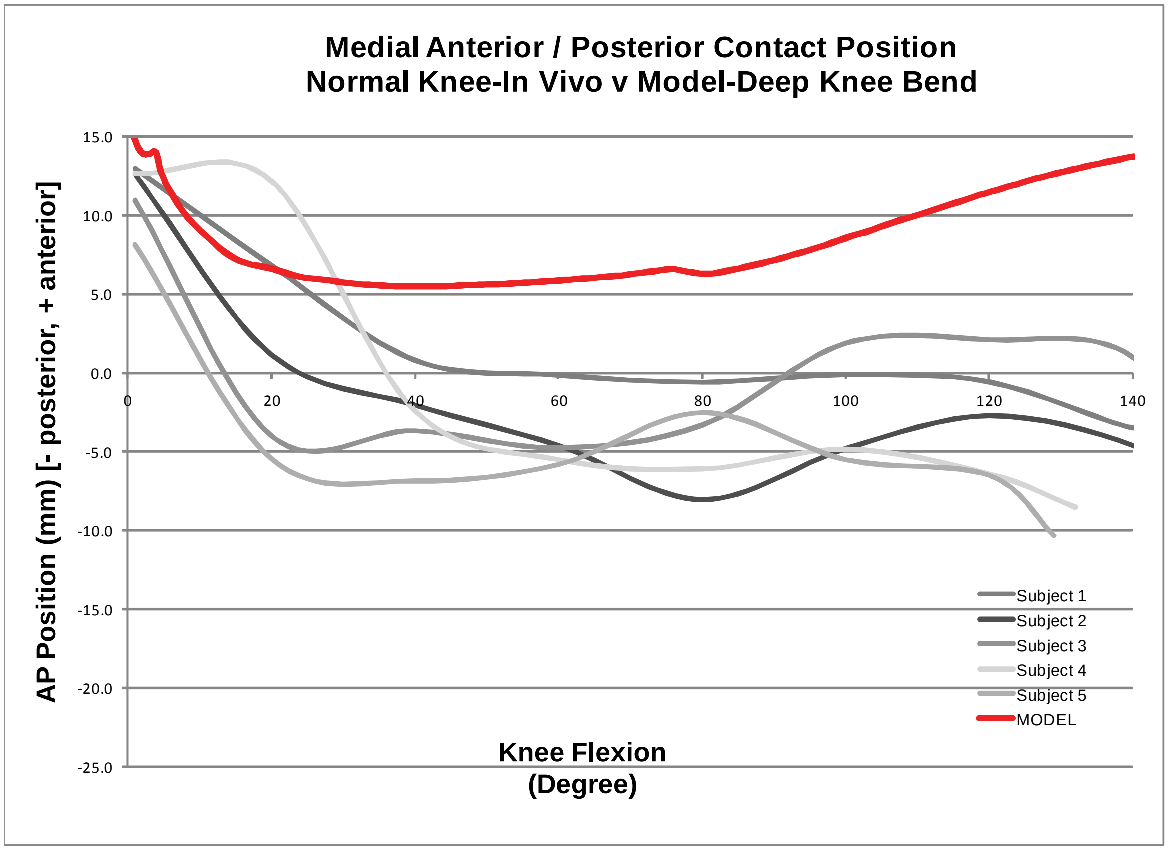

Figure 47: Medial anterior/posterior femorotibial contact position data from fluoroscopy and forward model simulation for a weight bearing deep knee bend activity. Geometry and soft tissue attachments were determined using models constructed from CT scans of Subject 3.

Teletibia Deep Knee Bend Model Validation

The Teletibia TKA implant was implanted to the normal model (Figure 48) and run from full extension to maximum flexion. The ACL and PCL were both removed from the model as this is a cruciate sacrificing design. To further validate the kinematic output and to validate the kinetic output from the model, the articulating geometry of the previously described telemetric TKA was virtually implanted in the normal deep knee bend model. Scans of the implanted subject were not available, therefore, the same parameters (soft tissue attachment, segment mass, length, COM, etc) from the normal model discussed above were used. Only one size of this implant was available. The size of the component CAD models were increased by 10% to fit Subject 3's femur and tibia. The parameters which determine the position of the assumed contact points on the femur and the articulating geometry of the tibial insert were determined using these scaled CAD models. The cruciate ligaments were removed since this particular implant design was a cruciate sacrificing TKA. The only other adjustments made from the normal knee model was the adjustment of the gains (K values) for the quadriceps PID controller. These were adjusted to reduce the oscillation of the quadriceps force and also to minimize the error between the actual and desired flexion for this new model. The kinematic and kinetic results from the model were compared to one subject as data for only one subject with this implant type was available.

The simulation predicted contact positions similar to what was seen in vivo (Figure 49). The general trend was similar, whereas minimal overall motion was detected to occur from full extension (0 degrees) to 120 degrees of knee flexion for both the medial and lateral condyles, compared to the normal knee. The in vivo data that was previously derived, showed that the contact points followed each other closely with the lateral condyle being slightly more posterior than the medial condyle. This pattern was also determined to occur in the simulation, although the offset is slightly less. The simulation predicted more of a posterior position from 10 to 80 degrees of knee flexion, then predicted a more anterior position of the medial condyle from 100 to 120 degrees of knee flexion.

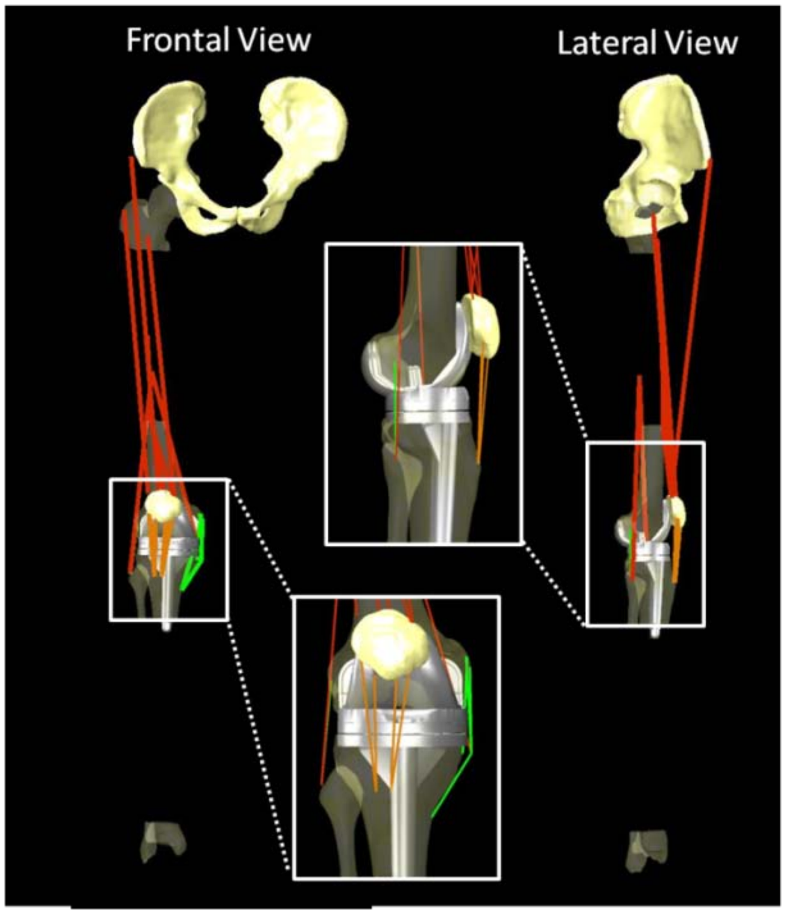

Figure 48: Deep knee bend normal model implanted with the Teletibia TKA. The PCL and ACL were removed for this simulation.

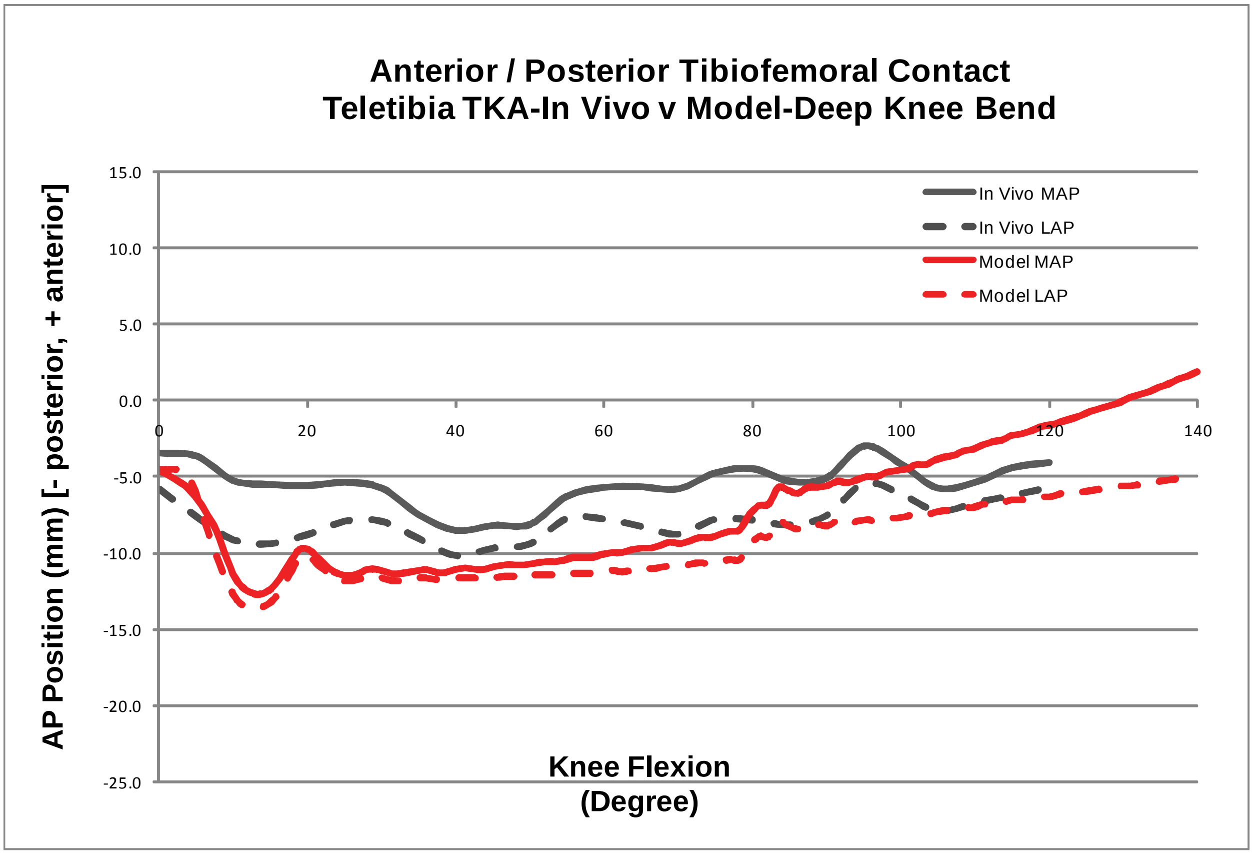

Figure 49: Lateral and Medial anterior/posterior femorotibial contact position data of a weight bearing deep knee bend from fluoroscopy of one subject with an instrumented TKA and forward model simulation with same TKA.

The overall pattern of axial force (the sum of the force at both contact points) simulated using the model was similar to the measured in vivo forces (Figure 50) derived using the telemetric implant, although the simulation underpredicted the force from full extension to 30 degrees of flexion and slighttly overpredicted the force from 30 to 100 degrees of knee flexion. The maximum force from the instrumented TKA was 3.84*BW occurring at 103 degrees of flexion. Using the model, the simulation predicted a maximum force of 3.96*BW at 78 degrees of knee flexion. If only maximum force at any flexion angle was the goal of this comparative analysis, the comparative error was 3.1%. At 103 degrees of knee flexion, the forward model simulation predicted a force of 3.80*BW, an error of 1.0% when compared to the in vivo force data.

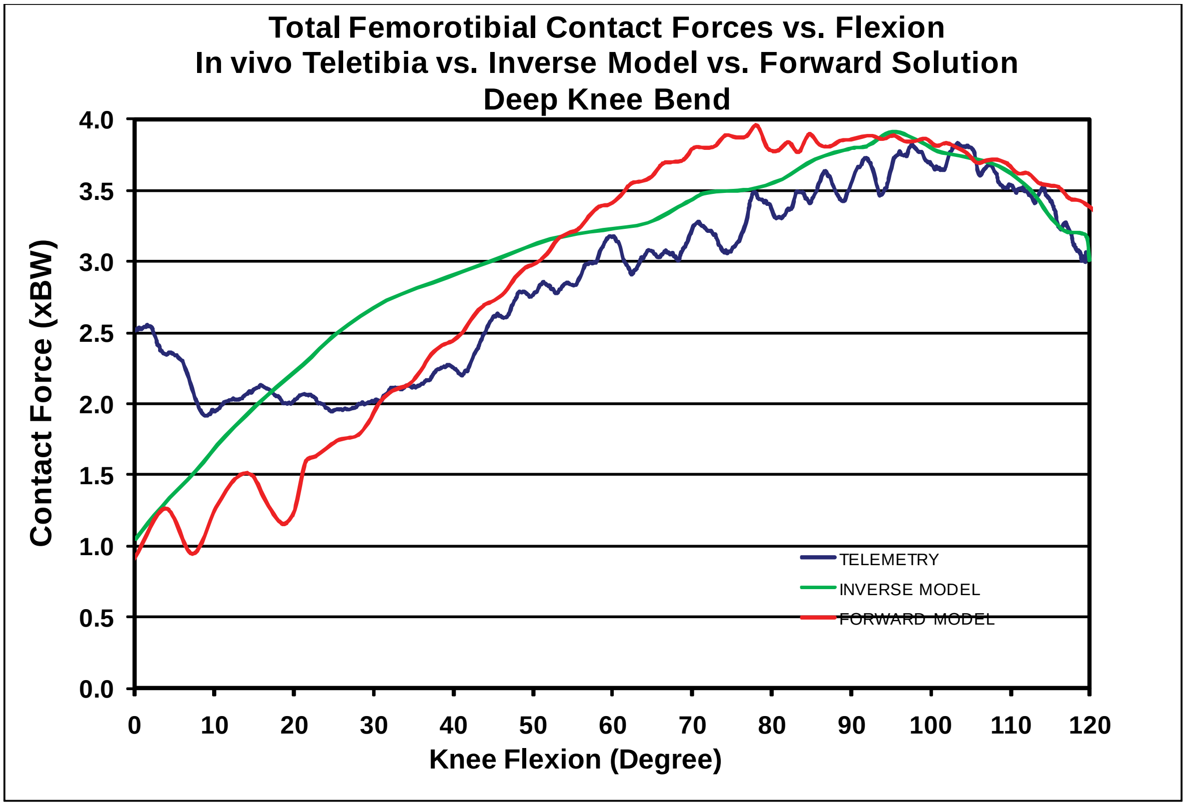

Figure 50: Comparison of the total axial force on the tibia from in vivo data from a subject implanted with an instrumented TKA performing a deep knee bend, a validated inverse model using the in vivo motions of from that subject and a forward simulation of a weight bearing deep knee bend with the same TKA geometry.

The forward solution model slightly underpredicted the lateral force from 0 to 40 degrees and overpredicted the force from 40 to 120 degrees flexion (Figure 51). The overall pattern of the force is consistent with what was determined to occur under in vivo conditions, with the force increasing from 20 to 105 degrees flexion and then decreasing after 105 degrees. The maximum in vivo force of 2.17 BW occurred at 107 degrees flexion. The simulation predicted a maximum force of 2.30 BW at 104 degrees flexion with an error of 6.0%. For comparison, the inverse model also overpredicts the force at times but matches up well with the maximum force at around 105 degrees.

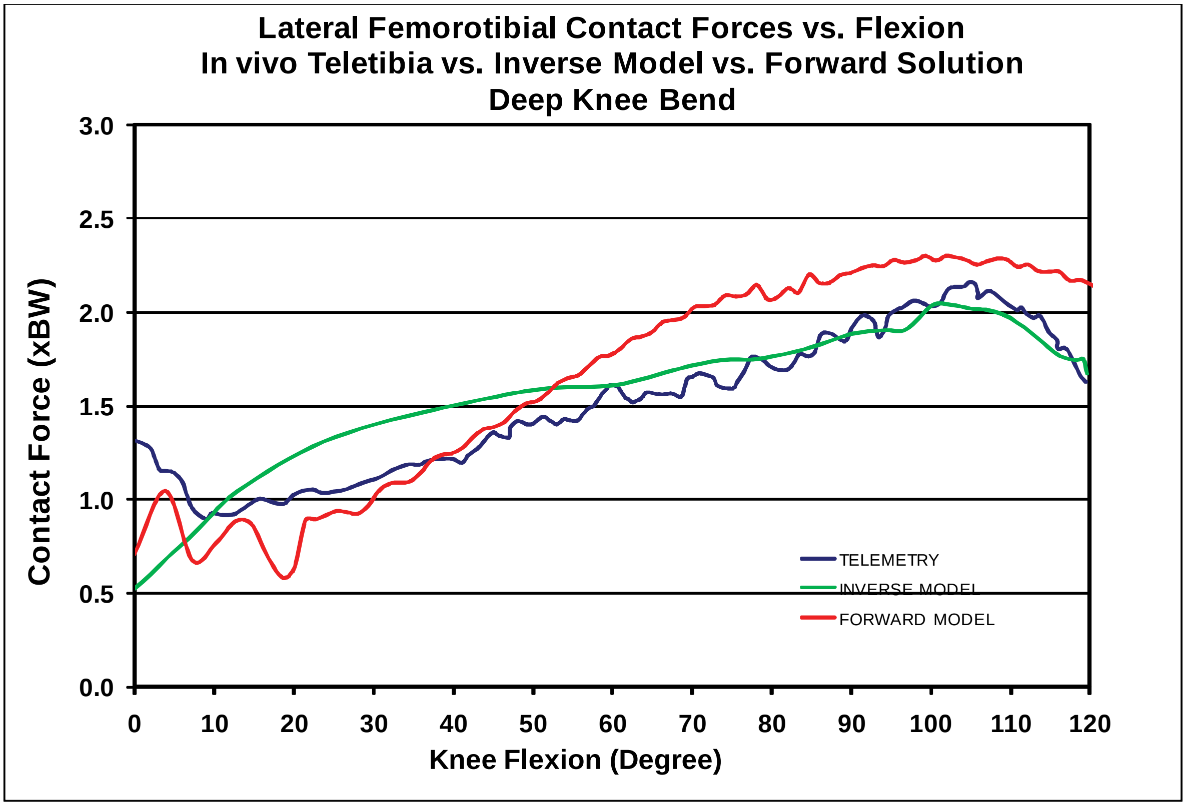

Figure 51: Comparison of the lateral contact force on the tibia from in vivo data from a subject implanted with an instrumented TKA performing a deep knee bend, a validated inverse model using the in vivo motions of from that subject and a forward simulation of the same activity with the same TKA geometry.

The overall pattern of the simulated medial contact force was similar to the in vivo force measurements after 30 degrees of knee flexion (Figure 52). The force was underpredicted from full extension to 30 degrees of flexion. The values matched well from 30 degrees to 80 degrees of knee flexion. Again the forward solution model underpredicted the force from 80 degrees to 120 degrees. The maximum measured force of 1.93 BW occurred at 98 degrees flexion. The maximum simulated force of 1.82 BW occurred at 80 degrees flexion. Again, if the goal was to determine the magnitude of the maximum force at any flexion angle,the comparative error was

5.7%. At 98 degrees flexion the simulation predicted a force of 1.57 BW with 18.7% error compared to the in vivo data.

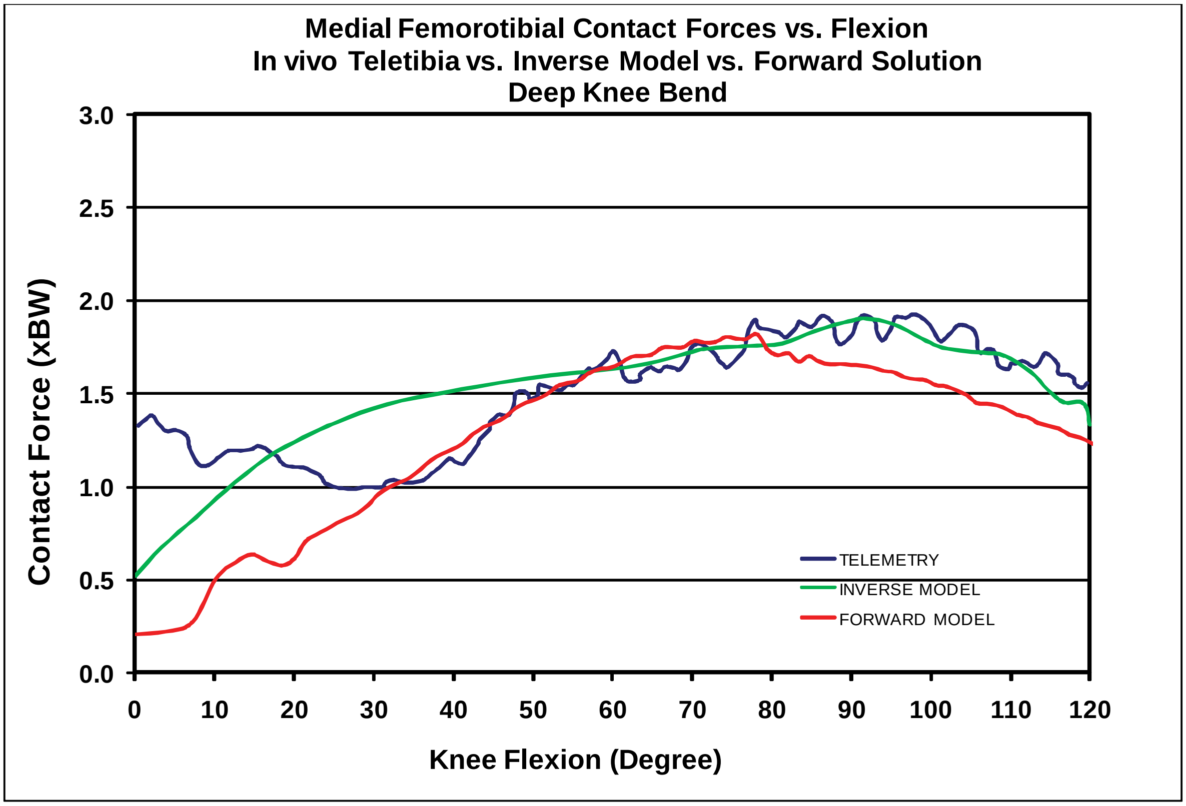

Figure 52: Comparison of the medial contact force on the tibia from in vivo data from a subject implanted with an instrumented TKA performing a deep knee bend, a validated inverse model using the in vivo motions from that subject and a forward simulation of the same activity with the same TKA geometry.

Chapter 5: Extension Model

Anterior/Posterior Tibiofemoral Positions

Medial Pivot TKA

In Vivo Kinematics Medial Pivot TKA

For 20 Medial Pivot TKA the average in vivo AP femorotibial, relative to the tibial component, (positive values indicate a position anterior of the component midline and negative numbers indicate a posterior position) contact position obtained using fluoroscopic analysis at initial extension (with an average knee angle of 80.2° (62° to 97°, SD=9.3°)) was -4.2 mm (-6.8 mm to 2.7 mm, SD=2.3 mm) and -3.5 mm (-7.8 mm to 3.0 mm, SD=2.4) for the medial and lateral condyle, respectively. At 40° of knee flexion, the medial and lateral contact point positions were -5.6 mm (-10.7 mm to 0.8 mm, SD=2.4 mm) and -2.3 mm (-6.7 mm to 1.4 mm, SD=2.0 mm), respectively. This resulted in 1.2 mm (-3.1 mm to 5.9 mm, SD=2.6 mm) and -1.4 mm (-8.2 mm to 1.4 mm, SD=2.1 mm) of medial and lateral of change in the contact position, respectively, where negative values indicate posterior motion and positive values indicate anterior motion.

At 20° of knee flexion, the medial and lateral AP contact positions were -6.2 mm (-11.8 mm to -2.9 mm, SD=2.0 mm) and -3.4 mm (-6.6 mm to 0.5 mm, SD=1.7 mm), respectively. This resulted in -2.0 mm (-9.4 mm to 1.6 mm, SD=2.8 mm) and 0.1 mm (-5.5 mm to 4.7 mm, SD=2.9 mm) of the medial and lateral condyle motion, respectively. Six (30%) subjects experienced anterior movement on the medial condyle and nine (55%) TKA experienced anterior movement on the lateral side from initial extension to 20° of knee flexion.

At full extension, the contact position was -6.8 mm (-10.2 mm to -4.0 mm, SD=1.5 mm) and -3.9 mm (-6.7 mm to 1.0 mm, SD=2.0 mm) for the medial and lateral condyles, respectively. The average overall movement from initial extension to full extension was -2.5 mm (-9.4 mm to 1.0 mm, SD=2.6 mm) and -0.4 (-7.7 mm to 5.5 mm, SD=3.3 mm). Three (15%) and nine (45%) of TKA analyzed in this study experienced anterior movement of the medial and lateral condyles, respectively, from initial extension to full extension.

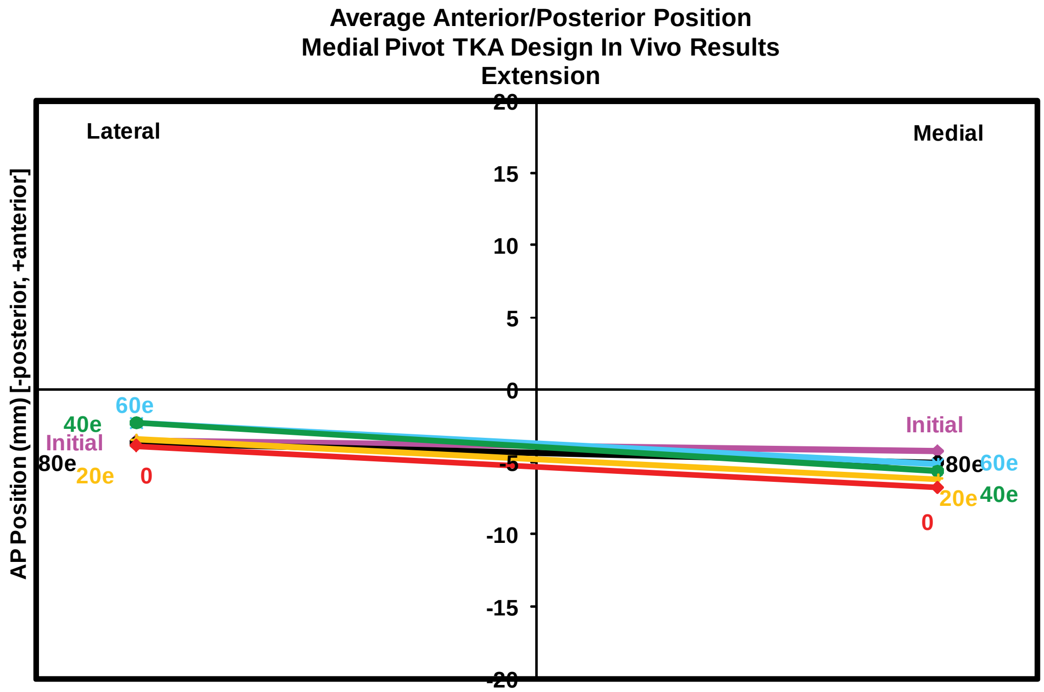

Figure 53: Anterior/Posterior in vivo tibiofemoral contact position for a non-weight bearing extension activity from initial extension to full extension obtained using fluoroscopic surveillance on 20 patients implanted with the Medial Pivot TKA.

Model Results

The simulation of the non-weight bearing extension activity with the Medial Pivot TKA design produced medial and lateral AP contact positions of -0.2 mm and -1.2 mm, respectively, at the initial position, which occurred when the knee was flexed at 90°. At 40° of knee flexion, the medial and lateral contact points moved in different direction, to the positions of 1.9 mm and -3.1 mm, respectively, resulting in 2.1 mm and -1.9 mm medial and lateral contact motion. The model predicted more anterior movement of the condylar contact points but within one standard deviation of the in vivo average, while the theoretical simulation predicted more posterior movement on the medial side, although this was also within the one standard deviation of the average for the in vivo data.

At full extension the model predicted a contact point of -8.2 mm and -10.0 mm for the medial and lateral sides resulting in -8.0 mm and -8.8 mm posterior medial and lateral movement. Although the medial condyle contact movement and position was still within the range seen in vivo it was outside one standard deviation of the average for these subjects. The model simulated more posterior contact position and movement on the lateral side than was seen in the in vivo data.

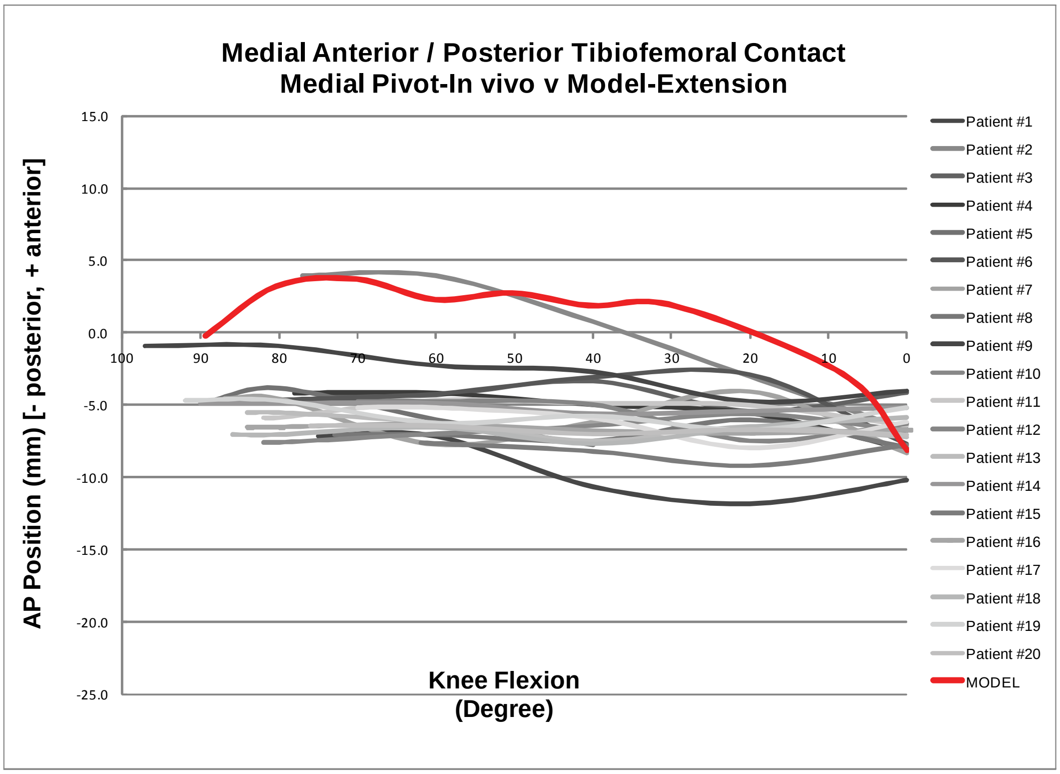

Figure 54: Anterior/posterior position of the medial tibiofemoral contact position of a Medial Pivot TKA from in vivo data obtained using fluoroscopy and simulated data obtained from the forward solution model.

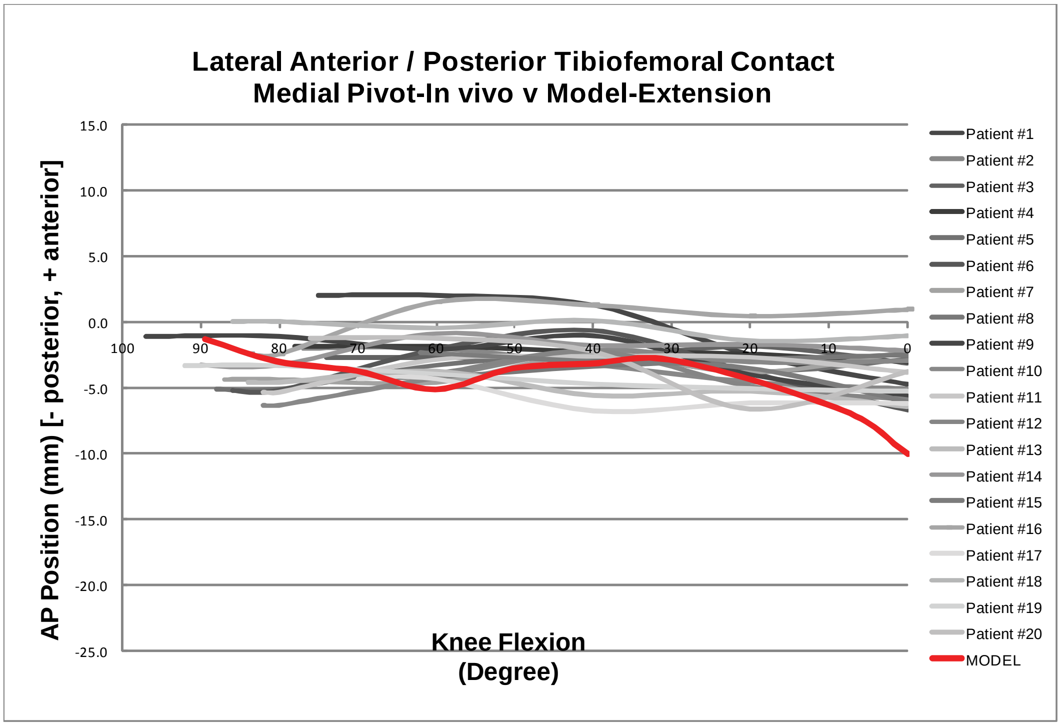

Figure 55: Anterior/posterior position of the lateral tibiofemoral contact position of a Medial Pivot TKA from in vivo data obtained using fluoroscopy and simulated data obtained from the forward solution model.

Quadriceps, Patella Ligament, Tibiofemoral and Patellofemoral Forces

The quadriceps forces for the normal and Medial Pivot TKA models increased from initial extension to a maximum of 1.00 BW and 0.85 BW, respectively at full extension. The patella ligament forces increased with the quadriceps force with the quadriceps to patella ligament force ratio reaching 1.00 for the normal simulation and 0.87 for the Medial Pivot TKA. The tibiofemoral forces were higher for the Medial Pivot design with 2.24 BW than the normal which saw a maximum of 1.26 BW. The model also predicted that the Medial Pivot design experienced a maximum patellofemoral force of 0.80 BW as opposed to the normal knee which saw a maximum of 0.56 BW. Both simulations predicted that the patellofemoral forces 0 BW at full extension. This result makes sense as the quadriceps force is acting roughly parallel to the patellofemoral contact surface at full extension. The patellofemoral force to quadriceps force ratio was the greatest at initial flexion with the Medial Pivot TKA design value a little over 1.00 and the normal value slightly less than 1.00. This ratio goes to 0.00 as the patellofemoral force goes to 0.00 in later extension.

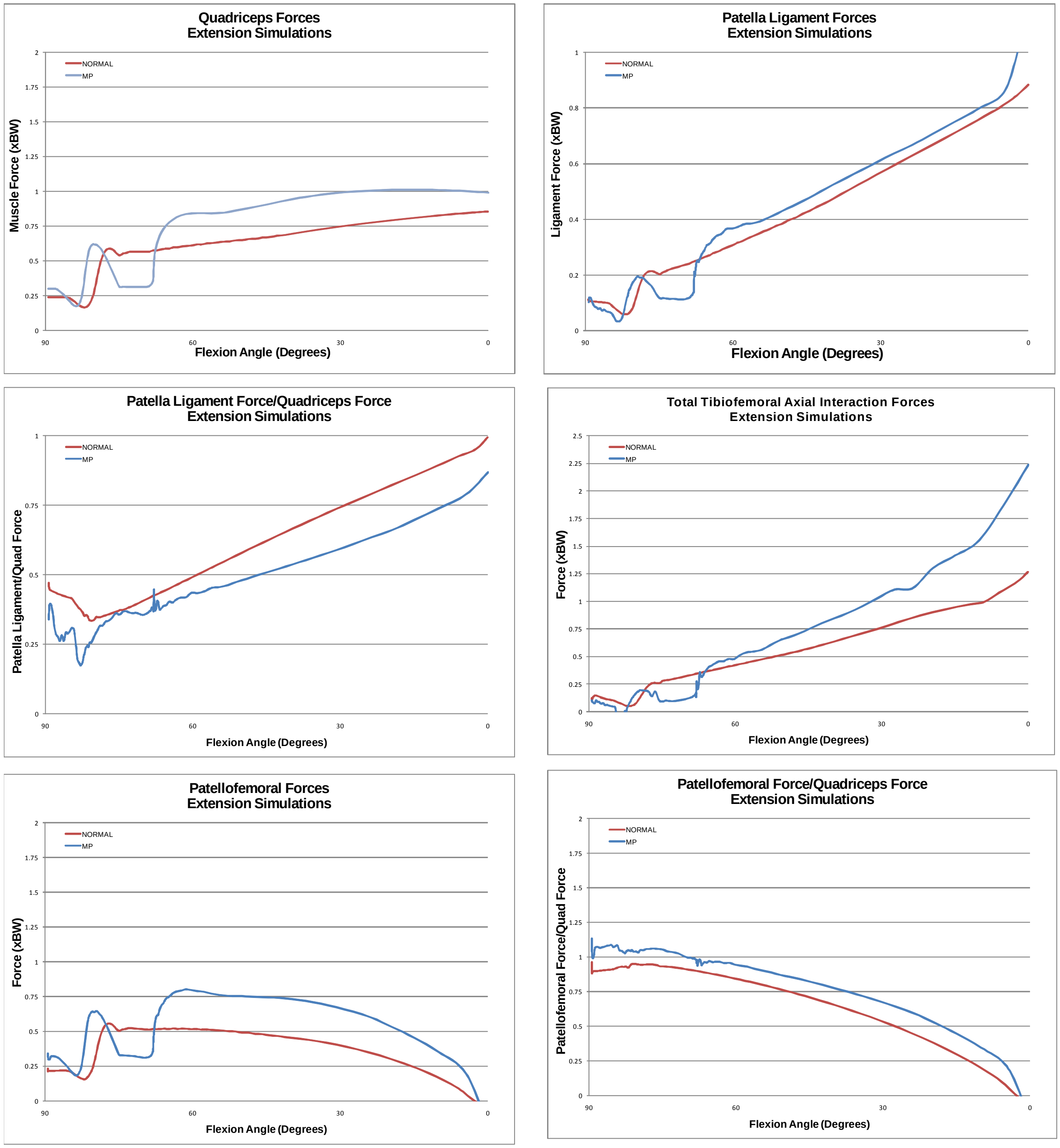

Figure 56: Quadriceps force, patella ligament force, patella ligament force to quadriceps force ratio, tibiofemoral axial force, patellofemoral force and patellofemoral to quadriceps force ratio for the extension simulations of a normal knee and Medial Pivot TKA design.

Knee Ligament Forces

In general the collateral ligaments were much more active in the Medial Pivot TKA design than in the normal knee simulation. The lateral collateral ligament increased throughout knee extension for both the normal and Medial Pivot design, but the Medial Pivot design had a maximum of 0.66 BW where the normal maximum was only 0.09 BW. The maximum medial collateral ligament force in the Medial Pivot TKA design was 0.49 BW at full extension with a maximum of 0.43 BW at 27° flexion. The normal knee model predicted the force in the ACL to be 0.1 BW at full extension. The maximum force in the PCL was higher in the normal simulation, with a maximum of 0.27 BW, compared to only 0.19 BW in the Medial Pivot design. Again, these findings are reasonable because it has been previously hypothesized that the PCL does not function properly in all subjects, post TKA.

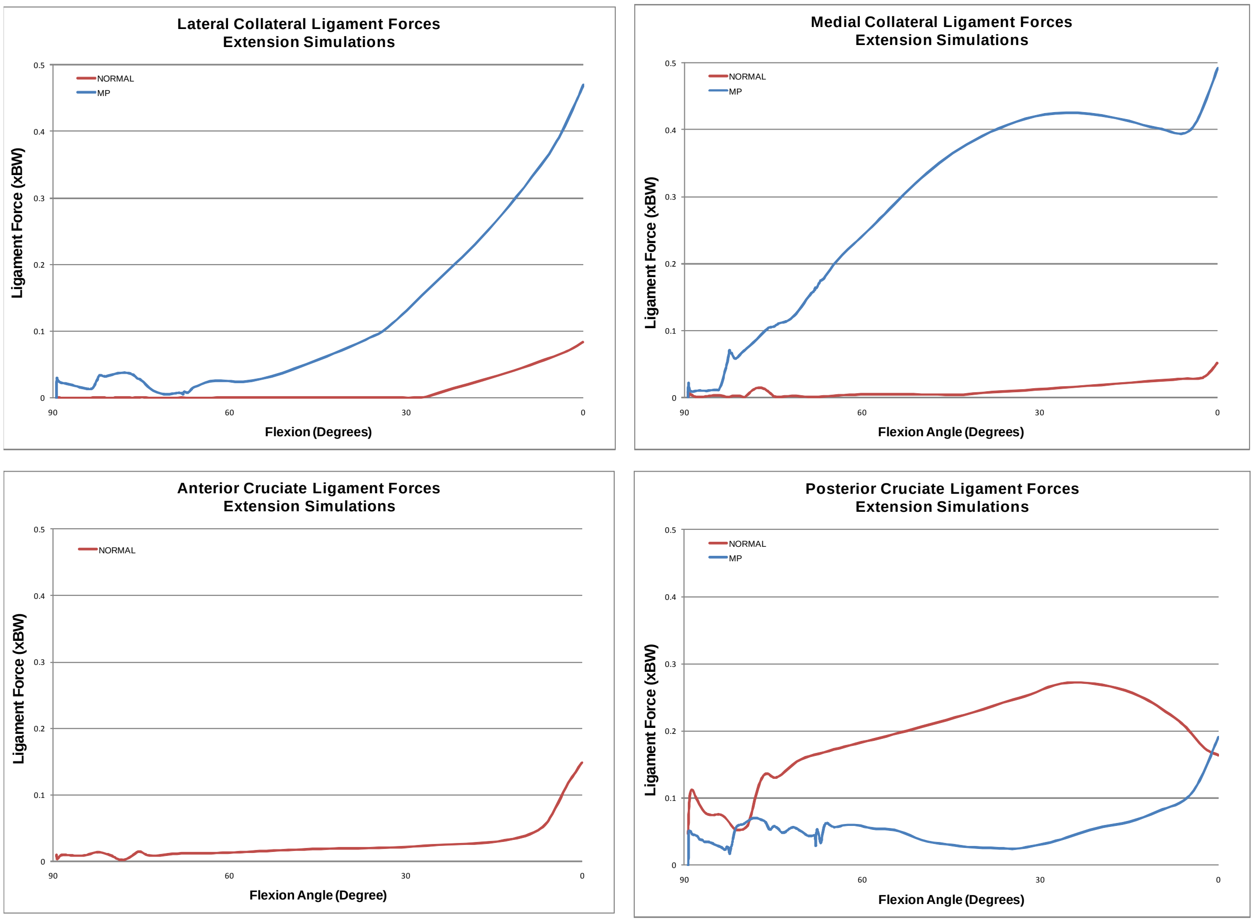

Figure 57: Lateral collateral, medial collateral, anterior cruciate and posterior cruciate ligament forces for the extension simulations of a normal knee and Medial Pivot TKA design.

Chapter 6: Deep Knee Bend Model

Anterior/Posterior Tibiofemoral Positions

Medial Pivot TKA

In Vivo Kinematics Medial Pivot TKA

For all 20 Medial Pivot TKA in which in vivo tibiofemoral contact kinematics were determined using fluoroscopy, the average medial and lateral condyle contact position at full extension was -6.9 mm (-10.5 mm to -5.3 mm, SD=1.3 mm) and -4.8 mm (-10.0 mm to -0.5 mm, SD=2.5 mm), respectively. At 100° weight bearing flexion, achieved by 15 (75%) of the TKA analyzed (including two in which 100° was the maximum flexion reached), the average medial and lateral condyle contact positions were -6.0 mm (-11.2 mm to -2.3 mm, SD=2.2 mm) and -7.4 mm (-11.4 mm to -1.6 mm, SD=3.2 mm). For the 15 TKA which reached 100°, this resulted in 0.8 mm (-1.2 mm to 3.6 mm, SD=1.4 mm) and -2.7 mm (-8.1 mm to 2.0 mm, SD=3.2 mm) medial and lateral contact point translation, respectively.

The in vivo tibiofemoral contact position for the six (30%) Medial Pivot TKA which achieved 120° weight bearing flexion (including one TKA in which 120° was the maximum) was -7.5 mm (-13.5 mm to -3.0 mm, SD=3.5 mm) and -8.9 mm (-13.9 mm to -5.7 mm, SD=3.0mm) for the medial and lateral condyles, respectively. This resulted in -0.7 mm (-6.7 mm to 2.9 mm, SD=3.3 mm) and -3.6 mm (-5.2 mm to -1.3 mm, SD=1.4 mm) of medial and lateral condylar contact movement in the six TKA which achieved from full extension to 120° weight bearing flexion, respectively.

At maximum weight bearing knee flexion for all 20 of the TKA, which averaged 105° (70° to 130°, SD=17°), the average medial condyle contact position was -7.0 mm (-13.7 mm to -2.2 mm, SD=-2.8 mm) and the lateral contact position moved in the posterior direction to -7.8 mm (-16.7 mm to 0.3 mm, SD=3.7 mm). Therefore, from full extension to each subject's maximum knee flexion, the average amount of posterior femoral rollback for the medial condyle was -0.1 mm (-6.9 mm to 3.4 mm, SD=2.3 mm) and the average amount of posterior femoral rollback for the lateral condyle was -3.0 mm (-8.1 mm to -2.3 mm, SD=3.0 mm) (Figure 58). Eight (40%) and 18 (90%) of the 20 TKA analyzed in this study experienced posterior motion of the medial and lateral contact points, respectively.

On average, in mid-flexion there was some anterior movement of the medial and lateral contact points and for the most part those TKA which exceeded the average 105° weight bearing flexion (Figure 58), the position of the lateral condyle was more posterior than those TKA which reached less than the average weight bearing flexion for this group. In summary, under in vivo conditions, this TKA experienced minimal movement of the medial condyle from full extension to maximum weight bearing flexion and a gradual posterior motion of the lateral condyle from full extension to maximum weight bearing flexion.

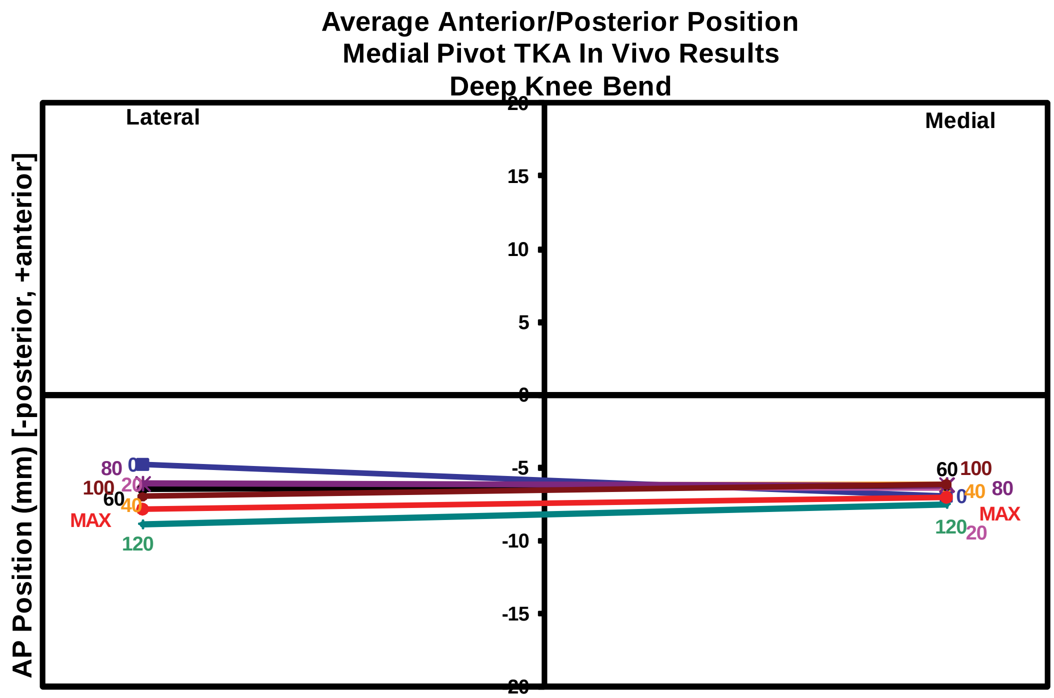

Figure 58: Average anterior/posterior contact positions obtained in vivo using fluoroscopy for 20 ADVANCE® Medial-Pivot TKA during a deep knee bend.

Medial Pivot TKA Model Results

At full extension, the initial contact positions of the medial and lateral condyles for the Medial Pivot TKA simulation were -8.3 mm and -8.5 mm (Figure 59-Figure 60). At 100° of knee flexion, the contact position of the medial and lateral condylar contact positions were -8.2 mm and -11.8 mm resulting in 0.1 mm of translation of the medial contact point in the anterior direction and -3.3 mm motion of the lateral condyle in the posterior direction. Comparing the results of the model to the average contact point movement of the 15 (75%) TKA which reached 100° weight bearing flexion in the in vivo study, there is a difference of -0.7 mm and -0.6 mm for the medial and lateral condyles, respectively. The amounts of translation seen in the simulation pertaining to both the medial and lateral condyles are within the minimum and maximum values observed under in vivo conditions and within one standard deviation of the average determined for the in vivo subjects.

At 120° of knee flexion, the simulated contact points for the medial and lateral side were -8.2 mm and -13.8 mm, respectively, resulting in 0.1 mm and -5.3 mm of condylar contact movement, respectively, from full extension to 120° of simulated weight bearing flexion. Compared to in vivo results, there was a difference of -0.8 mm and -1.7 mm in contact translation. The results pertaining to the medial condyle were well within one standard deviation of the average in vivo results. The simulation predicted greater posterior motion of the lateral side than was determined under in vivo conditions, with the overall motion being -0.2 mm outside the one standard deviation envelope. The small number of TKA included in the data set at 120° must be considered.

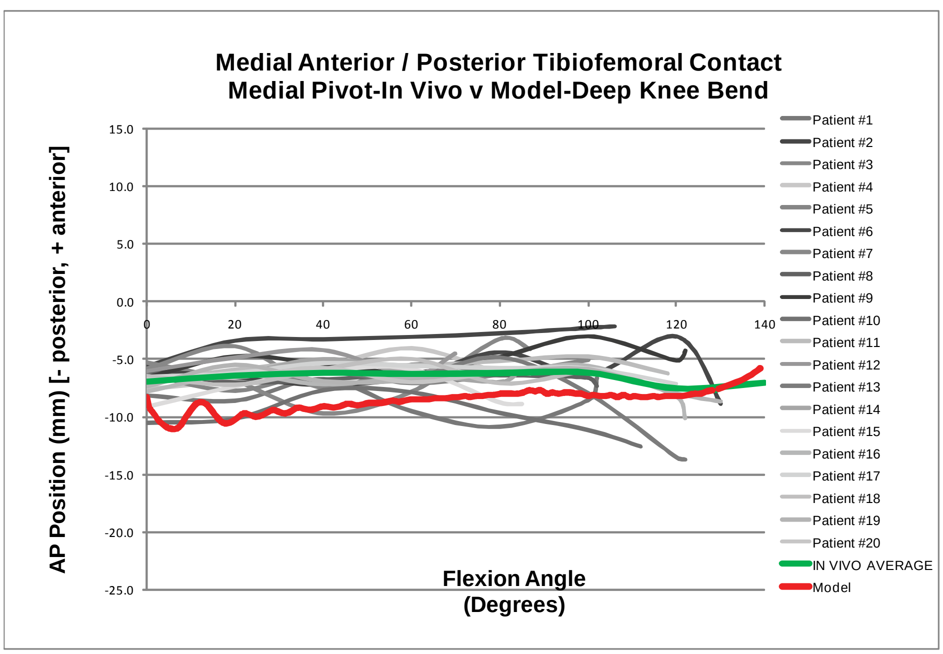

Figure 59: Anterior/posterior position of the medial tibiofemoral contact position of a Medial Pivot TKA from in vivo data obtained using fluoroscopy and simulated data obtained from the forward solution model.

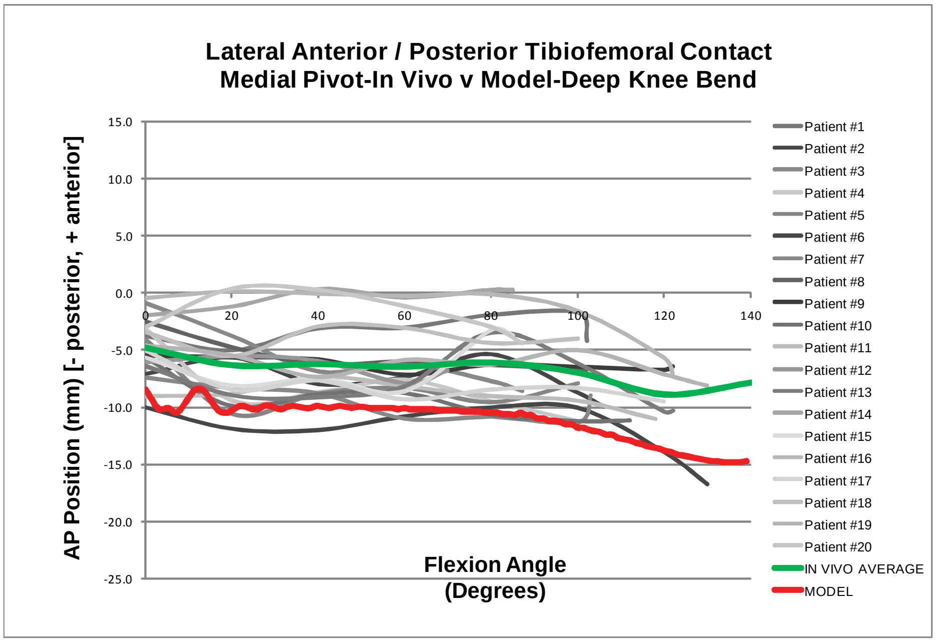

Figure 60: Anterior/posterior position of the lateral tibiofemoral contact position of a Medial Pivot TKA from in vivo data obtained using fluoroscopy and simulated data obtained from the forward solution model.

Natural Knee II Cruciate Retaining TKA with Congruent Polyethylene Insert

In Vivo Kinematics NKII CPE

On average, the 36 subjects implanted with a cruciate retaining NKII TKA with CPE inserts experienced anterior movement of the medial condyle and posterior femoral rollback of the lateral condyle contact position from full extension to maximum flexion (Figure 61) [Mueller 2009]. Contact positions at full extension for subjects with a NKII CR TKA with a CPE insert for the medial condyle averaged 1.1 mm (-2.5 to 7.1 mm, SD=1.9) and the lateral condyle averaged -1.0 mm (-6.9 to 5.0 mm, SD=2.5). At 90° of weight bearing knee flexion, the contact point positions for all 36 TKA for the medial condyle averaged 2.5 mm (-2.6mm to 10.1 mm, SD=2.9

mm) and -6.4 mm (-11.4 mm to -0.8 mm, SD=2.1 mm) for the lateral condyle. As a result, the condylar contact movement was 1.4 mm (-5.6 mm to 6.6 mm, SD=2.6 mm) and -5.5 mm (-10.8 mm to 0.3 mm, SD=2.6 mm) for the medial and lateral condyles, respectively. At 120° of knee flexion, of which 12 TKA (33%) experienced, the medial condyle contact position was 3.8 mm (-0.7 mm to 9.2 mm, SD=3.0 mm) and the lateral condyle contact position was -8.6 mm (-11.5 mm to -4.1 mm, SD=2.5 mm) resulting in 2.3 mm (-3.3 mm to -7.8 mm, SD=2.8 mm) and -7.8 mm (-12.3 mm to -1.8 mm, SD=3.0 mm) of condylar movement for the medial and lateral condyles, respectively.

At maximum knee flexion, for all TKA in this group, which averaged 112° (90° to 132°, SD=12.8°), the medial condyle contact position averaged a position of 2.7 mm (-5.6 to 8.8 mm, SD=3.2) anterior of the midline and -7.7 mm (-18.0 to -0.6 mm, SD=3.8) posterior for the lateral condyle. From full extension to maximum knee flexion, the condylar contact position moved 1.5 mm (-4.3 to 8.0 mm, SD=2.6) in the anterior direction for the medial condyle and -6.7 mm (-14.1 to 0.3 mm SD=3.7) in the posterior direction for the lateral condyle. Six of the 36 subjects (16.7%) experienced PFR of the medial condyle and all but one of the subjects experienced PFR of the lateral condyle (97.2%).

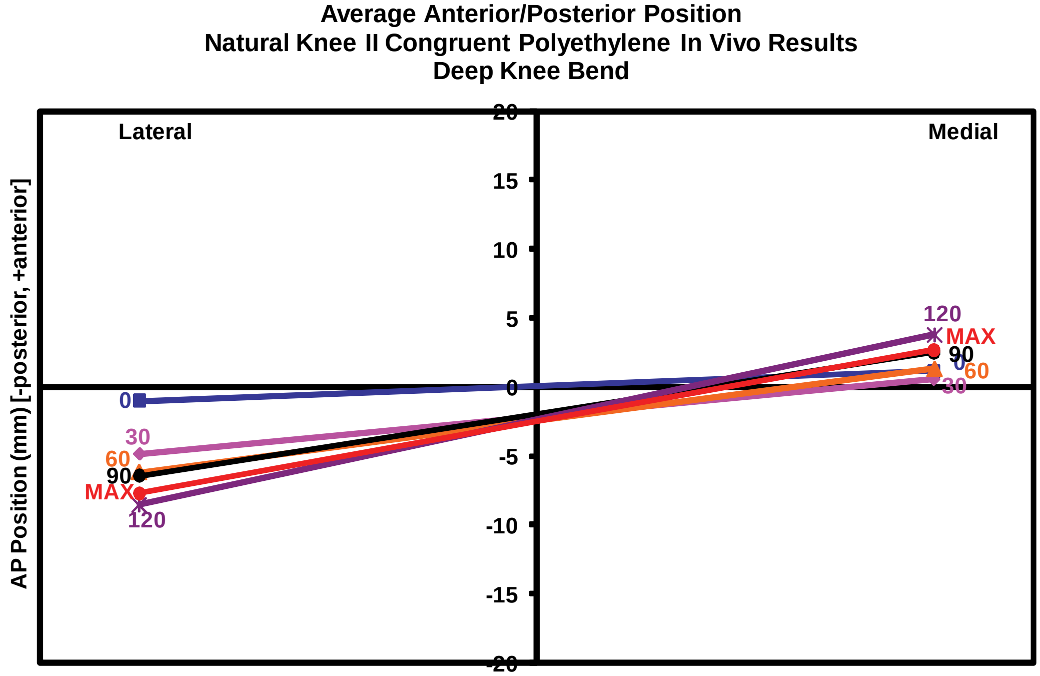

Figure 61: Average anterior/posterior contact positions obtained in vivo using fluoroscopy for 36 NKII Congruent Polyethylene TKA during a deep knee bend.

NKII CPE Model Results

For the deep knee bend simulation pertaining to the NK II CR TKA having a CPE insert the AP position for both the medial and lateral condyles was 0.3 mm (Figure 62 and Figure 63). At 90° of knee flexion the medial contact point moved in the posterior direction -4.4 mm, while the lateral condyle moved in the posterior direction -7.1 mm, resulting in AP contact point movement of -3.9 mm and -6.8 mm for the medial and lateral condyles, respectively. The medial condyle moved more posterior in the simulation than was determined to occur, on average, under in vivo conditions from full extension to 90° of knee flexion and this result was outside of one standard deviation of the average. The medial contact movement results were within the minimum and maximum translations seen in the in vivo study with two of the 36 TKA (5.6%) having more posterior motion than the simulation. The lateral condyle contact movement derived in the simulation was also greater in the posterior direction than the average in vivo results, but still within one standard deviation of the in vivo average and 9 of the 36 TKA (25%) achieving greater posterior motion from full extension to 90° flexion.

At 120° of knee flexion, the simulated medial and lateral condyle contact positions for this design were -3.7 mm and -7.8 mm, resulting in -3.4 mm and -7.5 mm of posterior movement for the medial and lateral condyles, respectively. This simulation predicted the medial condyle posterior movement to be slightly greater than the TKA subject (under in vivo conditions) having the most posterior movement in the in vivo study. The lateral condyle experienced slightly less posterior motion than the in vivo results, but was well within one standard deviation of the average.

The maximum simulated weight bearing flexion was 140°. The medial and lateral condyle contact positions, at maximum weight bearing flexion, were -0.4 mm and -6.3 mm for the medial and lateral condyles, respectively. Therefore, the overall motion was -0.1 mm and -6.0 mm of posterior motion for the medial and lateral condyle contact points, respectively. Although the maximum flexion for the in vivo group average 112° and revealed a maximum of 130°, comparing the simulation to the in vivo results, the total motion of the medial and lateral condyle from full extension to maximum flexion were well within one standard deviation of the average in vivo values.

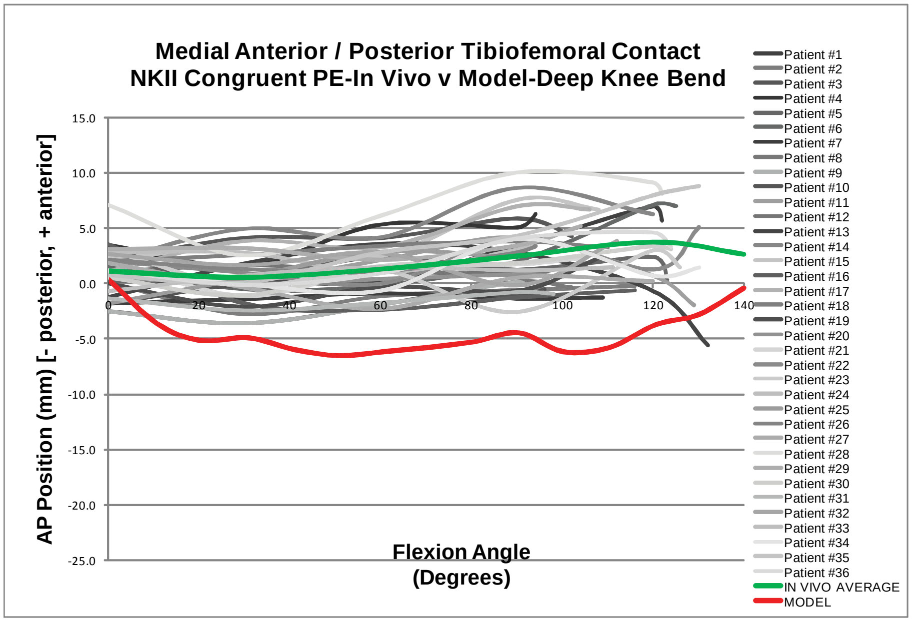

Figure 62: Anterior/posterior position of the medial tibiofemoral contact position of a Natural Knee II CR TKA with congruent polyethylene insert from in vivo data obtained using fluoroscopy and simulated data obtained from the forward solution model. The average in vivo value at 140° flexion is the average position at maximum flexion for all TKA.

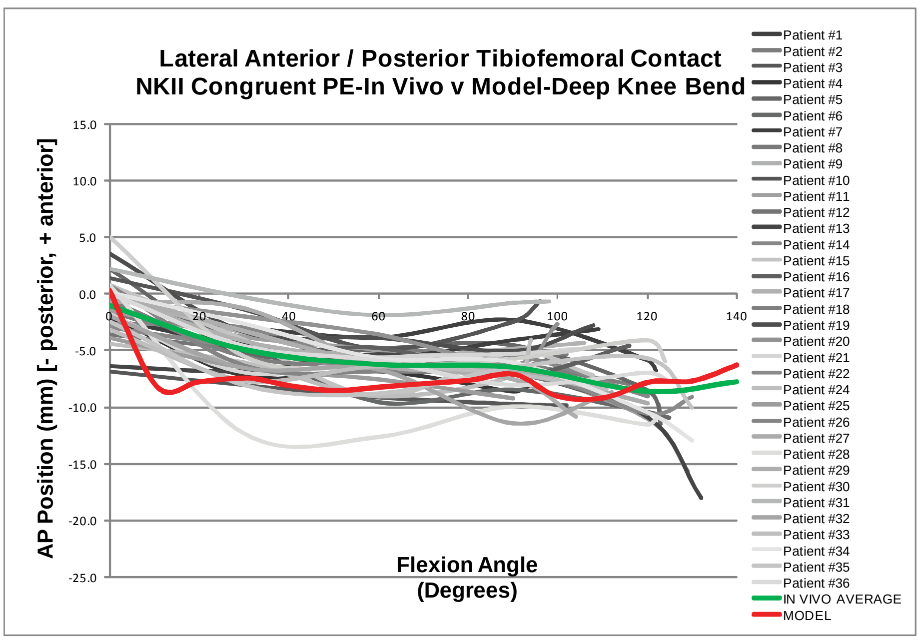

Figure 63: Anterior/posterior position of the lateral tibiofemoral contact position of a Natural Knee II CR TKA with congruent polyethylene insert from in vivo data obtained using fluoroscopy and simulated data obtained from the forward solution model. The average in vivo value at 140° flexion is the average position at maximum flexion for all TKA.

Natural Knee II TKA with UltraCongruent Polyethylene Insert

In Vivo Kinematics NKII UCPE

On average, from full extension to maximum knee flexion, the four subjects analyzed with NKII UCPE TKA experienced posterior femoral rollback of the lateral condyle and anterior paradoxical slide of the medial condyle. At full extension, the average medial and lateral condyle contact positions were -3.6 mm (-2.2 to -4.5 mm, SD=1.0) and -4.9 mm (-3.2 to -6.2 mm, SD=1.5), respectively (Figure 64). At 90° of knee flexion, of which all (100%) of the TKA in this study achieved, the medial and lateral condylar contact positions were -2.4 mm (-4.6 mm to -1.6 mm, SD=1.5 mm) and -7.6 mm (-9.0 mm to -5.8 mm, SD=1.5 mm) resulting in 1.3 mm (-0.7 mm to 2.7 mm, SD=1.6 mm) and -2.7 mm (-5.8 mm to 0.4 mm, SD=2.5 mm) of contact movement from full extension to 90° flexion.

At maximum knee flexion, which averaged 106° (96° to 122°, SD=11.5°) for these subjects, the average medial contact position moved in the anterior direction to -2.2 mm (-3.4 mm to -1.5 mm, SD=0.8) and the average lateral condyle contact position moved posteriorly to -7.9 mm (-11.2 mm to -6.6 mm, SD=2.2). From full extension to maximum knee flexion, the average movement for the medial condyle was 1.4 mm (2.5 to -1.2 mm, SD=1.8) in the anterior direction and the average amount of motion for the lateral condyle was -3.0 mm (-8.0 mm to -0.4 mm, SD=3.5) in the posterior direction. One (25%) of the NK II UCPE TKA experienced posterior motion of the medial condyle and 100% of the subjects experienced posterior motion of the lateral condyle.

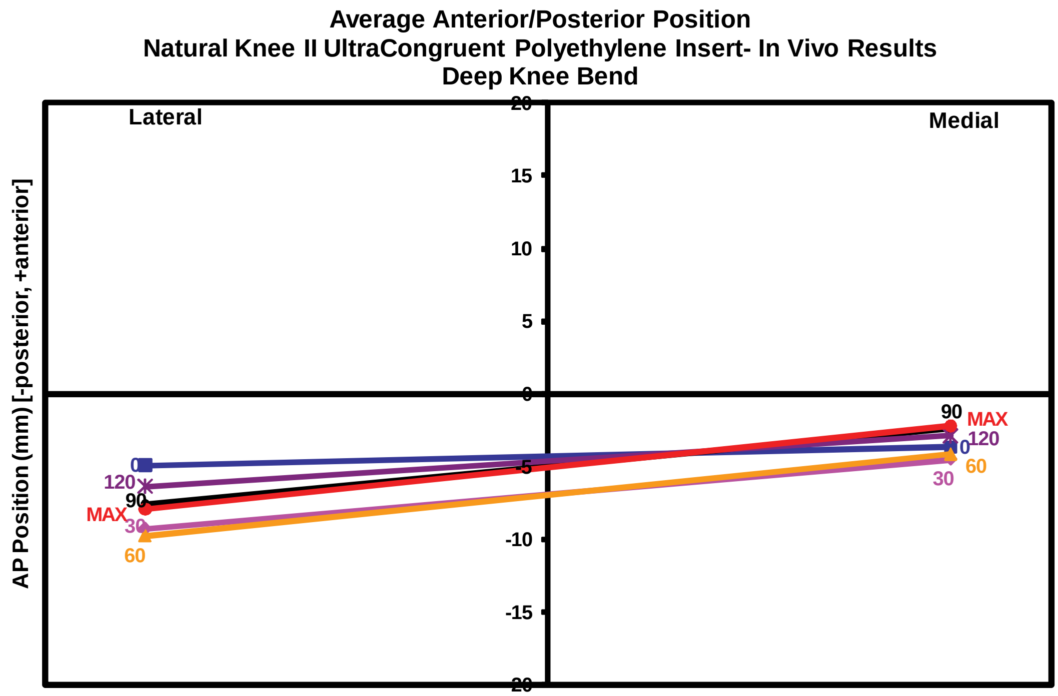

Figure 64: Average anterior/posterior contact positions obtained in vivo using fluoroscopy for 4 NKII UltraCongruent Polyethylene TKA during a deep knee bend.

NKII UCPE Model Results

At full extension, the simulation of medial and lateral AP contact point position for this implant was -4.7 mm for both condyles (Figure 66), respectively. At 90° of knee flexion the simulation predicted a contact position of -7.2 mm and -10.0 mm for the medial and lateral sides, respectively. This resulted in -2.5 mm and -5.3 mm posterior movement of the contact positions for the medial and lateral sides, respectively. The simulation predicted a more posterior contact position and movement for both the medial and lateral condylar contact points. The medial condyle experienced more than three times more posterior motion than the greatest posterior motion seen under in vivo conditions for this implant and the lateral movement was slightly greater than one deviation less than the average posterior movement of the four TKA analyzed in this group.

At a maximum knee flexion of 140°, the model simulated an AP contact position of -4.1 mm and -10.2 mm for the medial and lateral condyles, respectively. This resulted in 0.6 mm of anterior motion for the medial condyle and -5.5 mm of posterior motion for the lateral condyle, respectively. These values are both within the range determined to occur under in vivo conditions for this implant, from full extension to maximum weight bearing flexion. The medial and lateral condyle predictions are within one standard deviation of the average translation value.

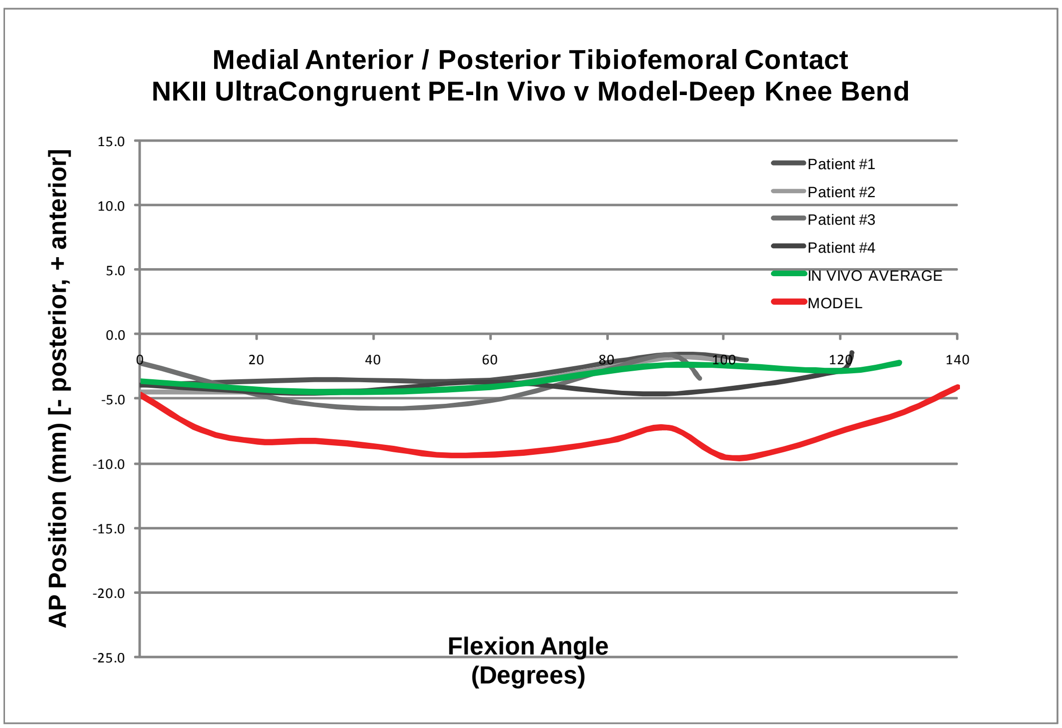

Figure 65: Anterior/posterior position of the medial tibiofemoral contact position of a Natural Knee II TKA with UltraCongruent polyethylene insert from in vivo data obtained using fluoroscopy and simulated data obtained from the forward solution model. The average in vivo value at 140° flexion is the average position at maximum flexion for all TKA.

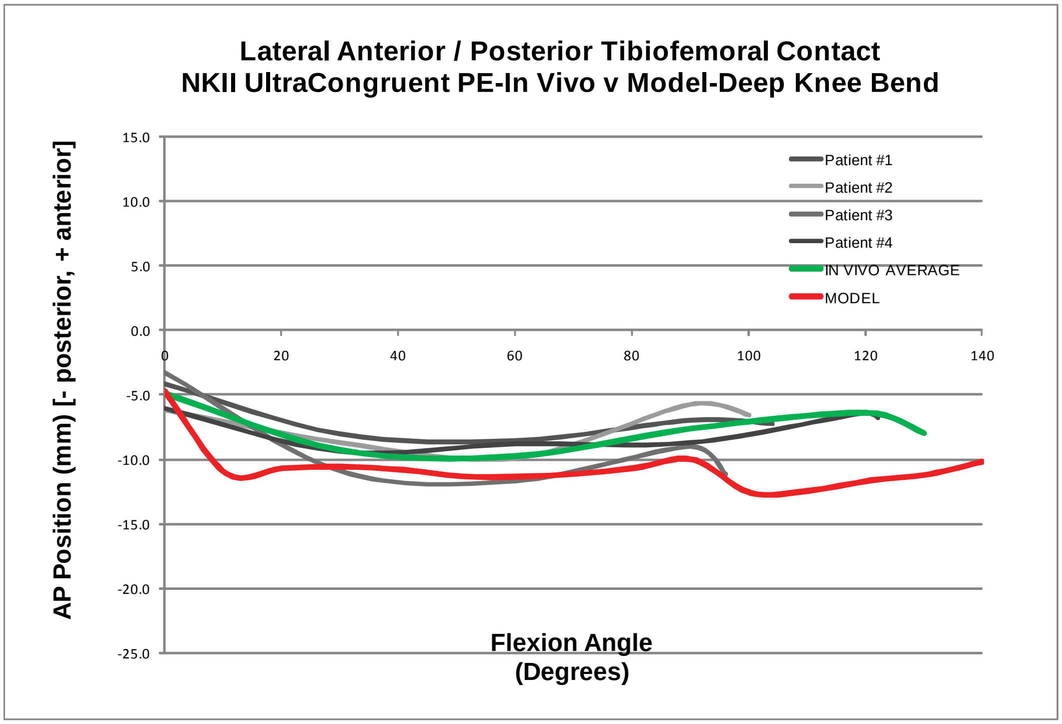

Figure 66: Anterior/posterior position of the lateral tibiofemoral contact position of a Natural Knee II TKA with UltraCongruent polyethylene insert from in vivo data obtained using fluoroscopy and simulated data obtained from the forward solution model. The average in vivo value at 140° flexion is the average position at maximum flexion for all TKA.

Comparison of Congruent PE Insert to UltraCongruent PE Insert

The in vivo results revealed that the average contact position for both condyles were more posterior for the TKA subjects having an UCPE insert than the subjects having a CPE insert throughout knee flexion, except for the lateral condyle in later flexion (Figure 67). The lateral condylar contact position for the UCPE group demonstrated less translation throughout knee flexion than the CPE group. The results from the model were consistent with the in vivo data trends, although the amount of translation for the lateral condyle, from full extension to maximum flexion, between the different insert designs was more similar than the in vivo results. The results from the simulation using the CPE and UCPE inserts, appears as if the UCPE results are simply shifted in the posterior direction. To insure that this is not the result of the starting position, a simulation was then conducted using a more anterior starting position for the UCPE insert design. This simulation with the more anterior starting position resulted in overall contact position results more similar to results from the original starting position after 10°, remaining posterior of the CPE results (Figure 68).

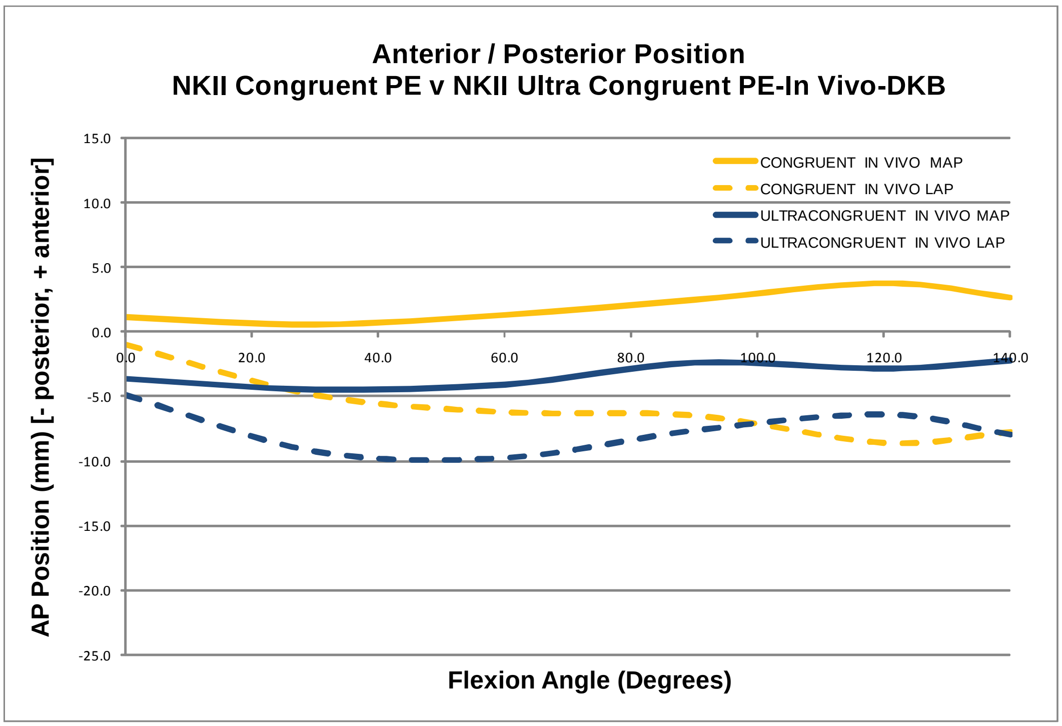

Figure 67: Comparison plot of the average anterior/posterior in vivo medial and lateral tibiofemoral contact positions obtained using fluoroscopy for 36 Natural Knee II TKA with Congruent polyethylene inserts and 4 Natural Knee II TKA with UltraCongruent polyethylene inserts. The average in vivo value at 140° flexion is the average position at maximum flexion for all TKA in the respective groups.

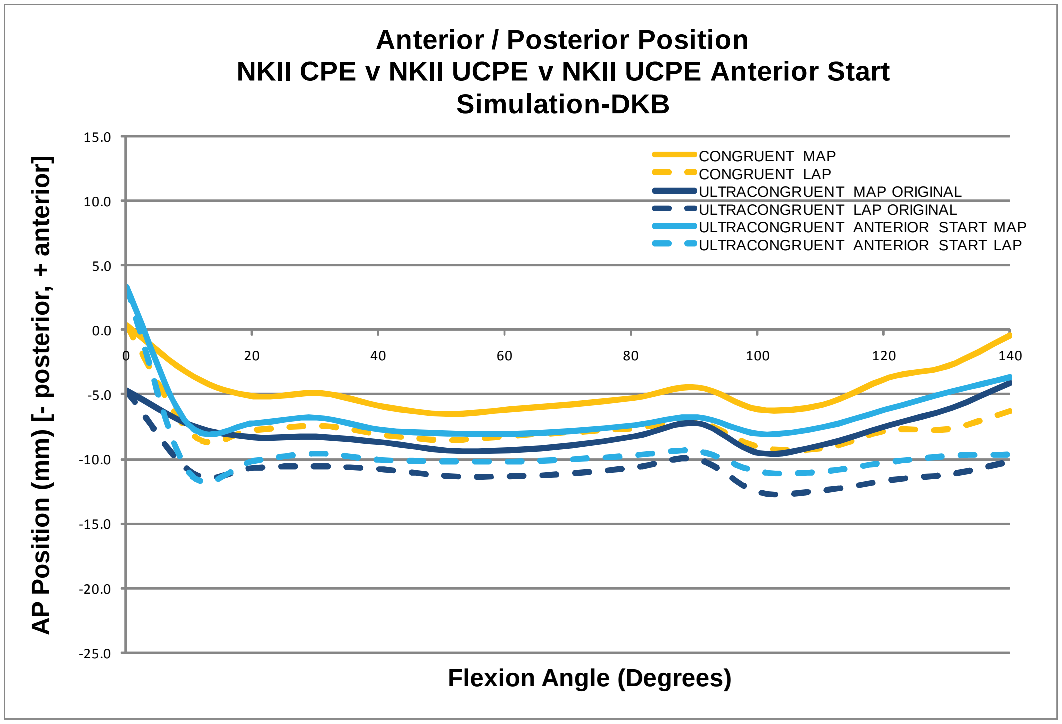

Figure 68: Comparison plot of the simulated anterior/posterior medial and lateral tibiofemoral contact positions obtained using the forward model for the original Natural Knee II TKA with Congruent and UltraCongruent polyethylene insert simulations and the results using the same NKII UltraCongruent design with a more anterior starting position showing that the UltraCongruent contact position remains posterior of the Congruent design contact positions regardless of the starting position.

WMT Axiom® ACL-Retaining TKA

In Vivo Kinematics Axiom® ACL-R

On average, the in vivo results obtained from fluoroscopy for 22 subjects implanted with a WMT Axiom® ACL Retaining (ACL-R) TKA revealed that from full extension to maximum knee flexion, the subjects experienced posterior femoral rollback (PFR) of the medial and lateral condyles (Figure 69). At full extension, the average medial and lateral condyle contact positions were 3.6 mm (-5.8 to 11.8 mm, SD=5.1mm) and -0.7 mm (-11.4 to 9.5 mm, SD=5.6 mm), respectively. At 90° of weight bearing knee flexion, the 20 TKA (90.9%) which achieved

90° of knee flexion had medial and lateral contact positions of -1.8 mm (-8.9 mm to 7.6 mm, SD=3.7 mm) and -9.8 mm (-8.0 mm to -4.6 mm, SD=3.0 mm), respectively, resulting in -5.3 mm (-13.2 mm to 5.5 mm, SD=4.8 mm) and -8.8 mm (-18.3 mm to -3.0 mm, SD=4.8 mm) of medial and lateral condyle posterior motion, respectively.

At maximum knee flexion, which averaged 104° (73° to 128°, SD=13.3°) for this group, the average medial condyle contact position moved in the posterior direction to -3.1 mm (-10.2 to 8.3 mm, SD=4.7 mm) and the average lateral condyle contact position moved posterior to -10.4 mm (-16.4 to -3.9 mm, SD=3.1 mm). From full extension to maximum knee flexion, the average amount of posterior movement for the medial condyle was -6.6 mm (-19.3 to 6.2 mm, SD=5.4 mm) and the average amount of posterior femoral rollback for the lateral condyle was -9.7 mm (-23.5 to -3.0 mm, SD=5.1 mm). Twenty of the 22 (90.9%) subjects experienced PFR of their medial condyle and 100% of the subjects experienced PFR of their lateral condyle from full extension to maximum knee flexion.

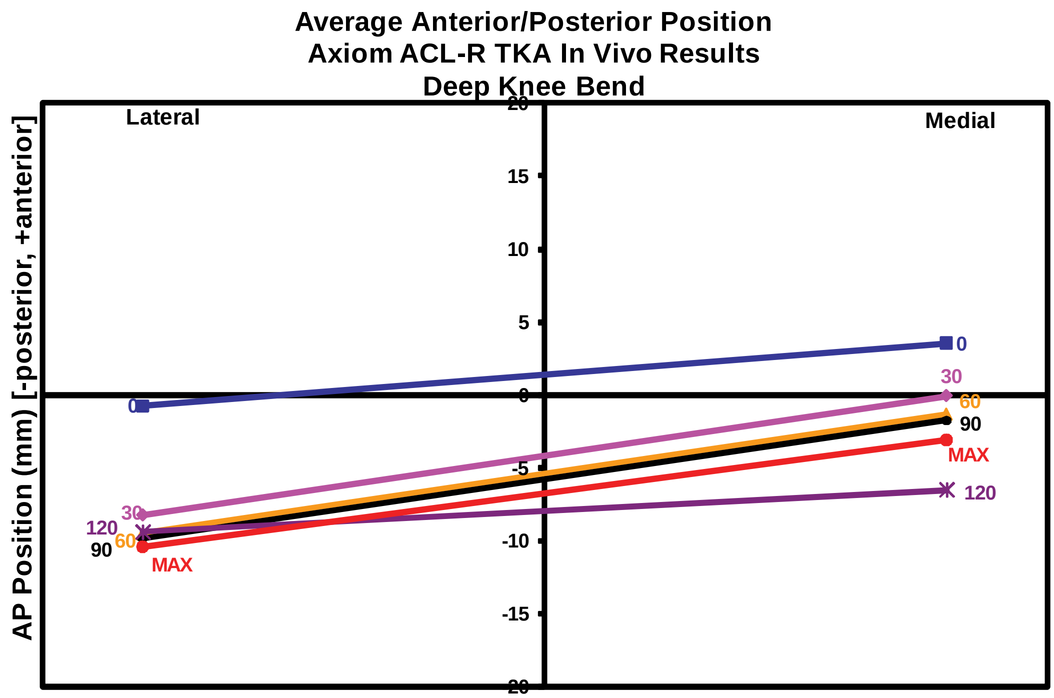

Figure 69: Average anterior/posterior contact positions obtained in vivo using fluoroscopy for 22 Axiom® ACL-Retaining TKA during a deep knee bend.

Axiom® ACL-R Model Results

The anterior-posterior medial and lateral condylar contact point positions from the simulation of the Axiom ACL-R TKA, at full extension, were -2.8 mm and -2.7 mm (Figure 70 and Figure 71), respectively. At 90° of simulated weight bearing knee flexion the medial and lateral contact points moved posteriorly to -14.2 mm and -19.9 mm, respectively, resulting in -11.5 mm and -17.2 mm posterior tibiofemoral contact motion, respectively. This is within the minimum and maximum translations seen in vivo for both the medial and lateral contact points for this TKA, however it is not within one standard deviation of the average result.

The maximum simulated weight bearing flexion for the Axiom ACL-R TKA was 140°. The simulated medial and lateral tibiofemoral contact positions at this flexion degree were -7.0 mm and -21.4 mm, respectively, resulting in -4.2 mm and -18.7 mm posterior tibiofemoral contact motion, respectively. Although the maximum in vivo weight bearing knee flexion was 128°, the posterior motion of both the medial and lateral contact points remained within the minimum and maximum values observed from full extension to maximum flexion in vivo and the simulated medial contact movement was within one standard deviation of the observed average.

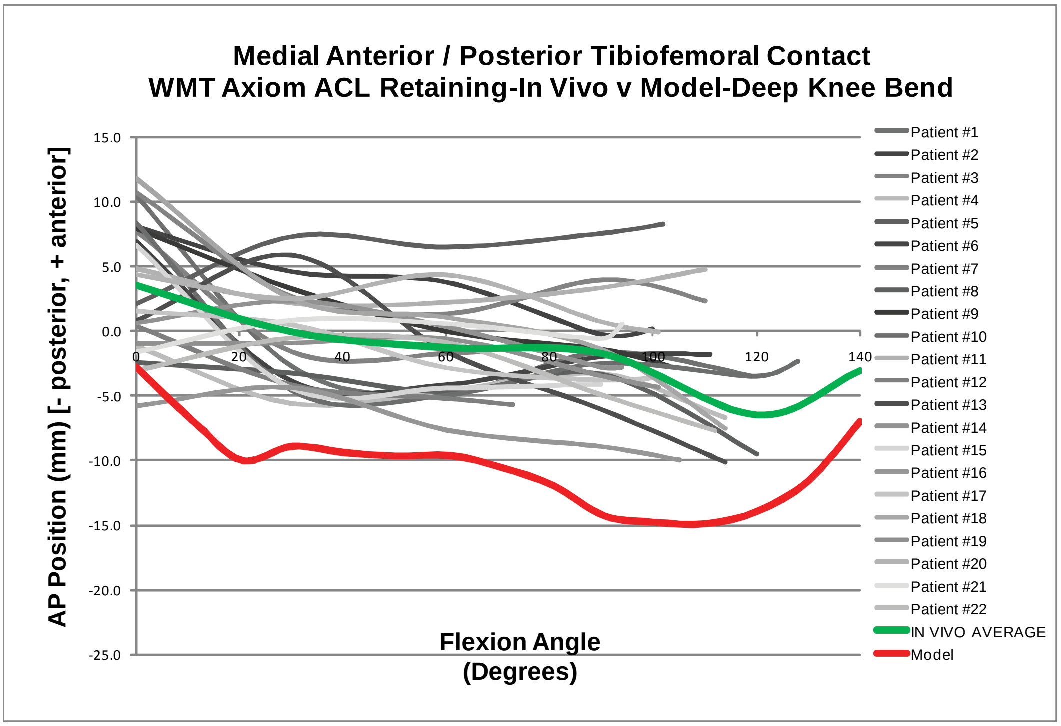

Figure 70: Anterior/posterior position of the medial tibiofemoral contact position of a Axiom® ACL-Retaining TKA from in vivo data obtained using fluoroscopy and simulated data obtained from the forward solution model. The average in vivo value at 140° flexion is the average position at maximum flexion for all TKA.

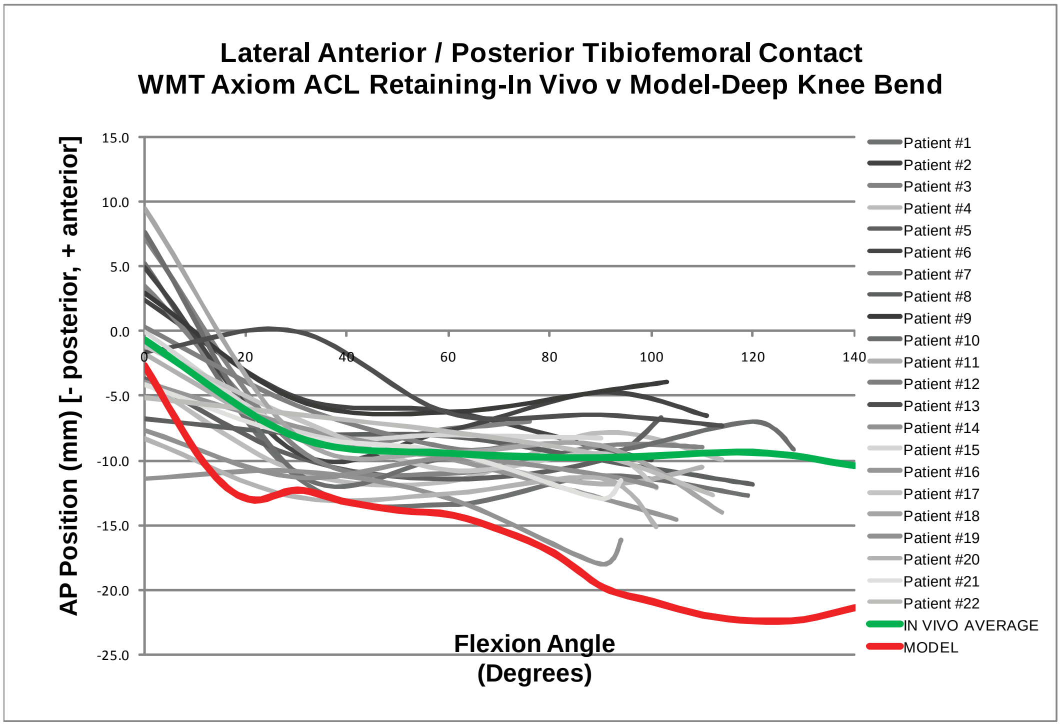

Figure 71: Anterior/posterior position of the medial tibiofemoral contact position of a Axiom® ACL-Retaining TKA from in vivo data obtained using fluoroscopy and simulated data obtained from the forward solution model. The average in vivo value at 140° flexion is the average position at maximum flexion for all TKA.

Ceraver Hermes® ACL-Retaining TKA

In Vivo Kinematics Hermes® ACL-R

The in vivo contact position for one Ceraver Hermes® ACL-Retaining (ACL-R) TKA at full extension was -0.4 mm and 5.1 mm for the medial and lateral condyles, respectively (Figure 72). At 20° of knee flexion the contact points moved to -14.1 mm and -14.2 mm for the medial and lateral condyles, respectively, resulting in -13.7 mm and -9.1 mm motion of the medial and lateral condyles, respectively. At maximum knee flexion of 112°, the medial and lateral AP condylar contact positions were -7.4 mm and -16.3 mm, resulting in AP medial and lateral contact translation of -7.0 mm and -21.4 mm, respectively.

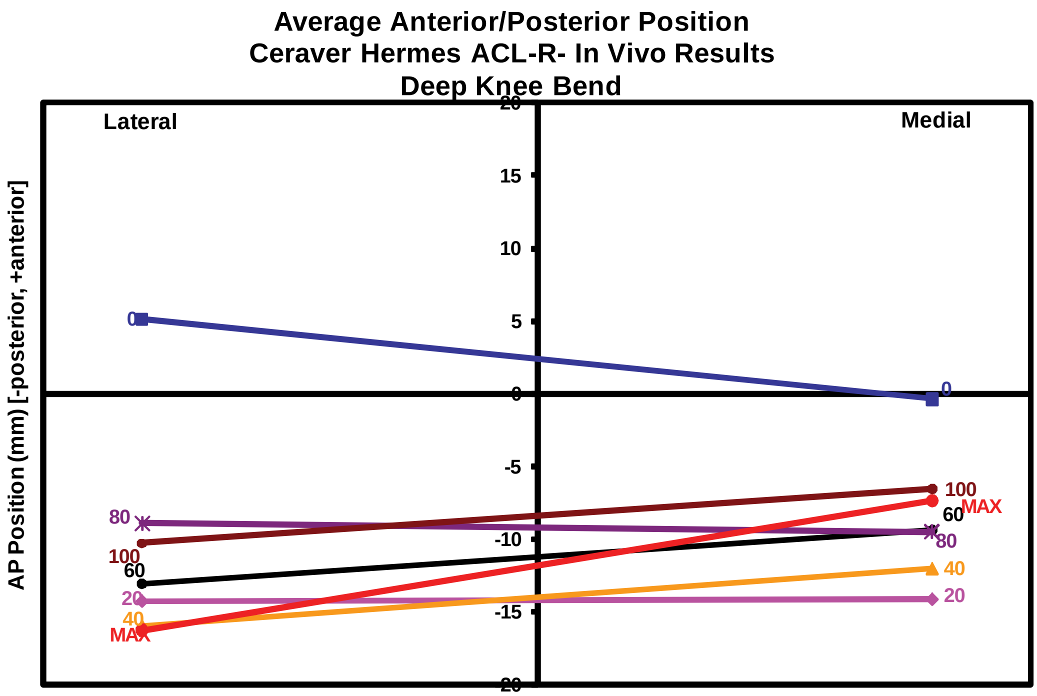

Figure 72: Anterior/posterior contact positions obtained in vivo using fluoroscopy for a single Hermes ACL-R TKA during a deep knee bend.

Hermes® ACL-R Model Results

The simulated contact positions at full extension for the Hermes® ACL-Retaining (ACL-R) TKA were -1.9 mm and -2.6 mm for the medial and lateral condyles, respectively. At 20° of knee flexion the contact points moved posteriorly to -14.3 mm and -13.3 mm resulting in -12.3 mm and -10.7 mm of condylar contact point translation on the medial and lateral condyles, respectively. The simulation resulted in 1.4 mm less posterior movement for the medial condyle and -1.8 mm more translation for the lateral condyle. The simulated pattern, revealing more medial movement than lateral condylar contact movement was consistent when comparing the simulation results to the in vivo results. At 112° of knee flexion the simulation contact positions were -12.5 mm and -15.6 mm for the medial and lateral condyles, respectively, resulting in -10.6 mm and -13.0 mm of condylar position change for the medial and lateral condyles, respectively. The simulation resulted in 3.6 mm of less posterior condyle movement for the medial condyle from full extension to 112° of knee flexion and 8.4 mm less movement for the lateral condyle. However the pattern of the lateral condyle moving more than the medial condyle remained consistent between the simulation and in vivo data results. The simulated model results experienced a maximum weight bearing flexion of 140°. The condylar contact positions at maximum knee flexion were -10.9 mm and -17.9 mm for the medial and lateral condyles, respectively resulting in -9.0 mm and -15.3 mm of movement for the medial and lateral condyle contact positions, respectively. The amount of simulated movement for the medial contact point was -2.0 mm more than the in vivo data and the lateral condyle was 6.1 mm less. However, a consistent pattern of more movement for the lateral condyle than the medial condyle at greater flexion angles was determined to occur between the simulation and in vivo data.

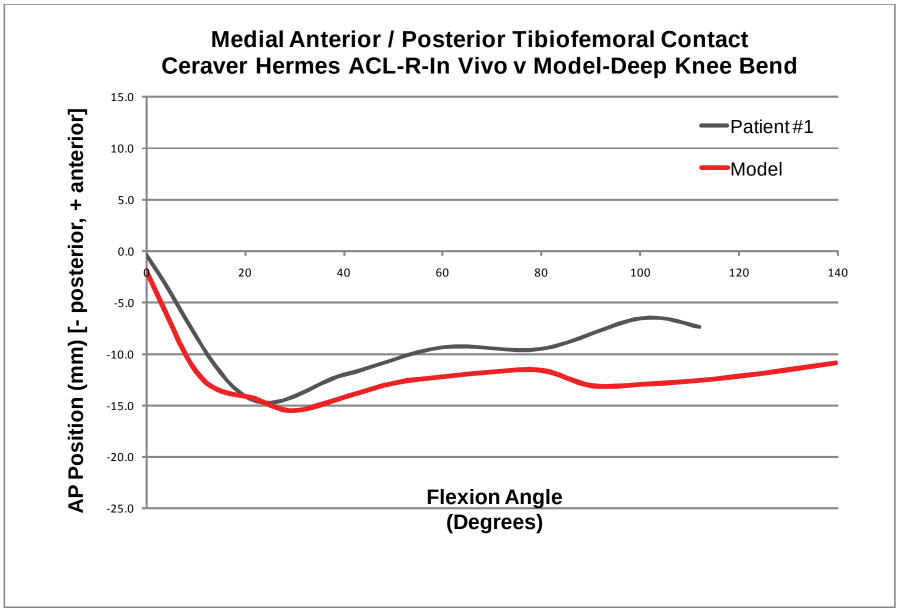

Figure 73: Anterior/posterior position of the medial tibiofemoral contact position of a single Hermes ACL-Retaining TKA from in vivo data obtained using fluoroscopy and simulated data obtained from the forward solution model.

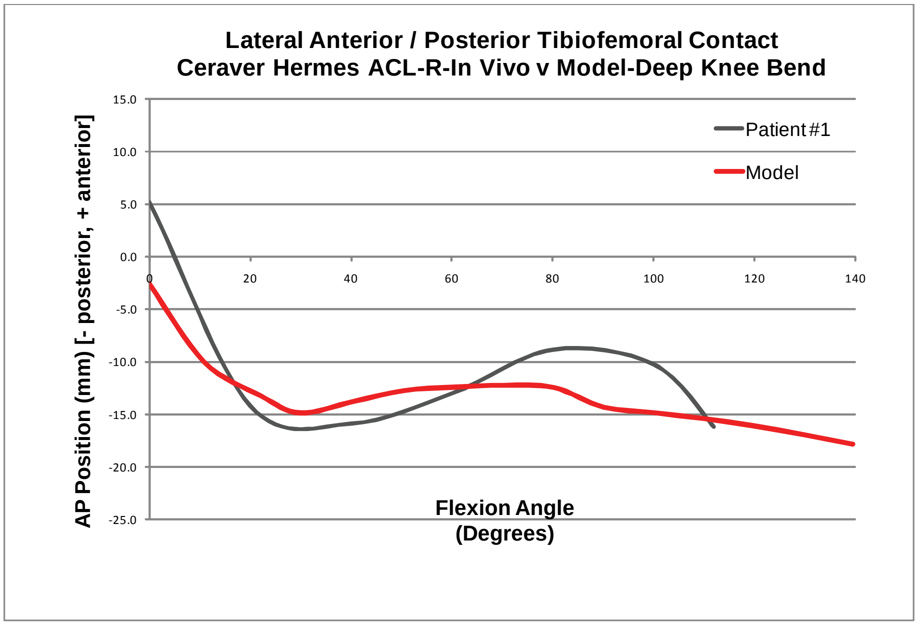

Figure 74: Anterior/posterior position of the lateral tibiofemoral contact position of a single Hermes ACL-Retaining TKA from in vivo data obtained using fluoroscopy and simulated data obtained from the forward solution model.

Pre-production ACL-Retaining TKA

Pre-production ACL-R Model Results

Further analysis was conducted for an ACL-Retaining TKA design that has been developed and tested, but not implanted or analyzed under in vivo conditions. Therefore, for this analysis a comparison to in vivo data could not be made at this time. The simulated contact positions at full extension for the medial and lateral condyle were -0.8 mm and -0.7 mm (Figure 75). At 40° flexion the medial and lateral contact points moved posteriorly to -15.5 mm and -15.9 mm, respectively, resulting in -14.7 mm and -15.2 mm posterior motion of the medial and lateral condylar contact points, respectively. At 140°, the maximum simulated weight bearing knee flexion for this theoretical design, the medial and lateral condylar contact point positions were -8.3 mm and -14.6 mm, resulting in -7.5 mm posterior motion of the medial condylar contact point and -13.9 mm motion of the lateral condylar contact point. These contact position results were similar in pattern to the other in vivo and simulated results from ACL-R TKA designs (Figure 76).

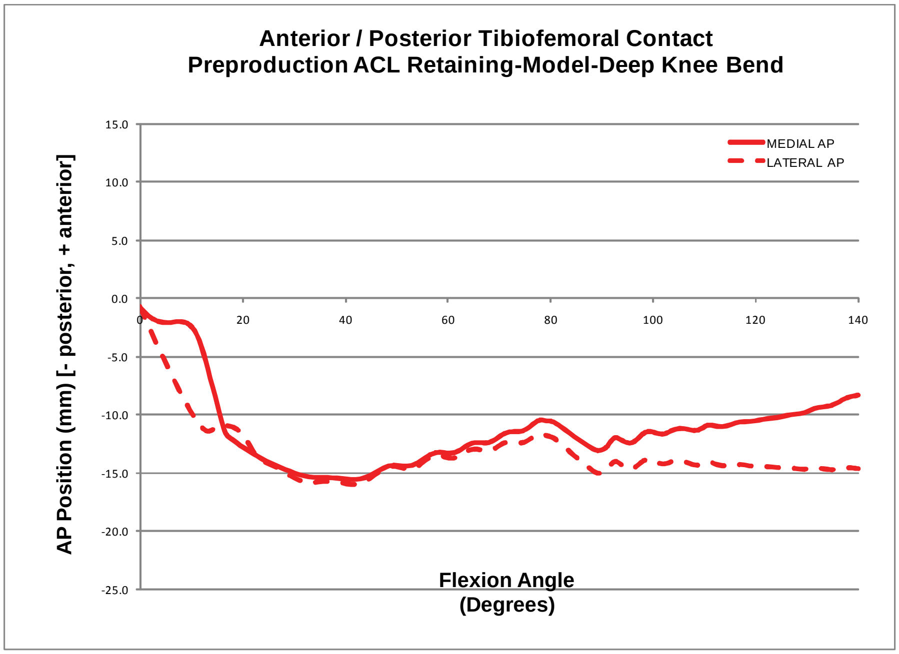

Figure 75: Simulated medial and lateral anterior/posterior tibiofemoral contact positions for a preproduction ACL-Retaining TKA.

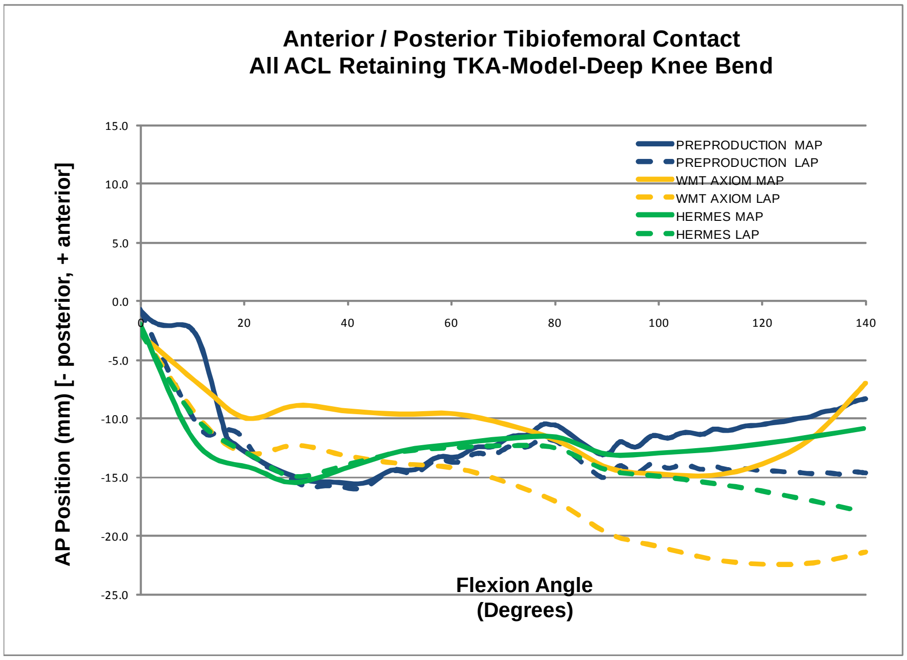

Figure 76: Simulated medial and lateral anterior/posterior tibiofemoral contact positions for all ACL-Retaining TKA analyzed.

PID Controller

The PID controller effectively controlled the rate of flexion after being tuned for each of the different designs that were evaluated using the model. The amount of tuning was typically minimal from one model to the next, generally involving an adjustment of the derivative gain. However the NKII CPE and NKII UCPE TKA proved to be a little more challenging, especially in later flexion. The PID controller provided relatively low error results (<1° flexion error) when comparing the actual simulated flexion to the desired flexion. Adjustments were made to the controller gains to minimize the oscillation of the process variable, in this case a coefficient which raised and lowered the force in the four quadriceps muscle. Oscillations of the quadriceps force could not be completely avoided with the current controller (Figure 77). Interestingly, oscillations were also detected with the telemetric knee, leading to a hypothesis that oscillations, under in vivo conditions, may be a normal occurrence ().

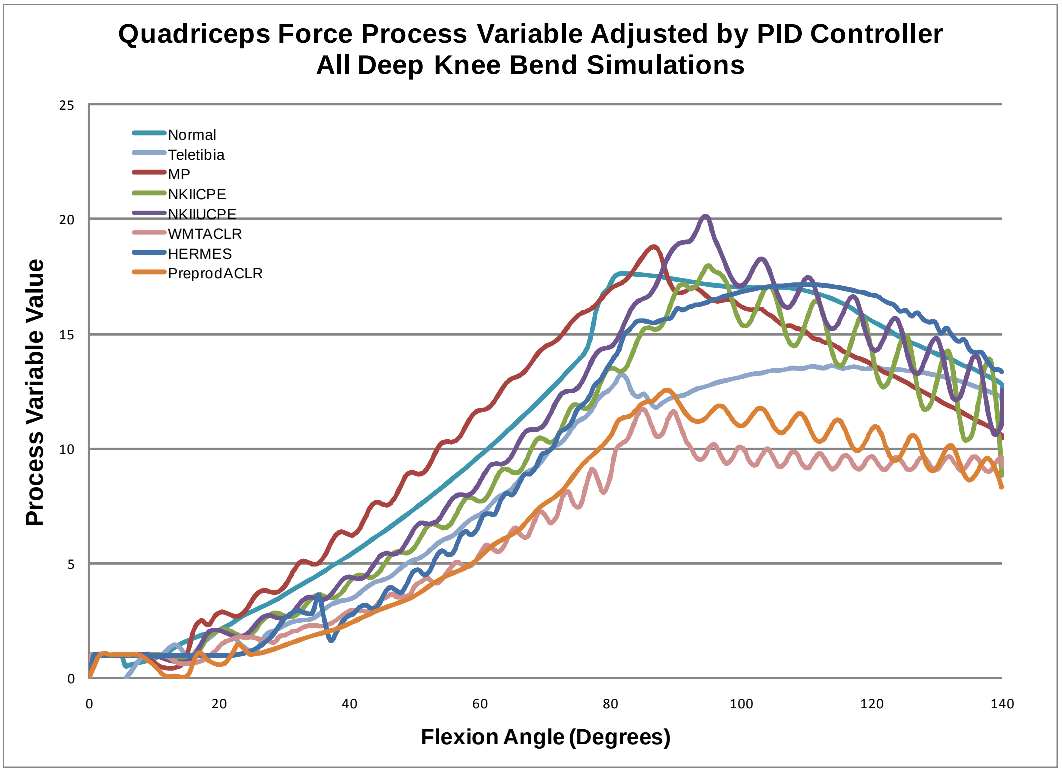

Figure 77: The quadriceps force process variable values adjusted by the PID controller for the normal knee simulation and all of the TKA design simulations.

The overall flexion of the simulations matches well with the desired flexion (Figure 78). Oscillations of varying frequency and amplitude were generally present in the error (Figure 79). The average absolute error for all of the simulations was 0.11° (0.08° to 0.77°, SD=0.11°). The average maximum absolute error was 0.34° (0.08° to 0.77°, SD=0.22°). The model, in which the controller allowed the largest absolute error value of 0.77°, was the normal model. The model which had the smallest maximum absolute error was the Hermes ACL-R TKA design with 0.08°.

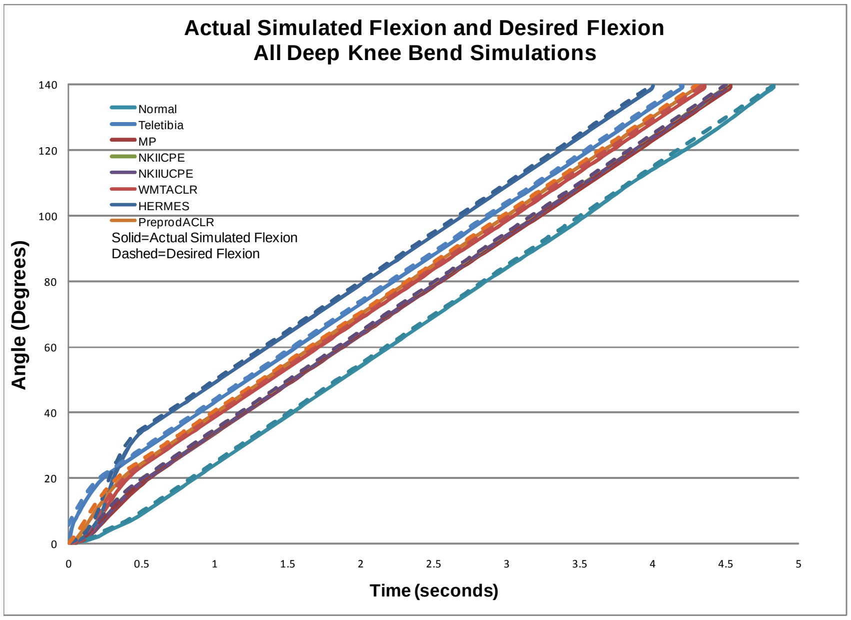

Figure 78: Actual Simulated Flexion from the model and desired flexion for the normal knee simulation and all of the TKA design simulations.

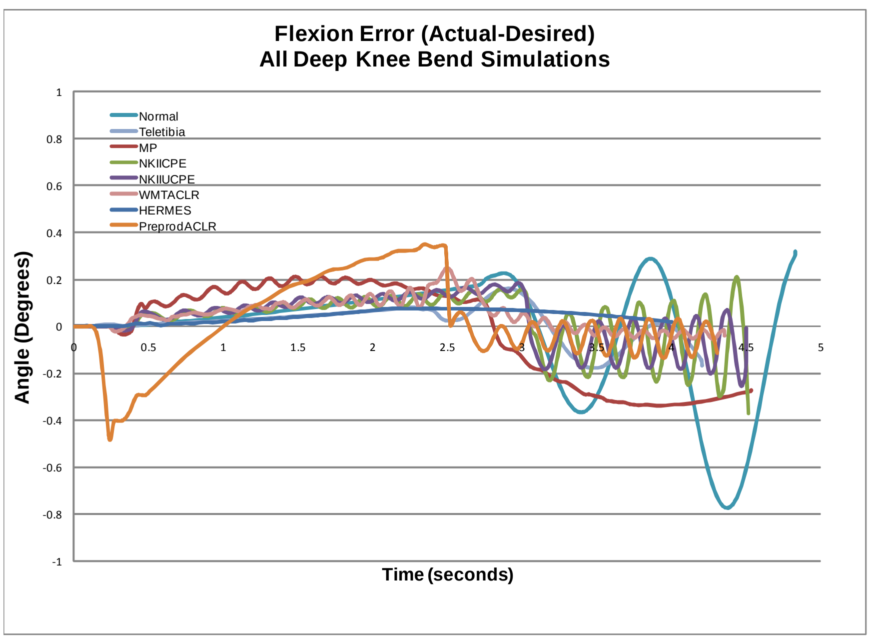

Figure 79: Flexion error (actual flexion – desired flexion) for the normal knee simulation and all of the TKA design simulations.

Quadriceps and Patella Ligament Forces

Total Quadriceps Force

Typically the quadriceps force peaked between 80° and 100° of knee flexion (Figure 80). The average maximum quadriceps force was 5.82 BW (4.73 BW to 7.06 BW, SD=0.82 BW). The greatest maximum quadriceps force was in the NK II CPE TKA with 7.06 BW at 94° flexion. The simulation experiencing the least maximum quadriceps force was the normal knee with 4.73 BW at 81° flexion. As was mentioned previously, the PID controller did adjust the quadriceps force in a way which resulted in the incidence of oscillations. The maximum quadriceps force and patterns in these results are within range of values from the literature [Lanovan 2009, Sharma 2008, Sharma 2007, Komistek 2005].

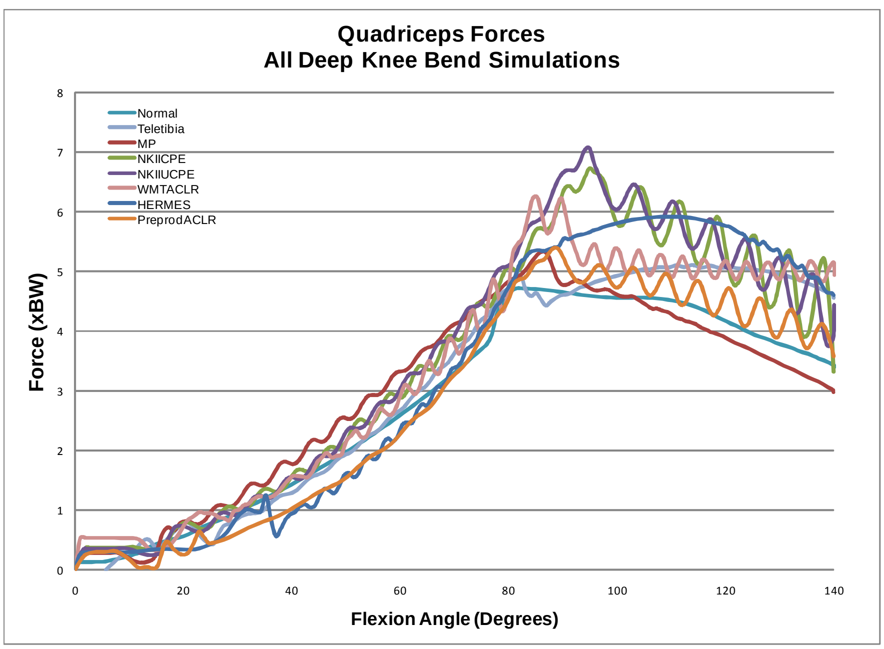

Figure 80: Total quadriceps force through flexion for the normal knee simulation and all TKA simulations.

Individual Quadriceps Forces

The maximum forces in the various quadriceps muscles varied from model to model (Figure 81). The maximum forces for the Vastus Lateralis, Rectus Femoris, Vastus Intermedius and Vastus Medialis were 1.73 BW (0.76 BW to 2.61 BW, SD=0.66 BW), 0.58 BW (0.44 BW to 0.75 BW, SD=0.13 BW), 2.57 BW (1.94 to 3.34 BW, SD=0.57 BW) and 1.08 BW (0.48 BW to 1.66 BW, SD=0.37 BW), respectively.

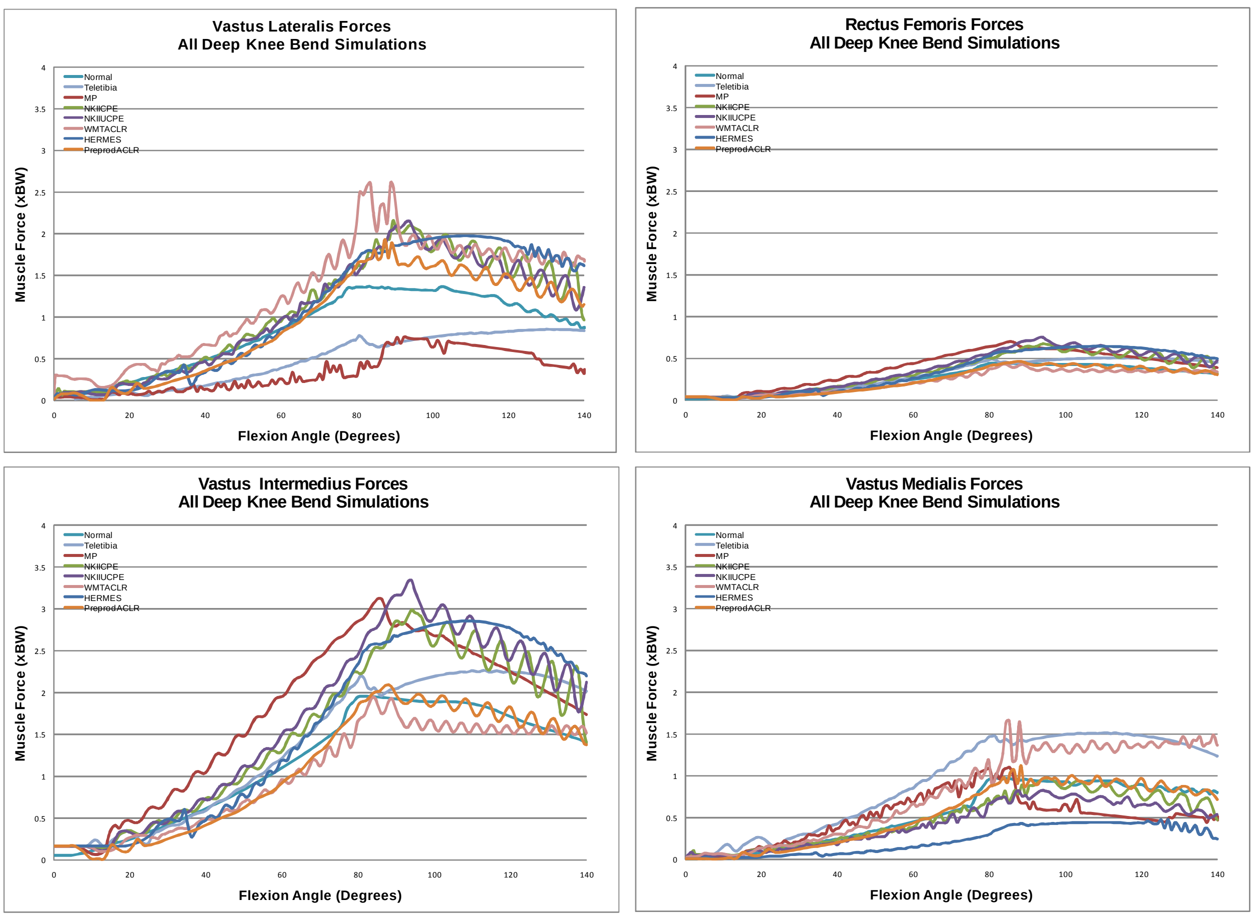

Figure 81: Individual quadriceps muscle forces for the normal knee simulation and all TKA simulations.

For the most part, the ratio of Vastus Lateralis to Vastus Intermedius stayed below 1.0 except for the case of the Axiom® ACL-R which was well over 1.0 for most of the simulation. The forces in the Vastus Medialis stayed lower than the Vastus Intermedius for all of the simulations.

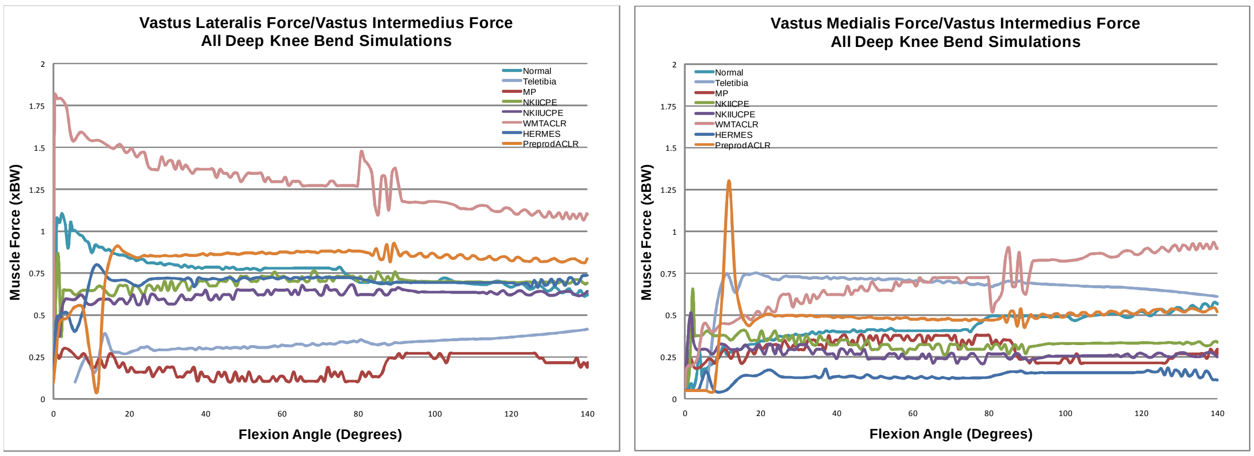

Figure 82: Ratio of Vastus Lateralis force to Vastus Intermedius force and Vastus Medialis force to Vastus Intermedius force.

Patella Ligament Force

The patella ligament force followed the general pattern of the quadriceps force in that it increased after full extension and then decreased in deeper flexion (Figure 83). The average maximum patella ligament force was 3.34 BW (2.39 BW to 4.83 BW, SD=0.81 BW). The greatest maximum patella ligament force was in the Hermes ACL-R TKA design with 4.83 BW at 106° flexion. The smallest maximum patella ligament force was in the WMTI Axiom® ACL-R TKA at 95° flexion.

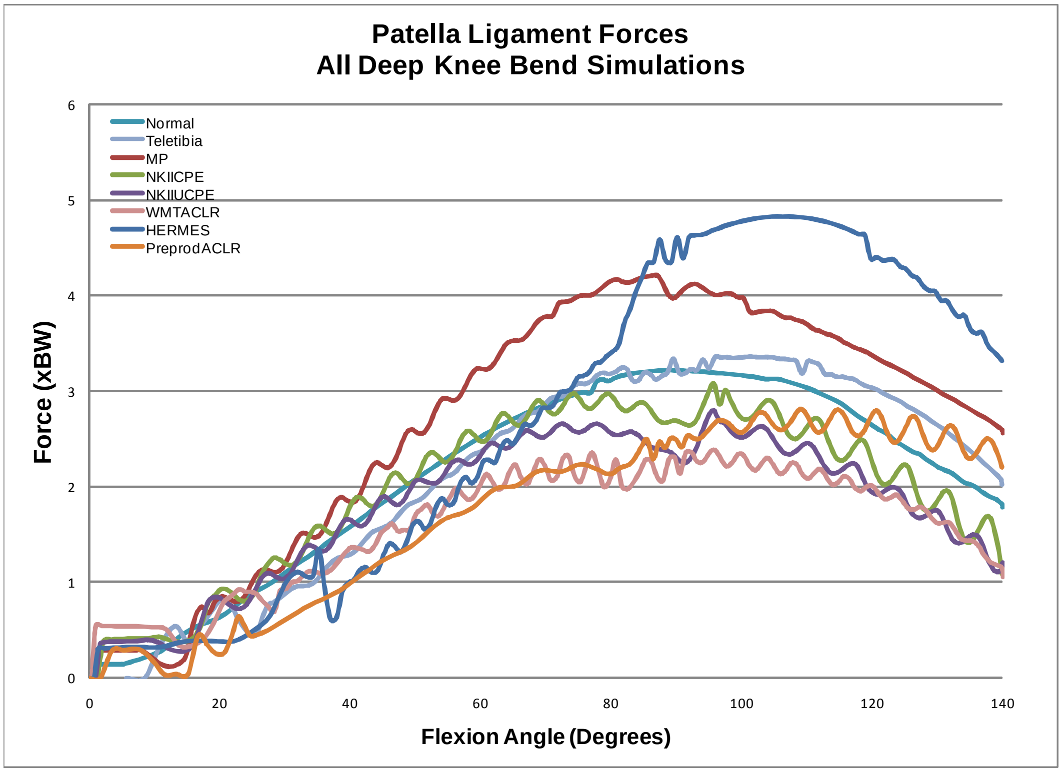

Figure 83: Patella ligament forces for the normal knee simulation and all TKA simulations.

The relationship between the patella ligament force and the quadriceps force is described by dividing the patella ligament force by the quadriceps force. This ratio, in all simulations, followed a general pattern at full extension greater than 1.0 to varying degrees depending on the design and steadily decreases until quadriceps wrapping occurs between 80° and 90° flexion, where the slope of the variable vs knee flexion plot changes and either gradually increases or decreases (Figure 84). The average maximum Patella Ligament/Quadriceps Force ratio was 1.10 (1.02 to 1.18, SD=0.06). The average minimum Patella Ligament/Quadriceps Force ratio was 0.46 (0.21 to 0.79, SD=0.20). The smallest minimum value of 0.21 was in the Axiom® ACL-R TKA at 140° flexion while the greatest minimum value was from the Medial Pivot TKA design at 85° flexion. The trend of the Patella Ligament Force/Quadriceps Force ratio is typical of results from literature [Lanovaz 2009, Sharma 2008, Ward 2005, Yamaguchi 1989, Shelbourne 1995].

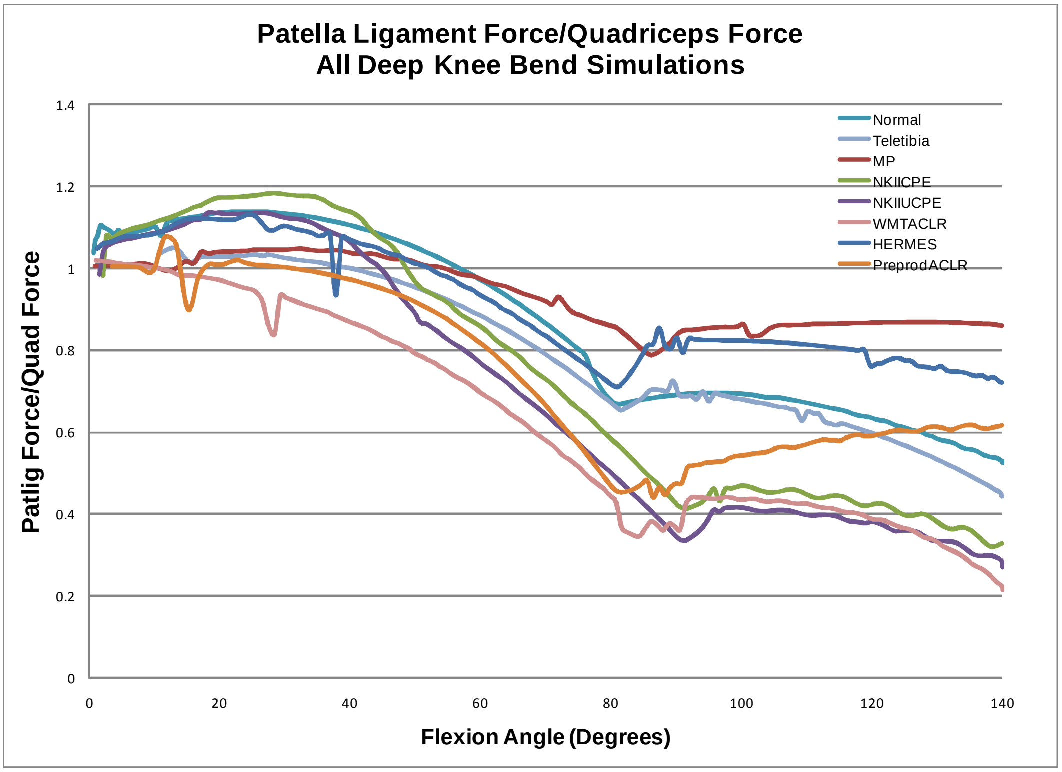

Figure 84: Patella ligament force/Quadriceps force ratio for the normal knee simulation and all TKA simulations.

Tibiofemoral Interaction Forces

Total Tibiofemoral Axial Force

The total tibiofemoral force is a summation of the medial and lateral contact interaction forces at each increment of knee flexion. In general, the total force started a less than 1.0 BW and increased and decreased with the patella ligament forces (Figure 85). The average maximum tibiofemoral force was 4.24 BW (3.32 BW to 6.77 BW, SD=1.13 BW). The design with the lowest maximum total axial force of 3.32 BW was the NKII UCPE TKA design at 95° flexion. The model with the greatest maximum axial force was the Hermes ACL-R design with 6.77 BW at 108° flexion. The normal knee experienced a maximum axial load of 3.70 BW at 87° flexion. The maximum axial forces occurred from 81° flexion in the Teletibia TKA design to 120° flexion in the Preproduction ACL-R TKA design.

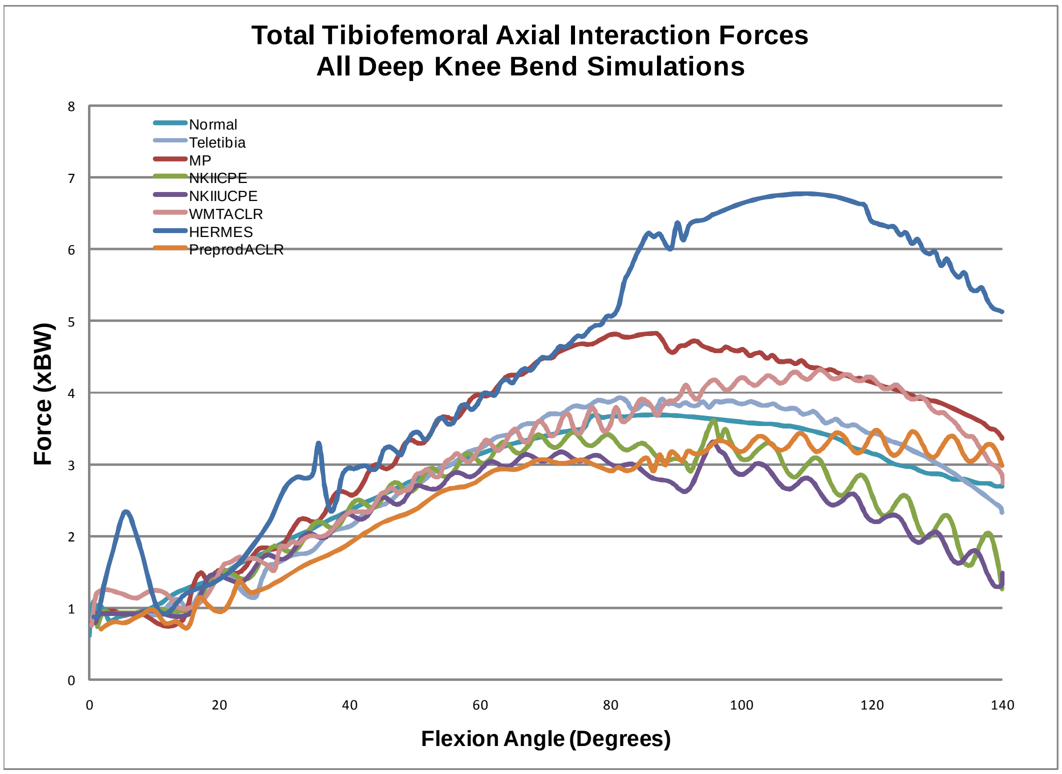

Figure 85: Total axial tibiofemoral interaction forces for the normal knee simulation and all TKA simulations.

Medial Contact Force

The medial contact force followed the trend of the total axial force, increasing and then decreasing in greater flexion (Figure 86). The maximum medial contact force averaged 2.13 BW (1.40 BW to 3.08 BW, 0.65 BW). The smallest maximum medial contact force of 1.40 BW was in the Preproduction ACL-R TKA design at 84°. The greatest maximum medial contact force was in the Hermes ACL-R TKA design with 3.08 BW at 102° flexion. The normal knee simulation predicted a maximum medial contact force of 1.99 BW at 87°. The occurrence of the maximum medial contact force during the simulation was at an average of 88° (72° to 108°, SD=12°). The earliest occurrence of the maximum force at 72° flexion was in the NKII UCPE TKA design and the latest at 108° flexion was in the Axiom® ACL-R TKA design.

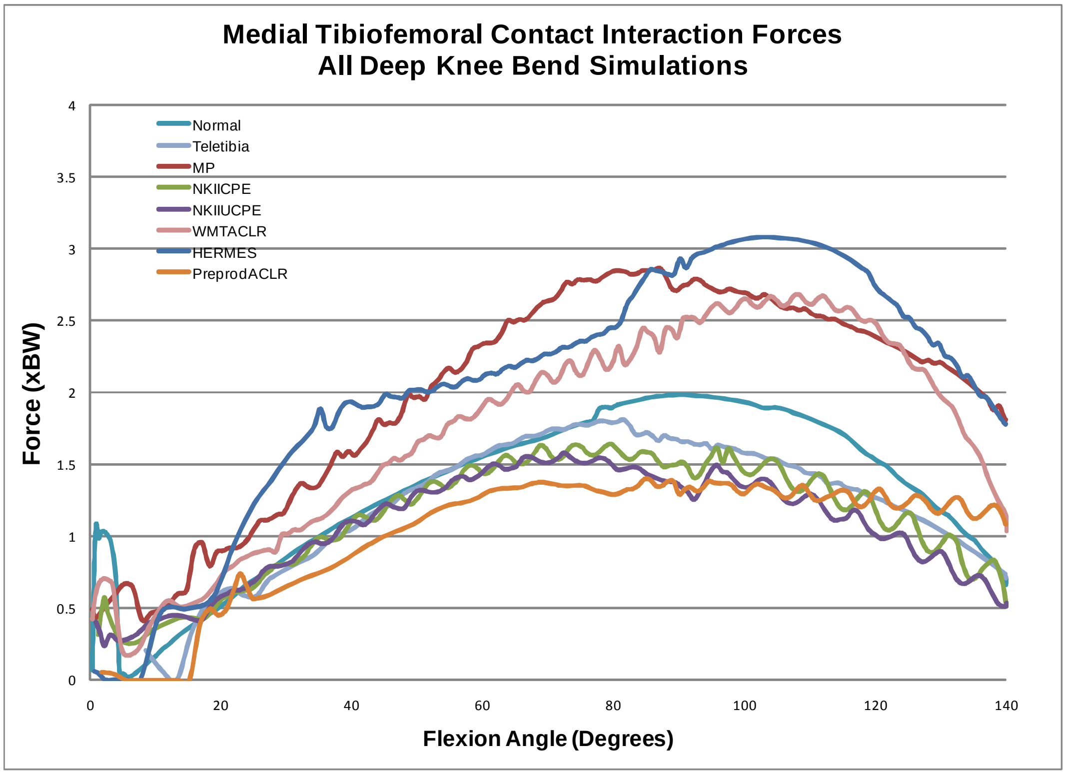

Figure 86: Medial tibiofemoral contact forces for the normal knee simulation and all TKA simulations.

Lateral Contact Forces

The average maximum lateral contact force for the normal knee model and all the TKA designs was 2.23 BW (1.79 BW to 3.77 BW, SD=0.64) (Figure 87), slightly higher than the medial contact force. The smallest maximum lateral contact force of 1.79 BW occurred in the Axiom® ACL-R TKA design at 135°. The greatest maximum lateral contact force of 3.77 BW occurred with the

Hermes ACL-R TKA design simulation at 118° flexion. This value is 1.46 BW greater than the next largest lateral contact force in the Teletibia TKA. The Hermes TKA simulation also predicted a spike between full extension and 10° flexion which was much greater than the other simulations in this flexion range. The normal knee simulation predicted a maximum of 2.04 BW at maximum flexion of 140°. The maximum lateral contact force occurred at an average flexion of 111° (80° to 140°, SD=21°), later in flexion than the maximum medial contact force. The earliest occurrence of the maximum at 80° was in the Medial Pivot TKA design and the latest occurrence at maximum flexion of 140° occurred in the normal knee.

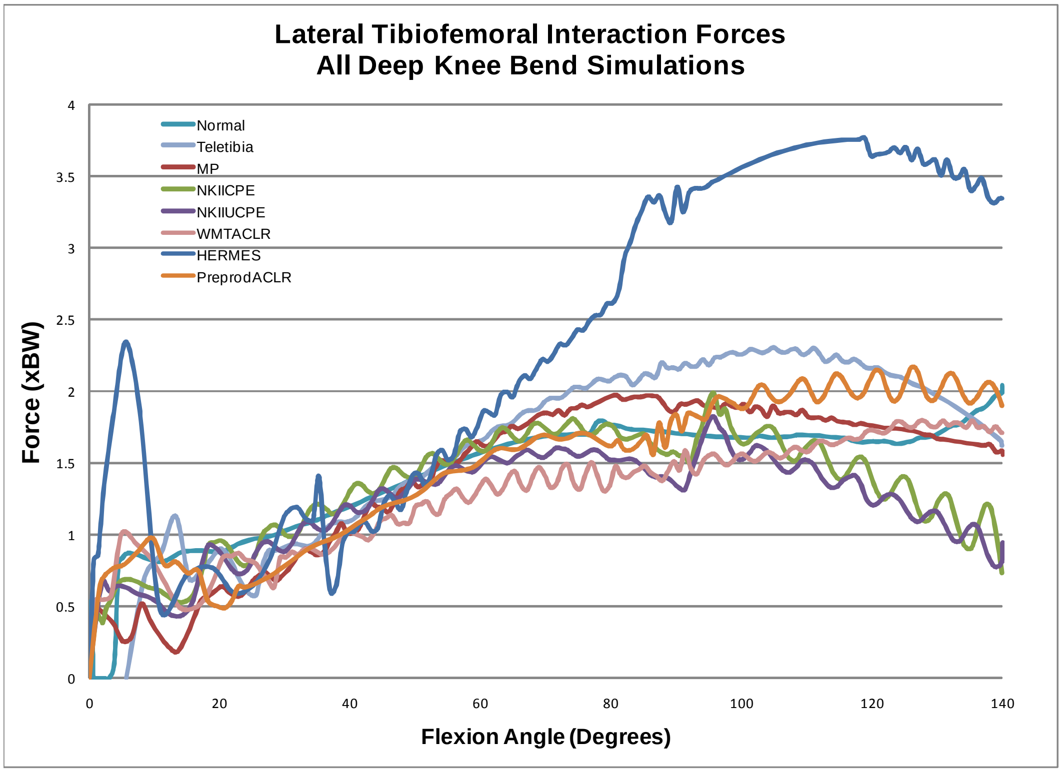

Figure 87: Lateral tibiofemoral contact forces for the normal knee simulation and all TKA simulations.

The ratio of medial contact force to lateral contact force is erratic and inconsistent between simulations from full extension to 55° flexion (Figure 88). After 55° flexion the values of the medial to lateral contact force ratio remains more similar. The average of the mean ratio values after 55° for each model was 0.98 (0.71 to 1.45, SD=0.29). The model which averaged the highest medial to lateral contact force ratio of 1.45 after 55° was the Axiom® ACL-R TKA and the lowest with 0.71 was the Preproduction ACL-R TKA. The normal knee saw an average ratio of 0.97.

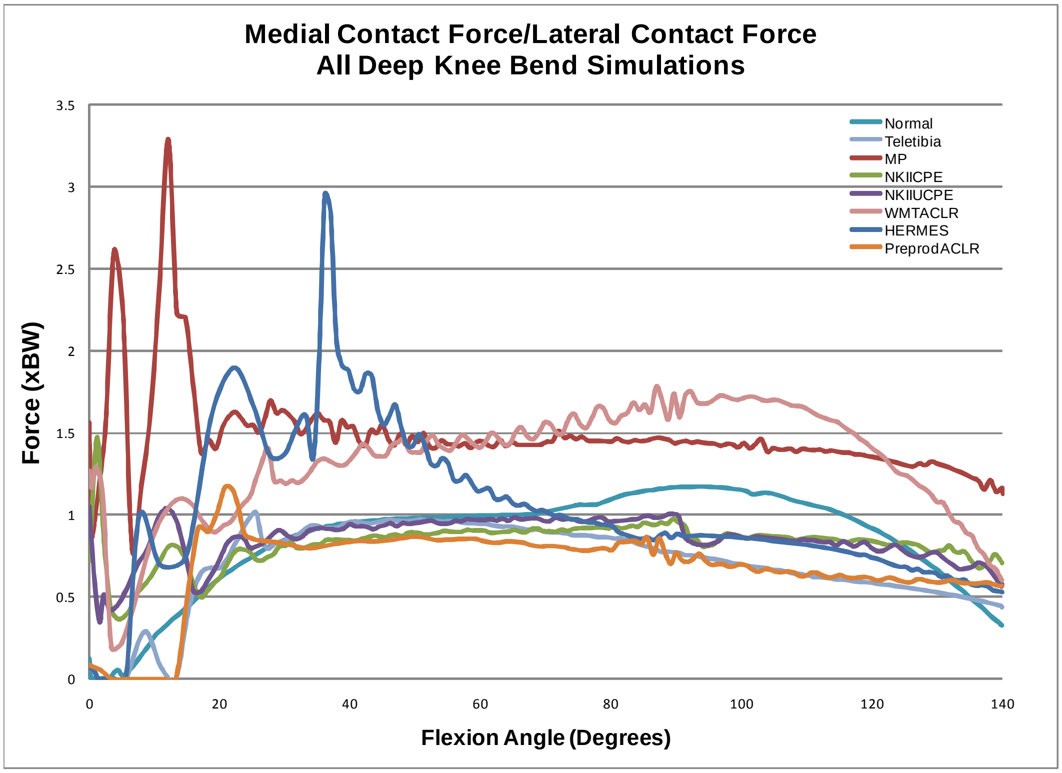

Figure 88: Medial to lateral contact force ratio for the normal knee simulation and all TKA simulations.

Patellofemoral Kinematics

Patella Tilt

Patella tilt, which was stabilized by a controller within the PID controller which controls knee flexion, varied from model to model (Figure 89). Generally the patella rotated about the PAT2> axis (physiologically known as patella tilt) in early flexion until the controller was able to stabilize the rotation by adjusting the forces in the Vastus Medialis and Vastus Lateralis elements in the model. The stabilized patella tilt angle differed from model to model. This tilt angle was typically between -2.0° and 5.0°, except in the case of the Hermes ACL-R TKA which stabilized around 13° patella tilt. After the patella reached this angle, the amount of rotation it experienced also varied from model to model but was typically under 2.0° rotation either in the internal (+) or external (-) directions, except in the case of the Axiom® ACL-R TKA which experienced about 4° of external tilt from 90° to 140° of flexion.

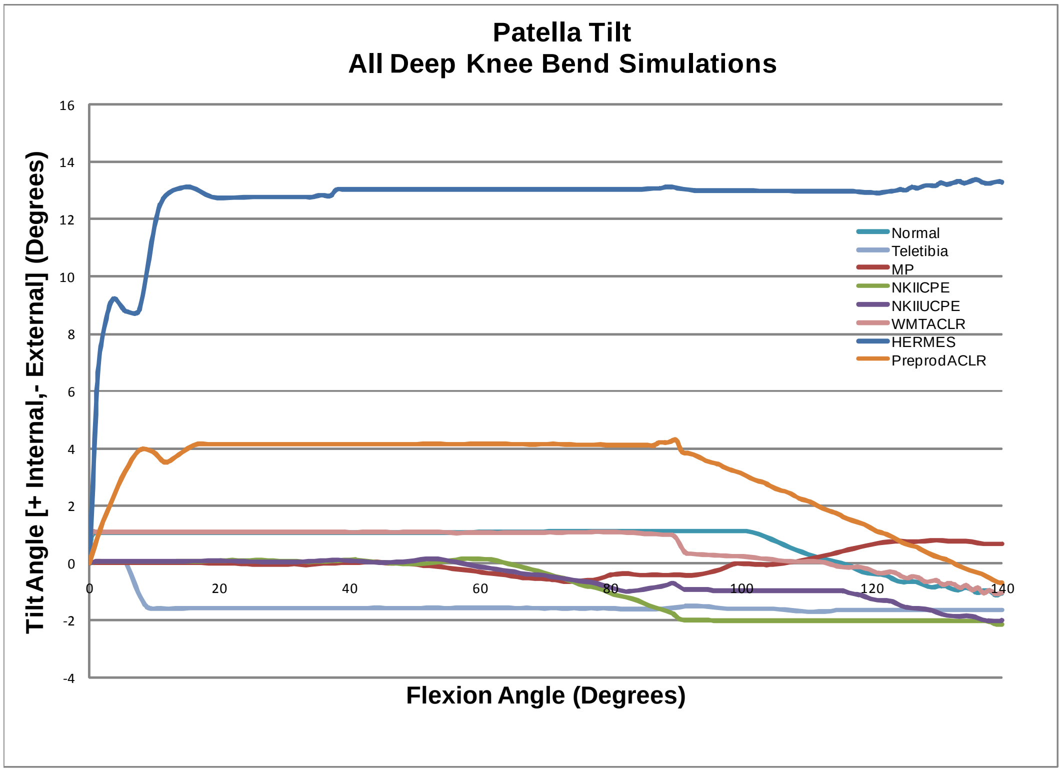

Figure 89: Patella tilt (rotation about PAT2> axis) controlled by a controller which adjusts the Vastus Medialis and Vastus Lateralis to stabilize the patella for the normal knee simulation and all TKA simulations.

Patella Rotation (Spin)

Patella rotation (rotation about the PAT1> axis) also differed for each simulation. In general the rotation stabilized between 20° and 40° knee flexion and then rotated medially (+) at various rates depending on the model until 140° flexion (Figure 90). The maximum patella rotation for each model averaged 7.6° (3.8° to 14.5°, SD=3.6°). The greatest patella rotation occurred in the normal knee with 14.5° at 140° flexion and the least maximum rotation occurred in the NKII UCPE TKA design with 3.8° at 90° flexion.

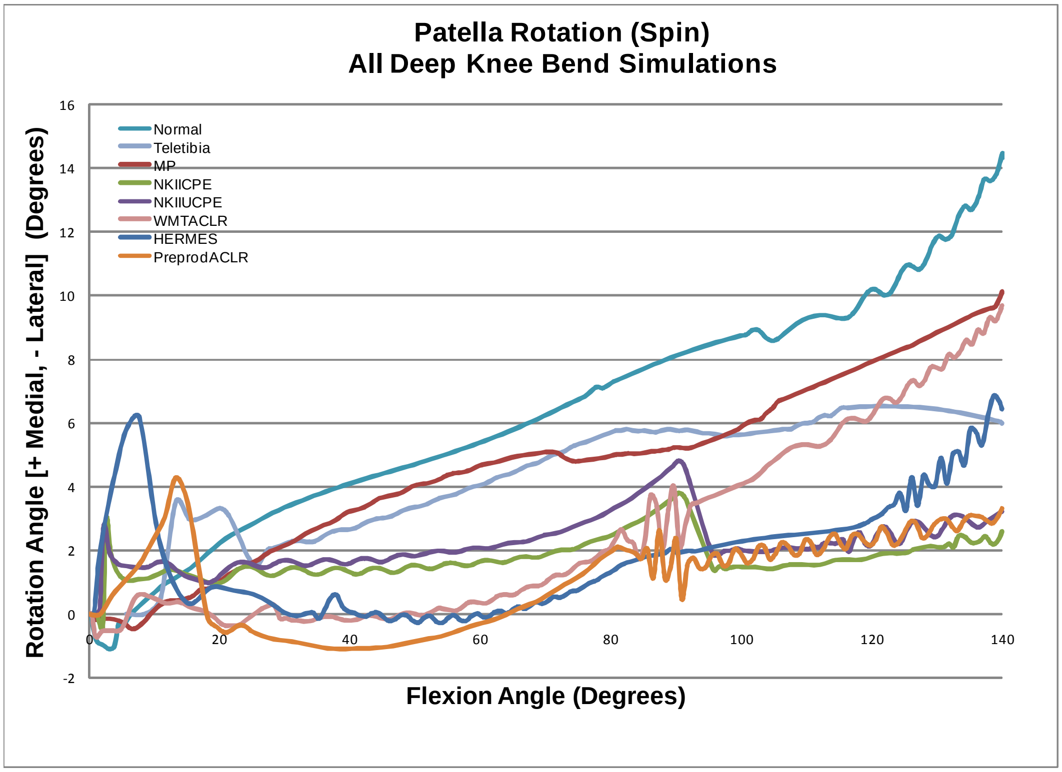

Figure 90: Patella rotation or spin (rotation about PAT1> axis) for the normal knee simulation and all TKA simulations.

Mediolateral Patella Translation

The average amount of maximum overall mediolateral movement of the patella (- medial, +lateral) was -0.3 mm (-5.2 mm to 4.9 mm, SD=3.0 mm) in the medial direction (Figure 91). Taking the absolute values of these maximum movements, the average maximum translation in either the medial or lateral direction was 2.2 mm (0.7 mm to 5.2 mm, SD=1.9 mm) in the lateral direction. The normal knee saw the most mediolateral movement of the patella with -5.2 mm in the medial direction. The Teletibia TKA design experienced the least amount of movement with -0.7 mm in the medial direction. The Hermes ACL-R TKA saw the most lateral translation of the patella with a maximum of 4.9 mm during the simulation.

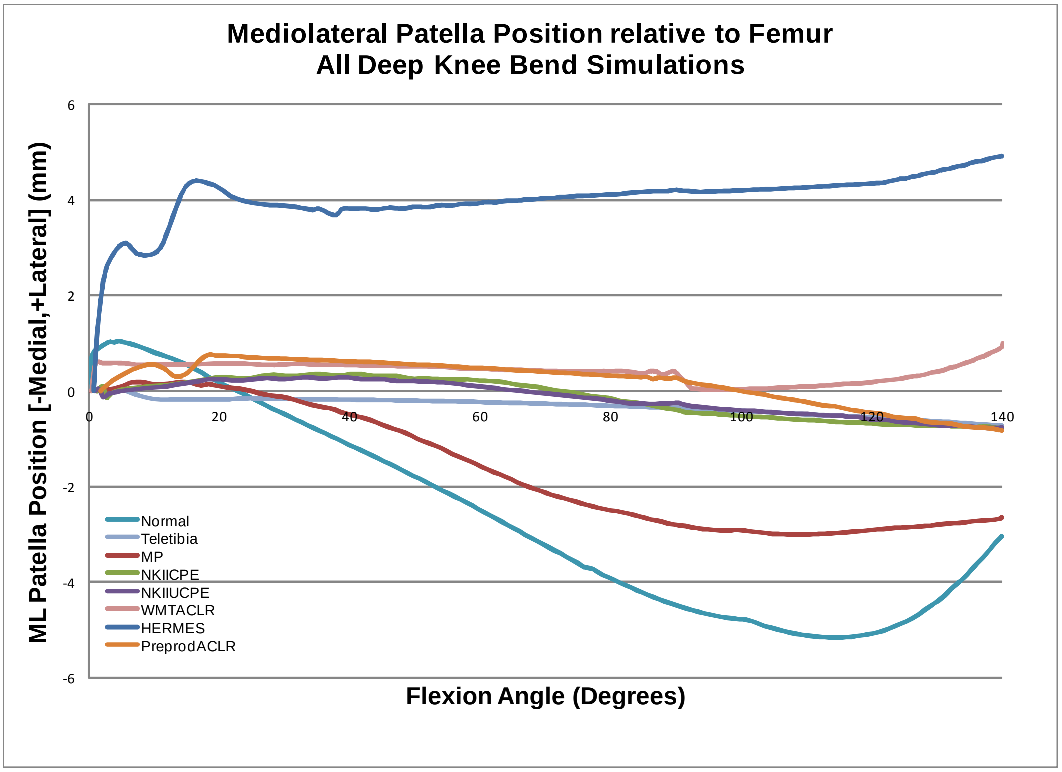

Figure 91: Mediolateral patella position relative to the femur for the normal knee simulation and all TKA simulations.

Patellofemoral Forces

The patellofemoral force pattern follows the quadriceps force pattern in that it increased until quadriceps wrapping occurred and decreased until full flexion (Figure 92). The average maximum force was 6.59 BW (5.31 BW to 8.15 BW, SD=1.07 BW). The maximum force occurred at an average flexion angle of 93° (80° to 113°, SD=11°). The greatest maximum force of 8.15 BW occurred in the NKII UCPE TKA design at 93° flexion. The smallest maximum patellofemoral force of 5.31 BW occurred in the Preproduction ACL-R at 87° flexion.

The ratio of the patellofemoral force to the quadriceps force started at full extension with an average of 0.24 (0.09 to 0.32, SD=0.08) and increases for all of the models until slightly before or during quadriceps wrapping when the values level off and usually slightly decrease until maximum flexion. The average maximum value for the patellofemoral force compared to the quadriceps force was 1.17 (1.03 to 1.26, SD=0.08) at an average flexion value of 85° (75° to 95°, 8.3°). The greatest maximum ratio of 1.26 occurred in the normal knee at 75°. The smallest maximum ratio value of 1.03 occurred in the Preproduction ACL-R at 78°. These results are consistent with findings from literature [Lanovaz 2009, Sharma 2008, Miller 1997, Ward 2005, Yamaguchi 1989, Shelbourne 1995].

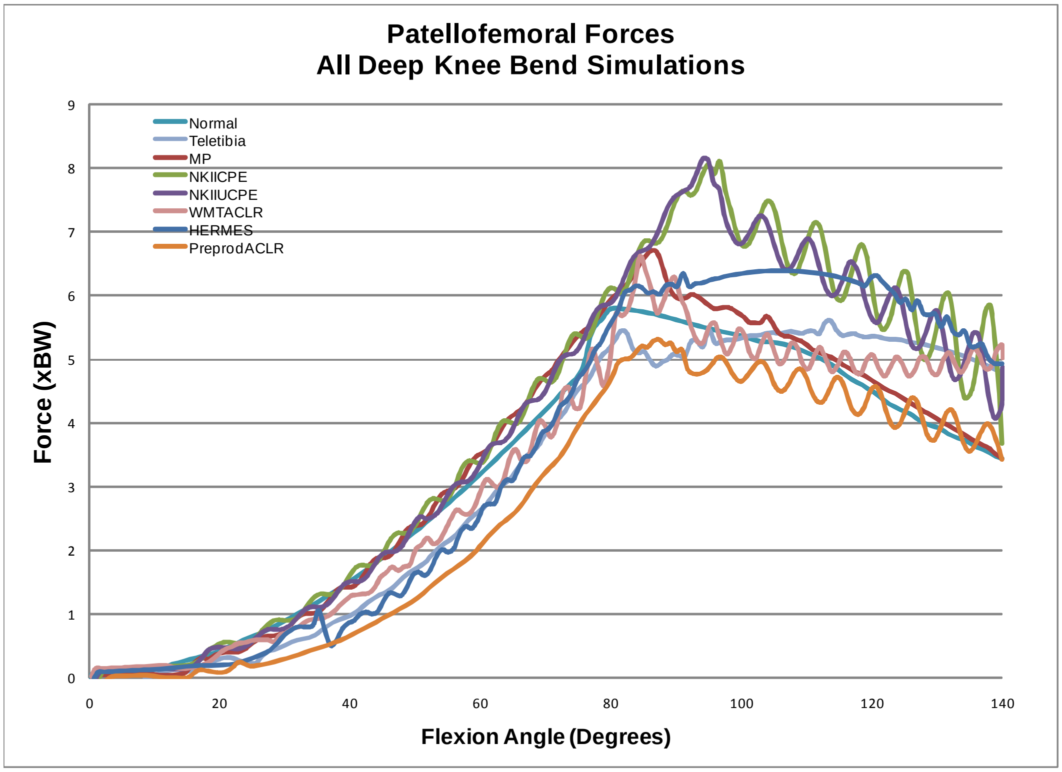

Figure 92: Patellofemoral forces for the normal knee simulation and all TKA simulations.

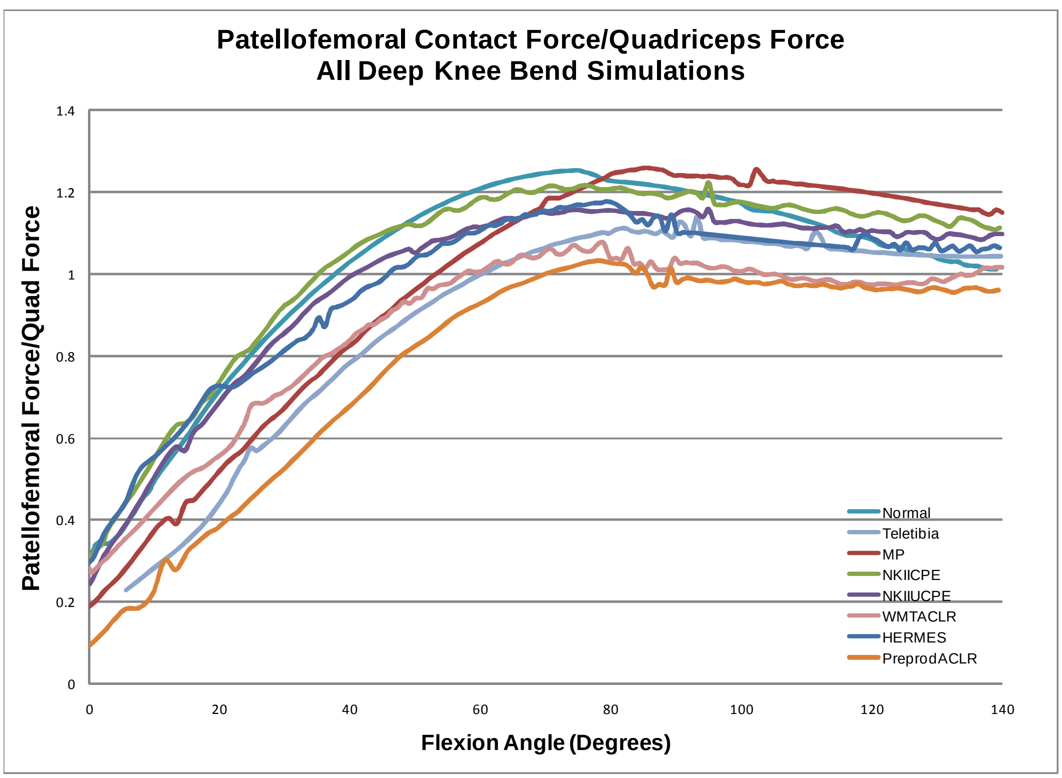

Figure 93: Patellofemoral force to quadriceps force ratio for the normal knee simulation and all TKA simulations.

Knee Ligament Forces

The magnitudes of the ligament forces were different for each simulation. However, the general pattern of their activation was similar (Figure 94). The lateral collateral ligament never became active during the simulations as the strain in this ligament never experienced a positive strain value (Figure 95) this is supported by findings in the literature [Blankevoort 1991].

The medial collateral ligament force rose from initial flexion to mid-flexion and then decreased into deeper flexion as has been reported in literature [Abdel-Rahman 1998]. The average maximum MCL force was 0.39 BW (0.09 to 1.08, SD=0.33). The greatest maximum MCL force of 1.08 BW occurred in the Hermes ACL-R TKA design at 56° flexion while the lowest maximum MCL force occurred in the NKII CPE TKA design at 54° flexion. The anterior cruciate ligament was generally active in early flexion with an average maximum force of 0.16 BW (0.09 BW to 0.28 BW, SD=0.09) which has been reported in literature [Beynnon 1995, Li 2004, Shelbourne 2008]. The Hermes ACL-R had the highest ACL force of 0.28 BW at 6° flexion while the normal knee experienced the lowest maximum ACL force of 0.09 BW at 5° flexion.

The posterior cruciate ligament had the highest average maximum force of any of the knee ligaments with 0.95 BW (0.15 BW to 1.9 BW, SD=0.68 BW) and had a pattern of increasing into deeper flexion. The pattern of the PCL increasing into deeper flexion has been reported in literature [Abdel-Rahmen 1998, Li 2004, Shelburne 1998]. The Axiom® ACL-R TKA design saw the highest PCL force of 1.9 BW at 125° flexion while the NKII CPE TKA design had the lowest maximum PCL force of 0.15 BW at 134° flexion. The patellofemoral ligaments, although present in the model were not active during any of the simulations.

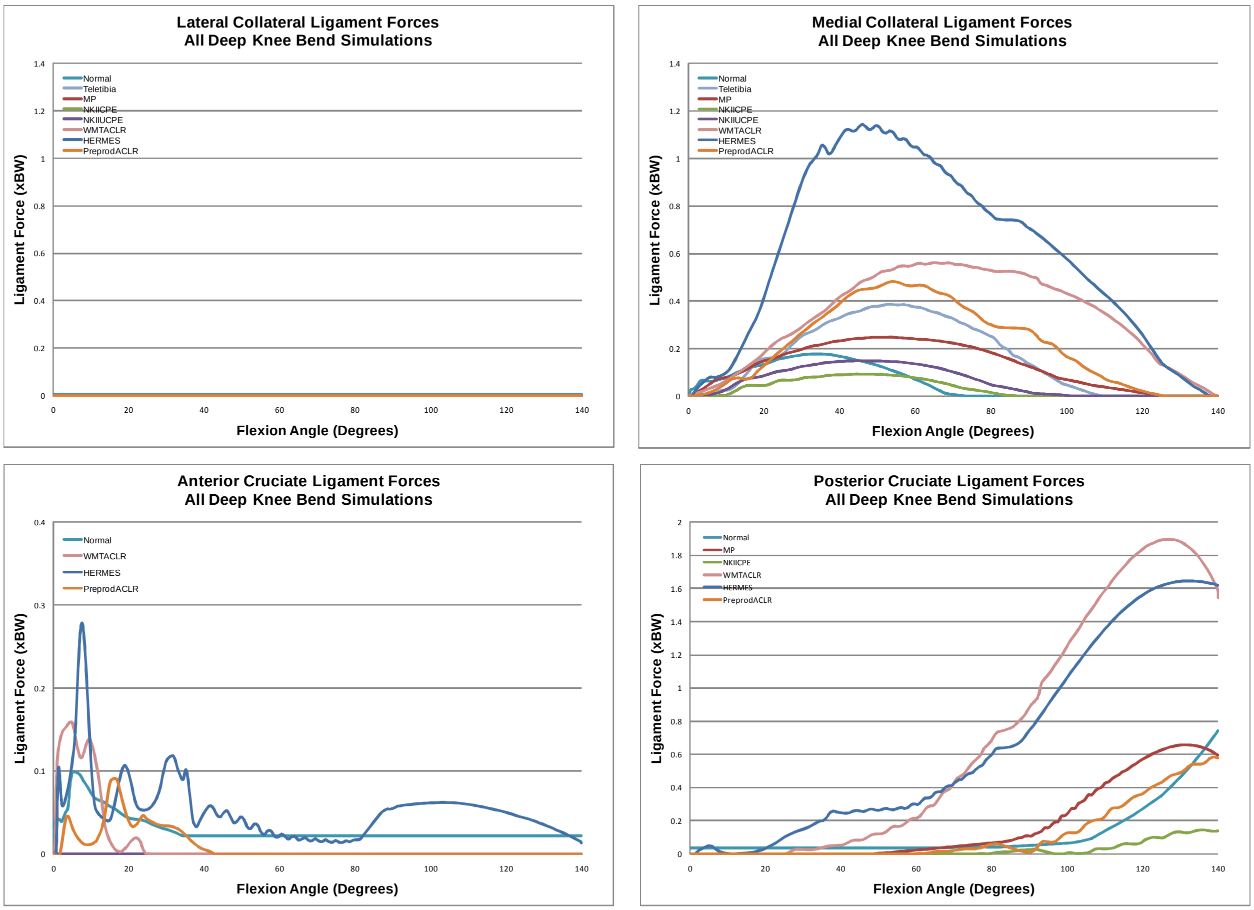

Figure 94: Ligament forces from all bundles for the LCL, MCL, ACL and PCL for the normal knee simulation and all TKA simulations.

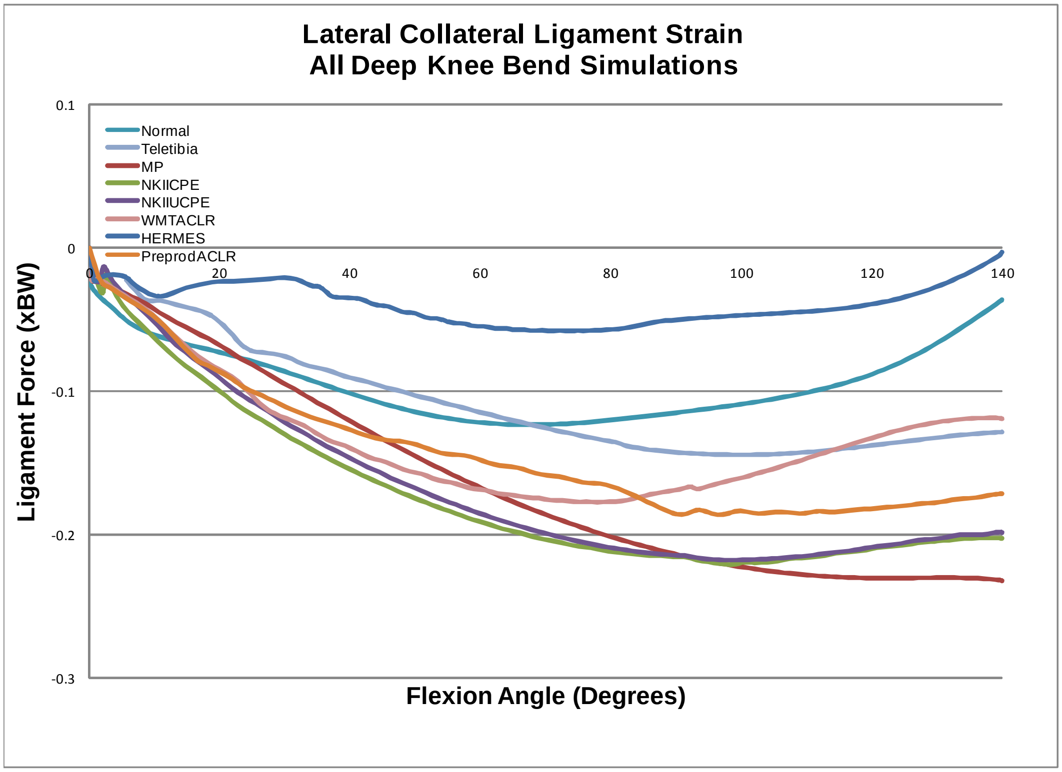

Figure 95: Average lateral collateral ligament strain values from the two spring elements making up the LCL for the normal knee simulation and all TKA simulations.

Ligament Slack Lengths

The following results are from simulations of the normal knee and Medial Pivot TKA design in which the ligaments were tightened. The ligament slack lengths for the deep knee bend and non-weight bearing extension simulations were tuned independently. The ligaments in the extension simulations were made tighter than in the deep knee bend because of the lack of physiological constraints in the model. The slack lengths in the following deep knee bend simulations were based on the extension slack lengths for the normal and Medial Pivot TKA. Some of the ligament forces were so tight they prevented the knee from progressing into flexion, therefore some were loosened on a trial bases until the simulation ran to 140° flexion. This finding has lead to hypothesis that under “true” conditions, implants could be surgically implanted, such that the MCL becomes too tight, which in-turn limits active, weight-bearing knee flexion.

Tightening the LCL resulted in a force in the beginning of flexion for the new Medial Pivot simulation while it resulted in a force in later flexion for the normal knee model (Figure 96). Tightening the MCL resulted in a greater force in the new simulation during a similar portion of flexion as the original model. In the Medial Pivot TKA design, however, the MCL ligament force appeared to be activated earlier, but did not reach the same magnitude as the original and went “slack” earlier than the original simulation. The force in the ACL did not experience a notable change. Most of the ligaments were adjusted but the ACL had to be “loosened” significantly in order for the simulation to begin flexion. The PCL experienced the most significant change from the original simulation to this altered new simulation. The force more than doubled in the Medial Pivot TKA design and tripled in the normal knee. The forces in the normal knee are probably higher than the tensile strength of the PCL in vivo.

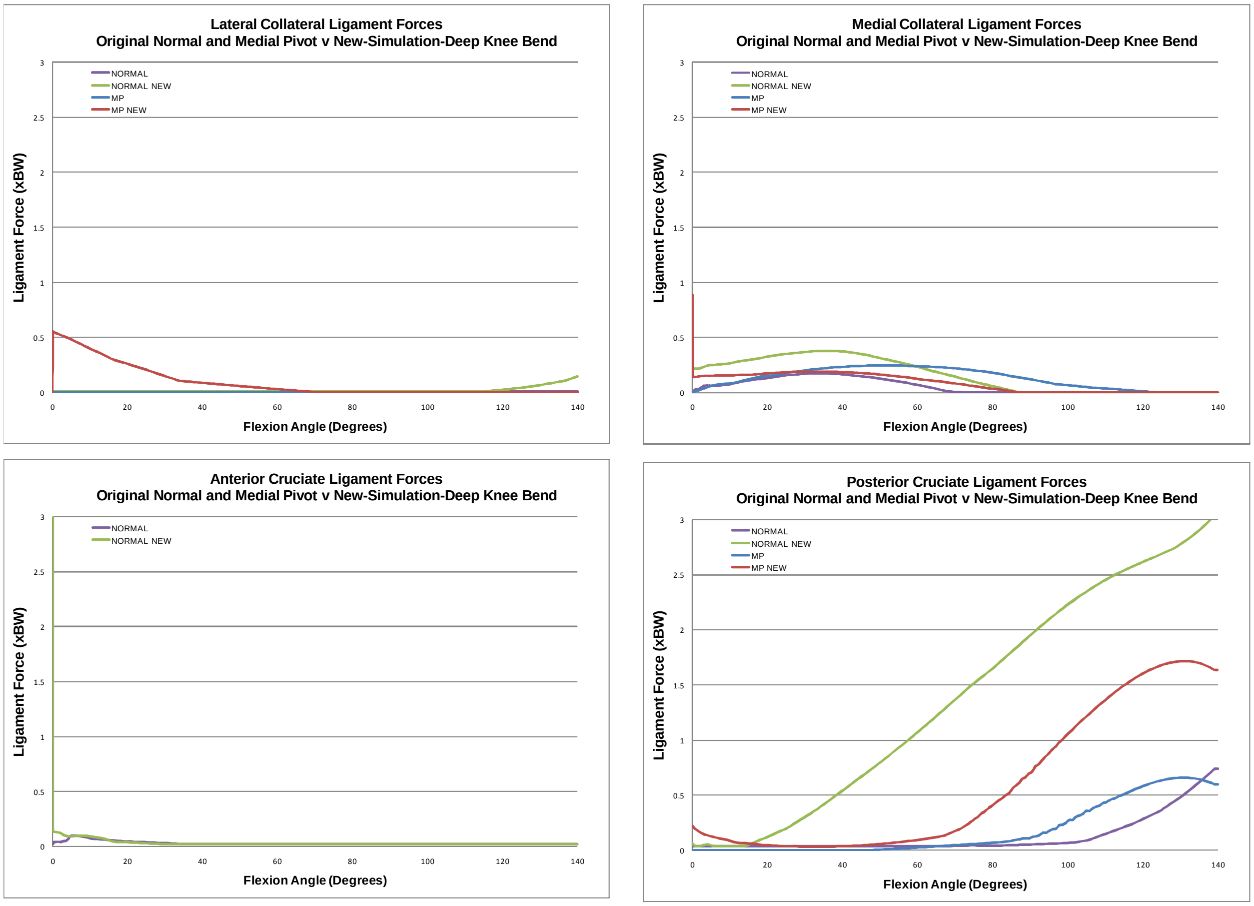

Figure 96: Ligament forces for the original normal and Medial Pivot TKA deep knee bend simulation and for a new simulation with tighter ligaments.

Changing the ligament slack lengths influenced both the kinematic and kinetic results derived using the model (Figure 97). The medial contact movement in the Medial Pivot TKA is not as erratic in early flexion and is probably due to the increased MCL force. The medial and lateral contact positions moved more posterior in later flexion for both the Medial Pivot TKA and changed almost 10 mm in the normal knee. This change is most likely due to the increased force in the PCL. The maximum tibiofemoral force almost doubled for the normal knee which is also attributed to the increased PCL force. The Medial Pivot TKA simulation also saw an increase in tibiofemoral force attributed to the increased force in the PCL. The quadriceps force changed slightly in later flexion but did not prove too sensitive to the change of ligament slack lengths.

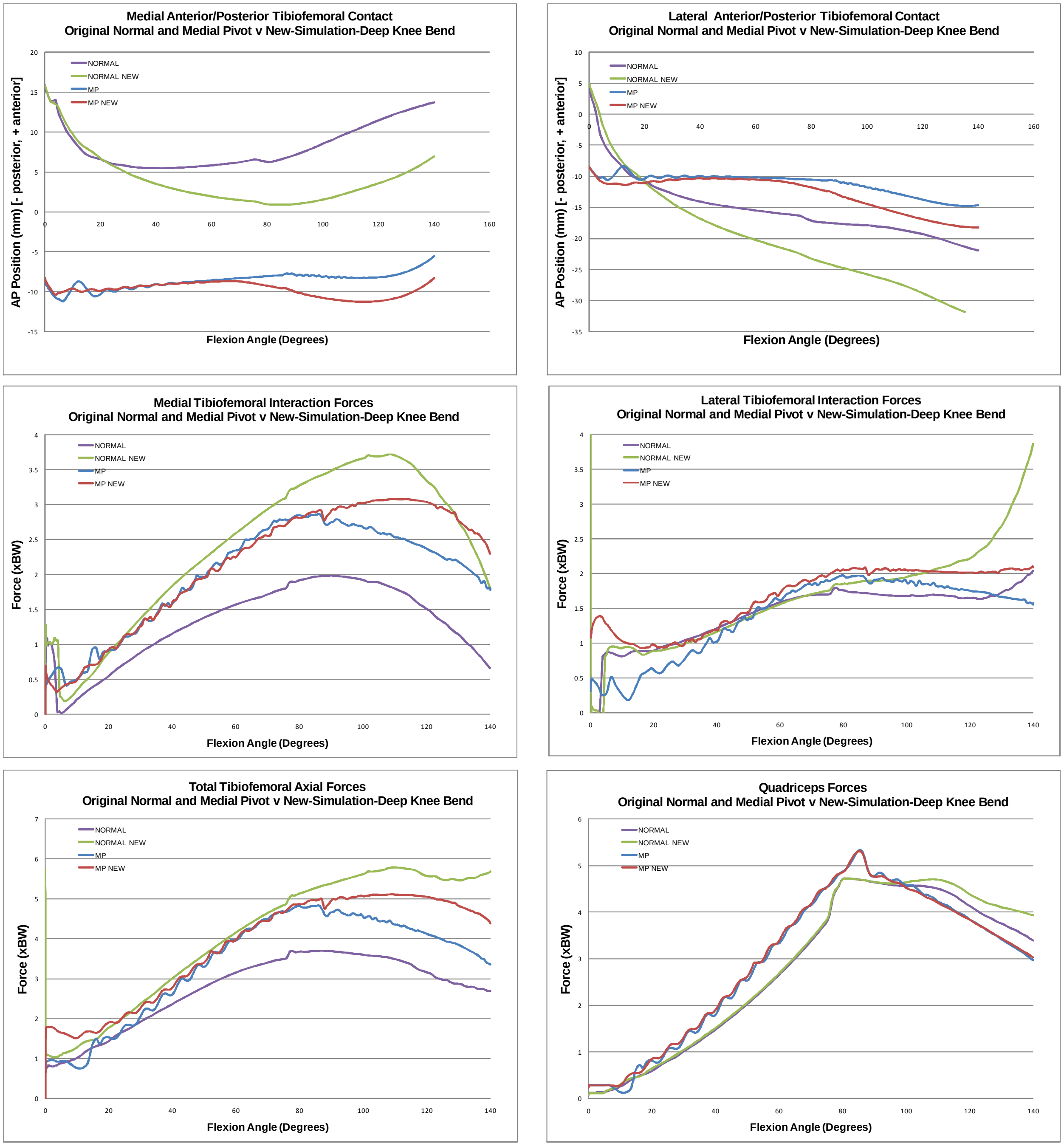

Figure 97: Tibiofemoral kinematics, kinetics and quadriceps force comparison for the original normal knee and Medial Pivot TKA implanted knee deep knee bend simulation and simulations with tightened ligaments.

Chapter 7: Sensitivity Analysis

The following results are from various sensitivity analysis of particular variables. Some of the variables were chosen for analysis with the purpose of examining the affect of assumptions in the model. These analyses were performed on the deep knee bend simulation using the Teletibia TKA design. In some cases not all of the results from simulations run are included in the results because of either numerical problems with the ordinary differential equations solver or because the quadriceps PID controller did not perform correctly giving results well outside realistic possibility. Also, because the solver struggles in early flexion especially, the simulations were started at 5 degrees to give the models a better chance to solve to 140 degrees flexion.

Rectus Femoris to Vastus Intermedius Force Ratio

One assumption made in this model is that the Rectus Femoris muscle force has a constant relationship to the Vastus Intermedius muscle. The ratio of Rectus Femoris force to Vastus Intermedius force was 0.225 in all simulations discussed previously. When modeling the lower leg the force in the Rectus Femoris is commonly calculated to be lower than in the Vastus Intermedius [Kim 2009, Shelburne 2002, Piazza 2001]. Changing this ratio does have a large effect on the tibiofemoral force results in the model and changes the shape and maximum value of the quadriceps force plot, although there is little affect on the AP contact position prediction (Figure 98). The quadriceps force reached the maximum allowable force for two of the simulations but interestingly reached almost the same value at maximum flexion for all simulations but one. The PID controller increased the overall quadriceps force more to slow the flexion rate as the Rectus Femoris/Vastus Intermedius force ratio increased. This was most likely due to the Rectus Femoris origin being on the anterior pelvis. The greater Rectus Femoris force created a flexion torque on the trunk, making it want to lean forward. This model resisted the rotation of the trunk by applying a constraining torque in the opposite direction. This constraining torque increases to counteract the affect of the higher Rectus Femoris forces, the torque on the trunk propagated to the femur and created a torque in the direction of greater flexion, which made the PID controller increase the overall quadriceps force more than when the Rectus Femoris force was lower (Figure 99). The flexion error seen in those simulations which reached the maximum quadriceps force was much higher than typically seen in other simulatons (Figure 100). Although increasing the Rectus Femoris/Vastus Intermedius force ratio did not have desirable affects, it showed that the model is sensitive to such changes and reacted in a way which, if not expected, makes sense.

Sensitivity Analysis of Rectus Femoris/Vastus Intermedius Force Ratio

Teletibia TKA-Deep Knee Bend Simulation

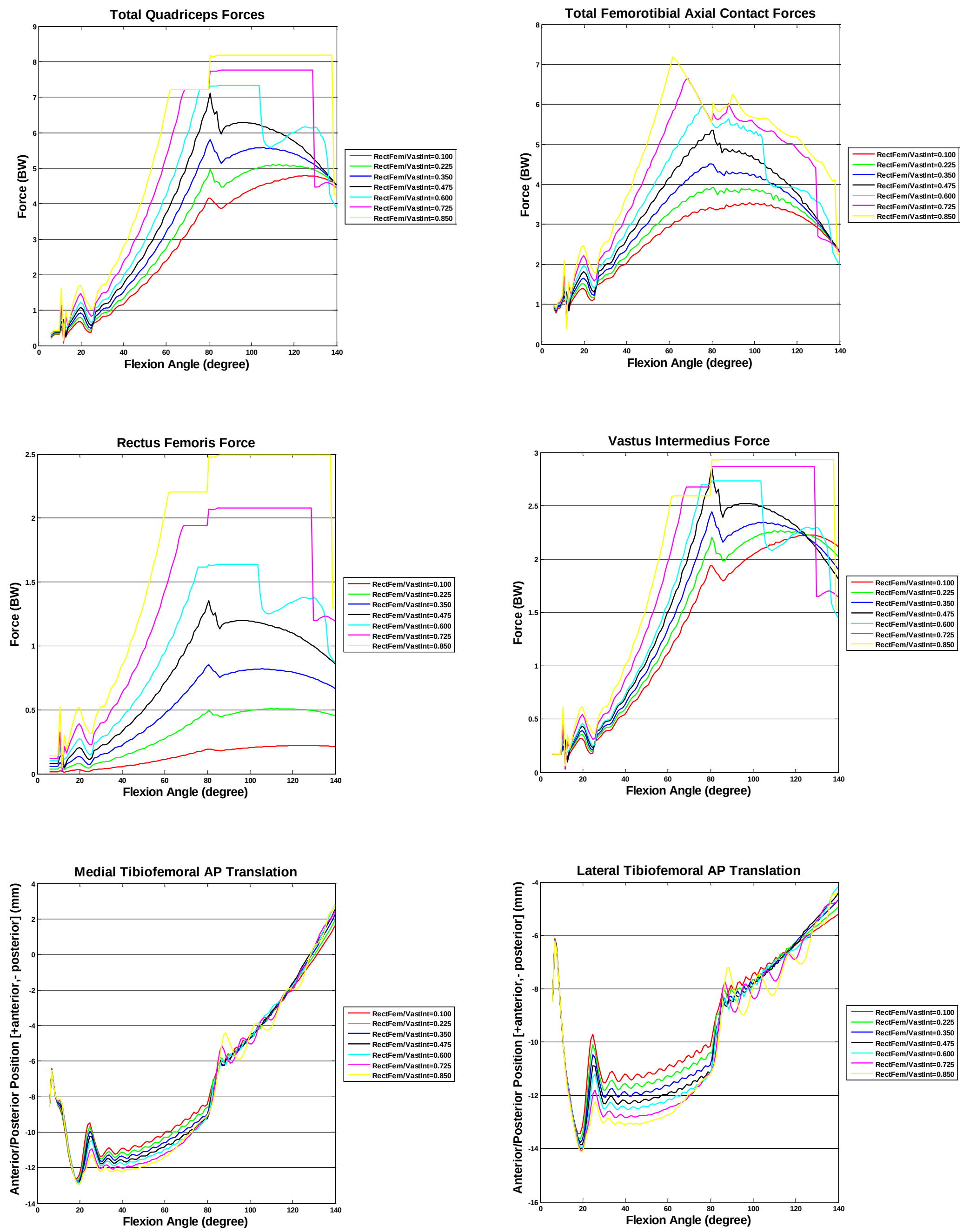

Figure 98: Sensitivity analysis results from increasing the Rectus Femoris / Vastus Intermedius force ratio. The model used for validation had a ratio of 0.225.

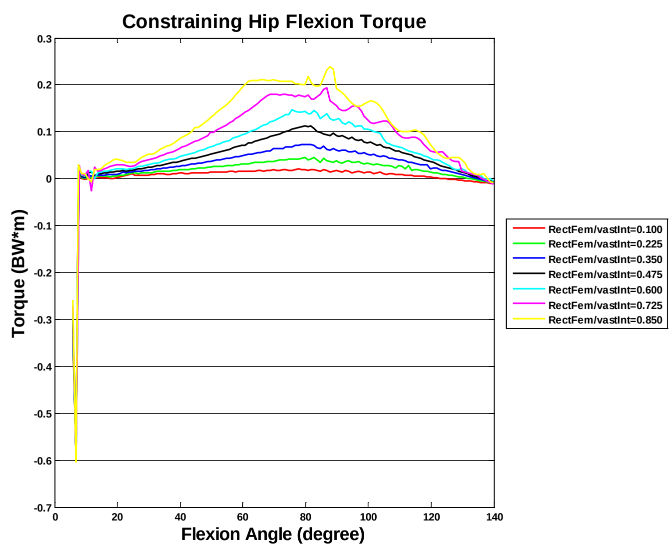

Figure 99: The torque applied to the trunk to constrain the trunk flexion for sensitivity analyses of the Rectus Femoris force ratio with the Vastus Intermedius muscle force. The increased torque seen in the simulations with increased Rectus Femoris/Vastus Intermedius force ratios probably increases the flexion torque on the femur and causes the increased overall quadriceps force controlled by the PID controller.

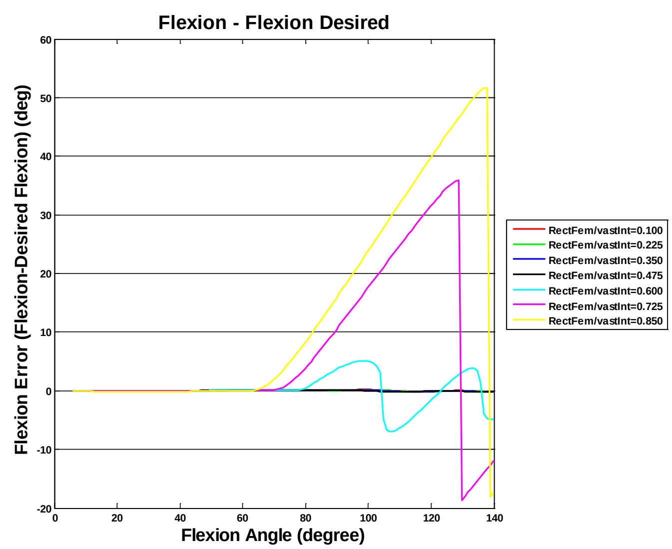

Figure 100: The flexion error (flexion-desired flexion) for sensitivity analyses of the Rectus Femoris force ratio with the Vastus Intermedius muscle force.

“Patella Button” Thickness

The thickness of the patella contact surface implant or “patella button” is examined in the following results (Figure 102). By changing the distance between the patella COM and the contact points, the patella position adjusts from the center of the femoral component and increases or decreases the distance between the contact points and the application of the force through the extensor mechanism. This increases or decreases the applied moment arm length. The results show that the model is sensitive to this variable and that changing the patellar button thickness by 1 cm can change the maximum tibiofemoral forces by 1*BW. This result is expected as increasing the length of the extensor mechanism moment arm should decrease the required force from the quadriceps or increase it as the moment arm is shortened sensitivity results from literature also show that models are sensitive to the patellar thickness [Halloran 2009].

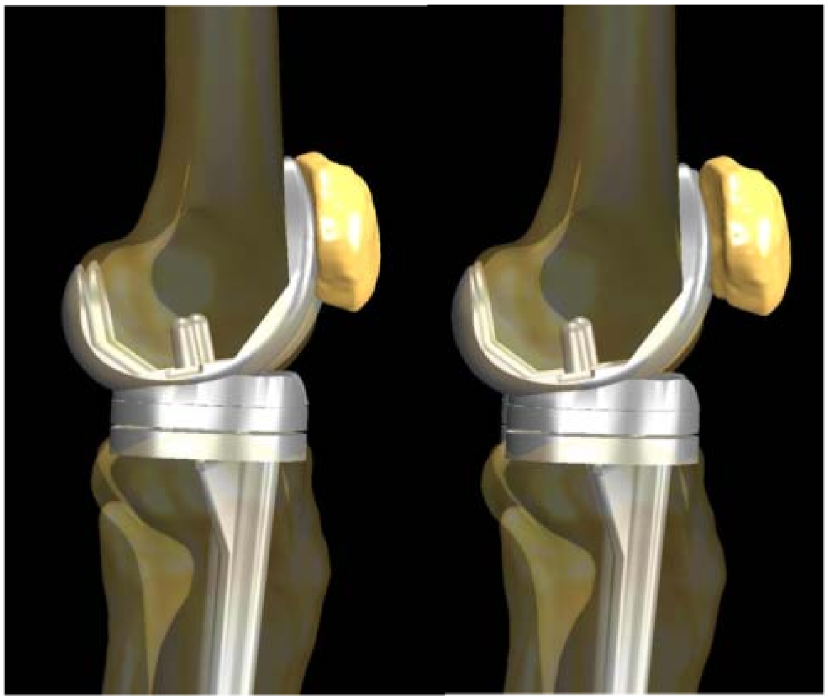

Figure 101: Although the "patellar button" is not visible in the above images the thickness is changed by keeping the patellofemoral contact points on the trochlear groove and moving the patella anterior from the femur. Pn the left is the thinnest patellar button analyzed, 9mm, and on the right the thickest, 19 mm.

Sensitivity Analysis of “Patella Button” Thickness
Teletibia TKA-Deep Knee Bend Simulation

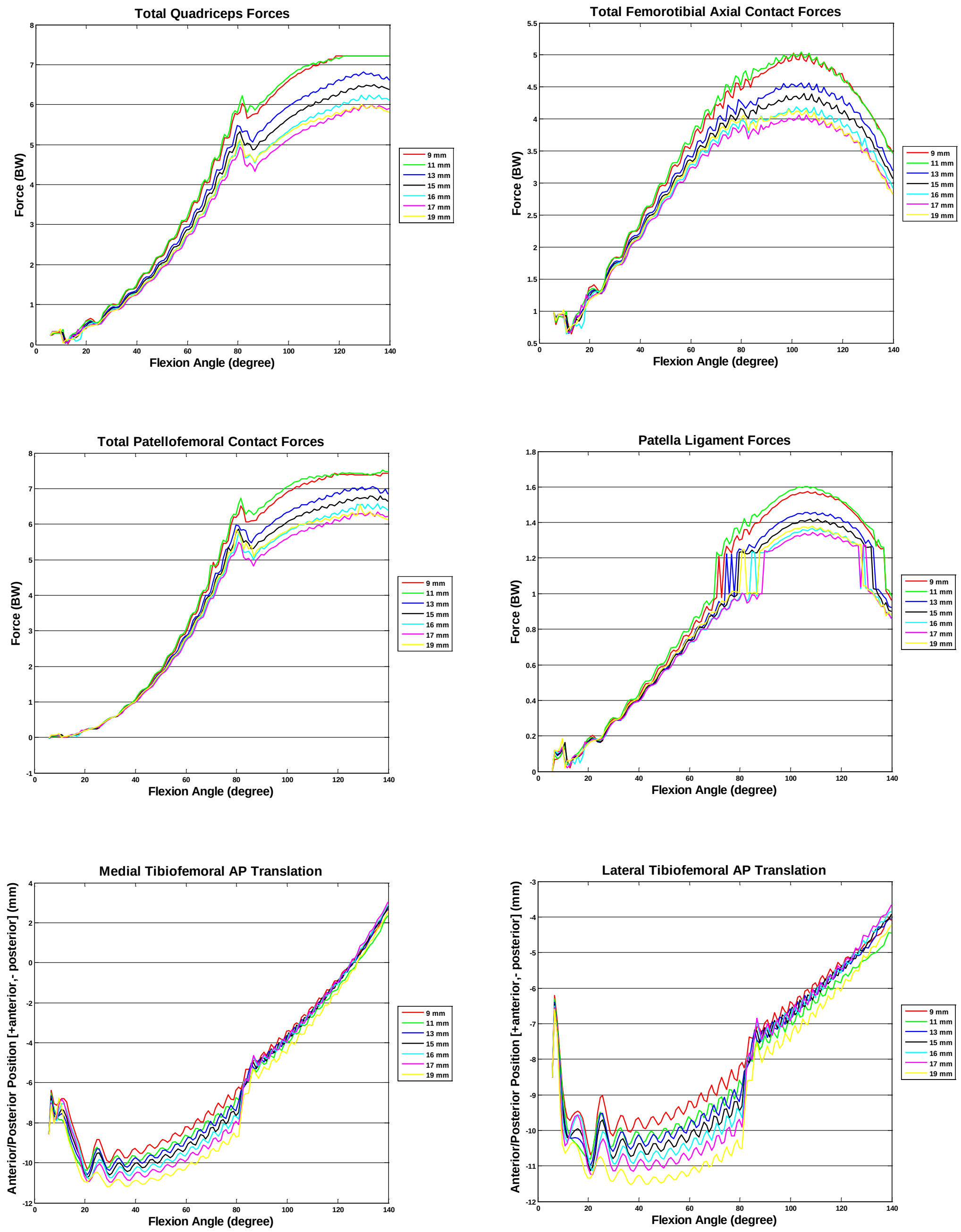

Figure 102: Sensitivity analysis results from increasing the “patella button” thickness. A thinner patella button moves the patella closer to the surface of the femoral component reducing the moment arm and a thicker one moves the patella away from the femoral component surface increasing the moment arm. Increasing the moment arm results in less quadriceps force and subsequently less tibiofemoral force. The value used in the validation results is a thickness of 13 mm.

Lateral and Medial Tibial Sagittal Geometry

The ultimate goal of this model is to predict the effects of implant design on the knee kinematics and kinetics. A sensitivity analysis was performed on the average sagittal geometry of the lateral (Figure 103) and medial (Figure 104) trays of the Teletibia TKA polyethylene insert. The curvature of the trays were adjusted from the actual average Teletibia TKA curvature (data set 4 in Figure 103 and data set 3 in Figure 104). For the lateral adjustment there were some effects on the quadriceps and axial knee forces but the greatest effect was on the tibiofemoral contact kinematics. The geometry with the largest radius allowed more overall translation and more posterior translation of the lateral AP contact point position. As would be expected the design which was more conforming allowed less translation and had a more anterior contact position. Interestingly, the profile of the medial tray affected the quadriceps and axial force values more than the lateral profiles and seemed to affect the kinematics of the contact point a little less. Interestingly, although not unexpected, changing the design parameters on one side of the insert also affects the kinematics of the contralateral side contact point. This is a case where more simulations were run than are presented here. The simulations not presented ran into numerical problems and did not run to completion, usually only making it to about 30 degrees. Many times these problems are not inherent to the model but the inputs. Either the PID controller controlling the quadriceps force or the controller stabilizing the patella usually are the sources of such problems.

Sensitivity Analysis of Lateral Tibial Tray Sagittal Profile

Teletibia TKA-Deep Knee Bend Simulation

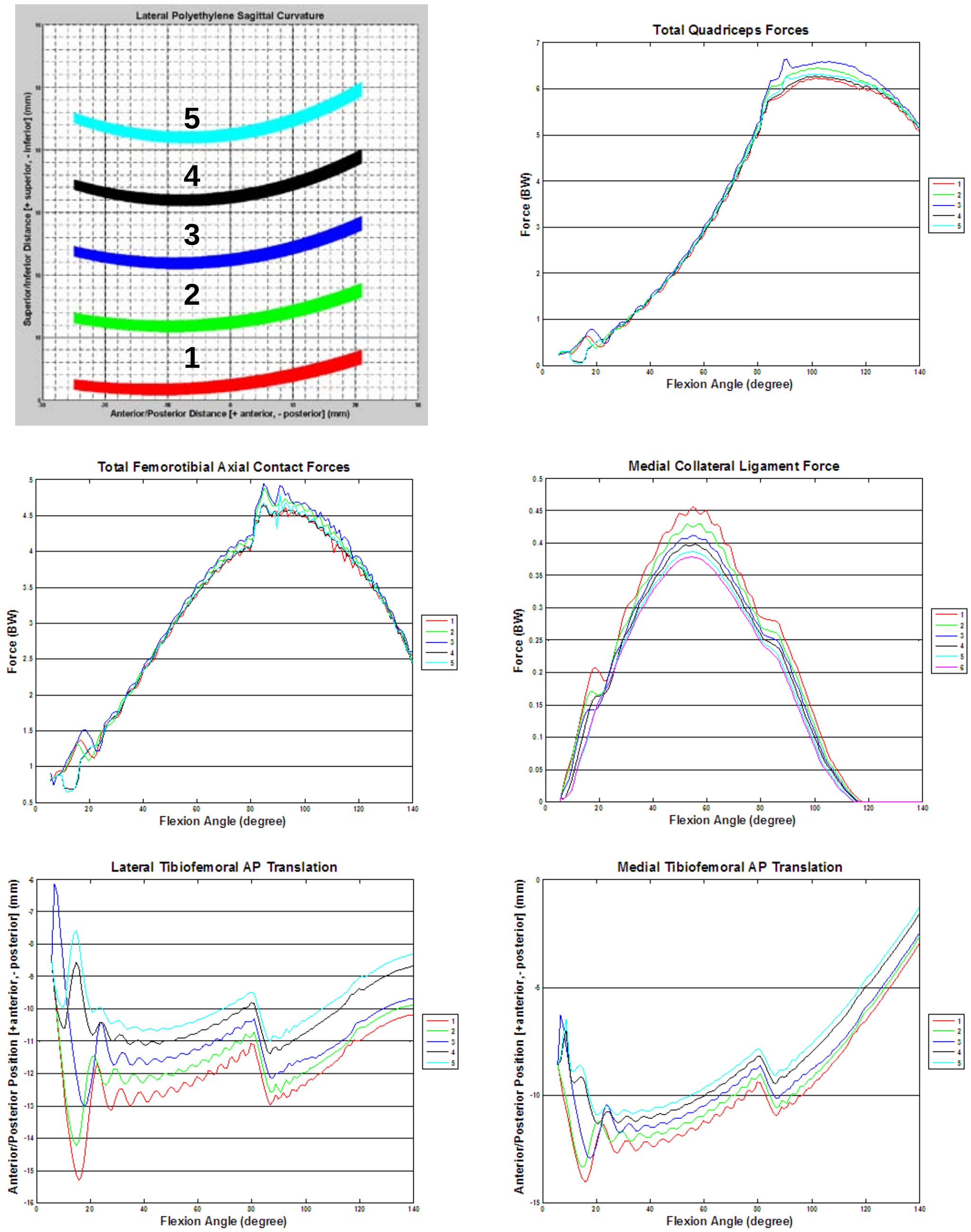

Figure 103: Sensitivity analysis of the lateral tibial tray curvature. The average curvatures simulated are shown in the upper left with data set 4 being the actual curvature of the Teletibia TKA. The "well point" changed moving more anterior in the more conforming design (5) and more posterior in the less constrained curvature (1-3).

Sensitivity Analysis of Medial Tibial Tray Sagittal Profile
Teletibia TKA-Deep Knee Bend Simulation

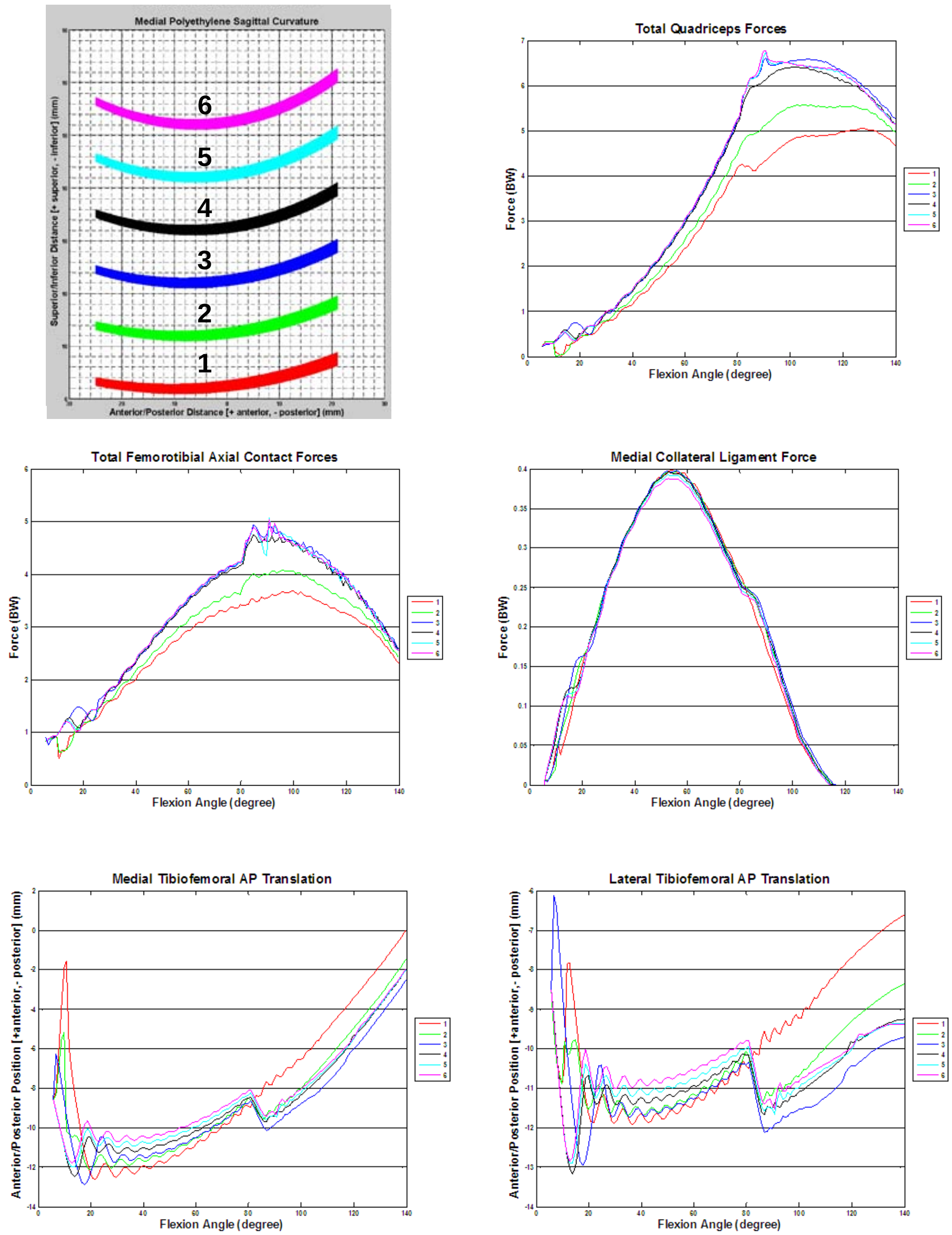

Figure 104: Sensitivity analysis of the medial tibial tray curvature. The average curvatures simulated are shown in the upper left with data set 3 being the actual curvature of the Teletibia TKA. The "well point" changed moving more anterior in the more conforming designs (4-6) and more posterior in the less constrained curvature (1-2).

Lateral and Medial Femoral Sagittal Geometry

The shapes of the lateral and medial sagittal geometry curvature was changed for this sensitivity analysis. There were no major or obvious affects from the changes of the geometry. However, there were differences which showed that changing the location of the contact points of the femur does have some affect on how the model behaves.

Sensitivity Analysis of Lateral Femoral Sagittal Profile (1)
Teletibia TKA-Deep Knee Bend Simulation

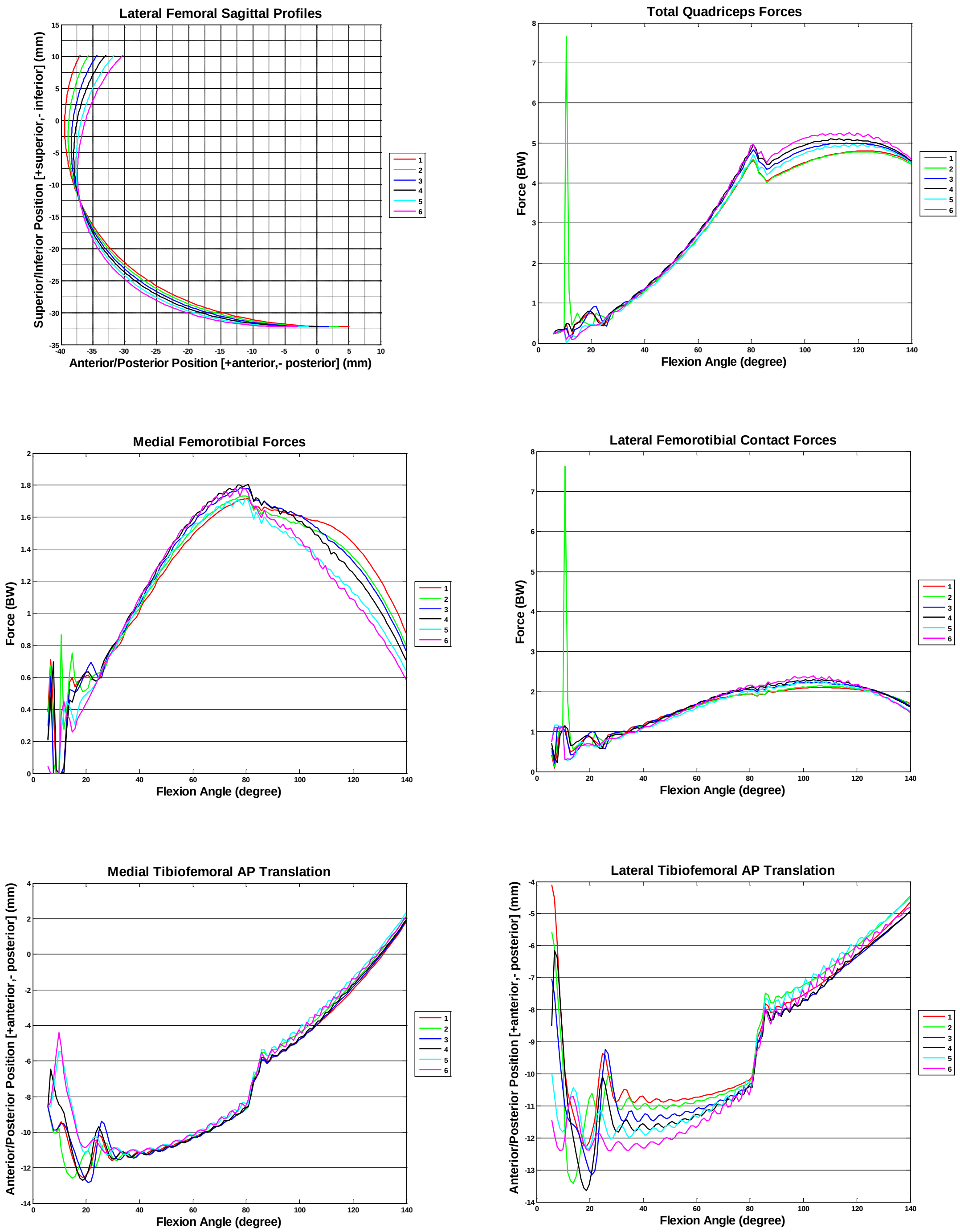

Figure 105: Sensitivity analysis of the lateral sagittal femoral curvature. The curvatures simulated are shown in the upper left with data set 4 being the actual curvature of the Teletibia TKA.

Sensitivity Analysis of Medial Femoral Sagittal Profile (1)
Teletibia TKA-Deep Knee Bend Simulation

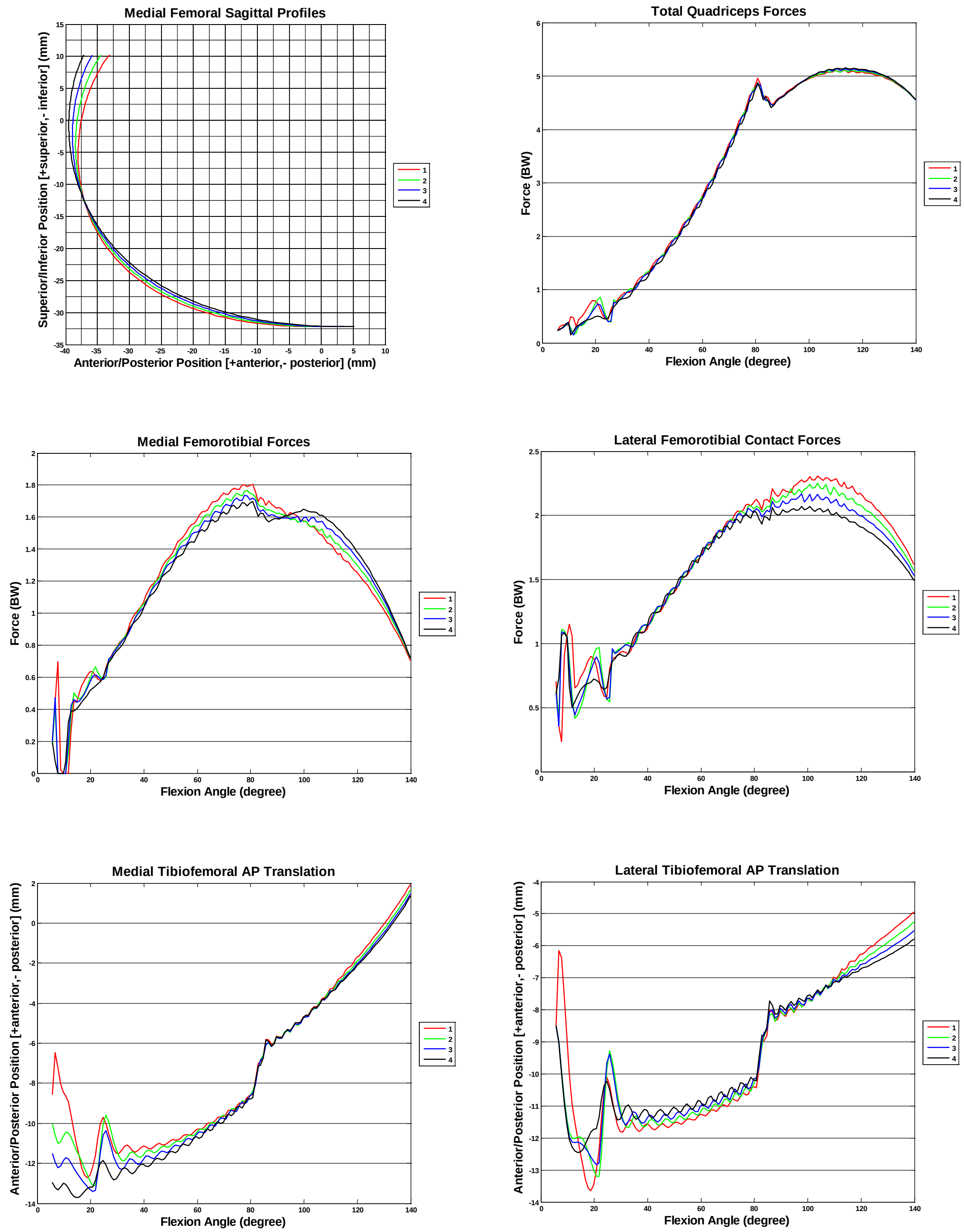

Figure 106: Sensitivity analysis of the medial sagittal femoral curvature. The curvatures simulated are shown in the upper left with data set 1 being the actual curvature of the Teletibia TKA.

Body Weight

The segment masses including the mass/weight of the trunk are calculated based on the total body weight assigned to the model. For all of the models discussed so far the body weight has been 900 N. The total body weight was adjusted to see if the resulting affects are expected and what the affect a person's weight can have on TKA mechanics. The quadriceps force, when in units of body weight as commonly described, unexpectedly looked higher for the lower body weight (Figure 107). However, when the units were changed to newtons, the expected increase in quadriceps force with body weight was evident. The maximum quadriceps force increases almost linearly with the changing body weight, doubling from a little over 3000 N in the lowest body weight of 600 N to 6000 N in the highest of 1200 N, which made sense since the quadriceps force in units of BW were so close to each other. This linear relationship was unexpected but not surprising since the trunk and femur weights doubled with the doubling of the body weight. The total femorotibial axial force also increased with increasing body weight. The medial and lateral contact positions were also affected but not by more than one mm.

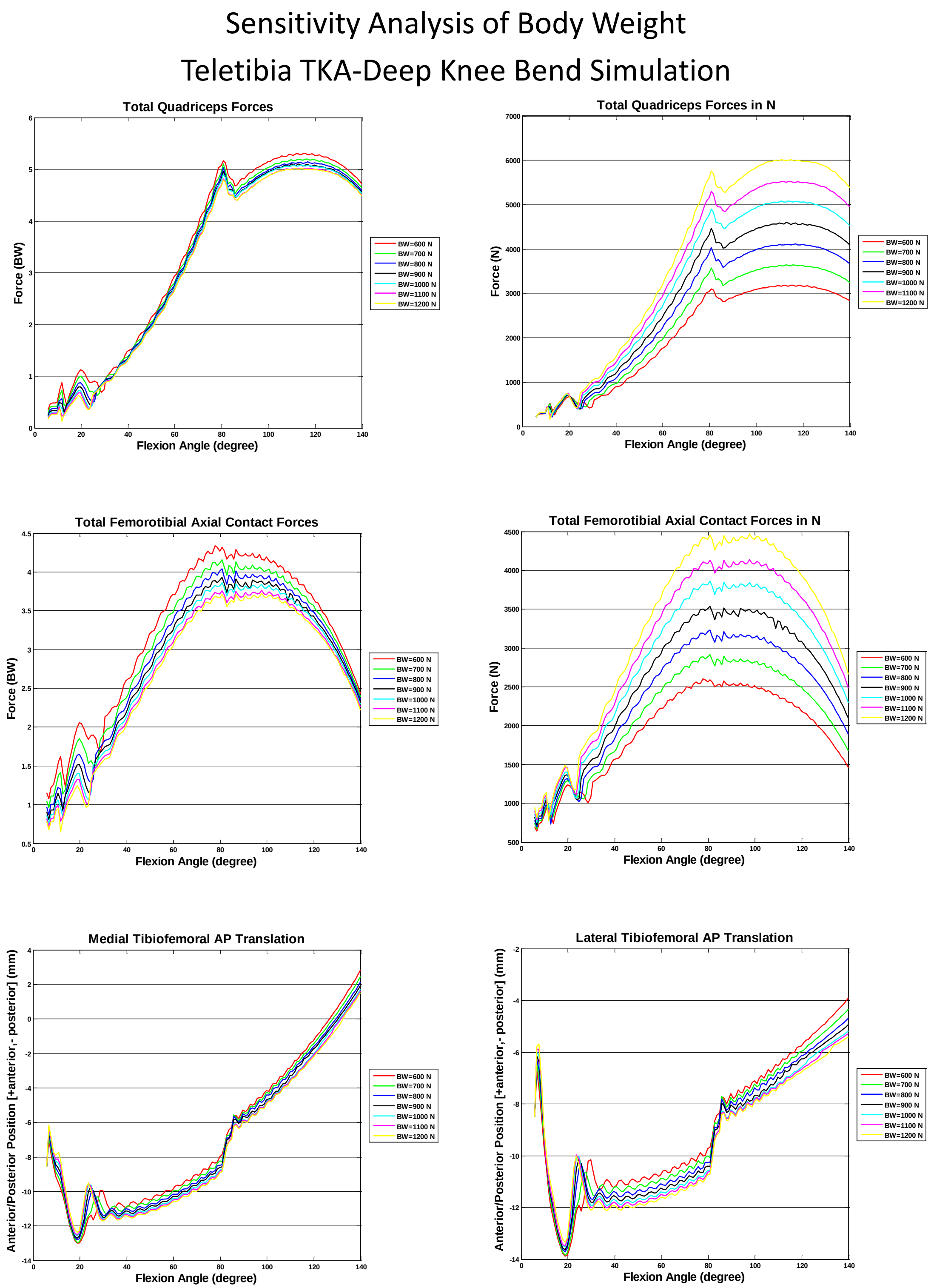

Figure 107: Sensitivity analysis of the total body weight parameter. The original body weight is 900 N. The quadriceps and total axial forces are in the top two rows in units of BW on the left and N on the right.

Tibial Component Rotational Orientation

For the component orientation analysis, the position of the tibial TKA component was adjusted relative to the tibia body. The femoral component was also adjusted so that it remained in the same initial position as previous simulations relative to the tibial component's new orientation. This analysis adjusted the orientation of the tibia in the coronal plane (Figure 108). Coronal alignment is such a concern in TKA that tools such as surgical navigation have been developed to assist surgeons in providing the correct alignment during implantation [Kim 2005]. There was little effects were minor on the quadriceps force and total axial force, except in later flexion. There was, however, a fairly large effect on the tibiofemoral contact kinematics. There was a difference of almost five mm between the two most extreme rotations in opposite directions for the medial and lateral contact points. This resulted in large differences in internal/external rotation (in this case calculated as the angle between the line connecting the medial and lateral contact points and the mediolateral line of the tibial component (Figure 109)). The greater external rotation, however, seen in the simulations with negative rotations of the tibial component, was a result of greater anterior slide of the medial contact point, while the simulations with lower external rotation saw greater anterior slide of the lateral condyle. The original orientation of the tibial component saw the least amount of internal/external rotation but avoided extreme amounts of anterior slide of either condyle. Improper coronal alignment has been thought to increase the risk of failure and wear in TKA [Bargren 1983]. The increased anterior slide of the contact points with increased coronal rotation could contribute to increased wear of the polyethylene insert.

Sensitivity Analysis of Tibial Component Coronal Orientation
Teletibia TKA-Deep Knee Bend Simulation

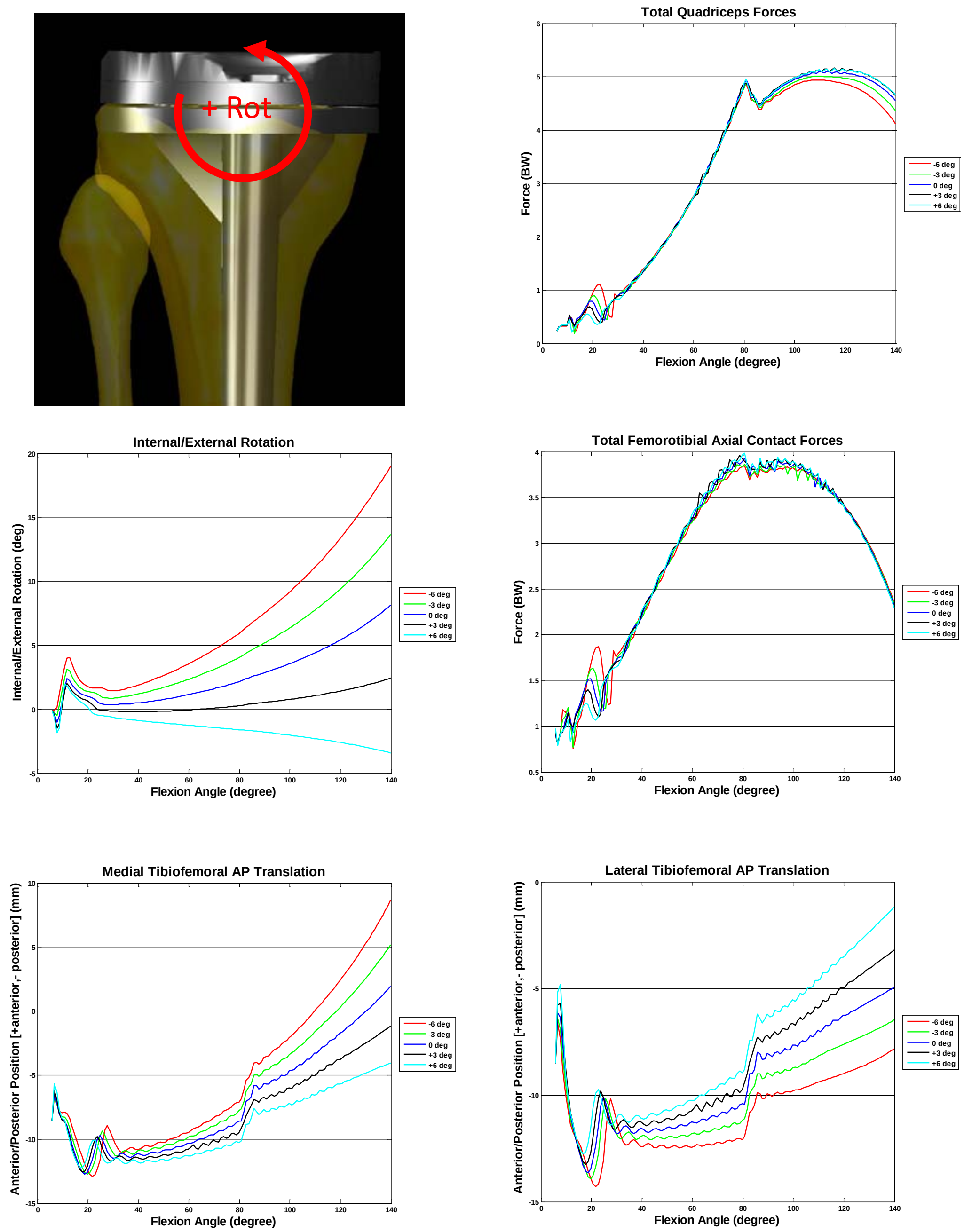

Figure 108: Sensitivity analysis of the rotation of the tibial component in the coronal plane (image in upper left describes rotational direction). The data sets are described by the rotation from the original orientation used for the validation. Internal/External rotation (middle plot on the left) in this case is calculated as the angle between the line connecting the contact points and the mediolateral line of the tibial component.

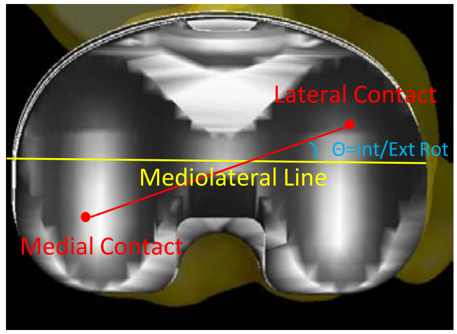

Figure 109: Description of internal/external rotation calculation in Figure 108

Femoral Component Rotational Orientation

The femoral component coronal orientation, along with the tibial alignment is thought to be important to the longevity of the femoral implant. The model was sensitive to the variable in that any rotations over 5 degrees in either rotation resulted in numerical failure before 30° degrees flexion. Again, this could be due to the PID controller, which if more refined may have controlled flexion better and allowed those simulations to run past 30°. However, radiological analysis of coronal component alignment from both traditional TKA and TKA using computer navigation show that malrotation is usually well under 5° [Kim 2005] and sensitivity of another model stayed within 5° of the original orientation [Lenovaz 2009]. The model did not prove to be very sensitive to the adjustments. However, the slack length of the ligaments for these simulations were recalculated whenever the implant position was changed (See Appendix for more sensitivity analysis including some which did not adjust the ligament slack lengths).

Sensitivity Analysis of Femoral Component Coronal Orientation
Teletibia TKA-Deep Knee Bend Simulation

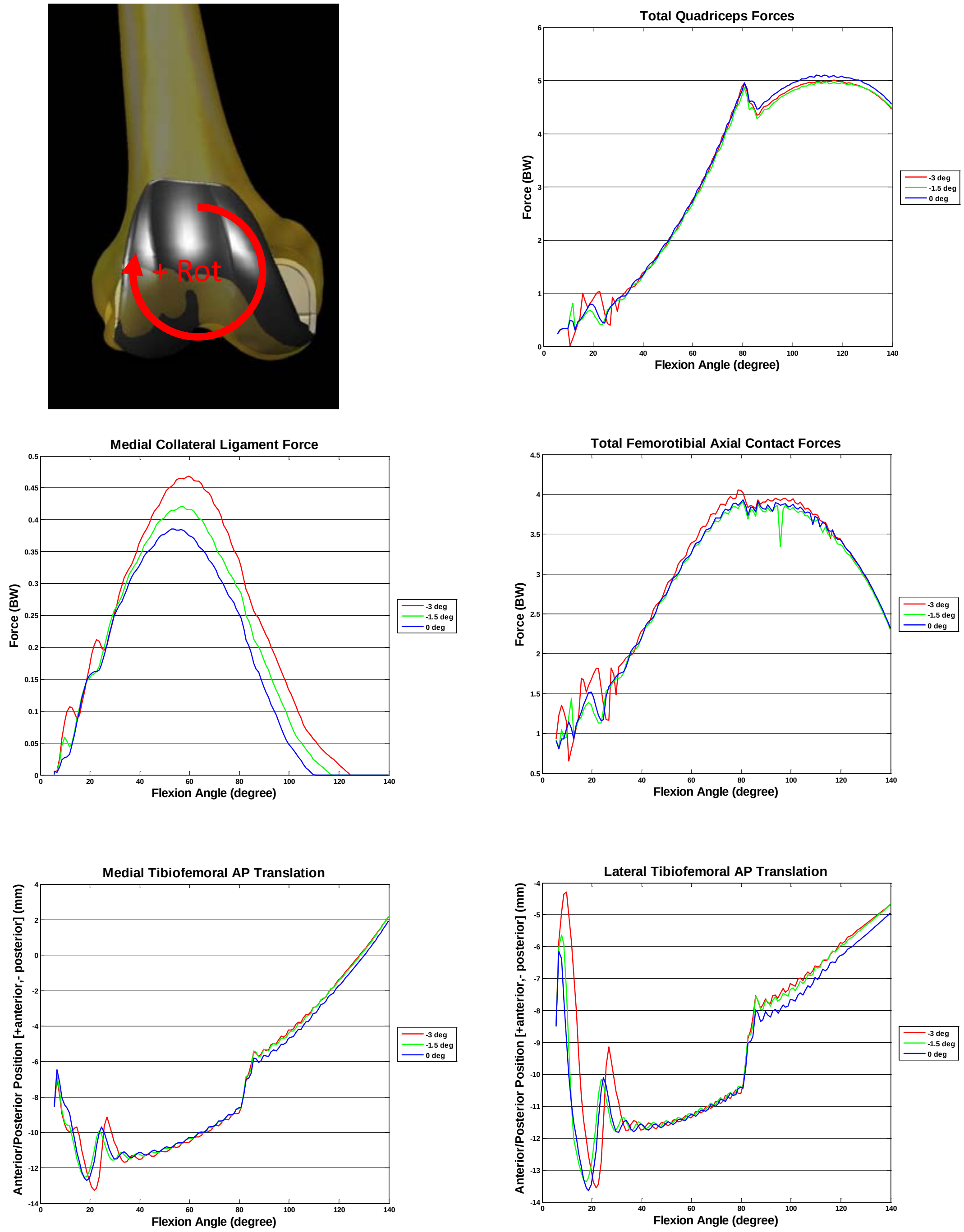

Figure 110: Sensitivity analysis of the coronal alignment of the femoral component.

Chapter 8: Conclusions

This dissertation project resulted in the successful creation of a predictive physiological rigid-body dynamic model of the lower leg. It is physiologically based, models the tibiofemoral and patellofemoral joint of a subject performing two activities as if in the real world and includes the ankle and hip joint and moving trunk mass. All parameters in the model can be adjusted, therefore making it a true design tool that can be used to evaluate new TKA and UKA components and investigate “what if” scenarios. Kinematic profiles from the simulation of several virtually implanted existing TKA designs matched well with what was previously determined under in vivo conditions and also altered the contact force and quadriceps profiles depending on the design that was analyzed.

The two most important plots were presented early in this document (Figure 49 and Figure 50). No other truly forward dynamic predictive physiological model of the knee has been validated with in vivo kinematic and kinetic data to the extent that this model has been validated. The accuracy of the results for the telemetric implant, and the accuracy of the results from the other implant designs, are testament to the performance of this model. The versatility and potential for this simulation platform is endless with the data, tools and researchers available at the Center for Musculoskeletal Research at The University of Tennessee. Future work on this model could result in a tool which orthopaedic manufacturers could use to help create the best performing, longest lasting joint replacement systems manufactured to date.

Chapter 9: Contributions

At present, there is a tremendous need in orthopaedics to evaluate newly developed implant devices. In orthopaedics, new implants are evaluated after five and ten years, using "long-term follow-up studies" where the surgeons evaluate the success of a product, determining how many implants are still in use. Unfortunately, having to wait five or ten years to determine if a product is successful is not acceptable as it does not provide the developer proper feedback in a timely manner. Therefore, it is imperative that a new evaluation process be developed that will allow the company, engineers and surgeons an accurate process that gives them immediate feedback. In this research study, a new process is presented that allows for newly developed implant designs to be evaluated, immediately after they are designed, giving the developer instant feedback that can be used to predict implant viability. This new process is the development of a theoretical simulator, using a forward solution mathematical model, that predicts implant mechanics.

The following are the major contributions to the field of biomechanics:

1. According to Dr. Richard Brand, the editor for Clinical Orthopaedics and Related Research, in a letter written in 1993, he stated, "it is impossible to develop an accurate mathematical model of the human leg, especially one using forward solution modeling techniques." It was assumed for many years that Dr. Brand was correct because as of today, no one has developed an accurate, validated forward solution mathematical model of the human leg. All previous

attempts were for passive conditions and none attempted to accurately develop a model that can be used to analyze implants during in vivo weight-bearing conditions. Therefore, the primary contribution pertains to the development of a dynamic physiological rigid-body predictive forward solution model of the knee that could be used to evaluate the non implanted or implanted knee. The model is intended to simulate in-vivo non-weight bearing (active open-kinetic-chain extension) and weight bearing (deep knee bend) activities and will be developed from the ground up, including simultaneous simulation of the patellofemoral and tibiofemoral joint, muscle forces, soft tissue structures and articulating geometry for both joints with the end goal of predicting kinematics and contact kinetics of the normal knee and also virtually implanted total knee arthroplasty (TKA).

2. As mentioned previously, Dr. Brand, a pioneer with respect to orthopaedic mathematical modeling and telemetry research, stated that he believed an “accurate”, validated mathematical model could not be developed. Therefore, one of the most important aspects of any new mathematical model is the validation of the results. The kinematic output of the normal knee model will be validated using fluoroscopic data from the database at the Center for Musculoskeletal Research.

3. Although this is a forward solution mathematical model, the use of Kane’s Method of Dynamics, allows for the determination of interactive forces, simultaneously with the determination of the kinematics of the lower leg. This is a major contribution because other models only attempt to determine kinematics, but are unable to assess many of the kinetics in the system.

4. Once the model has been kinematically validated using in vivo normal knee kinematic data for both activities, the newly developed forward solution model will be used to evaluate existing TKA, as they will be virtually implanted and simulated. The output from the model pertaining to various TKA, again validated using fluoroscopic data, will lead to the development of a data base comparing various implanted conditions and designs.

5. The kinetic output from the model, namely tibiofemoral interaction forces which act at the contact points between the femoral component and polyethylene insert of a TKA, will be validated using in vivo results of a telemetric implant which measures forces at the tibial base plate on both the medial and lateral side.

6. Although researchers routinely model soft-tissue structures, such as ligaments and muscles, the preloads in ligament structures has not been previously determined. Ligaments are always in tension, but without the knowledge of the loads in these ligaments under passive and/or static conditions, an accurate determination of muscle and interactive forces cannot be made. Therefore, another contribution to the literature is the development of a theoretical approach to determining ligament preloads and the determination of those preloads in the anterior cruciate ligament (ACL), posterior cruciate ligament (PCL), medial collateral ligament (MCL) and lateral collateral ligament (LCL) if they exist in the theoretical model.

7. Since the model was originally used to determine the mechanics of the normal and present-day implanted knees, this model could be used to design future TKA and UKA using the developed data base.

8. This forward solution mathematical model also allows for input of either temporal or flexion dependent shape functions, or shape structures, determining how femur, patella, or tibial shapes affect knee mechanics.

9. It has been proven that previous mathematical models have inaccurately modeled contact mechanics, including slip vs. roll and the interaction occurring at both the medial and lateral condylar interfaces with the tibial plateau. This newly developed model uses an accurate methodology to model the interactions occurring at the femorotibial and patellofemoral interfaces.

10. A unique controller was developed to adjust the quadriceps forces in order to control knee flexion and stabilize the patellofemoral joint. This controller uses both flexion error, flexion acceleration error and patella tilt as the process variable. The controller provides smooth, accurate tibiofemoral and patellofemoral motions during simulation and quadriceps forces which match force profiles and magnitudes seen in validated inverse dynamic models of similar activities. This control scheme emulates motor control strategies found in the human nervous system while stabilizing the numerical solution of the model.

11. Finally, several existing TKA were evaluated using this model and compared to results seen in vivo. The output from this model will be used as a first-step to develop a virtual knee simulator that can be used to evaluate and predict the in vivo behavior of different existing or under development TKA under various conditions.

Chapter 10: Future Work

It is proposed that the following future work could be conducted the further enhance this mathematical model:

1. More muscles and physiological structures should be added including more hamstring muscle elements and muscle of the lower leg, increasing the potential for more activities.

2. Continue to refine the controller. This should include an automated tuning of the controller gains and gain scheduling during the simulation.

3. Increase speed and robustness of the numerical solver. Although numerical problems are rare with the types of simulations shown in this dissertation, numerical issues can arise, as they do in all forward solution algorithms, when new designs are implanted or extreme adjustments to parameters are made. The numerical solution of this model is also tied in with the muscle force controller. Resolving number 2 in this list could eliminate most numerical issues. Speed should always be improved as long as accuracy is not sacrificed.

4. Expand and refine the articulating 3-D geometry representation of the tibial tray and trochlear groove. This could include using splines and the ability to use NURBS.

6. Add a foot and eventually the contralateral leg to the model.

7. Expand and refine the wrapping of muscles and ligaments.

8. Expand the GUI to make more user friendly and allow instant simulation with a new TKA design.

9. Further validation with other telemetric implants.

10. Allow for condylar lift off in the model.

11. Add additional constraints so that posterior stabilized knees can be modeled and also add mobility to the insert so that rotating platform and mobile bearing TKA can be analyzed.

12. Integrate with the discrete spring model to estimate contact area, stress and wear and make this truly a computational wear simulator.

13. Obtain data needed from more CT scans so a library of subjects in various shapes, sizes and genders are available for implantation. Also implement an easy scaling scheme so the height and weight of subjects can easily be adjusted.

14. Simulate more activities, including gait.

List of References

Abdel-Rahman E, Hefzy MS. A two-dimensional dynamic anatomical model of the human knee joint. J Biomech Eng. 1993 Nov;115(4A):357–65.

Abdel-Rahman EM, Hefzy MS. Three-dimensional dynamic behavior of the human knee joint under impact loading. Med Eng Phys. 1998 Jun;20(4):276–90.

Amis AA, Gupte CM, Bull AMJ, Edwards A. Anatomy of the posterior cruciate ligament and the meniscofemoral ligaments. Knee Surg Sports Traumatol Arthrosc. 2006 Mar;14(3):257–63.

Anderson FC, Pandy MG. Dynamic Optimization of Human Walking. J Biomech Eng. 2001 Oct;123(5):381–90.

Andriacchi TP, Mikosz RP, Hampton SJ, Galante JO. Model studies of the stiffness characteristics of the human knee joint. J Biomech. 1983;16(1),23–29.

Baldwin MA, Clary C, Maletsky LP, Rullkoetter PJ. Verification of predicted specimen-specific natural and implanted patellofemoral kinematics during simulated deep knee bend. J Biomech. 2009 Oct 16;42(14):2341-8.

Bargren JH, Blaha JD, Freeman MAR. Alignment in total knee arthroplasty: correlated biomechanical and clinical observations. Clin Orthop 1983;173:178.

Barink M, De Waal Malefijt M, Celada P, Vena P, Van Kampen A, Verdonschot N. A mechanical comparison of high-flexion and conventional total knee arthroplasty. Proc Inst Mech Eng H. 2008 Apr;222(3):297-307.

Barink M, van Kampen A, de Waal Malefijt M, Verdonschot N. A three-dimensional dynamic finite element model of the prosthetic knee joint: simulation of joint laxity and kinematics. Proc Inst Mech Eng H. 2005 Nov;219(6):415-27.

Bartel DL, Burstein AH, Toda MD, Edwards DL. The effect of conformity and plastic thickness on contact stresses in metal-backed plastic implants. J Biomech Eng. 1985 Aug;107(3):193–9.

Bendjaballah MZ, Shirazi-Adl A, Zukor DJ. Biomechanical response of the passive human knee joint under anterior-posterior forces. Clin Biomech (Bristol, Avon). 1998 Dec;13(8):625–33.

Bei Y. Dynamic simulation of knee joint contact during human movement [dissertation]. [Gainesville]: University of Florida; 2003.

Bei, Y., Fregly, B.J. Multibody dynamic simulation of knee contact mechanics. Med. Eng. Phys. 2004;26: 777–789.

Bertozzi L, Stagni R, Fantozzi S, Cappello A. Knee model sensitivity to cruciate ligaments parameters: a stability simulation study for a living subject. J Biomech. 2007;40 Suppl 1:S38-44.

Beynnon BD, Fleming BC, Johnson R, Nichols C, Renström PA and Pop MH. Anterior Cruciate Ligament Strain Behavior During Rehabilitation Exercises In Vivo. Am J Sports Med. 1995; 23:24.

Blankevoort L, Huiskes R, de Lange A. Recruitment of knee joint ligaments. J Biomech Eng. 1991 Feb;113(1):94–103.

Blankevoort L, Kuiper JH, Huiskes R, Grrotenbeor HJ. Articular contact in a three-dimensional model of the knee. J Biomech. 1991;24(11):1019-31.

Burny F, Donkerwolcke M, Moulart F, Bourgois R, Puers R, Van Schuylenberg K, Barbosa M, Paiva O, Rodes F, Begueret JB, Lawes P. Concept, design and fabrication of smart orthopedic implants. Med Eng Phys. 2000 Sept;22(7):469–79.

Chao EY. Graphic-based musculoskeletal model for biomechanical analyses and animation. Med Eng Phys. 2003 Apr;25(3):201–12.

Cohen ZA, Henry JH, McCarthy DM, Mow VC, Ateshian GA. Computer simulations of patellofemoral joint surgery. Patient-specific models for tuberosity transfer. Am J Sports Med. 2003 Jan–Feb;31(1):87–98.

Cohen ZA, Roglic H, Grelsamer RP, Henry JH, Levine WN, Mow VC, Ateshian GA. Patellofemoral stresses during open and closed chain exercises. An analysis using computer simulation. Am J Sports Med. 2001 Jul–Aug;29(4):480–7.

Crowninshield R, Pope MH, Johnson RJ. An analytical model of the knee. J Biomech. 1976;9(6):397–405.

Crowninshield RD, Wimmer MA, Jacobs JJ, Rosenberg AG. Clinical performance of contemporary tibial polyethylene components. J Arthroplasty. 2006 Aug; 21(5):754-61.

Currier JH, Bill MA, Mayor MB. Analysis of wear asymmetry in a series of 94 retrieved polyethylene tibial bearings. J Biomech. 2005 Feb;38(2):367-75.

DesJardins JD, Walker PS, Haider H, Perry J. The use of a force-controlled dynamic knee simulator to quantify the mechanical performance of total knee replacement designs during functional activity. J Biomech. 2000 Oct;33(10):1231-42.

Dhaher YY, Kahn LE. The effect of vastus medialis forces on patello-femoral contact: a model-based study. J Biomech Eng. 2002 Dec;124(6):758–67.

D'Lima DD, Chen PC, Colwell CW Jr. Polyethylene contact stresses, articular congruity, and knee alignment. Clin Orthop Relat Res. 2001 Nov;392:232–8.

D'Lima DD, Steklov N, Fregly BJ, Banks SA, Colwell CW Jr. In vivo contact stresses during activities of daily living after knee arthroplasty. J Orthop Res. 2008 Dec;26(12):1549–55.

D'Lima DD, Townsend CP, Arms SW, Morris BA, Colwell CW Jr. An implantable telemetry device to measure intra-articular tibial forces. J Biomech. 2005 Feb;38(2):299–304.

Eberhardt AW, Keer LM, Lewis JL, Vithoontien V. An analytical model of joint contact. J Biomech Eng. 1990 Nov;112(4):407–13.

Elias JJ, Wilson DR, Adamson R, Cosgarea AJ. Evaluation of a computational model used to predict the patellofemoral contact pressure distribution. J Biomech. 2004 Mar;37(3):295–302.

Erdemir A, McLean S, Herzog W, van den Bogert AJ. Model-based estimation of muscle forces exerted during movements. Clin Biomech (Bristol, Avon). 2007 Feb;22(2):131-54.

Fernandez JW, Akbarshahi M, Kim HJ, Pandy MG. Integrating modelling, motion capture and x-ray fluoroscopy to investigate patellofemoral function during dynamic activity. Comput Methods Biomech Biomed Engin. 2008 Feb;11(1):41–53.

Fregly BJ, Bei Y, Sylvester ME. Experimental evaluation of an elastic foundation model to predict contact pressures in knee replacements. J Biomech. 2003 Nov;36(11):1659–68.

Fuss FK. Anatomy of the cruciate ligaments and their function in extension and flexion of the human knee joint. Am J Anat. 1989 Feb;184(2):165–76.

Giddings VL, Kurtz SM, Edidin AA. Total knee replacement polyethylene stresses during loading in a knee simulator. Journal of Tribology. 2001 Oct;123:843.

Godest AC, Beaugoninb M, Haug E, Taylor M, Gregson PJ. Simulation of a knee joint replacement during a gait cycle using explicit finite element analysis. J Biomech. 2002 Feb;35(2):267–75.

Godest AC, de Cloke CS, Taylor M, Gregson PJ, Keane AJ, Sathasivan S, Walker PS. A computational model for the prediction of total knee replacement kinematics in the sagittal plane. J Biomech. 2000 Apr;33(4):435–42.

Goodfellow J, O'Connor J. The mechanics of the knee and prosthesis design. J Bone Joint Surg Br. 1978 Aug;60-B(3), 358–69.

Goodfellow JW, Tibrewal SB, Sherman KP, O'Connor JJ. Unicompartmental Oxford Meniscal knee arthroplasty. J Arthroplasty. 1987;2(1):1–9.

Grood ES, Suntay WJ, Noyes FR and Butler DL. Biomechanics of the knee-extension exercise. Effect of cutting the anerior-cruciate ligament. J Bone Joint Surg Am. 1984;66:725-734.

Guess TM, Maletsky LP. Computational modelling of a total knee prosthetic loaded in a dynamic knee simulator. Med Eng Phys. 2005 Jun;27(5):357–67.

Halloran JP, Easley SK, Petrella AJ, Rullkoetter PJ. Comparison of deformable and elastic foundation finite element simulations for predicting knee replacement mechanics. J Biomech Eng. 2005 Oct;127(5):813–8.

Halloran JP, Erdemir A, van den Bogert AJ. Adaptive surrogate modeling for efficient coupling of musculoskeletal control and tissue deformation models. J Biomech Eng. 2009 Jan;131(1):011014.

Halloran JP, Petrella AJ, Rullkoetter PJ. Explicit finite element modeling of total knee replacement mechanics. J Biomech. 2005 Feb;38(2):323–31.

Harman M, DesJardins J, Banks S, Benson L, LaBerge M, Hodge W. Damage patterns on polyethylene inserts after retrieval and after wear simulation. Proceedings 47th Orthopaedic Research Society, 1003; 2001.

Harman MK, DesJardins J, Banks SA, Benson L, LaBerge M, Hodge WA. Damage patterns on polyethylene inserts after retrieval and after wear simulation. J Bone Joint Surg Br. 2001;86-B(Suppl IV):425.

Hefzy MS, Yang H. 1993. A three-dimensional anatomical model of the human patello-femoral joint, for the determination of patello-femoral motions and contact characteristics. J Biomed Eng. 1993 Jul;15(4):289–301.

Heinlein B, Kutzner I, Graichen F, Bender A, Rohlmann A, Halder AM, Beier A, Bergmann G. Complete data of total knee replacement loading for level walking and stair climbing measured in vivo with a follow-up of 6–10 months. Clin Biomech (Bristol, Avon). 2009 May;24(4):315–26.

Innocenti B, Follador M, Salerno M, Bignardi C, Wong P, Labey L. Experimental and numerical analysis of patello-femoral contact mechanics in TKA. IFMBE Proceedings 22; 2008. 1789–93 p.

Kane TR, Levinson DA. Dynamics: theory and applications. New York: McGraw-Hill; 1985.

Kessler O, Patil S, Colwell CW Jr, D’Lima DD. The effect of femoral component malrotation on patellar biomechanics. J Biomech. 2008 Dec 5;41(16):3332–9.

Khanna A, Gougoulias N, Longo UG, Maffulli N. Minimally invasive total knee arthroplasty: a systematic review. Orthop Clin N Am. 2009 Oct;40(4):479–89.

Kiguchi K, Fukuda T, Koga Y, et al. Development of a physiological knee motion simulator. Advanced Robotics. 1999;13:171-88.

Kim SJ, MacDonald M, Hernandez J, Wixson RL. Computer Assisted Navigation in Total Knee Arthroplasty: Improved Coronal Alignment. J Arthroplasty . 2005; 20(7 Supp 3): 123-131.

Kim HJ, Fernandez JW, Akbarshahi M, Walter JP, Fregly BJ, Pandy MG. Evaluation of predicted knee-joint muscle forces during gait using an instrumented knee implant. J Orthop Res. 2009 Oct;27(10):1326-31.

Komistek RD, Kane TR, Mahfouz M, Ochoa JA, Dennis DA. Knee mechanics: a review of past and present techniques to determine in vivo loads. J Biomech. 2005 Feb;38(2):215-28.

Komistek RD, Stiehl JB, Dennis DA, Paxson RD, Soutas-Little RW. Mathematical Model of the Lower Extremity Joint Reaction Forces using Kane's Method of Dynamics. J Biomech. 1998 Feb;31(2):185-9.

Kwak SD, Blankevoort L, Ateshian GA. A mathematical formulation for 3D quasi-static multibody models of diarthroidal joints. Comput Methods Biomech Biomed Engin. 2000;3(1):41–64.

Landon RL, Hast MW, Piazza SW. Robust contact modeling using trimmed NURBS surfaces for dynamic simulations of articular contact. Comput Methods Appl Mech Engrg. 2009;198:2339–2346.

Lanovaz JL, Ellis RE. A cadaverically evaluated dynamic FEM model of closed-chain TKR mechanics. J Biomech Eng. 2009 May;131(5):051002-1.

LaPrade RF, Engebretsen AH, Ly TV, Johansen S, Wentorf FA, Engebretsen L. The anatomy of the medial part of the knee. J Bone Joint Surg Am. 2007 Sep;89(9):2000–10.

Lavernia CJ, Sierra RJ, Hungerford DS, Krackow K. Activity level and wear in total knee arthroplasty: a study of autopsy retrieved specimens. J Arthroplasty. 2001 Jun;16(4):446–53.

Laz PJ, Pal S, Fields A, Petrella AJ, Rullkoetter PJ. Effects of knee simulator loading and alignment variability on predicted implant mechanics: a probabilistic study. J Orthop Res. 2006 Dec;24(12):2212-21.

Leszko F, Sharma A, Komistek RD, Mahfouz MR, Cates HE and Scuderi GR. Comparison of In Vivo Patellofemoral Kinematics for Subjects Having High-Flexion Total Knee Arthroplasty Implant With Patients Having Normal Knees. The Journal of Arthroplasty 2009. Article in Press.

Lewis G. Contact stress at articular surfaces in total joint replacements. Part II: Analytical and numerical methods. Biomed Mater Eng. 1998;8(5-6):259-78.

Li G, Gil J, Kanamori A, Woo SL. A validated three-dimensional computational model of a human knee joint. J Biomech Eng. 1999 Dec;121(6):657–62.

Li G, Sakamoto M, Chao EY. A comparison of different methods in predicting static pressure distribution in articulating joints. J Biomech. 1997 Jun;30(6):635–8.

Li G, DeFrate, Sun H, Gill TJ. In vivo elongation of the anterior cruciate ligament and posterior cruciate ligament during knee flexion. Am J Sports Med. 2004; 32:1415.

LifeModeler [Internet]. San Clemente (CA): LifeModeler, Inc. 2009. Available from: http://www.lifemodeler.com/content/modernizing-product-development

Lin YC, Haftka RT, Queipo NV, Fregly BJ. Surrogate articular contact models for computationally efficient multibody dynamic simulations. Med Eng Phys. 2010; 32(6): 584-594.

Lin YC, Haftka RT, Queipo NV, Fregly BJ. Two-dimensional surrogate contact modeling for computationally efficient dynamic simulation of total knee replacements. J Biomech Eng. 2009 Apr;131(4):041010.

Lin YC, Walter JP, Banks SA, Pandy MG, Fregly BJ. Simultaneous prediction of muscle and contact forces in the knee during gait. J Biomech. 2010; 43(5), 945-952.

Lu TW, Taylor SJ, O'Connor JJ, Walker PS. Influence of muscle activity on the forces in the femur: an in vivo study. J Biomech. 1997 Nov-Dec;30(11-12):1101–6.

Mahfouz MR, Hoff WA, Komistek RD, Dennis DA. A robust method for registration of three-dimensional knee implant models to two-dimensional fluoroscopy images. IEEE Trans Med Imaging. 2003 Dec;22(12):1561-74.

Maletsky LP, Hillberry BM. Simulating Dynamic Activities Using a Five-Axis Knee Simulator. J Biomech Eng. 2005 Feb;127(1):123-33.

McDevitt TW. Treatment of frictional contact problems. Proceedings of 2002 North American MSC.ADAMS Users Conference; 2004; Scottsdale, AZ.

Meister BR, Michael SP, Moyer RA, Kelly JD, Schneck CD. Anatomy and kinematics of the lateral collateral ligament of the knee. Am J Sports Med. 2000 Nov-Dec;28(6):869-78.

Miller RK, Murray DW, Gill HS, O'Connor JJ, Goodfellow JW. In vitro patellofemoral joint force determination by a noninvasive technique. Clinical Biomechanics. 1997;12: 1–7.

Moeinzadeh MH, Engin AE, Akkas N. Two-dimensional dynamic modelling of human knee joint. J Biomech. 1983;16(4):253–64.

Mommersteeg TJ, Blankevoort L, Huiskes R, Kooloos JG, Kauer JM. Characterization of the mechanical behavior of human knee ligaments: a numerical-experimental approach. J Biomech. 1996 Feb;29(2):151–60.

Moran MF, Bhimji S, Racanelli F, Piazza SJ. Computational assessment of constraint in total knee replacement. J Biomech. 2008;41(9):2013–20.

Morra EA, Rosca M, Greenwald JF, Greenwald AS. The influence of contemporary knee design on high flexion: a kinematic comparison with the normal knee. J Bone Joint Surg Am. 2008 Nov;90 Suppl 4:195-201.

Morra EA, Harman MK, Greenwald AS. Computational models can predict polymer insert damage in total knee replacements. Surgery of The Knee (Fourth Ed). J.N. Insall, W.N. Scott, editors. 2006;1:271–83.

Morrison JB. The mechanics of the knee joint in relation to normal walking. J Biomech. 1970 Jan;3(1):51–61.

Mueller JKP, Longenecker S, Anderle MR, Komistek RD, Mahfouz MR. In Vivo Comparison Of TKA Kinematics with Ultra Congruent and Congruent Polyethylene Inserts in Natural Knee II CR TKA. Podium. International Society of Technology in Arthroplasty Annual Conference. Paris, France. 2007.

Mueller JKP, White RR, Komistek RD, Anderle MR, Mahfouz MR. In Vivo Determination of Knee Kinematics for Subjects Having an ACL Retaining TKA. Podium. American Academy of Orthopedic Surgeons Annual Conference. Las Vegas, NV. 2009.

Murray DW, Goodfellow JW, O'Connor JJ. The Oxford medial unicompartmental arthroplasty: a ten-year survival study. J Bone Joint Surg Br. 1998 Nov;80(6):983–9.

Nuño N, Ahmed AM. Sagittal profile of the femoral condyles and its application to femorotibial contact analysis. J Biomech Eng. 2001 Feb;123(1):18-26.

Pandy MG, Sasaki K, Kim S. A three-dimensional musculoskeletal model of the human knee joint. Part 1: Theoretical construction. Comput Methods Biomech Biomed Engin. 1998;1(2):87–108.

Pandy MG, Sasaki K. A three-dimensional musculoskeletal model of the human knee joint. Part 2: Analysis of ligament function. Comput Methods Biomech Biomed Engin. 1998;1(4):265–83.

Patil S, Colwell CW Jr, Ezzet KA, D'Lima DD. Can normal knee kinematics be restored with unicompartmental knee replacement? J Bone Joint Surg Am. 2005 Feb;87(2):332–8.

Peña E, Calvo B, Martinez MA, Doblaré M. A three-dimensional finite element analysis of the combined behavior of ligaments and menisci in the healthy human knee joint. J Biomech. 2006;39(9):1686–701.

Peña E, del Palomar AP, Calvo B, Martínez MA, Doblaré M. Computational modelling of diarthrodial joints. Physiological, pathological and post-surgery simulations. Arch Comput Meth Engin. 2007;14(1):1–54.

Perez-Gonzalez P, Fenollosa-Esteve C, Sancho-Bru JL, Sanchez-Marın FT, Vergara M, Rodrıguez-Cervantes PJ. A modified elastic foundation contact model for application in 3D models of the prosthetic knee. Med Eng Phys. 2008 Apr;30(3):387–98.

Petersen W, Zantop T. Anatomy of the anterior cruciate ligament with regard to its two bundles. Clin Orthop Relat Res. 2007 Jan;454:35–47.

Piazza SJ, Delp SL. Three-dimensional simulation of total knee replacement motion during a step-up task. J Biomech Eng. 2001 Dec;123(6):599–606.

Post ZD, Matar WY, van de Leur T, Grossman EL, Austin MS. Mobile-bearing total knee arthroplasty better than a fixed-bearing? J Arthroplasty. 2009 Sep 22.

Rawlinson JJ, Furman BD, Li S, Wright TM, Bartel DL. Retrieval, experimental, and computational assessment of the performance of total knee replacements. J Orthop Res. 2006 Jul;24(7):1384–94.

Rohrbach M, Lüem M, Ochsner PE. Patient and surgery related factors associated with fatigue type polyethylene wear on 49 PCA and DURACON retrievals at autopsy and revision. J Orthop Surg. 2008 Feb 22;3:8.

Sathasivam S, Walker PS. A computer model with surface friction for the prediction of total knee kinematics. J Biomech. 1997 Feb;30(2):177–84.

Sharma A. A method to calculate the femoro-polyethylene contact pressures in total knee arthroplasty in vivo [master's thesis]. [Knoxville (TN)]: University Of Tennessee; 2005.

Sharma A, Komistek RD, Ranawat CS, Dennis DA, Mahfouz MR. In vivo contact pressures in total knee arthroplasty. J Arthroplasty. 2007 Apr;22(3):404 –416.

Sharma A. Development of a computational model to predict the in-vivo contact mechanics of modern total knee arthroplasty [dissertation]. [Knoxville (TN)]: University of Tennessee; 2008.

Sharma A, Leszko F, Komistek RD, Scuderi GR, Cates HE Jr, Liu F. In vivo patellofemoral forces in high flexion total knee arthroplasty. J Biomech. 2008;41(3):642–8.

Sharma A, Komistek RD, Scuderi GR, Cates HE Jr. High Flexion TKA Designs: what are their in vivo contact mechanics? Clin Orthop Relat Res. 2007 Nov;464:117-26.

Shelburne KB and Pandy MG. A Musculoskeletal Model of the Knee for Evaluating Ligament Forces During Isometric Contractions. J Biomech. 1997;30:163–176.

Shin CS, Chaudhari AM, Andriacchi TP. The influence of deceleration forces on ACL strain during single-leg landing: a simulation study. J Biomech. 2007;40(5):1145–52.

Taylor M, Barrett DS. Explicit finite element simulation of eccentric loading in total knee replacement. Cling Orthop Relat Res. 2003 Sep;(414):162–71.

Taylor SJ, Walker PS. Forces and moments telemetered from two distal femoral replacements during various activities. J Biomech. 2001 Jul;34(7):839–48.

Tumer ST, Engin AE. Three-body segment dynamic model of the human knee. J Biomech Eng. 1993 Nov;115(4A):350–6.

Varadarajan KM, Harry RE, Johnson T, Li G. Can in vitro systems capture the characteristic differences between the flexion–extension kinematics of the healthy and TKA knee? Med Eng Phys. 2009 Oct;31(8):899-906.

Walker PS, Blunn GW, Perry JP, Bell CJ, Sathasivam S, Andriacchi TP, Paul JP, Haider H, Campbell PA. Methodology for long-term wear testing of total knee replacements. Clin Orthop Relat Res. 2000 Mar;372:290-301.

Ward SR, Terk MR, Powers CM. Influence of patella alta on knee extensor mechanics. J Biomech. 2005; 38: 2415–2422.

Wasielewski RC, Galante JO, Leighty RM, Natarajan RN, Rosenberg AG. Wear patterns on retrieved polyethylene tibial inserts and their relationship to technical considerations during total knee arthroplasty. Clin Orthop Relat Res. 1994 Feb;299:31-43.

Wasielewski RC, Parks N, Williams I, Surprenant H, Collier JP, Engh G. Tibial insert undersurface as a contributing source of polyethylene wear debris. Clin Orthop Relat Rex. 1997 Dec;345:53-9.

Weiss JA, Gardiner JC. Computational modeling of ligament mechanics. Crit Rev Biomed Eng. 2001;29(3):303–71.

Weiss JM, Noble PC, Conditt MA, Kohl HW, Roberts S, Cook KF, Gordon MJ, Mathis KB. What functional activities are important to patients with knee replacements? Clin Orthop Relat Res. 2002 Nov;404:172-88.

Wimmer MA, Andriacchi TP. Tractive forces during rolling motion of the knee: implications for wear in total knee replacement. J Biomech. 1997 Feb;30(2):131–7.

Wismans J, Veldpaus F, Janssen J, Huson A, Struben P. A three-dimensional mathematical model of the knee joint. J Biomech. 1980;13(8):677–85.

Yamaguchi GT, Zajac FE. A planar model of the knee joint to characterize the knee extensor mechanism. J Biomech. 1989; 22: 1–10.

Appendix

Anatomical Definitions

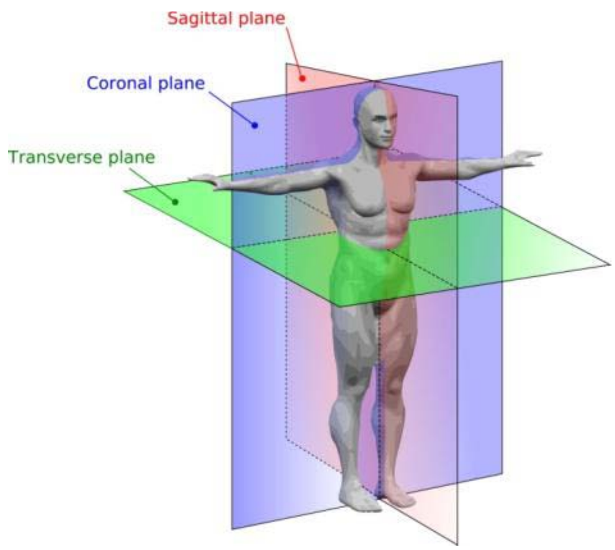

Figure 111:Human anatomy planes. Source: Wikipedia http://en.wikipedia.org/wiki/Abduction_(kinesiology)

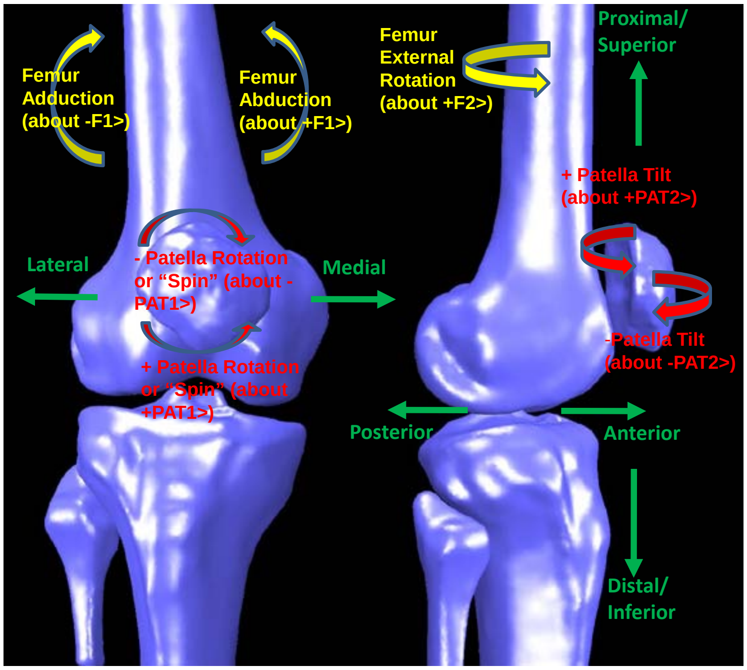

Figure 112: Definitions of some femoral and patellar rotations and anatomical directions.

Extension Model Progression

Initial Model

The gradual development of the extension model was a method of verification. By adding elements or changes to the model one by one, the effect of these changes can be seen and the determined to be correct or reasonable assumptions. The first extension model consisted of the femur which is attached to the Newtonian and one body, the tibia connected to the femur with a pin joint representing the TFJ with no translation, three degrees of rotational freedom and massless frames representing the patella and patella ligament which both had prescribed rotations relative to the tibial reference frame (Figure 113). Constraining the translation of the tibia at the pin joint requires three constraining interaction forces. Keeping the tibia from penetrating the femur using some form of an interaction force or forces is common for all of the iterations of this extension model. The constraining forces acting in the ML and AP directions in this first pin joint model were eventually replaced by elements which replicate a physiological structure in the knee.

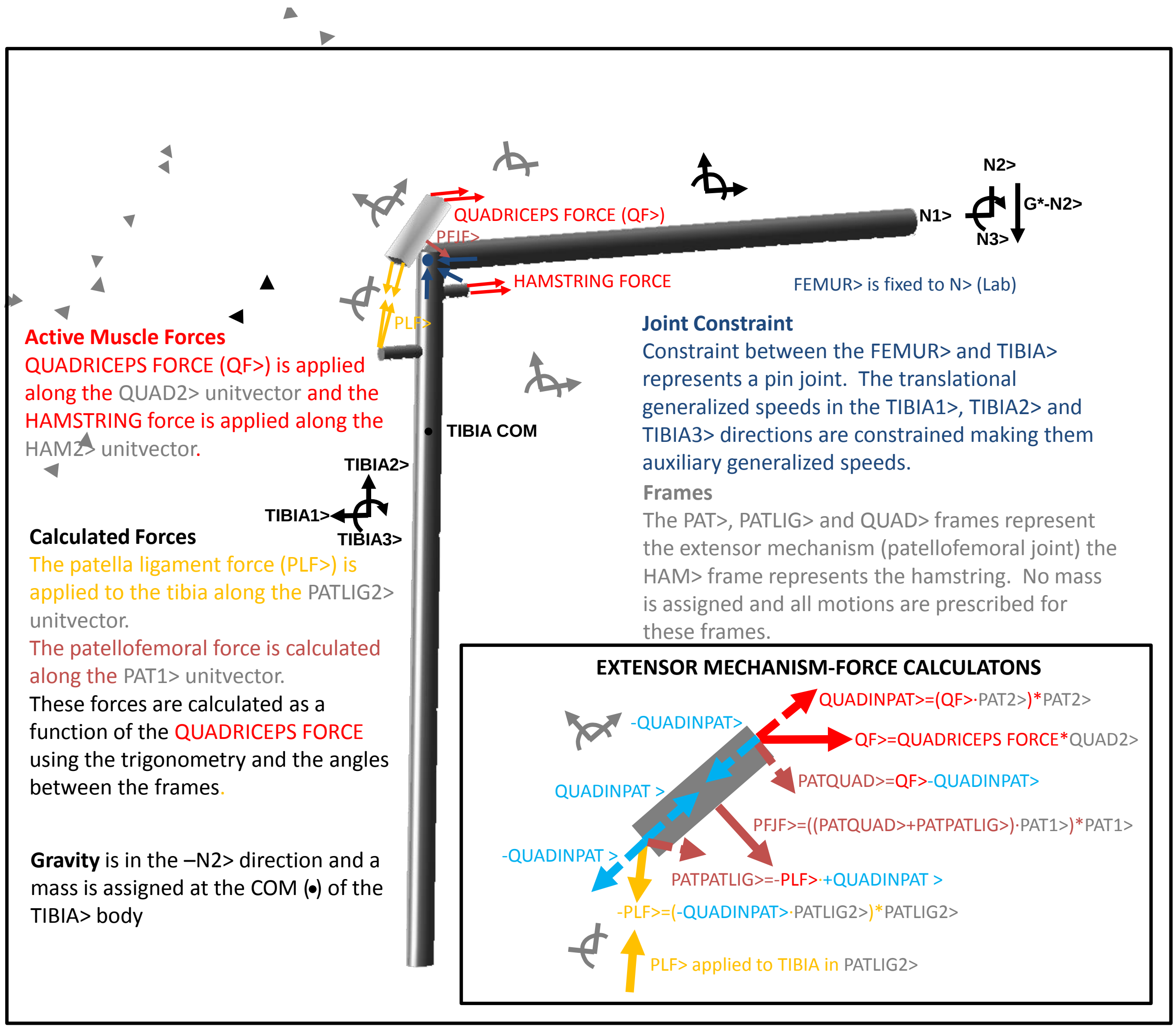

Figure 113: Description of a simple extension model with an idealized pin joint representing the TFJ and frames with specified motions representing the extensor mechanism. The inlay shows the calculations for the patellar mechanism forces including the patellar ligament force and patellofemoral force which are represented using massless frames. This model includes one body (TIBIA) free to rotate in all three directions with one tibiofemoral contact point with the femur fixed to the Newtonian reference frame. Active quadriceps and hamstring forces are applied along unitvectors in their respective reference frames.

Moving Tibiofemoral Contact and Constrained Patella Body

The next big change in the modeling of the lower leg bodies and contact was adding a degree of freedom to the tibia body, allowing translation in the anterior/posterior direction, and adding the patella as a body. Professor Thomas Kane the father of Kane's Dynamic said "go slow, we do not have time to go fast." This seems like a large jump to make this early. This step in the modeling progression was a bottleneck for this project. The goal of this model was originally to focus on the tibiofemoral contact points and forces. Therefore, adding translation to the TFJ was the next logical step. Another goal for the project was to control the kinematics of the model with force input, rather than simply changing the displacement. After hundreds of attempts, the only way that garnered reasonable results with quadriceps force as the input was by adding the patella as a body. Therefore, we have this jump which includes both tibiofemoral translation and adding the patella as a body. The benefit from this struggle, however, was a dynamic model of the patellofemoral joint which was developed along with the tibiofemoral joint.

In this stage of the model the femorotibial and patellofemoral contact points were described on the femur as a function of knee flexion using polynomials. These functions were generic and simplified. The contact point was allowed to move on the tibia, relative to the tibia in the AP direction (TIBIA1>) and was constrained in the ML (TIBIA3>) and Axial (TIBIA2>) directions using constraining and interaction forces (Figure 114).

The patella only had one degree of freedom, it was allowed to translate along its own SI axis (PAT2>). It was constrained in all other translational and rotational directions. The patella body, similar to the femur, had an interaction force acting in the AP direction of the patella (PAT1>). It also had a constraining force which acted at the contact point keeping the patella from "subluxing" or basically falling off the medial or lateral side of the femur. The patella also had three constraining torques applied to its mass center which described its rotational motion relative to the femur (Figure 114). The patella flexion (about PAT3>) relative to the femur is prescribed with a linear relationship determined from in vivo data.

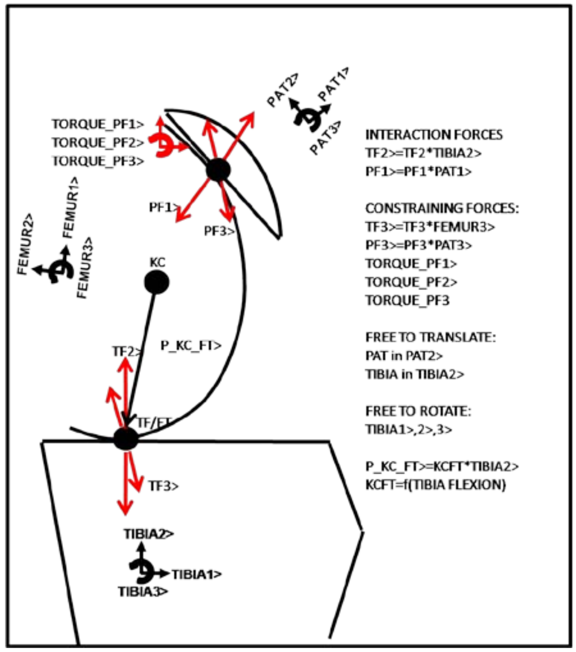

Figure 114: Schematic of the contact points and constraining forces for an initial model of extension. The patella is a body as is the tibia. The femorotibial and patellofemoral contact points are prescribed on the femur as a function of tibial flexion. Interaction forces keep the patella and tibia from penetrating the femur, constraining forces constrain the motion of the bodies. Ligaments and muscles are not shown.

Two moving TFJ Contact Points and Allowing Ligaments to Constrain

To better represent the knee and also to add more stability to the tibia, the single contact point was changed to two contacts, representing the medial and lateral condyles of the knee. The constraining force in the ML direction was removed and the tibia unconstrained in the ML direction. In order to calculate the force at the second femorotibial contact point, the tibia was constrained in the abduction/adduction plane (about TIBIA1>). This is a reasonable assumption, since the abduction/adduction rotation was minimal for previous simulations.

The only translational constraint on the tibia was in the axial direction. In rigid body dynamics, contact constraints act in both directions. Therefore, if all the ligaments were removed, the femur would apply a tension force at the tibial contact points, constraining the movement in the axial direction of the tibia, holding the tibia in place. This, of course, is not realistic. However, it is realistic if the forces during the simulation are always in compression. In most cases the TFJ and patellofemoral joint are always in compression.

Another important addition was patellofemoral ligaments. Ligaments become essential as constraining forces represented with auxiliary generalized speeds are removed from the model. The collateral and cruciate ligaments were added to the extension model in between the pin joint model and model previous to this one. Not until now, when constraints are removed, have they played an important role in determining the predicted kinematics from this model. This iteration removes the two torque constraints besides that which controls patella flexion. The patellofemoral ligaments added to this model acted as passive constraints, replacing the constraining torques, and keeping the patella tilt and rotation within reasonable bounds. Unlike the tibiofemoral joint in this model, the patella only had one contact, therefore the kinematics were affected by out of plane forces. Thus, the patellofemoral ligaments were more active in this iteration of the extension model than they are in vivo or in later iterations which include patellofemoral geometry. Generic models of the femur, tibia and patella were used in this model to determine segment lengths, ligament attachments and the position of the TF and PF contact points on the femur.

Data from Computed Tomography Models

After the last iteration of the model using a generic femur, tibia and patella models achieved reasonable results, attachment points, segment length and measured contact point positions were obtained from bone models constructed using computer CT images.

Points were chosen for all position vectors in this model from a set of femur, tibia/fibula and patella models built from CT scans (Figure 115). The positions of the landmarks were found relative to the segment centers of mass. The coordinates for the bony landmarks were found using Rapidform 2006 (Inus Technology, Inc., Seoul, Korea). The path of the femorotibial and patellofemoral contact points on the femur were also determined and modeled with polynomials. The position vectors for these contact points changed as a function of knee flexion in this extension model.

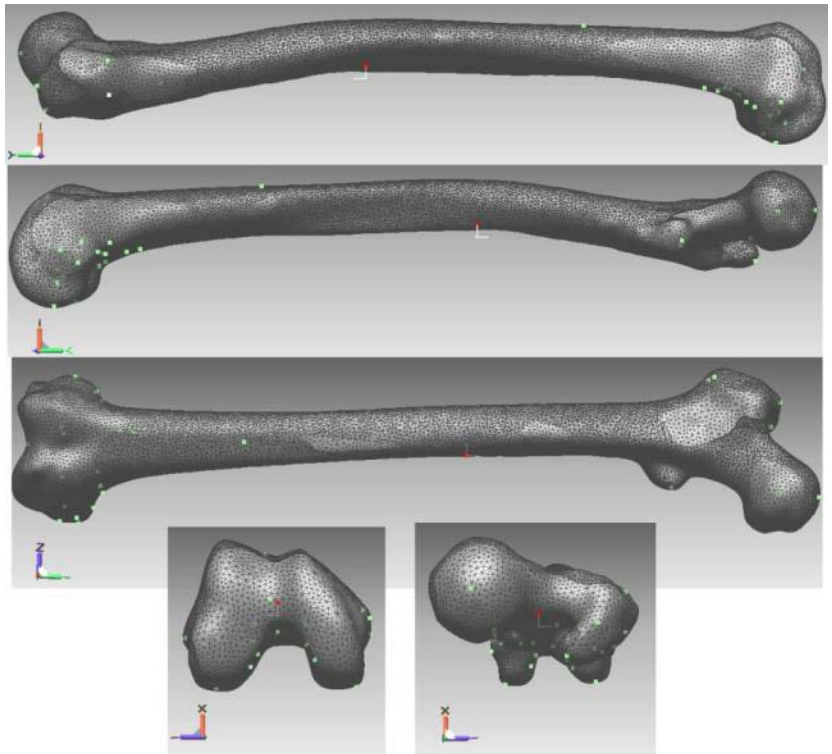

Figure 115: From top to bottom: Lateral, medial, anterior, distal and proximal view of a femur bone model constructed from CT scans with boney landmarks. The position of the contact points on the femur were also measured from this model.

For the initial model using data from CT scans, the femorotibial contact points were in contact with a flat plane that represented the tibial condyles (Figure 116). The contact points were free to translate in any direction within this plane whose normal was the long axis of the tibia. The patellofemoral contact point was described on the femur but the corresponding point on the patella was free to move along the proximal/distal (PD) line of the patella (Figure 117). Therefore after application of a simulated quadriceps force which acted at an angle to long axis of the patella that changed with flexion, the patella was free to translate along the trochlear groove, which resulted in the extension of the tibia. The patella was constrained in the patellar AP (PAT1>) direction and in the ML (PAT3>) direction by applying an interaction force and a constraining force at the patellofemoral contact point. The patella body was still free to rotate and tilt and the forces constraining this motion were the patellofemoral ligaments.

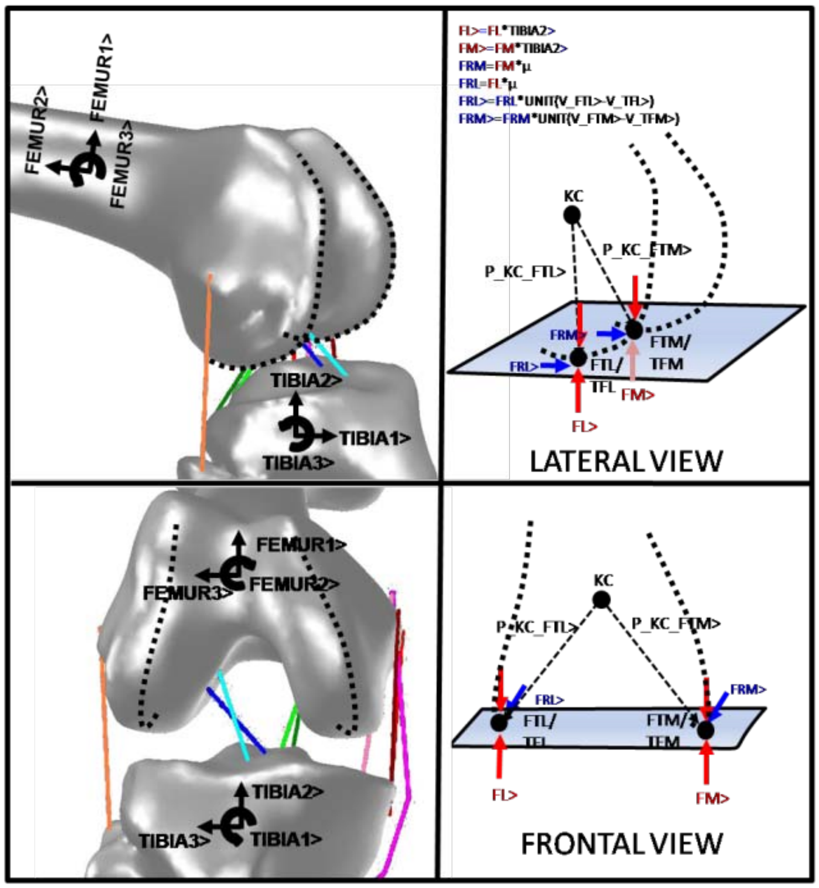

Figure 116: Diagram showing how tibiofemoral contact is modeled in early models. The geometry of the medial and lateral femur is expressed as a point on the medial (FTM) and lateral (FTL) condyle. FTM and FTL change position in the femoral reference frame as a function of flexion. TFL and TFM are the tibial contact points. The distance between TFL and FTL and TFM and FTM is set to 0>. TFL and TFM can translate relative to the tibia in the TIBIA3> and TIBIA1> directions. Medial (FM>) and lateral (FL>) contact forces are in the TIBIA2> direction. FRL> and FRM> are friction forces.

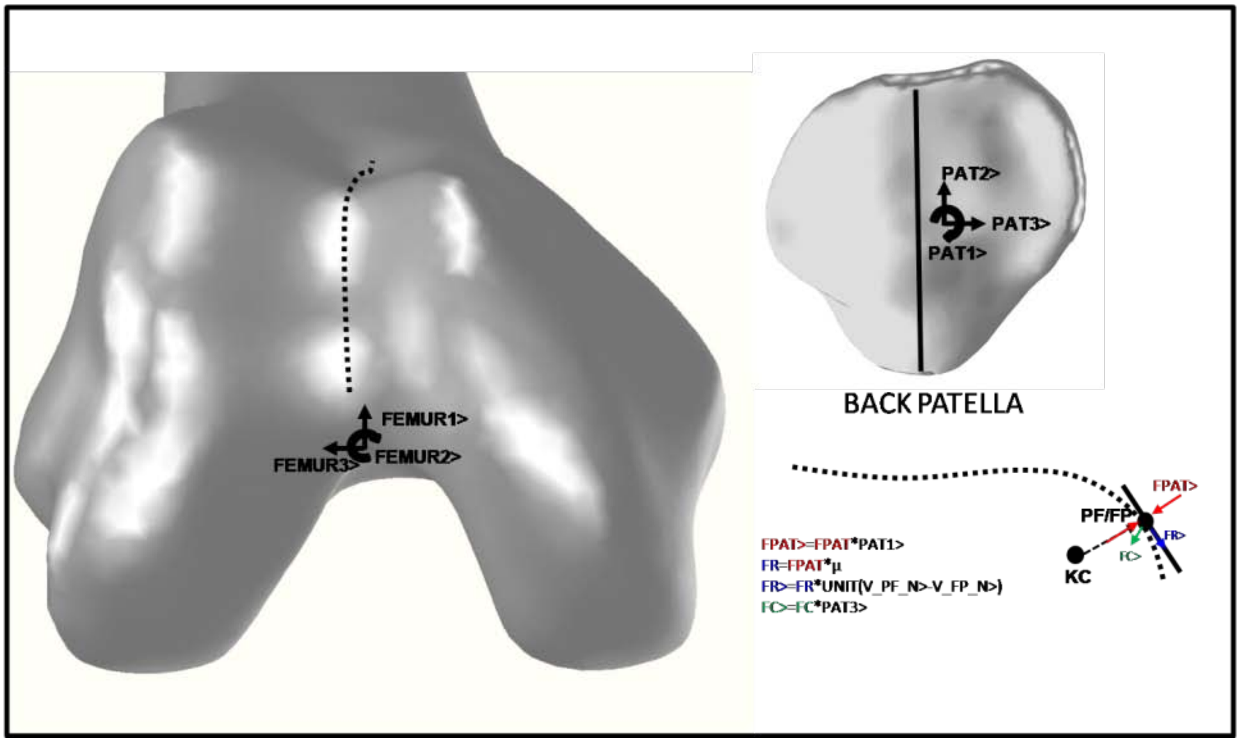

Figure 117: Diagram showing how patellofemoral contact is modeled in early models. The geometry of the trochlear groove is expressed as a point, FP, on the femur. FP changes position in the femoral reference frame as a function of tibial flexion. PF is the contact point on the patella. The distance between FP and PF is set to 0>. PF can translate relative to the patella only in the PAT2> direction. The patellofemoral contact force, FPAT> is in the PAT1> direction. FC> is a constraining force in the FEMUR3> direction for this iteration of the model. FR> is a friction force.

More Model Iterations

Many iterations later, including those in Figure 118 and Figure 119, the model reported in the Methods section of this dissertation came to be.

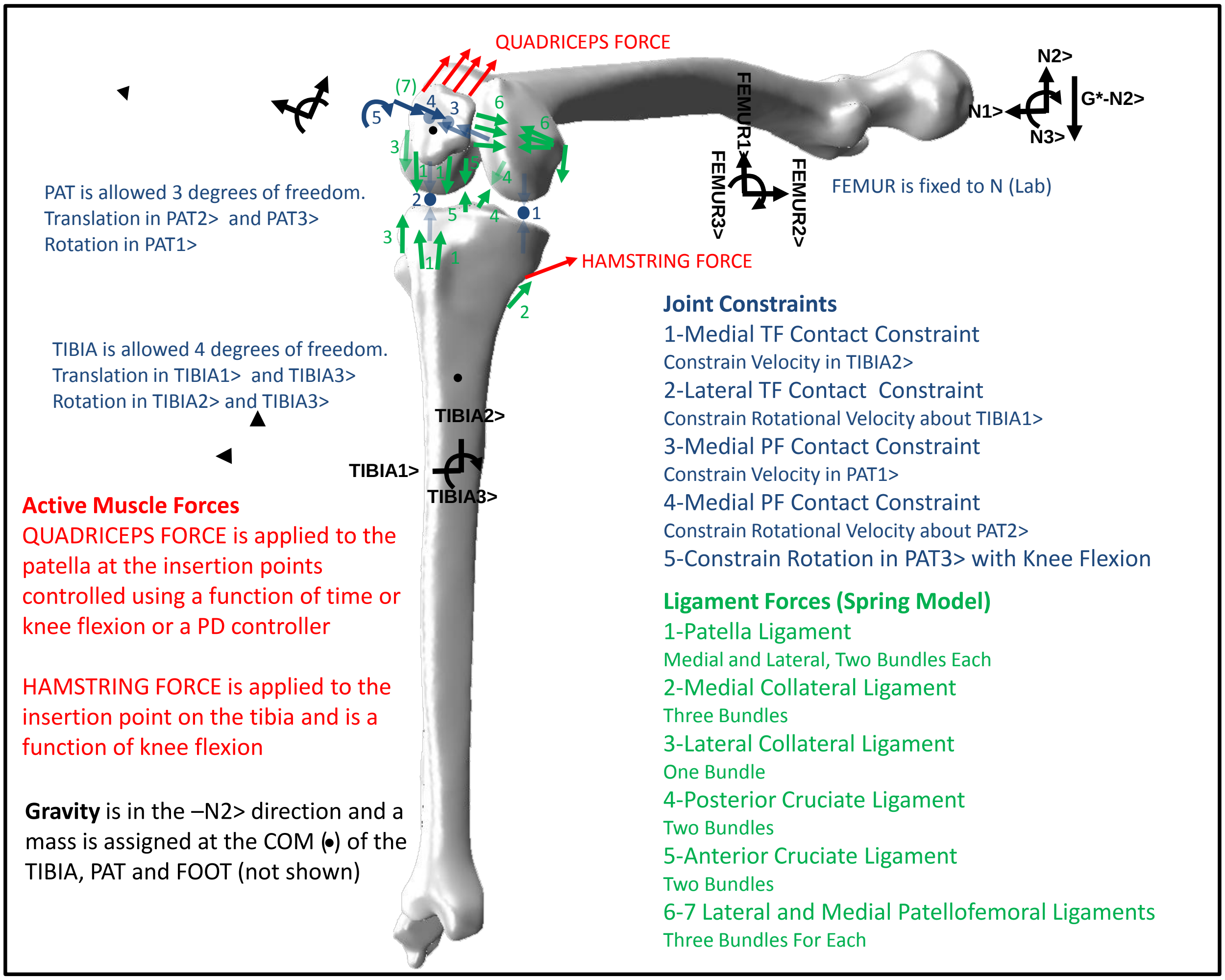

Figure 118: Description of the extension model before insertion of geometry including constraining forces, ligament forces, active muscle forces. This model includes two bodies, TIBIA and PAT with the FEMUR attached to the NEWTONIAN reference frame (LAB). The PAT body representing the patella has two contact points with the FEMUR and three DOF. The TIBIA body representing the tibia also has two contact points with the FEMUR and has four DOF. The ligaments forces are modeled as spring-damper systems with two spring elements per bundle. The QUADRICEPS and HAMSTRING forces are inputs to the model and are applied at attachment points on the patella and tibia, respectively, at angles relative to the femur.

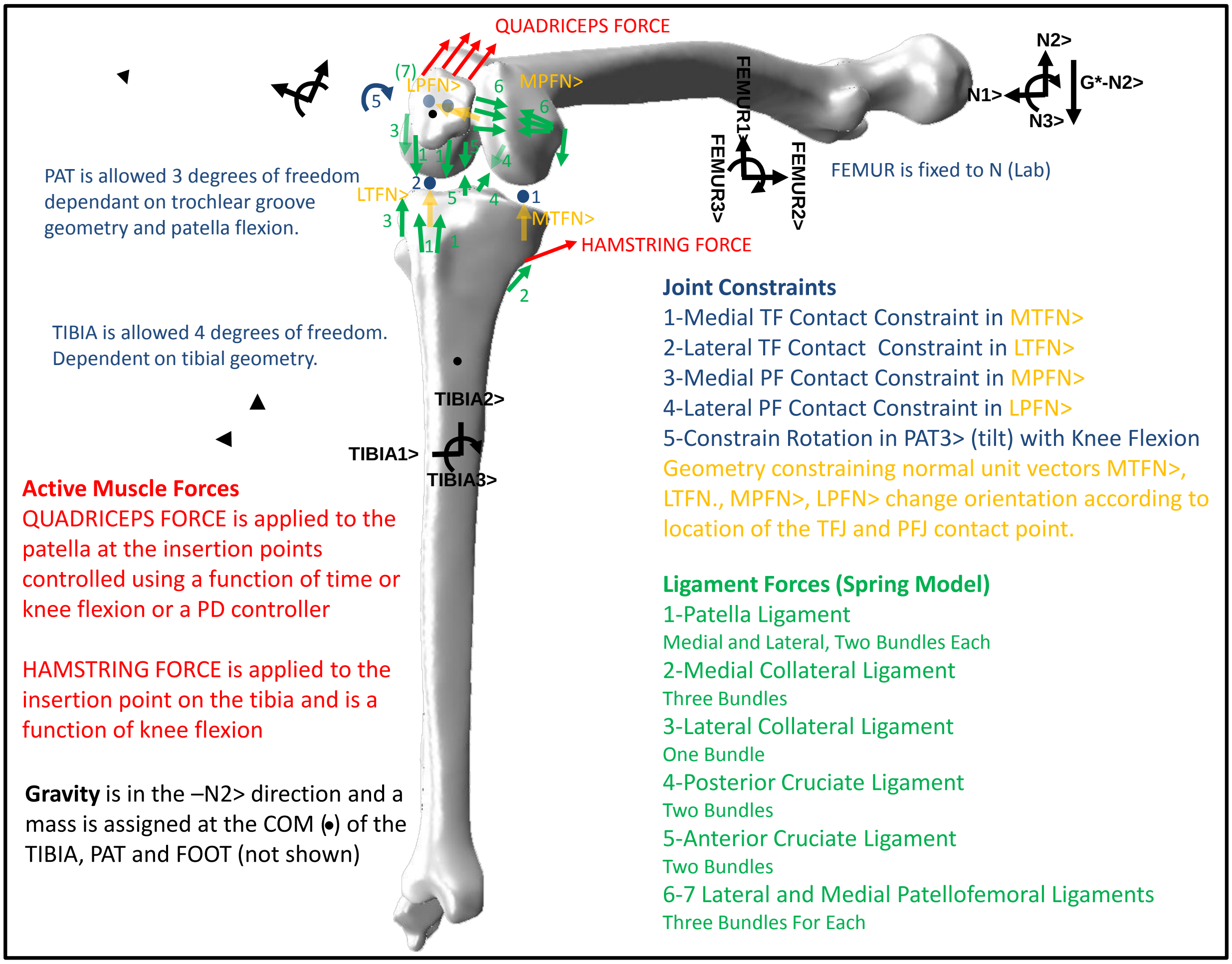

Figure 119: Free body diagram of extension model with articulating geometry. The TFJ and PFJ contact constraints were constrained using normals from the tibial or polyethylene insert and trochlear groove geometry.

2D Patella Kinematics

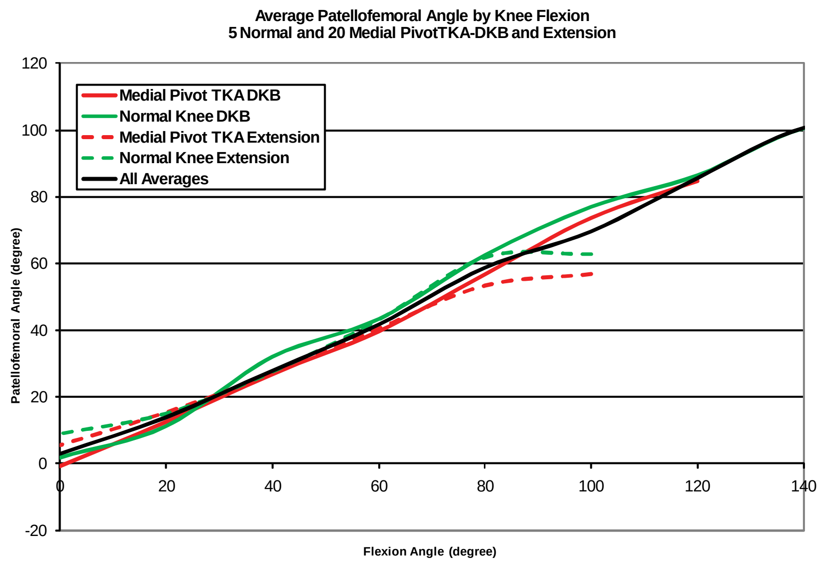

Z

Figure 120: Average in vivo patellofemoral angle versus flexion angle determined using fluoroscopy for both weight-bearing deep knee bend and non-weight bearing activities for a group of 5 normal subjects and 20 Medial Pivot TKA.

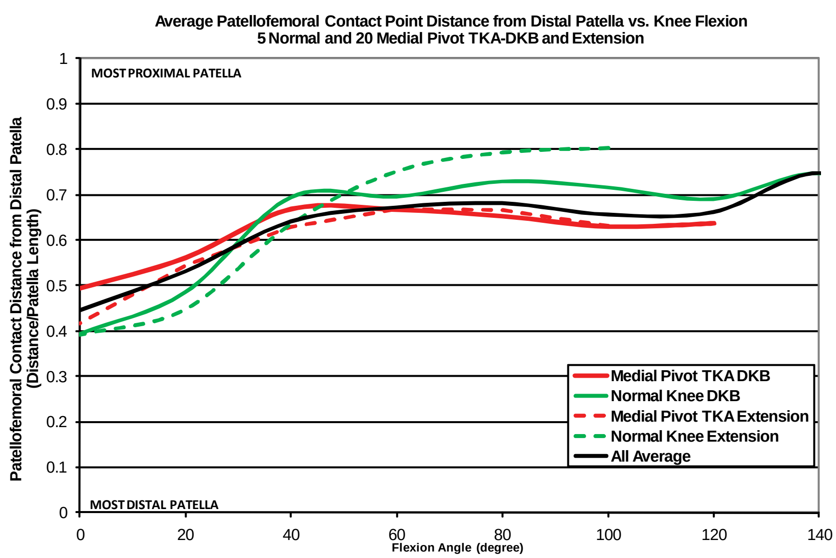

Figure 121: In vivo patellofemoral contact position on the patella determined with fluoroscopy measured from the most distal point on the patella and normalized by the length of the patella for 5 subjects with a normal knee and 20 implanted with a Medial Pivot TKA during weight bearing deep knee bend and non-weight bearing flexion.

Model Point Definitions

Table 3: Description of points in the final deep knee bend model and code. The extension model has similar definitions but instead of the ankle being fixed to the Newtonian reference frame the pelvis and femur are both fixed to the Newtonian and the tibia is free to move.

Point Descriptions				
	On Tibia	On Femur	On Patella	On Pelvis/Trunk
Segment Center of Mass and Reference Points	Tibia is represented by body **A**	Femur is represented by body **F**	Patella is represented by body **PAT**	Pelvis and Trunk are one body represented by **PELVIS**
ANKLE REFERENCE	NO/ANKLECENTER (NOTE: fixed to lab or Newtonian represented by **N** not **A**)			
REFERENCE POINTS	AN (same local as ANKLECENTER but attached to **A**) AREF (Located at intercondyloid emminence)	FREF (Located at the geometrical center of femoral head) CONDYLECENTER (midpoint of the centers of femoral condyles)	PATO (located at the **PAT** center of mass)	PELVISREF (Located at PELVISF Interaction point between the **PELVIS** and **F**)
SEGMENT CENTER OF MASS	AO	FO	PATO (also used as PAT reference point)	PELVISO (Pelvis/Trunk center of Mass)
TKA Component Reference Frame Points	Tibial Component massless reference frame fixed to **A** is **TIBIACOMP**	Femoral component massless reference frame fixed to **F** is **FEMURCOMP**	Patella component massless reference frame fixed to **PAT** is **PATELLACOMP**	
	TIBIACOMPO, ATIBIACOMPO, COMPREF, AFCOMPREF	FEMURCOMPO, FFEMURCOMPO, FACOMPREF	PATPATCOMPO, PATELLACOMPO	
Generalized speeds location (translational)				
U4-U6	ANKLECENTER→AN in **N** reference frame			
U10-U12	AFCOMPREF →	FACOMPREF in **TIBIACOMP** reference frame		
U16-U18		FACOMPREF →	PATELLACOMPO in **TIBIACOMP** reference frame	
U22-U24		FPELVIS →		PELVISF in **N** reference frame

Table 3: Continued

Point Descriptions (continued 1)				
	On Tibia	On Femur	On Patella	On Pelvis/Trunk
Interaction and Constraint Force Points				
ANKLE CONTACT	AN (NA fixed to lab, ground reaction forces calculated here)			
TIBIOFEMORAL CONTACT (Medial and Lateral)	AFL,AFM (In Tibial Component Reference Frame)	FAL,FAM (In Femoral Component Reference Frame, position described as function of flexion)		
PATELLOFEMORAL CONTACT (Medial and Lateral		FPATL,FPATM (in Femoral Component Reference Frame	PATFL,PATFM (in Patella Component Reference Frame, position described as function of flexion)	
FEMUR/PELVIS INTERACTION		FPELVIS		PELVISF
CONSTRAINING M/L HIP FORCE (DKB)		HIPFORCE (same as FELVIS)		
CONSTRAINING M/L TIBIAL FORCE (Extension)	AREF			

Table 3: Continued

Point Descriptions (continued 2)				
	On Tibia	On Femur	On Patella	On Pelvis/Trunk
Ligament Origin and Insertion				
MCL	AMCL{3,2} 6 points(MCL wrapping points included in these)	FMCL{3,2} 6 points		
LCL	ALCL{1,2} 2 points	FLCL{1,2} 2 points		
ACL	AACL{2,2} 4 points	FACL{2,2} 4 points		
PCL	APCL{2,2} 4 points	FPCL{2,2} 4 points		
Patella Ligament (Lateral and Medial Bundle)	APATLIGL{2,4}, APATLIGM{2,4} 16 points		PATLIGPATL{2,4}, PATLIGPATM{2,4} 16 points	
Patellofemoral Ligaments Medial and Lateral	AMPML{1,3} 3 points	FLPFL{3,2}, FMPFL{3,2} 12 points	PATLPFL{3,2}, PATMPFL{3,2}, PATMPML{1,3} 15 points	
Quadriceps Insertion and Origin		GREATTROCH{4} MIDFEMPOSTL{4} Vastus Lateralis DISTFEMANT{4} MIDFEMANT{4} Vastus Intermedius VASTMED{4} MIDFEMPOSTM{4} Vastus Medialis 24 points	PATQUADL1{4} Vastus Lateralis PATQUADL2{4} Rectus Femoris PATQUAM1{4} Vastus Medialis PATQUAM2{4} Vastus Intermedius 16 points	RECTFEM{4} Rectus Femoris 4 points
Quadriceps Wrapping		QUADWRAPLAT{2,4}, QUADWRAPMED{2,4} 16 points		
Hamstring Force Insertion and Origin	ALCL1{2} AMCL1{2} 4 points	MIDFEMPOSTL{2} MIDFEMPOSTM{2} 4 points		

Additional Deep Knee Bend Sensitivity Analyses

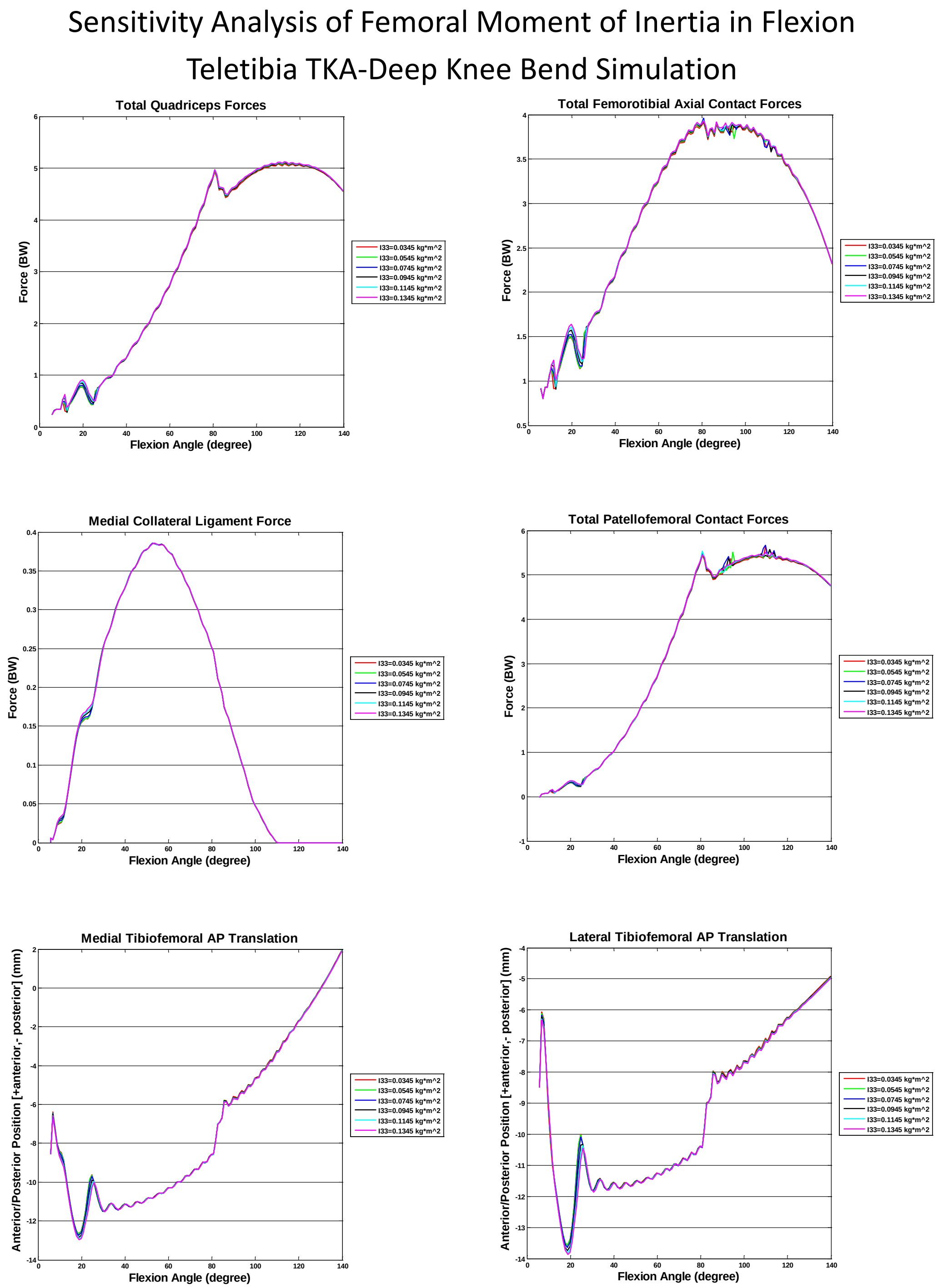

Figure 122: Sensistivity analysis of the femur moment of inertial value in the sagittal plane. The original value is 0.0645 kg*m^2.

Sensitivity Analysis of LCL Reference Strain (Slack Length)
Teletibia TKA-Deep Knee Bend Simulation

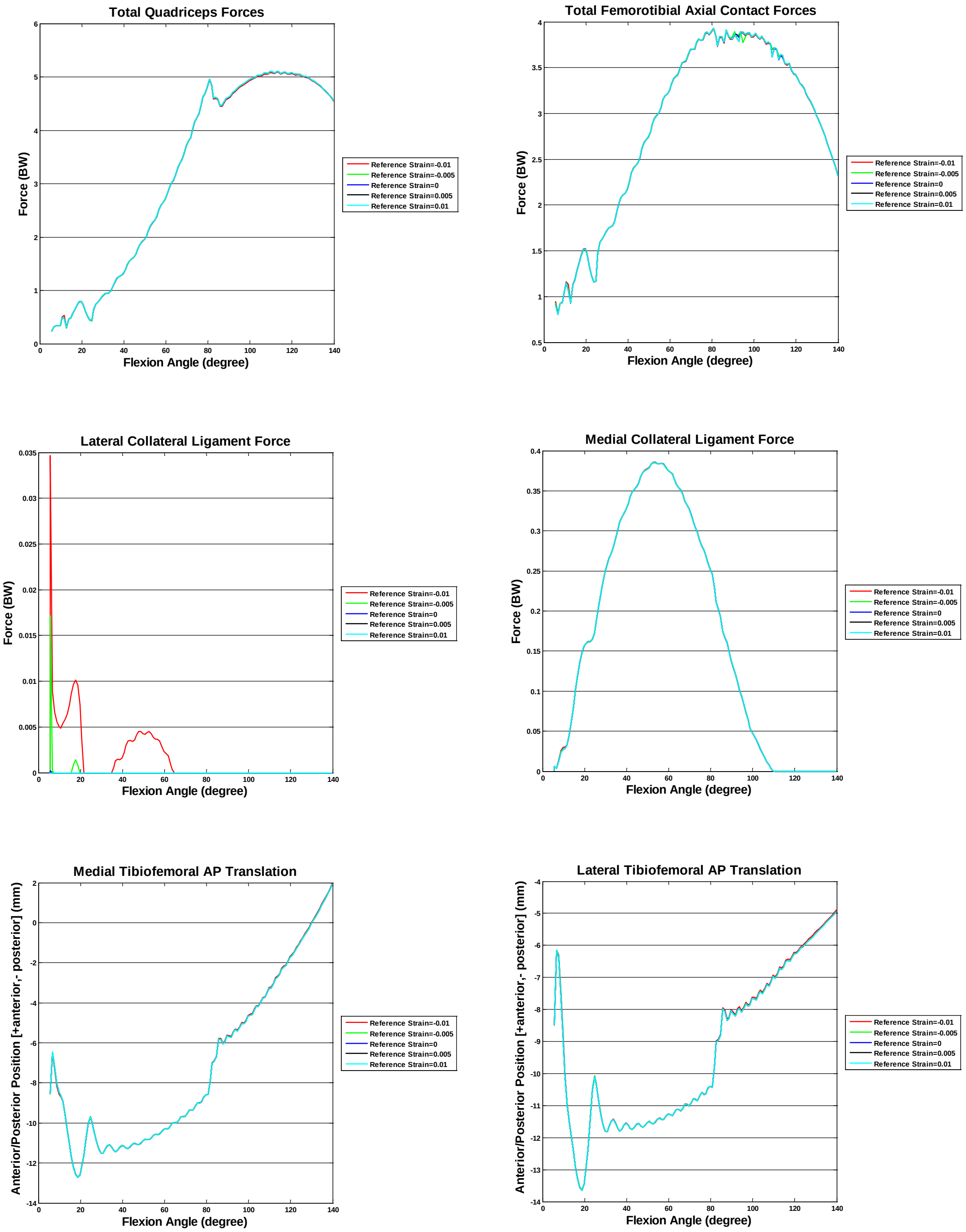

Figure 123: Sensitivity analysis of the lateral collateral ligament reference strain which adjusts the LCL slack length, calculated by multiplying the length of the ligament at full extension with the reference strain.

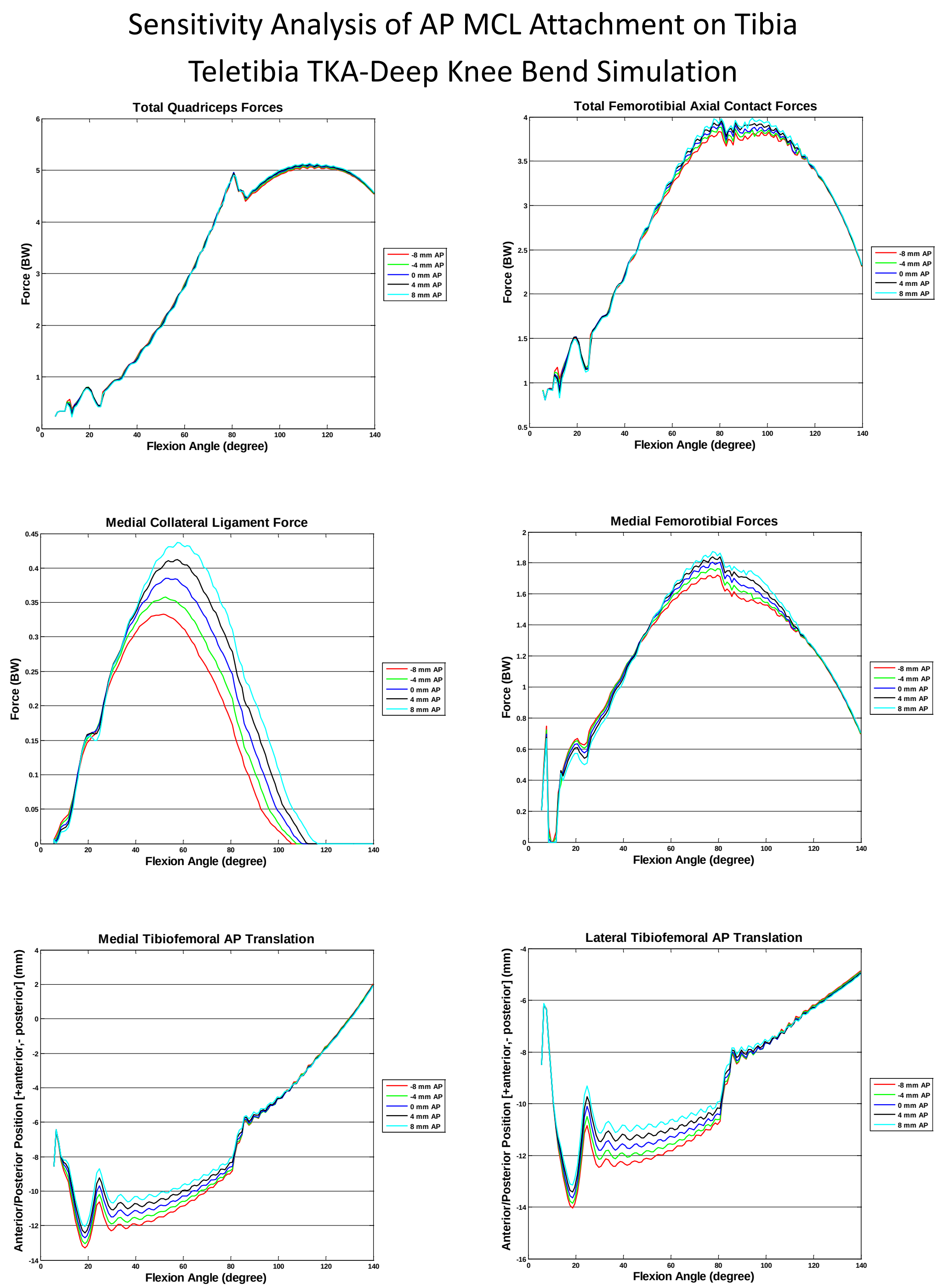

Figure 124: Sensitivity analysis of the attachment point of the MCL on the tibia. All three bundle attachments were moved in the anterior/posterior direction relative to the original position.

Sensitivity Analysis of Tibial Component Transverse Orientation
Teletibia TKA-Deep Knee Bend Simulation

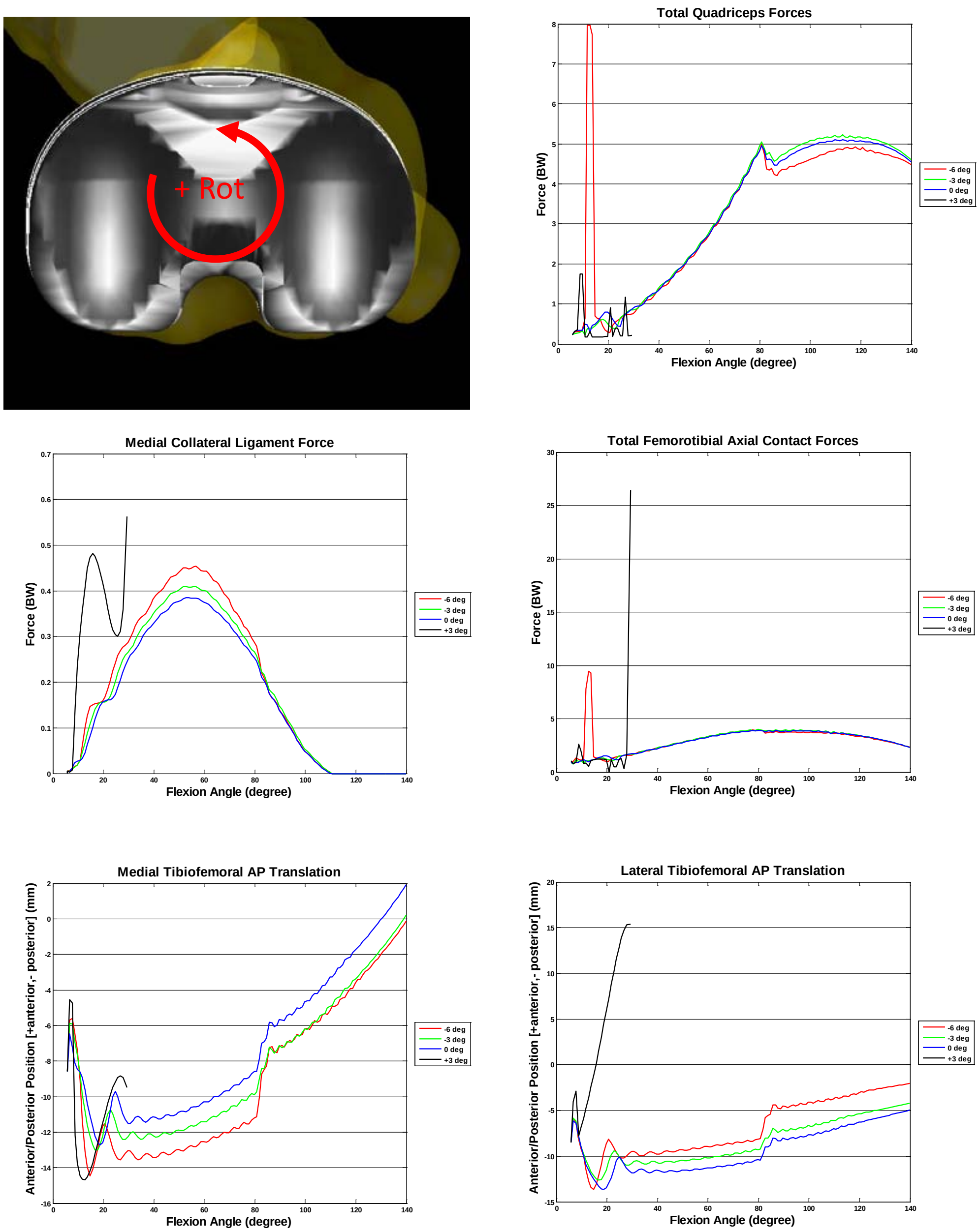

Figure 125: Sensitivity analysis of the tibial component orientation in the transverse plane. Adjustments were made from the original orientation (0 deg). Once the rotation became positive the model failed to solve (+3 deg). This is probably due to the quadriceps force applied by the PID controller or adjusted by the controller which stabilizes the patella. The femur and femoral component and patella locations were adjusted so that the relative starting position to the tibial component was the same at each new location.

Sensitivity Analysis of Tibial Component Sagittal Plane Orientation

Teletibia TKA-Deep Knee Bend Simulation

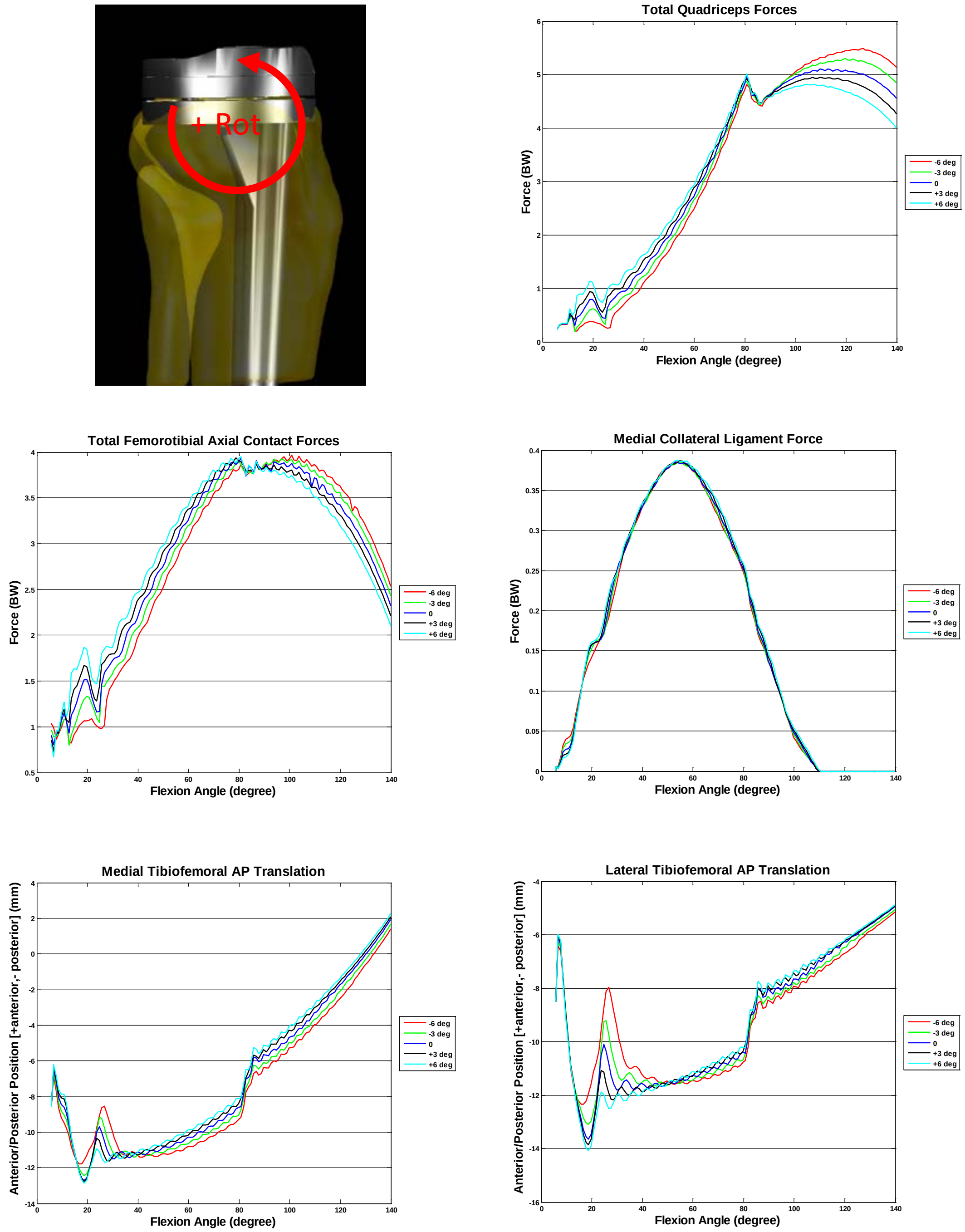

Figure 126: Sensitivity analysis of the tibial component orientation in the sagittal plane. Adjustments were made from the original orientation (0 deg). The femur and femoral component and patella locations were adjusted so that the relative starting position to the tibial component was the same at each new location.

Sensitivity Analysis of Femoral Component Transverse Orientation
Teletibia TKA-Deep Knee Bend Simulation

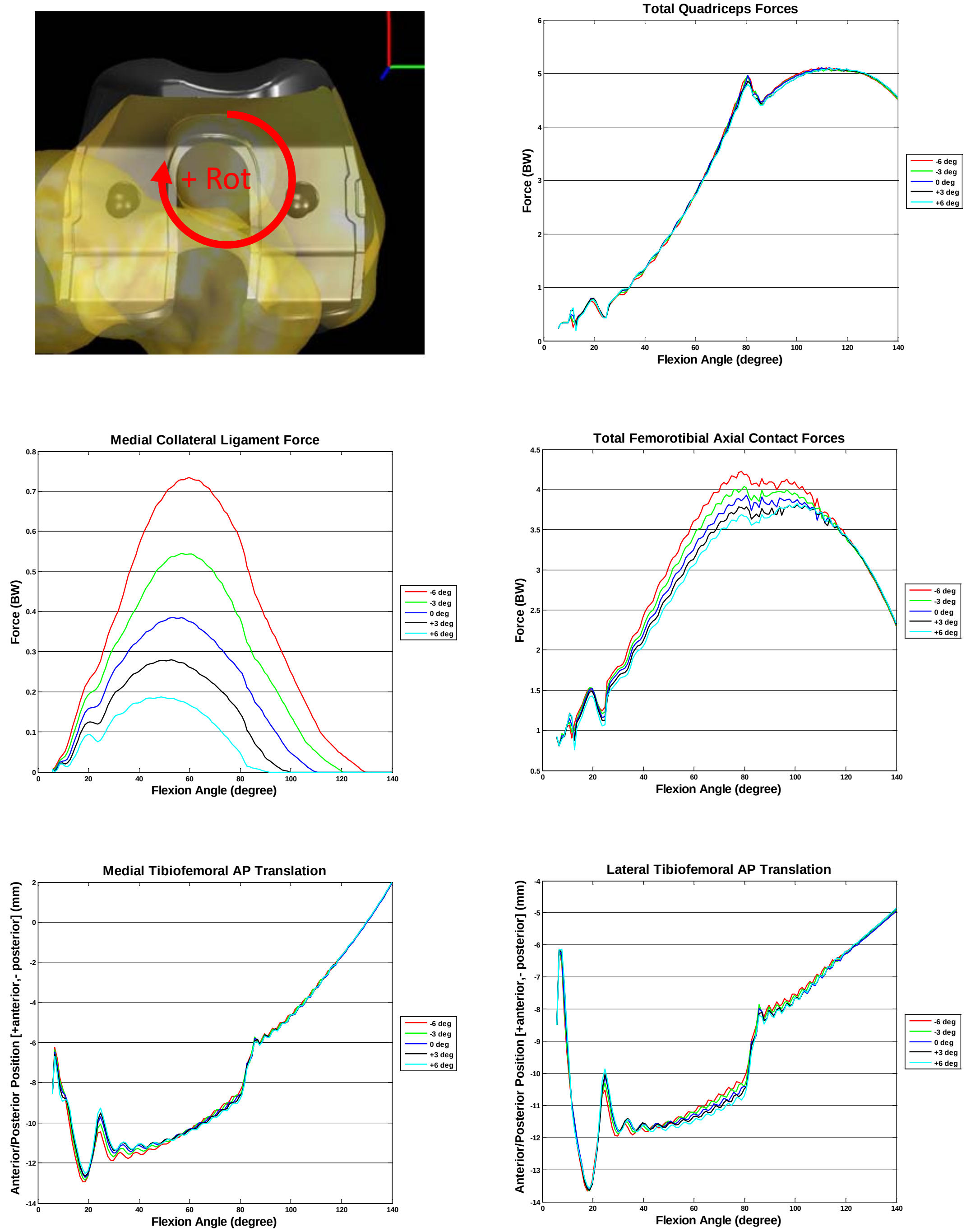

Figure 127: Sensitivity analysis of the femoral component orientation in the transverse plane (see figure in upper left for rotation direction). Adjustments were made from the original orientation (0 deg). The relative starting positions of the tibial, femoral and patellar components remained the same for all simulations.

Sensitivity Analysis of Femoral Component Sagittal Orientation
Teletibia TKA-Deep Knee Bend Simulation

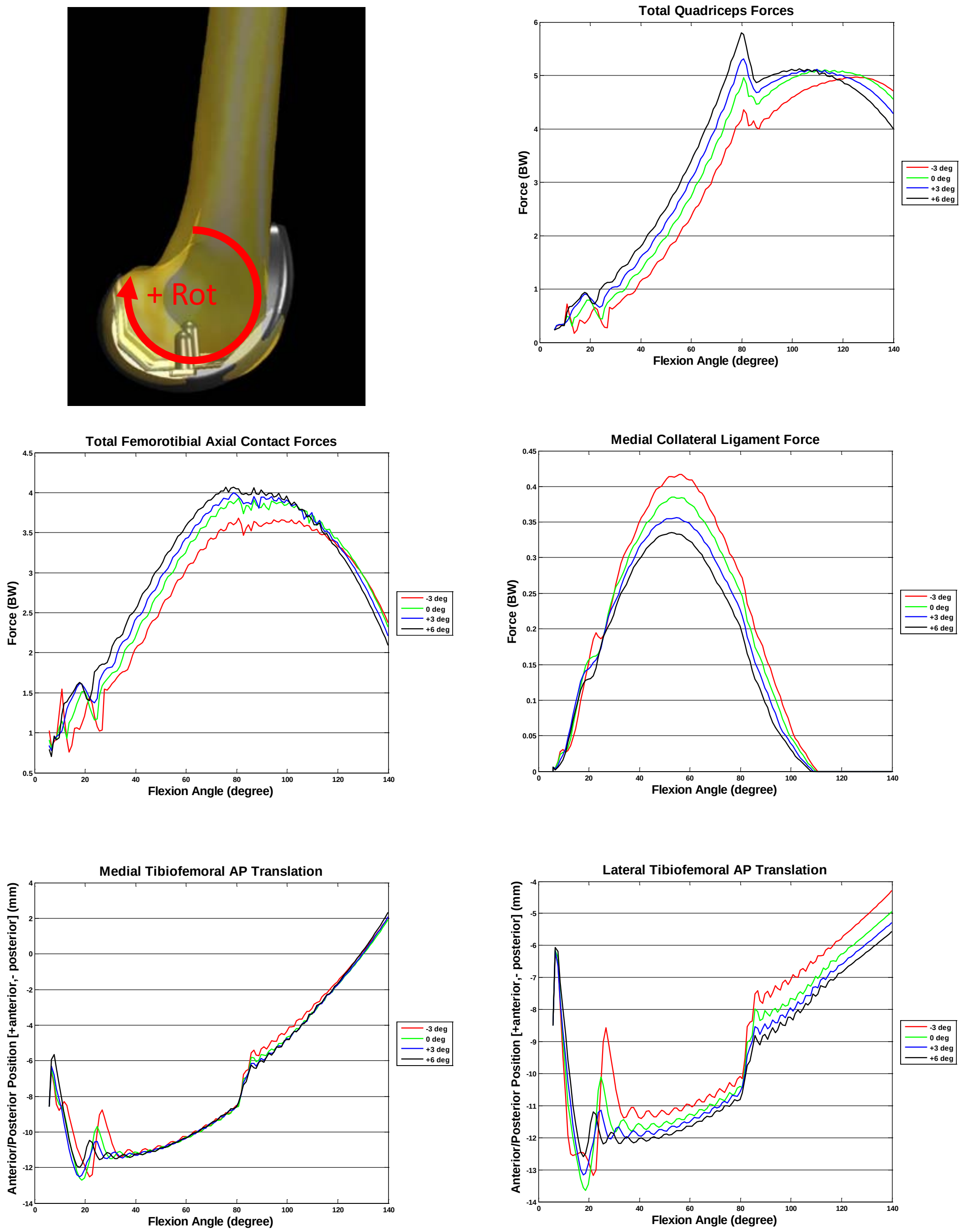

Figure 128: Sensitivity analysis of the femoral component orientation in the sagittal plane (see figure in upper left for rotation direction). Adjustments were made from the original orientation (0 deg). A rotation from the original of -6 degrees was run but the model failed to solve. The relative starting positions of the tibial, femoral and patellar components remained the same for all simulations.

Sensitivity Analysis of Femoral Component Coronal Orientation
Teletibia TKA-Deep Knee Bend Simulation (No Lig Adjust)

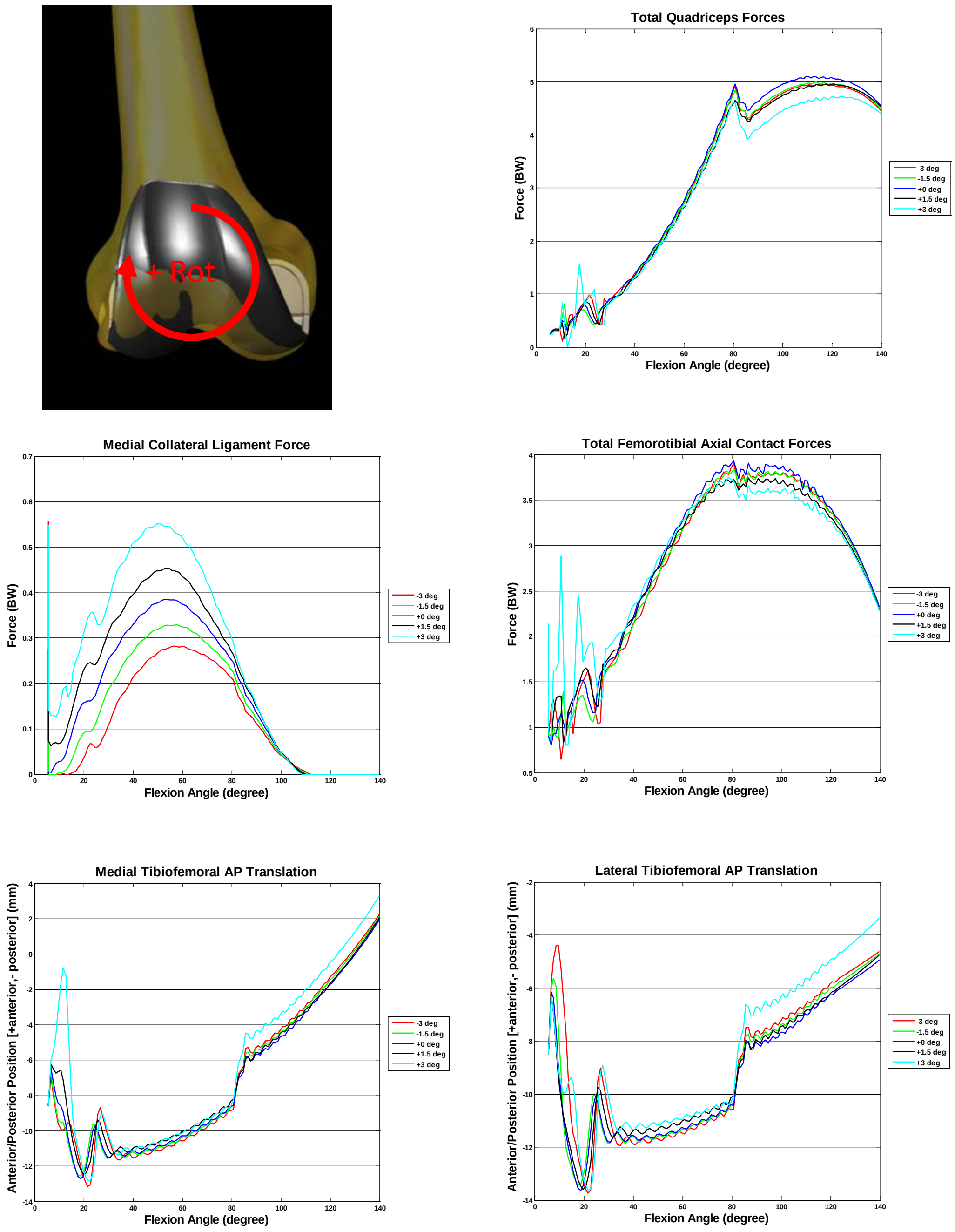

Figure 129: Sensitivity analysis of the femoral component orientation in the coronal plane (see figure in upper left for rotation direction). Adjustments were made from the original orientation (0 deg). Unlike the results Figure 110 the ligament slack lengths were kept the same for each orientation of the components.

Sensitivity Analysis of Tibial Component AP Location
Teletibia TKA-Deep Knee Bend Simulation

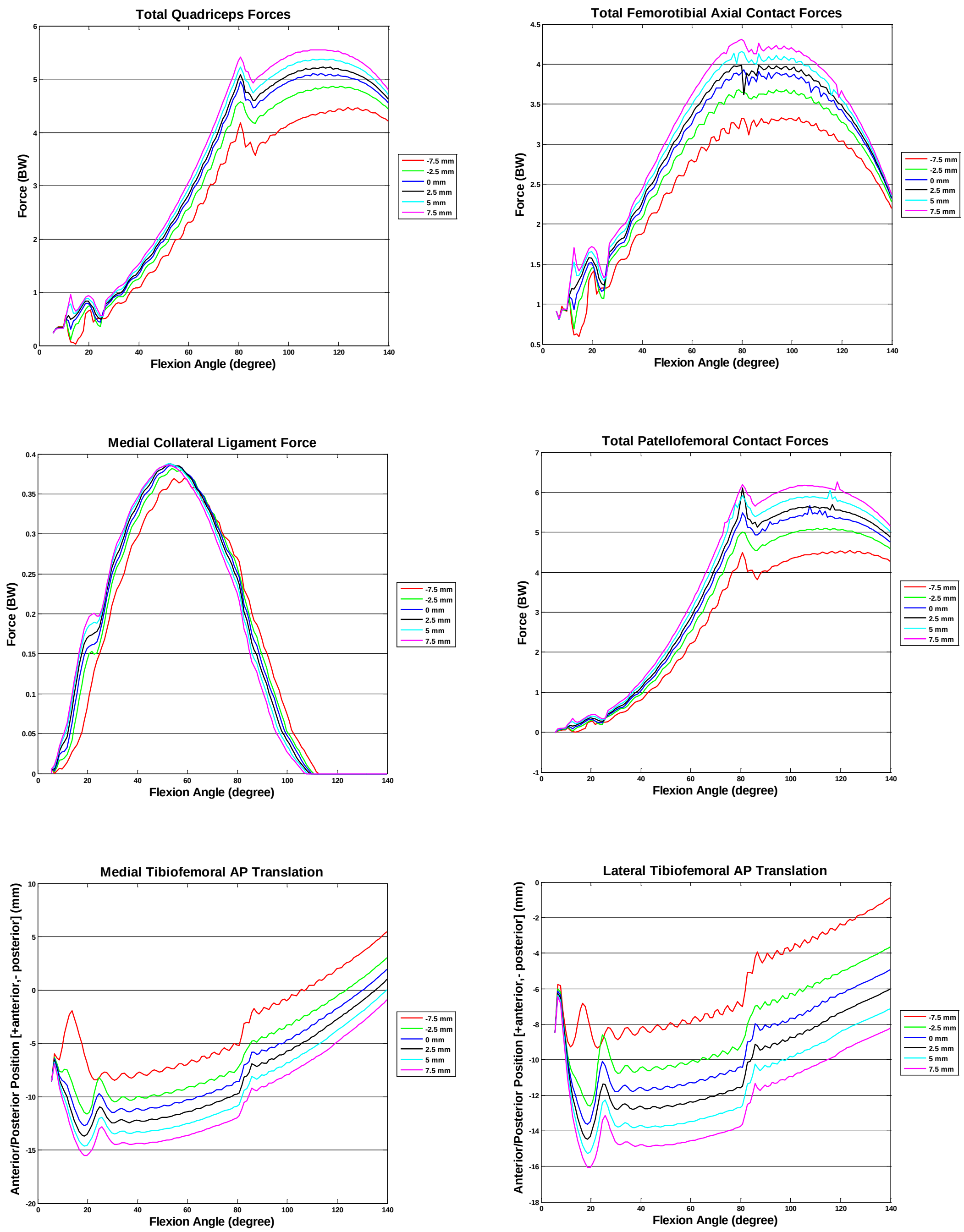

Figure 130: Sensitivity analysis of the tibial component location relative to the tibia in the Anterior/Posterior direction (+anterior,-posterior). The femur and femoral component and patella locations were adjusted so that the relative starting position to the tibial component was the same at each new location.

Sensitivity Analysis of Medial Femoral Sagittal Profile (2)
Teletibia TKA-Deep Knee Bend Simulation

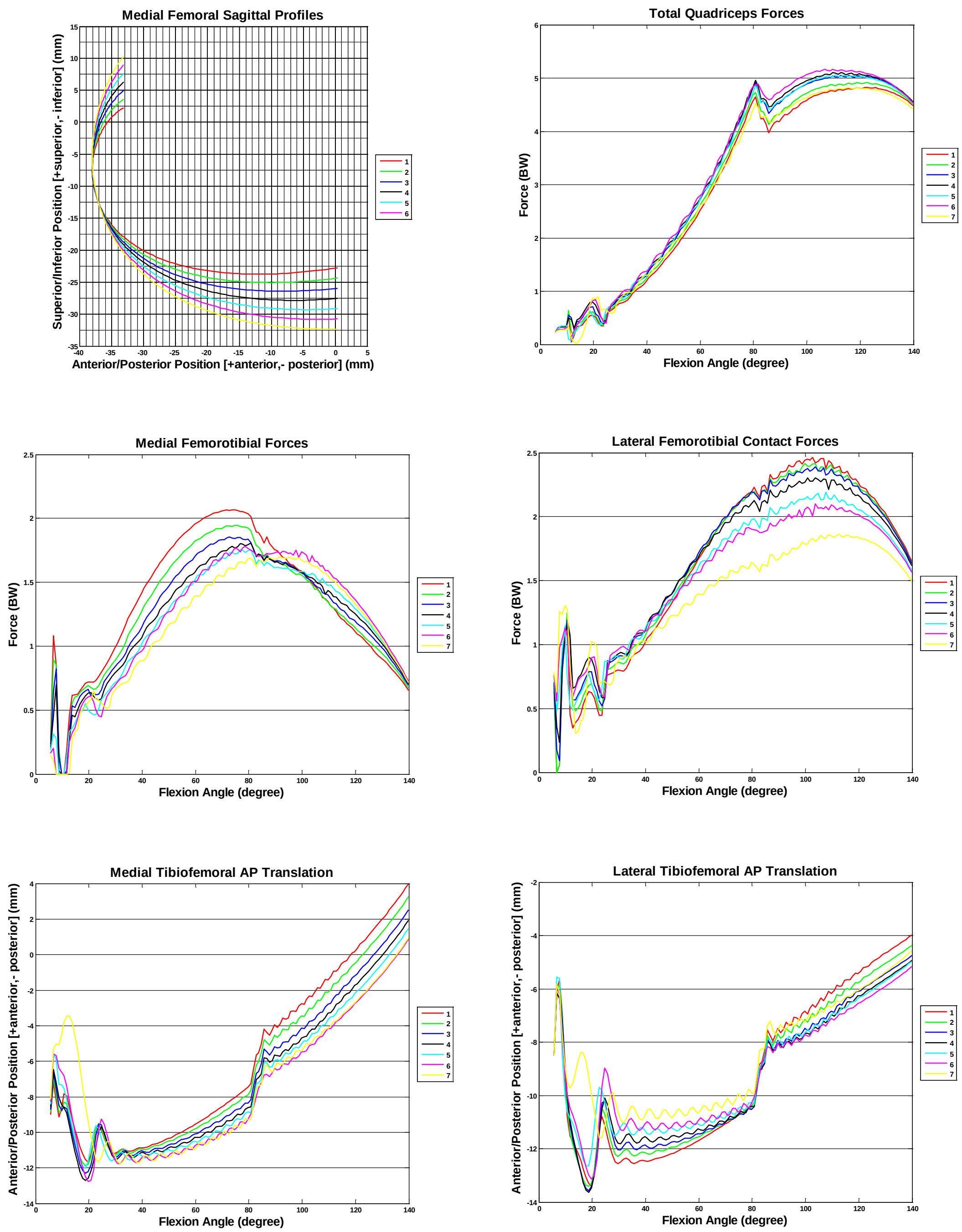

Figure 131: A second sensitivity analysis of the medial femoral sagittal profile. The sagittal profile is seen in upper left figure. The original profile of the Tibiofemoral TKA is data set 4.

Sensitivity Analysis of Laterral Femoral Sagittal Profile (2)

Teletibia TKA-Deep Knee Bend Simulation

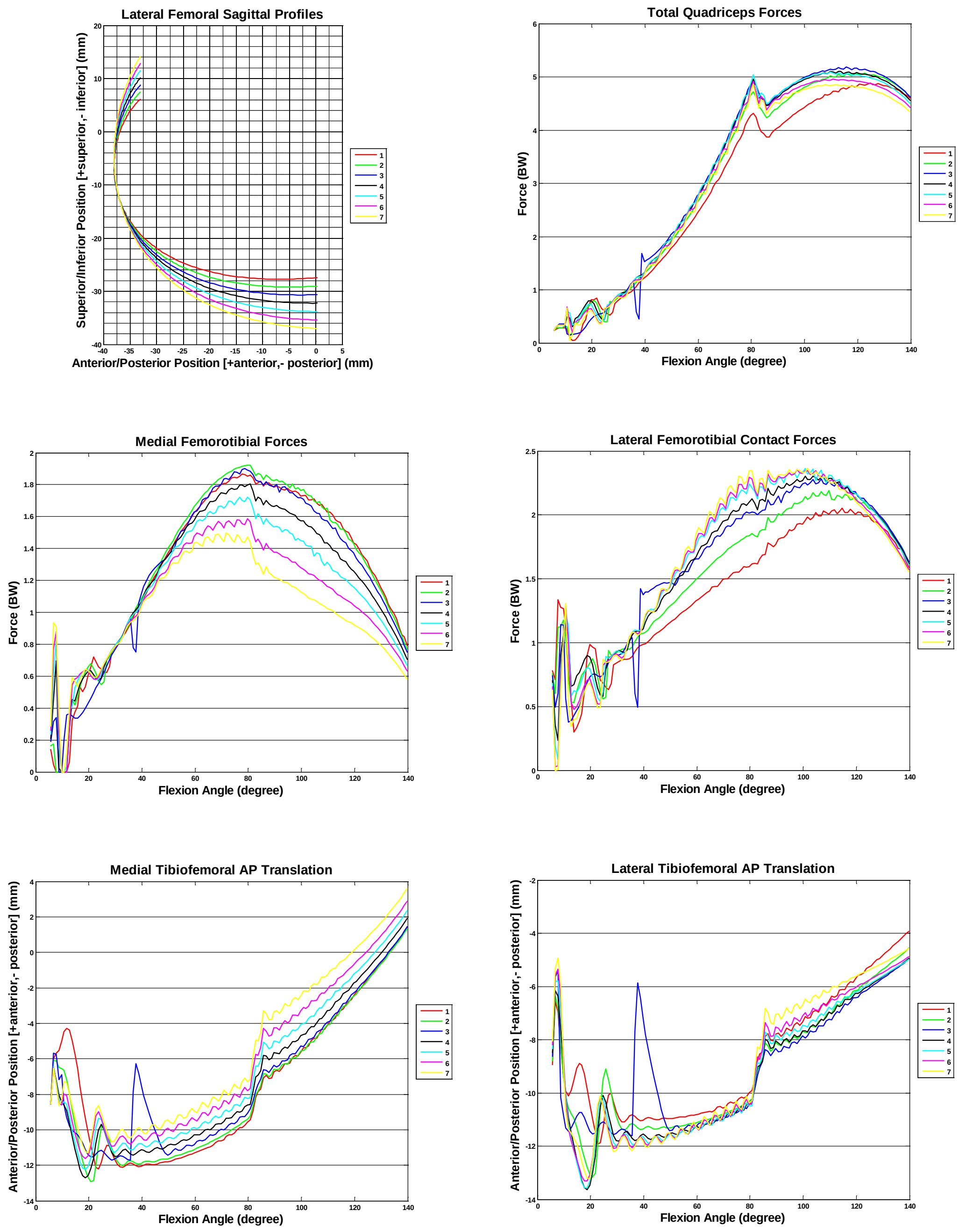

Figure 132: A second sensitivity analysis of the lateral femoral sagittal profile. The sagittal profile is seen in upper left figure. The original profile of the Tibiofemoral TKA is data set 4.

Sensitivity Analysis of Prescribed Pelvis/Torso Flexion
Teletibia TKA-Deep Knee Bend Simulation

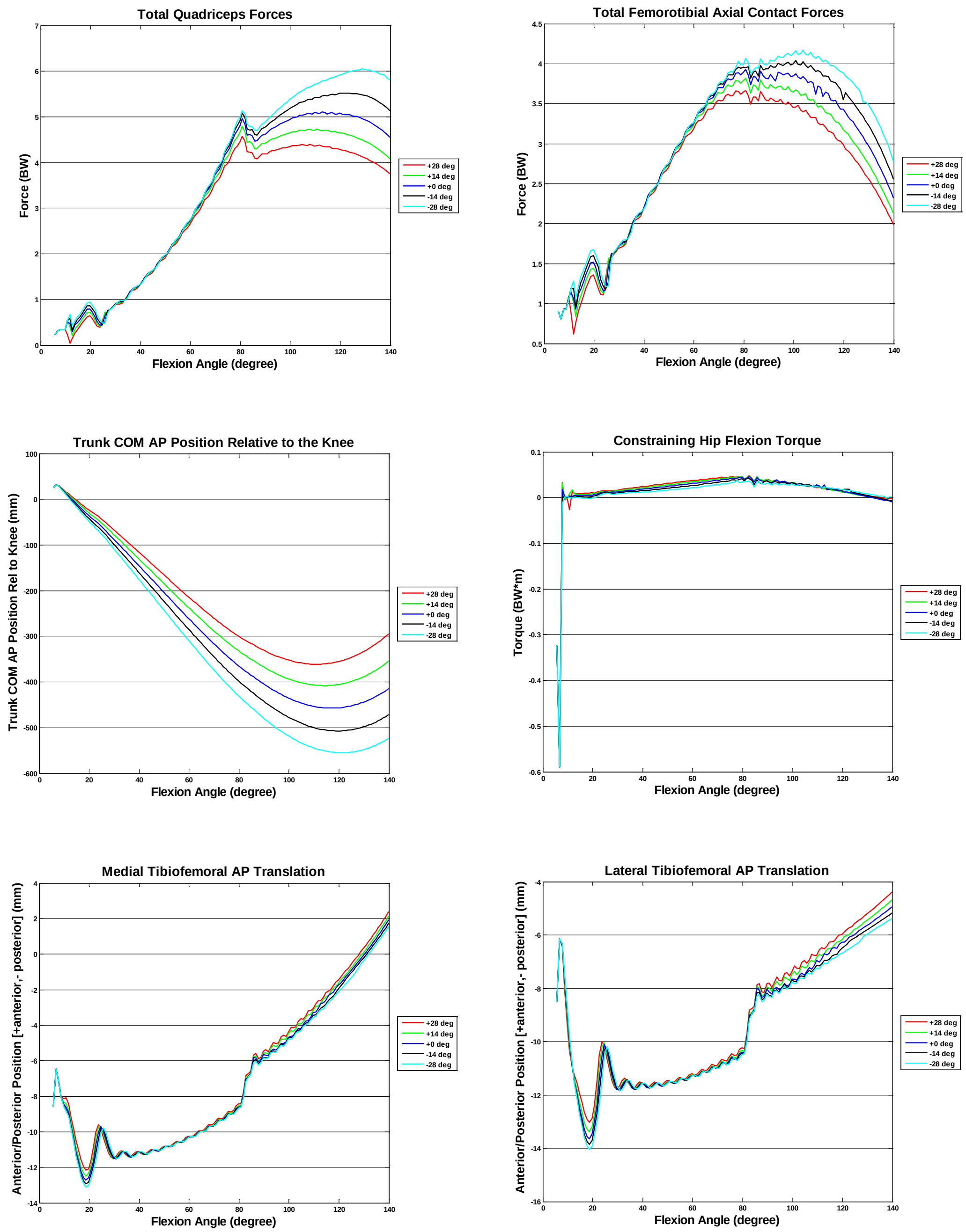

Figure 133: Sensitivity analysis of increasing or decreasing the amount of flexion in the hip, causing the torso to lean more forward (+) or less (-). The numbers in the legends for this figure is the total amount of flexion at the hip added or subtracted from the simulation.

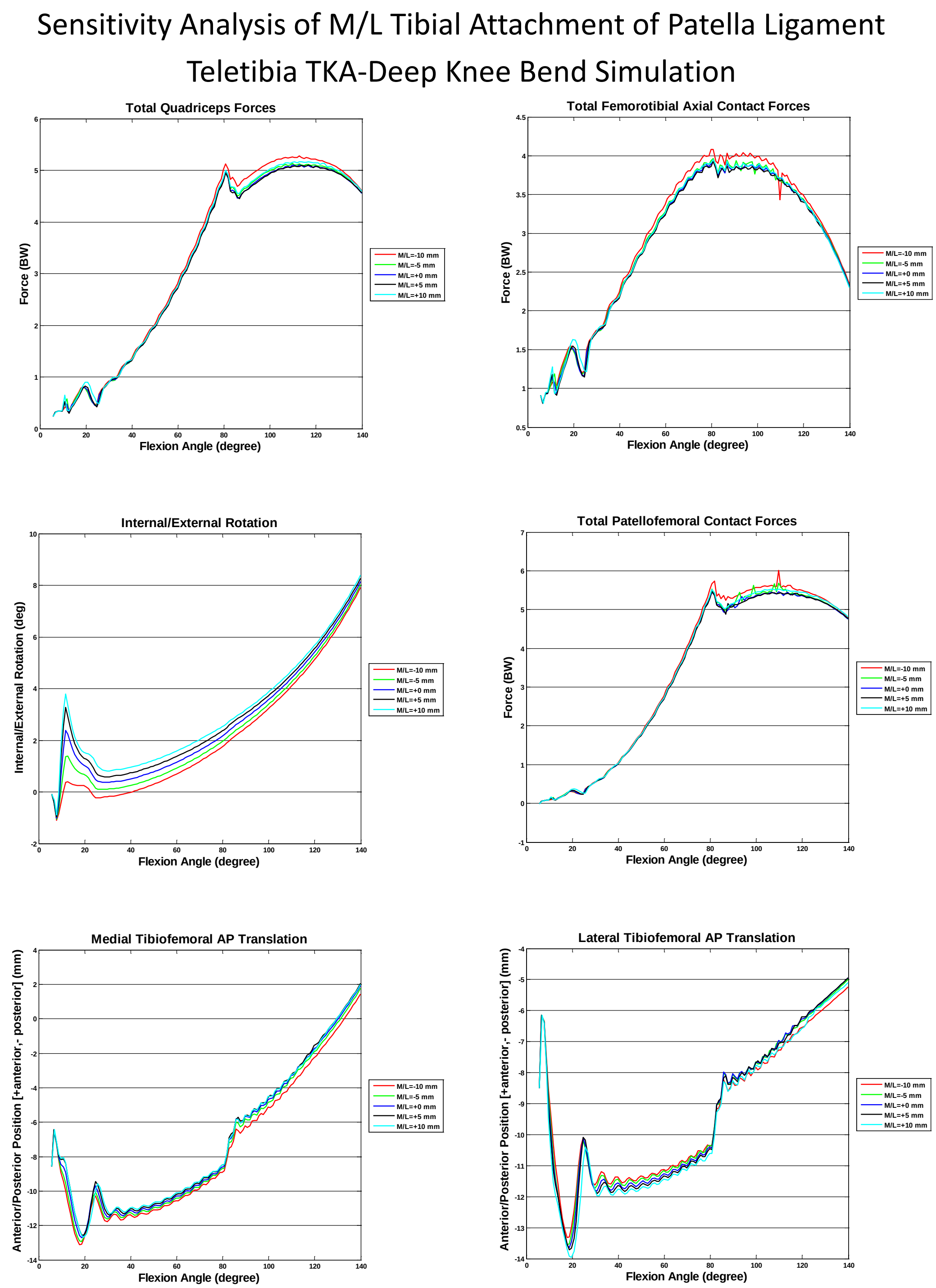

Figure 134: Sensitivity analysis of increasing moving the attachment of the patella ligament on the tibia in the medial or lateral direction from the choosen position on the CAD models built by CT scans. For these simulations the slack length of the patella ligament was recalculated using the new initial length for each simulation.

Sensitivity Analysis of M/L Tibial Attachment of Patella Ligament

Teletibia TKA-Deep Knee Bend Simulation (No Lig Adjust)

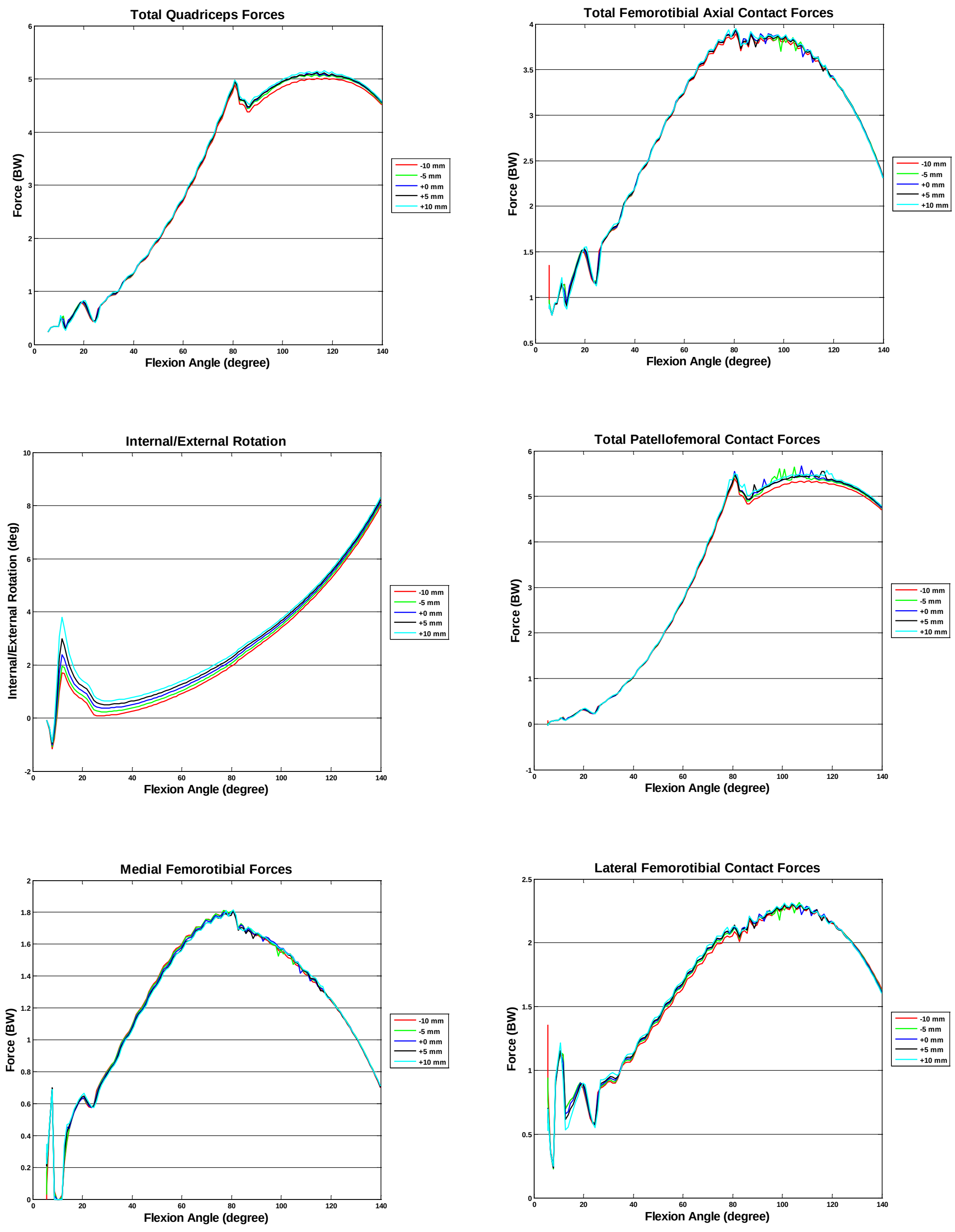

Figure 135: Sensitivity analysis of moving the attachment of the patella ligament on the tibia in the medial or lateral direction from the choosen position on the CAD models built by CT scans. For these simulations no adjustment of the slack length from simulation to simulation was made.

Vita

John Kyle Patrick Mueller is the third son of Dale and Mary Ellen Mueller of Cedarburg, WI. He has three brothers who all rowed at the University of Wisconsin-Madison. His eldest brother, Eric, is a two time Olympian and silver medalist in rowing and coached the men's crew at the University of Wisconsin and currently purchases and rehabs houses in Wisconsin. The second oldest, Timothy, works in internet marketing in Chicago and has two beautiful identical twin daughters and another on the way. John Kyle's youngest brother, Daniel, is a software developer in New York City and also has a beautiful baby girl. Dale and Mary Ellen still reside in Cedarburg where Mary Ellen works as an artist and Dale is a retired federal law enforcement agent.

John Kyle was educated in the Jesuit tradition at Marquette University High School where he was first taught to think critically and with social conscience. He also eventually started for the boy's varsity basketball team and this led to an offer to play basketball at another Jesuit institution, Marquette University in Milwaukee, WI. At Marquette he continued to develop his critical thinking and utilized his mathematical talents by majoring in Biomechanical Engineering. He was always interested in research topics presented in his classes, especially in motion analysis, neurological control theory, physiology and overall biomechanics of the human body. He also earned a starting spot on the Men's Basketball team throughout his Junior and Senior year and during his tenure helped his team make two post-season showings.

After receiving his bachelor's degree, John Kyle worked at the Motion Analysis Lab at the Medical College of Wisconsin under Dr. Richard Harris while taking master's courses at Marquette. During this year he decided his basketball career should not end yet. He played for several professional minor league teams in the US the following year and then was hired to play for a team in the National Basketball League of Australia. During his second season in Australia John was injured and decided to start his post-basketball life.

This led him to Knoxville to the University of Tennessee to work for Dr. Richard Komistek at the Center for Musculoskeletal Research (CMR). Dr. Komistek knew that much of what John learned while playing athletics at the highest levels could be applied to working in orthopaedic research. At CMR, John Kyle pursued his interests in human motion analysis, biomechanics, clinical orthopaedics, multibody dynamics, Kane's dynamics and software design. He was afforded the opportunity to manage several projects, in addition to his PhD project, analyzing in vivo kinematics of the normal knee and TKA for most of the major orthopaedic companies in the market. This sent him across the country and to Europe several times. On these projects he had the opportunity to manage many undergraduate student researchers, work with other graduate researchers at CMR, work with the top orthopaedic surgeons in the country and the world, and researchers in industry. He also had the opportunity to work with Dr. Thomas Kane, father of Kane's dynamics. John Kyle was able to present and publish several of these kinematic studies on TKA, UKA and the normal knee and wrote a book chapter on the topic. He also manages to play basketball whenever he gets a chance.

John Kyle hopes the work he started for his dissertation project continues and spawns many more projects at the Center for Musculoskeletal Research. He currently works as a Research Associate at Oak Ridge National Laboratory under Dr. Boyd Evans. He is developing a system to help clinicians get better performance out of lower leg prosthesis for soldiers injured in the wars in Iraq and Afghanistan.